NON-FEEDBACK DISTRIBUTED BEAMFORMING

Pongnarin Sriploy

A Thesis Submitted in Partial Fulfillment of the Requirements for the

Degree of Doctor of Philosophy in Telecommunication Engineering

Suranaree University of Technology

Academic Year 2015

การก่อรูปลำคลื่นแบบกระจายโดยไม่ใช้การป้อนกลับ

นายพงษ์นรินทร์ ศรีพลอย

วิทยานิพนธ์นี้เป็นส่วนหนึ่งของการศึกษาตามหลักสูตรปริญญาวิศวกรรมศาสตรดุษฎีบัณฑิต
สาขาวิชาวิศวกรรมโทรคมนาคม
มหาวิทยาลัยเทคโนโลยีสุรนารี
ปีการศึกษา 2558

NON-FEEDBACK DISTRIBUTED BEAMFORMING

Suranaree University of Technology has approved this thesis submitted in partial fulfillment of the requirements for the Degree of Doctor of Philosophy.

Thesis Examining Committee

_____

(Asst. Prof. Dr. Wipawee Hattagam)

Chairperson

_____

(Assoc. Prof. Dr. Monthippa Uthansakul)

Member (Thesis Advisor)

_____

(Assoc. Prof. Dr. Peerapong Uthansakul)

Member

_____

(Asst. Prof. Dr. Chanchai Thaijiam)

Member

_____

(Dr. Dheerasak Anantakul)

Member

_____

(Prof. Dr. Sukit Limpijumnong)

Vice Rector for Academic Affairs and Innovation

_____

(Assoc. Prof. Flt. Lt. Dr. Kontorn Chamniprasart)

Dean of Institute of Engineering

พงษ์นรินทร์ ศรีพลอย : การก่อรูปลำคลื่นแบบกระจายโดยไม่ใช้การป้อนกลับ (NON-FEEDBACK DISTRIBUTED BEAMFORMING) อาจารย์ที่ปรึกษา : รองศาสตราจารย์ ดร.มนต์ทิพย์ภา อุฑารสกุล, 194 หน้า.

การก่อรูปลำคลื่นแบบกระจายเป็นวิธีที่สามารถช่วยเพิ่มระยะการสื่อสารและเพิ่มคุณภาพของสัญญาณหรืออัตราส่วนสัญญาณต่อสัญญาณรบกวนได้ อย่างไรก็ตามการก่อรูปลำคลื่นแบบกระจายต้องอาศัยวิธีการซิงโครไนซ์เฟสในการก่อรูปลำคลื่น ซึ่งวิธีการซิงโครไนซ์เฟสสำหรับการก่อรูปลำคลื่นแบบกระจายตามที่ได้สำรวจปริทัศน์วรรณกรรมยังมีจุดด้อยดังนี้ วิธีแบบป้อนกลับสัญญาณ 1 บิต (one-bit feedback technique) และแบบไม่มีสัญญาณป้อนกลับ (zero-feedback technique) ที่ต้องการให้โนดส่งสัญญาณซ้ำเป็นจำนวนมาก ซึ่งความต้องการนี้ส่งผลกระทบต่อแบตเตอรี่ของโนดเคลื่อนที่ซึ่งมีพลังงานจำกัด ขณะที่วิธีแบบอาศัยการป้อนกลับระหว่างโนดแม่กับโนดลูก (master-slave technique) และแบบอาศัยการส่งสัญญาณไปกลับ (round-trip technique) ที่ต้องการส่งสัญญาณอ้างอิงระหว่างโนด ซึ่งส่งผลให้การทำงานของโนดซับซ้อนขึ้น ดังนั้นวิทยานิพนธ์นี้จึงได้นำเสนอการก่อรูปลำคลื่นแบบกระจายที่เรียกว่า การก่อรูปลำคลื่นแบบกระจายโดยไม่ใช้การป้อนกลับ (non-feedback distributed beamforming) ซึ่งมีแนวคิดในการนำเอาสัญญาณของแต่ละโนดมาแยกออกจากกันโดยอาศัยทฤษฎีเมตริกซ์ผกผันที่ใช้ในการแก้สมการเชิงเส้นมาประยุกต์ใช้ในการแยกสัญญาณ จากนั้นจึงทำการซิงโครไนซ์เฟสที่สถานีฐาน โดยวิธีดังกล่าวไม่ต้องการสัญญาณป้อนกลับและสัญญาณอ้างอิงระหว่างโนด ทำให้วิธีการที่นำเสนอมีความซับซ้อนน้อยกว่าวิธีแบบอาศัยการป้อนกลับระหว่างโนดแม่กับโนดลูกและแบบอาศัยการส่งสัญญาณไปกลับ อีกทั้งยังต้องการจำนวนการส่งสัญญาณซ้ำน้อยกว่าวิธีแบบป้อนกลับสัญญาณ 1 บิต และแบบไม่มีสัญญาณป้อนกลับ ผลจากการจำลองแบบและการสร้างชุดทดสอบในทางปฏิบัติแสดงให้เห็นว่าการก่อรูปลำคลื่นแบบกระจายโดยไม่ใช้การป้อนกลับที่นำเสนอสามารถให้อัตราขยายการก่อรูปลำคลื่นสูงสุด และมีอัตราความผิดพลาดบิตน้อยกว่าวิธีการซิงโครไนซ์เฟสที่ได้ศึกษาในปริทัศน์วรรณกรรม

สาขาวิชา วิศวกรรมโทรคมนาคม ลายมือชื่อนักศึกษา _____

ปีการศึกษา 2558 ลายมือชื่ออาจารย์ที่ปรึกษา _____

PONGNARIN SRIPLOY : NON-FEEDBACK DISTRIBUTED BEAMFORMING. THESIS ADVISOR : ASSOC. PROF. MONTHIPPA UTHANSAKUL, Ph.D., 194 PP.

COLLABORATIVE COMMUNICATION/ DISTRIBUTED BEAMFORMING/ PHASE SYNCHRONIZATION/ SPACE-TIME COMMUNICATION

A distributed beamforming can increase a transmission range and enhance Signal-to-Noise Ratio (SNR). However, major phase-synchronization techniques for distributed beamforming suffer from the problems as follows. One-bit feedback and zero-feedback techniques require a large number of retransmissions. This requirement reduces the battery-lifetime of mobile nodes. The master-slave and round-trip techniques require the reference signal among transmitting nodes which introduces a complexity to all transmitting nodes. Therefore, this thesis proposes an alternative technique, so called non-feedback beamforming. The proposed technique concept is to extract and synchronize a combined signal at the base station. The concept of extraction is based on solving a linear equation without the requirement of feedback or reference signals from base station. This proposed technique provides a lower complexity compared with the ones found in literatures. Also, the number of retransmissions are less compared with other techniques. The simulation and experimental results reveal that the proposed technique provides the optimum beamforming gain. Furthermore, it provides a lower bit error rate compared with other technique.

School of Telecommunication Engineering Student's Signature _____

Academic Year 2015 Advisor's Signature _____

ACKNOWLEDGEMENTS

The author wishes to acknowledge the funding support from The Royal Golden Jubilee Ph.D. Program (RGJ).

The grateful thanks and appreciation are given to the thesis advisor, Assoc. Prof. Dr. Monthippa Uthansakul for her consistent supervision and thoughtfully comment on several drafts and advice towards the completion of this study.

My thanks go to Asst. Prof. Dr. Wipawee Hattagam, Assoc. Prof. Dr. Peerapong Uthansakul, Asst. Prof. Dr. Chanchai Thaijiam and Dr. Dheerasak Anantakul for their valuable suggestion and guidance given as examination committees. Many thanks are also extended to Assoc. Prof. Dr. Stevan Berber who commented on the manuscript.

The author is also grateful to the financial support from Suranaree University of Technology (SUT).

Finally, I would also like to express my deep sense of gratitude to my parents for their support and encouragement me throughout the course of this study at the Suranaree University of Technology.

Pongnarin Sriploy

TABLE OF CONTENTS

Page

ABSTRACT (THAI) I

ABSTRACT (ENGLISH) II

ACKNOWLEDGMENTS III

TABLE OF CONTENTS IV

LIST OF TABLES VIII

LIST OF FIGURES IX

LIST OF ABBREVIATIONS XV

CHAPTER

I INTRODUCTION 1

1.1 Background and problems 1

1.2 Thesis objectives 5

1.3 Scope of study 6

1.4 Contributions 6

1.5 Thesis organization 7

II BACKGROUND THEORY 8

2.1 Introduction 8

2.2 Relaying technique 9

2.3 Array antenna 11

TABLE OF CONTENTS (Continued)

Page

2.3.1 Linear array 11
2.3.2 Planar array 15
2.3.3 Circular array 19
2.4 Beamforming 22
2.4.1 Smart antenna 23
2.4.2 Distributed beamforming 26
2.5 Chapter summary 40
III PHASE SYNCHRONIZATION FOR DISTRIBUTED BEAMFORMING 42
3.1 Introduction 42
3.2 One-bit feedback phase synchronization 43
3.3 Master-slave phase synchronization 50
3.4 Round-trip phase synchronization 58
3.5 Zero-feedback phase synchronization 66
3.6 Chapter summary 73
IV NON-FEEDBACK DISTRIBUTED BEAMFORMING 76
4.1 Introduction 76
4.2 Proposed non-feedback distributed beamforming 77
4.2.1 RF frontend receiver 78
4.2.2 Spatial-temporal extraction 82
4.2.3 Optimum weight 90

TABLE OF CONTENTS (Continued)

Page

4.3 Effect of phase variation on proposed non-feedback distributed beamforming 94
4.4 Performance comparison 102
4.4.1 Beamforming gain comparison 104
4.4.2 BER gain comparison 106
4.4.3 Complexity gain comparison 108
4.5 Chapter summary 113
V AN EXPERIMENTAL STUDY OF NON-FEEDBACK DISTRIBUTED BEAMFORMING 115
5.1 Introduction 115
5.2 Software defined radio 116
5.2.1 Equipment list 117
5.2.2 GNU Radio Companion 121
5.3 An experiment on received power 121
5.4 An experiment on BER 131
5.5 Chapter summary 140
VI CONCLUSION 141
6.1 Conclusion 141
6.2 Future studies 142

TABLE OF CONTENTS (Continued)

Page

REFERENCES 144

APPENDIX A PUBLICATIONS 149

BIOGRAPHY 195

LIST OF TABLES

Table **Page**

3.1 Disadvantages of existing phase synchronization techniques from literatures. ... 74

4.1 Mean and standard deviation of measured phase 102

4.2 Number of FLOPS of the basic mathematical operation 109

4.3 FLOPS calculation of the one-bit feedback technique 109

4.4 FLOPS calculation of PLL 110

4.5 FLOPS calculation of the master-slave technique 110

4.6 FLOPS calculation of the round-trip technique 111

4.7 FLOPS calculation of the zero-feedback technique 111

4.8 FLOPS calculation of the proposed non-feedback technique 111

4.9 Requirement comparison between proposed non-feedback and literatures 114

5.1 Mean and standard deviation of measured average magnitude 131

5.2 Mean and standard deviation of measured BER 140

LIST OF FIGURES

Figure **Page**

2.1 Route map for Chapter II 9

2.2 Relaying network in WLANs 10

2.3 *N*-element linear array 12

2.4 Radiation pattern of linear array where $N = 4$ 15

2.5 $N \times M$ rectangular planar array 16

2.6 Radiation pattern of 2×2 rectangular planar array 18

2.7 Circular array of *N*-elements 20

2.8 Radiation pattern of circular array where $N = 10$ 21

2.9 Base station in a mobile network with beamforming technique 23

2.10 2×1 smart antenna systems 24

2.11 Distributed beamforming networks 27

2.12 Radiation pattern of distributed beamforming with perfect phase synchronization 32

2.13 Average beam pattern with imperfection in network radius estimation, r_n 38

2.14 Average beam pattern with imperfection in phase estimation, ψ_n 39

2.15 Plot of main beam's gain degradation with respect to imperfection of estimated node location (radius and phase) 40

3.1 Route map of organization in Chapter III 43

LIST OF FIGURES (Continued)

Figure **Page**

3.2 Configuration of distributed nodes employing the one-bit feedback phase synchronization technique 44

3.3 Convergence of feedback control algorithm 47

3.4 Beamforming gain with a number of iteration, *i* 49

3.5 Configuration of distributed nodes employing a master-slave phase synchronization technique 51

3.6 Round-trip phase calibration for master-slave technique 52

3.7 Schematic of a slave node for master-slave technique 55

3.8 Time-division duplexing for master-slave technique 56

3.9 Simulation of oscillator time-varying phase drift in PLL 56

3.10 Time-slotted round-trip carrier synchronization system with two source nodes 58

3.11 Summary of the two-source time-slotted round-trip carrier synchronization protocol 64

3.12 *M*-source round-trip distributed beamforming system 65

3.13 Two distributed transmitters ($N = 2$) with carrier frequency offsets of $\Delta f_2 = 2\Delta f_1 = f_0$ 68

3.14 Steady-state (time-independent) alignment probability lower bound as a function of number of distributed transmitter (M), with normal carrier offset distribution 71

LIST OF FIGURES (Continued)

Figure **Page**

3.15 Expected number of symbols (out of τ_c = 100) with N = 3 aligned signals within at most a phase offset ¤$_0$ (a = cos(φ_0)), and [¤$_1$, ¤$_2$, ¤$_3$] = [6.19, 0.24, 1.77] 72

4.1 Route map of study in Chapter IV 77

4.2 Block diagram of the RF front end receiver 83

4.3 Block diagram of the proposed non-feedback technique 83

4.4 Proposed phase shifting pattern 84

4.5 Four original transmitted signals 88

4.6 Combined retransmission signals 89

4.7 Four extracted signals 89

4.8 Summary flow chart of proposed phase synchronization 91

4.9 Normalized beamforming gain vs. weighting step 92

4.10 Received signal at base station from 4 transmitting nodes 92

4.11 Beamforming gain of proposed non-feedback with several standard deviations 95

4.12 Floor plan of measuring area 97

4.13 Measurement setup 97

4.14 Transmitter setup 98

4.15 Receiver setup 98

4.16 Phase histogram at measured location 1 100

LIST OF FIGURES (Continued)

Figure **Page**

4.17 Phase histogram at measured location 2 100
4.18 Phase histogram at measured location 3 101
4.19 Phase histogram at measured location 4 101
4.20 Combined signal affected by phase variation (σ = 6°) 103
4.21 Average beamforming gain using proposed non-feedback under the worst phase variation (σ = 6°) condition 103
4.22 Beamforming gain of proposed non-feedback technique vs. other techniques 105
4.23 BER comparison where number of retransmissions is unlimited 107
4.24 BER comparison where number of retransmissions is limited to 50 times 107
4.25 FLOPS comparison of proposed non-feedback technique vs. existing techniques 112
5.1 Route map of study in Chapter V 116
5.2 Configuration of SDR 117
5.3 USRP1 module 119
5.4 USRP B100 module 119
5.5 XCVR2450 daughterboard 120
5.6 SBX daughterboard 120
5.7 VERT2450 antenna 120
5.8 Configuration of measurement for received signal power 122

LIST OF FIGURES (Continued)

Figure **Page**

5.9 Configuration of the two transmitting nodes on received signal power 123

5.10 Configuration of the base station on received signal power 123

5.11 Calibrated transmitting power of USRP1 124

5.12 Programming block diagram of transmitting nodes on received signal power 125

5.13 Programming block diagram of base station on received signal power 125

5.14 Programming block diagram of the proposed “Extraction” 126

5.15 Programming block diagram of the weighting and combining signal 126

5.16 Magnitude of transmitting signal from node A (1×1 A) 128

5.17 Magnitude of transmitting signal from node B (1×1 B) 128

5.18 Magnitude of signal from two nodes at the 1st transmission (2×1 1st) 129

5.19 Magnitude of signal from two nodes at the 2nd transmission (2×1 2nd) 129

5.20 Magnitude of transmitting signal with proposed technique (2×1 on) 130

5.21 Magnitude of transmitting signal without phase synchronization (2×1 off) 130

5.22 Configuration of measurement for BER 132

5.23 Two transmitting nodes employing USRP B100 132

5.24 Calibrated transmitting power of USRP B100 133

5.25 Programming block diagram of transmitting nodes for experimental BER 134

5.26 Programming block diagram of base station for experimental BER 134

5.27 Programming block diagram of the weighting and combining signal 135

LIST OF FIGURES (Continued)

Figure **Page**

5.28 Programming block diagram of base station for experimental BER 135

5.29 BER of transmitting signal from node #A (1×1 A) 137

5.30 BER of transmitting signal from node #B (1×1 B)..... 137

5.31 BER of signal from two nodes at the 1st transmission (2×1 1st) 138

5.32 BER of signal from two nodes at the 2nd transmission (2×1 2nd)..... 138

5.33 BER of transmitting signal with proposed technique (2×1 on) 139

5.34 BER of transmitting signal without phase synchronization (2×1 off)..... 139

SYMBOLS AND ABBREVIATIONS

α_n	=	Attenuation in channel between n^{th} node and a base station
β	=	Phase difference between antenna elements
γ	=	Direction of propagation
$\Delta\zeta_{n,l}$	=	Phase variation effect of the n^{th} node at the sending time l
Δ¤$_n$	=	Phase offset
$\Delta\omega_n$	=	Frequency offset
$\Delta\Omega_n$	=	Frequency offset
$\Delta\mathbf{A}_{NN}$	=	Phase adjustment pattern matrix
Δf_n	=	Carrier frequency offset of n^{th} node
£$_.$	=	Location error in terms of phase
£$_r$	=	Location error in terms of radius
δr_n	=	Random variables of estimated node location error
$\delta\psi_n$	=	Random variables of estimated node location error
θ_n	=	Initial phase of n^{th} node
λ	=	Wave length
$\eta(t)$	=	Noise
σ	=	Standard deviation of phase values
±$^2_{..}$	=	Variance of the phase noise
±$_R$	=	Mean deviation
ς	=	Sampling time

SYMBOLS AND ABBREVIATIONS (Continued)

²	=	Time delay
φ	=	Measured phase value
φ_0	=	Mean of phase values
ϕ_0	=	Nominal phase
¤$_n^d(t)$	=	Phase drift of n^{th} slave
¤$_n$	=	Phase of received signal
¤$_n^h$	=	Effective phase noise
Φ_n	=	Phase offset
ψ_n	=	Direction angle of n^{th} node referred to x-axis
ω_c	=	Carrier frequency
µ$_{LO}$	=	Local Oscillating (LO) frequency
Ω_{DLO}	=	Digital local oscillator frequency
a	=	Alignment parameter
A	=	Carrier amplitude
A_φ	=	Attenuation given by phase offset
A_d	=	Desired signal
$\mathbf{A}_{NN}$	=	Proposed phase adjustment pattern matrix
ADC	=	Analog-to-Digital Converter
AF	=	Array Factor
BER	=	Bit Error Rate
C_p	=	Magnitude of the phase step in radians

SYMBOLS AND ABBREVIATIONS (Continued)

d	=	Antenna element spacing
d_n	=	Distance between the node and the base station
DAC	=	Digital to Analog Converter
dB	=	Decibel
DBPSK	=	Differential Binary Phase Shift Keying
DDC	=	Digital Down-Converter
DOA	=	Direction Of Arrival
DSP	=	Digital Signal Processing
DUC	=	Digital UP-Converter
${}_pF_q(x)$	=	Generalized hypergeometric function
f_c	=	Carrier frequency
FLOPS	=	FLoating-point Operations Per Second
FPGA	=	Field-Programmable Gate Array
f_{out}	=	Output frequency
f_{ref}	=	Reference frequency
GRC	=	GNU Radio Companion
H	=	Product of the individual feedback transfer function
$\hat{h}_n$	=	Complex channel gain of n^{th} node
I	=	Excitation coefficient
i.i.d.	=	independent and identically distributed
k	=	Wave number
$L_{\text{BF}}[b]$	=	Beamforming gain factor

SYMBOLS AND ABBREVIATIONS (Continued)

LNA	=	Low Noise Amplifier
LPF	=	Low-Pass Filter
LOS	=	Line-Of-Sight
mod	=	Modulo operation
mW	=	milliwatts
N	=	Number of transmitting nodes
N_p	=	Phase noise
PA	=	Power Amplifier
PLL	=	Phase Locked Loop
pdfs	=	Probability Density Functions
ppm	=	Part per million
P_{av}	=	Average beam pattern
$p_{\Delta f}(\Delta f)$	=	Frequency offset distribution
P_R	=	Received power
P_T	=	Transmitted power
$Q(x)$	=	Distribution function of a standard Gaussian random variable
R	=	Radius of network
RF	=	Radio frequency
r_n	=	Distance between n^{th} node and network center
SDR	=	Software Defined Radio
SNR	=	Signal to Noise Ratios
T_s	=	Sampling rate

SYMBOLS AND ABBREVIATIONS (Continued)

U	=	Number of iteration in the optimum weighting operation
UHD	=	USRP Hardware Driver
USRP	=	Universal Software Radio Peripheral
V	=	Number of iteration in PLL
VCO	=	Voltage-Controlled Oscillator
$W_{BB}(\varsigma)$	=	Base-band additive white Gaussian noise
$W_{BB,N}(\mathrm{s})$	=	Vector of baseband white Gaussian noise
$W_{PB}(t)$	=	Pass-band additive white Gaussian noise
WLAN	=	Wireless Local Area Networks
$x(t)$	=	Data message
$y_n'(t)$	=	Signal from the n^{th} node
$\mathbf{y}_N(\mathrm{s})$	=	Vector of transmitted message from all transmitting nodes
$Y''(\mathrm{s})$	=	Received digital base-band signal at a base station
$\mathbf{Y}_N''(\mathrm{s})$	=	Vector of combined received signal
$Y_{opt}(\mathrm{s})$	=	Output signal

CHAPTER I

INTRODUCTION

1.1 Background and problems

Nowadays, wireless communication networks provide a variety of applications such as Wireless Local Area Networks (WLANs), cellular networks or wireless sensor networks. These wireless networks have lots of advantages in flexibility and mobility for users compared with wire line systems. However, the transmission range of wireless communication systems is limited due to signal attenuation (Sriploy, P., et.al, (2013)). Therefore, nodes or sensors in the systems requires higher transmitting power to compensate the mentioned attenuation. This requirement is not practical due to the limited battery life time of nodes. To tackle the problem, a relaying technique has been presented (Dohler, M. et.al, (2010)). The relay increases a transmission rangs by sending the information among nodes which pass on the information to a base station. Nevertheless, the relaying technique is ineffectiveness when the relaying network is situated far away from a base station. This is because the transmitted signal is distorted when travelling through long distance. On the other hand, an array antenna may be employed at individual devices in order to enhance beamforming gain (Balanis C. A., (1997); Meerasri P., et.al, (2014); Innok A., et.al, (2012); Uthansakul M. et.al (2005); Bunsanit C. et.al (2012) and Uthansakul P., et.al, (2011)). Unfortunately, the installation of multiple antenna elements on a mobile terminal is difficult due to its size and the requirement of limited power consumption (Rayal F., (2005); Kosanovic M., et.al, (2012) and Kaiser T., (2005)). Recently, a distributed

beamforming has been proposed to handle the problem (Lo Y. T., (1964) and Ochiai H., et.al, (2005)), which has many advantages such as a significant increase in transmission range and enhancement of both energy efficiency and Signal-to-Noise Ratio (SNR) (Amini S., (2015); Yang L. (2013) and Dohler, M. et.al, (2010)). This is because the beamforming gain of distributed beamforming networks is N^2, where N is the number of transmitting nodes in distributed beamforming networks.

The distributed beamforming concept is similar to smart antennas but the position of antennas (or nodes) is random. Also, it could be said that the distributed beamforming is similar to virtual array antennas in which each node sends the same data at the same time to base station (Yao K., et.al, (1998)). The transmitting nodes have to perform the carrier phase synchronization so that the transmitted signals are combined at a base station. Otherwise, the phase offsets or phase errors among all transmitted signals would reduce the power of combined signal at a base station. Thus, phase synchronization is the key success for distributed beamforming networks.

Recently, several phase synchronization techniques have been proposed. Those techniques can be divided into two general types which are closed loop and open loop synchronization techniques (Mudumbai R., et.al, (2009)). The closed loop technique needs some feedbacks from base station to adjust phase offsets between base station and transmitting nodes. A one-bit feedback is one of the best techniques for closed loop synchronization (Mudumbai R., et.al, (2005); Mudumbai R., (2010) and Rahman M. M, at.al, (2012)). According to this technique, every transmitting node in the networks adjusts its carrier phase randomly. Then, all nodes transmit the same data to base station. After the SNR of received signal is estimated at the base station, one bit (0 or 1) is fed back to all nodes. The bit “0” means that SNR is worse

than before so that each node has to randomly adjust their phases again. While bit “1” means that SNR is better so that all nodes have to update their latest phase adjustment. Otherwise, all nodes do this closed loop technique again in order to update the best phase adjustment. This technique requires a large number of retransmissions (or feedback signal) from all nodes to a base station. In addition, this technique requires at least 5*N* iterations in order to achieve 75% guarantee of perfect or maximum beamforming gain (Mudumbai R., et.al, (2009)). This may be considered impractical as the battery lifetime of nodes or mobile terminals is very limited. Moreover, closed-loop feedback from base station to transmitting nodes may be unreliable when the communication channel between base station and nodes is weak.

In order to overcome the mentioned problems, two open loop phase synchronization techniques have been proposed to reduce interaction between the base station and nodes, so called the master-slave and the time-slot round-trip techniques. For the master-slave technique, a node in the network is selected as a master node while all remaining nodes are assigned as slave nodes. The phase synchronization is achieved by sending the reference signals between master and slave nodes (Mudumbai R., (2007)). Alternatively, for time-slot round-trip technique, phase synchronization among nodes is obtained by sending a reference data round between nodes (Brown D.R., et.al, (2008); Ozil I. et.al, (2007) and Brown D.R., et.al, (2010)). The idea is based on the equivalence of round-trip transmission delays through a multi-hop chain between transmitting nodes and base station. According to these procedures, the open loop techniques reduce the interaction among nodes and base station. However, both master-slave and round-trip techniques require some feedbacks from the base station. This interaction between nodes increases complexity to all

transmitting nodes. In addition, nodes require a special hardware such as the phase-locked loops (PLLs) to obtain reference signals when performing open-loop feedback in order to achieve phase synchronization.

Alternatively, a zero-feedback technique for phase synchronization has been lately proposed (Bletsas A., et.al, (2010) and Sklivanitis G., et.al, (2011)). This technique does not require any feedback signal from the base station. All transmitting nodes are also assumed as the conventional radio transceivers employing no special hardware. The utilized technique employs a carrier frequency offset between transmitting nodes for the phase synchronization. However, the zero-feedback technique requires a large number of packet retransmissions. For example, in case of having 3 nodes, this technique requires at least 50 retransmissions (iterations) to obtain a beamforming gain at 9.1 dB. Note that the maximum gain for this case is 9.5 dB (Bletsas A., et.al, (2010)). In addition, the number of retransmissions exponentially increase when the number of nodes increases. Thus, this technique is also not practical.

From the above literatures, the major disadvantage of existing phase synchronization techniques, one-bit feedback and zero-feedback, is that they require a large number of retransmissions. This requirement reduces the battery-lifetime of mobile nodes. Also, the master-slave and round-trip openloop techniques require a reference signal among transmitting nodes, which increases complexity for all transmitting nodes.

To overcome these limitations, a Non-Feedback Distributed Beamforming technique is proposed in this thesis. The proposed technique does not require any feedback signal from base station or any interaction between nodes. A few number of

retransmissions from nodes, which is only the same as the number of beamforming nodes, *N*, is required. This number is relatively small comparing to the case of one-bit feedback and zero-feedback techniques. The proposed non-feedback beamforming employs an inverse matrix to extract the combined signal at the base station. The concept of extraction is based on solving a linear equation using the inverse matrix method (Kreyszig E., (1999)). After performing signal extraction, each extracted signal is weighted for phase synchronization at the base station, instead of nodes. Finally, the base station obtains a combined signal with maximum beamforming gain. However, the retransmitted signals may be distorted due to phase variations when travelling through the communication channel. To investigate the mentioned effect, the phase variation effect in real circumstance is taken into account in this thesis. Please note that the term use "non-feedback" is used to avoid any confusion with the conceptual term defined for "zero-feedback" which has been presented in (Bletsas A., et.al, (2010) and Sklivanitis G., et.al, (2011)).

1.2 Thesis objectives

(i) To study the basic principles and theories of the phase synchronization for the distributed beamforming.

(ii) To propose a new distributed beamforming technique which does not require any feedback signal from a base station or any interaction between transmitting nodes for the phase synchronization procedure.

(iii) To investigate the performance of the proposed distributed beamforming technique in a real circumstance.

1.3 Scope of study

(i) The phase of transmitting signals can be synchronized by utilizing the proposed non-feedback distributed beamforimg.

(ii) All simulation results are performed using MATLAB.

(iii) For simulation, the transmitting node's location are uniformly distributed in a network. The transmitting nodes and base station are equipped with a single isotropic antenna. Also, the mutual coupling effect between nodes is negligible because the antennas are sufficiently separated.

(iv) A testbed of the proposed non-feedback distributed beamforimg consists of two transmitting nodes and one base station.

(v) The performance comparison between the proposed technique and a system without phase synchronization are investigated.

(vi) The measured power and Bit Error Rate (BER) are considered.

1.4 Contributions

This thesis proposes the new distributed beamforming technique, so called non-feedback distributed beamforming technique which the outcome can be categorized as follows :

(i) The proposed technique is attractive as it can be practically implemented because it requires a few number of retransmissions and does not require any feedback or reference signals from a base station.

(ii) This thesis has presented the experimental study of received power and BER for the proposed technique compared to a system without phase synchronization.

1.5 Thesis organization

The remainder of this thesis is organized as follows. Chapter II presents the background theory including relay and beamforming technique which includes smart antennas and distributed beamforming. This chapter presents that the distributed beamforming is more interesting than the relay and smart antennas.

Chapter III presents the existing phase synchronization techniques for distributed beamforming. This chapter presents that the existing phase synchronization techniques have some drawbacks as they require a large number of retransmissions, feedback signal and interaction among transmitting nodes.

Chapter IV presents the proposed non-feedback distributed beamforming which does not require any interaction between nodes and feedback signals. The simulation results of the proposed technique are also presented in this chapter. Moreover, the phase variation in real circumstance is taken into account in this chapter.

Chapter V presents the practical measurement of the proposed the non-feedback distributed beamforming. A full testbed is constructed. The testbed consisting of two transmitting nodes and one base station was developed under SDR (Software-Defined Radio) technology. The experimental results reveal that the proposed technique provides the optimum beamforming gain. Furthermore, it can reduce BER in the systems.

Chapter VI provides the conclusion of the research work and suggestion for further study.

CHAPTER II

BACKGROUND THEORY

2.1 Introduction

Recently, wireless communication systems such as Wireless Local Area Networks (WLANs) have gained lots of consideration into several applications in various areas. This is because WLANs have advantages in terms of flexibility and mobility. Moreover, it can support a high speed data transmission. However, WLANs have a major limitation in terms of transmission range. Generally, the transmission range is typically 30 meters for indoor communications and 100 meters for outdoor communications. Therefore, this chapter discusses the relay and beamforming technique which can tackle the mentioned problem. Figure 2.1 demonstrates a route map of this chapter. Section 2.1 is an introduction of this chapter which presents the limitation of communication range of WLANs. Then, some techniques for increasing communication range are presented in the Sections 2.2, 2.3 and 2.4. Section 2.2 discusses the relaying technique which can increase communication range by sending the signal among the relay nodes. Section 2.3 presents the theories of the array antennas which are the basic theory of beamforming technique presented in Section 2.4. The beamforming technique can increase communication range by increasing a directivity. Finally, Section 2.5 points out the advantages and disadvantages of the relay and beamforming technique.

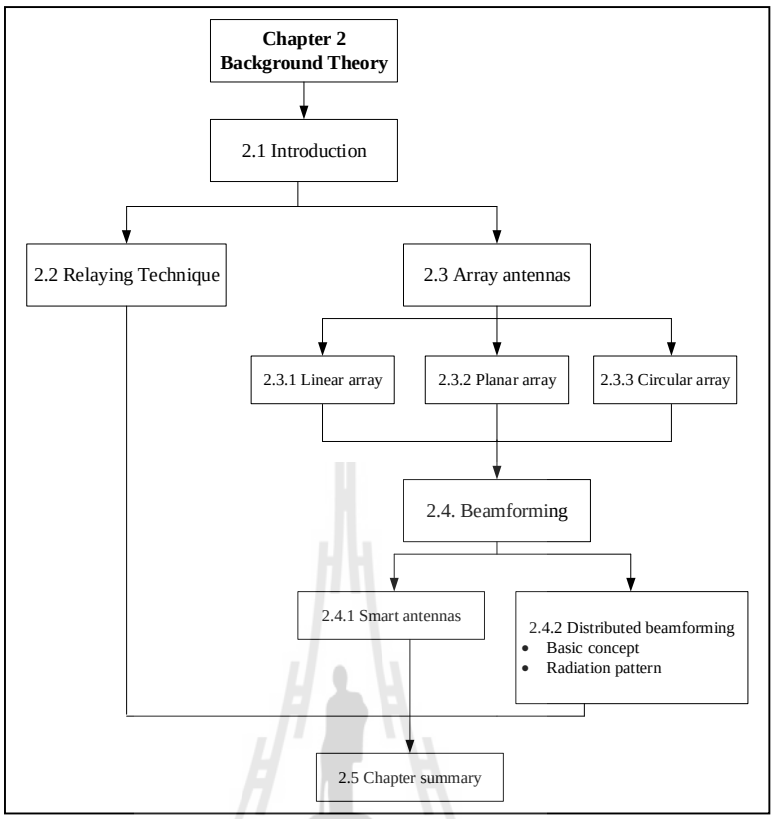

Figure 2.1 Route map for Chapter II.

2.2 Relaying Technique

A relaying technique is a cooperative method in which the source node and base station are interconnected by means of cooperative nodes (Dohler M. et.al, (2010)). The cooperative relaying technique consists of source, destination and relay nodes supporting the direct communication between source and destination. If the direct transmission of a signal from source to destination is not successful, the overheard signal from the source is forwarded by the relay to reach the destination via a different path. Figure 2.2 shows an example of cooperative relaying networks where

the direct communication between a WLAN access point in home #1 and a WLAN access point

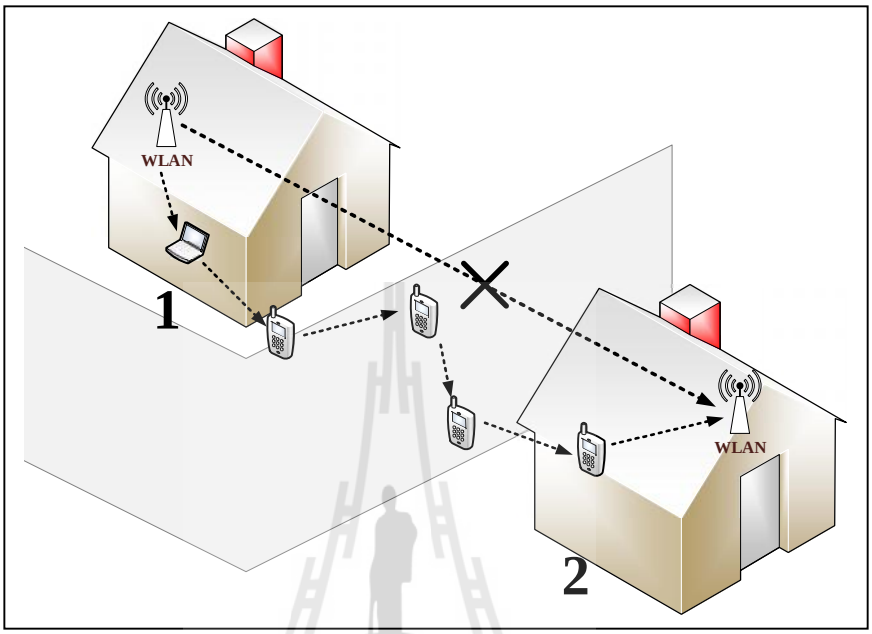

Figure 2.2 Relaying network in WLANs.

in home #2 is not successful. Thus, the WLAN access point in home #1 transmits a signal via the relays nodes such as laptop or mobile phone to the WLAN access point in home #2. The relaying protocol can be classified into two groups as follows

(i) **Amplify-and-Forward (AF)** : AF is the simplest relaying protocol in which each relay amplifies the received noisy signals and forwards them to the base station. According to the noise component in the signals is also amplified, thus the BER can be degraded (Issariyakul T., et.al, (2009)).

(ii) **Decode- and-Forward (DF)** : The received signals are decoded by the relay then the relay re-encodes signals and transmitted to base station, also the received signals are amplified. The DF provides a higher quality

signal over the AF. However, the DF has higher complexity in terms of signal processing (Hwang K. S., et.al, (2008)).

According to these procedures, the relay can extend a communication range by interconnecting among nodes. However, the relaying technique is ineffective when the relaying network is situated far away from base station. As seen in Figure 2.2 if the network has no any relay node between home and street. Then, the base station cannot transmit signals to the nodes on the street. In this case, the beamforming technique is more attractive in which it can point the main beam to the desired direction. The next section presents the array antennas which are the basic theory for beam formation.

2.3 Array antennas

Array antennas are a set of individual antenna elements which are connected together (Bletsas A., et.al, (2010)). The signals from the antennas are combined in order to improve the directional characteristics. The array geometry can be roughly classified into three types e.g. linear, planar and circular array.

2.3.1 Linear array

The linear array is the simplest array geometry. All antenna elements are aligned along a straight line. Figure 2.3 shows a linear antenna array which has N antenna elements. The element spacing, d, can be usually calculated by

$$d = \frac{\lambda}{2}, \tag{2.1}$$

where λ is the wavelength.

For simplification, we assume that all elements have a uniform inter-element spacing and have an equal transmitted power. Thus, we can derive the array factor in the far field region as follows

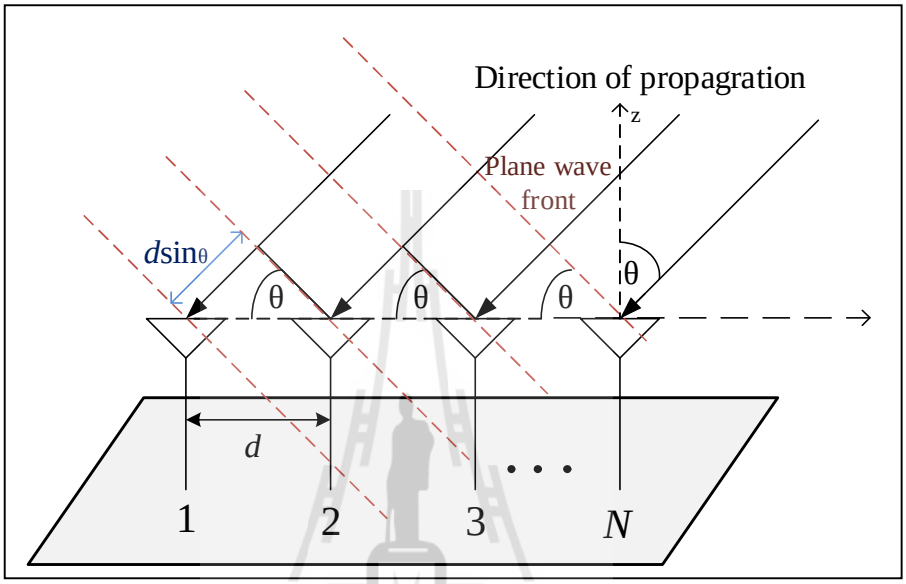

Figure 2.3 *N*-element linear array.

$$\begin{aligned} AF &= 1 + e^{+j(kd\sin\theta + \beta)} + e^{+j2(kd\sin\theta + \beta)} + \ldots + e^{+j(N-1)(kd\sin\theta + \beta)} \\ &= \sum_{n=1}^{N} e^{j(n-1)kd(\sin\theta + \beta)} \\ &= \sum_{n=1}^{N} e^{j(n-1)\Psi}, \end{aligned} \tag{2.2}$$

where $\psi = kd\sin\theta + \beta$, θ is an angle as measured from the z-axis, k is the wave number where $k = 2\pi/\lambda$ and β is an electrical phase difference between two adjacent antenna elements. The most common mode of operation for linear array is in the broadside mode, thus β generally is 0. In the case of end-fire linear array, the phase difference is

that $\beta = -kd$. In the case of smart antennas, the phase difference is that $\beta = -kd\sin\theta_0$ where θ_0 is the desired direction.

The array factor appeared in (2.2) can be expressed in a compact form by multiplying both side of (2.2) by $e^{j\psi}$ as follows

$$(AF)e^{j\cdot} = e^{j\cdot} + e^{j2\cdot} + e^{j3\cdot} + \ldots + e^{j\cdot(N-1)} + e^{jN\cdot} . \tag{2.3}$$

Subtracting (2.2) from (2.3), the array factor is reduced to

$$(AF)(e^{j\cdot} - 1) = (-1 + e^{jN\cdot}) , \tag{2.4}$$

which can be rewritten as

$$\begin{aligned} AF &= \left[\frac{e^{jN\cdot} - 1}{e^{j\cdot} - 1} \right] \\ &= e^{j[(N-1)/2]\cdot} \left[\frac{e^{j(N/2)\cdot} - e^{-j(N/2)\cdot}}{e^{j(1/2)\cdot} - e^{-j(1/2)\cdot}} \right] \\ &= e^{j[(N-1)/2]\cdot} \left[\frac{\sin\left(\frac{N}{2}\cdot\right)}{\sin\left(\frac{1}{2}\cdot\right)} \right]. \end{aligned} \tag{2.5}$$

If the reference point is at the physical center of the array then the array factor of (2.5) can reduce to

$$AF = \left[\frac{\sin\left(\frac{N}{2}\cdot\right)}{\sin\left(\frac{1}{2}\cdot\right)} \right]. \tag{2.6}$$

In the case of having a small ψ, the (2.6) can be minimized to

$$AF \cong \left[\frac{\sin\left(\frac{N}{2}\cdot\right)}{\frac{\cdot}{2}} \right]. \tag{2.7}$$

As the maximum values of (2.6) and (2.7) equal to the number of elements, N, we need to normalize the array factor as follows

$$\left(AF\right)_n = \frac{1}{N}\left[\frac{\sin\left(\frac{N}{2}\cdot\right)}{\sin\left(\frac{1}{2}\cdot\right)} \right] \tag{2.8}$$

or

$$\left(AF\right)_n \cong \left[\frac{\sin\left(\frac{N}{2}\cdot\right)}{\frac{N}{2}\cdot} \right]. \tag{2.9}$$

According to (2.9), Figure 2.4 presents the radiation pattern of linear array where the number of antennas is 4, $d = \lambda/2$ and the direction of propagation, θ, is 45°. Therefore, the phase difference among the antennas is $\beta = -kd\sin 45°$ which

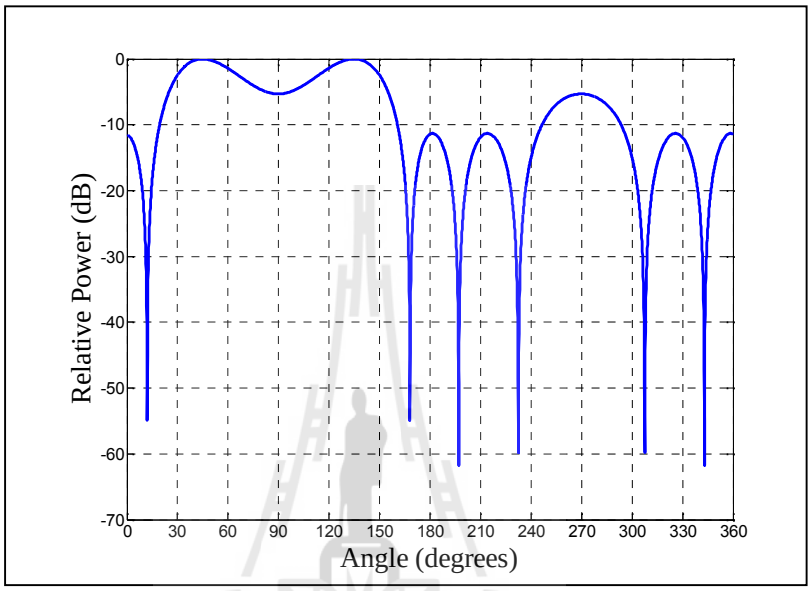
Relative Power (dB)
0
-10
-20
-30
-40
-50
-60
-70
0
30
60
90
120
150
180
210
240
270
300
330
360
Angle (degrees)

$$\cos\¥ = \hat{x}\cdot\hat{r} = \hat{x}\cdot\left(\hat{x}\sin^{-}\cos¤ + \hat{y}\sin^{-}\sin¤ + \hat{z}\cos^{-}\right) = \sin^{-}\cos¤\,, \qquad (2.10)$$

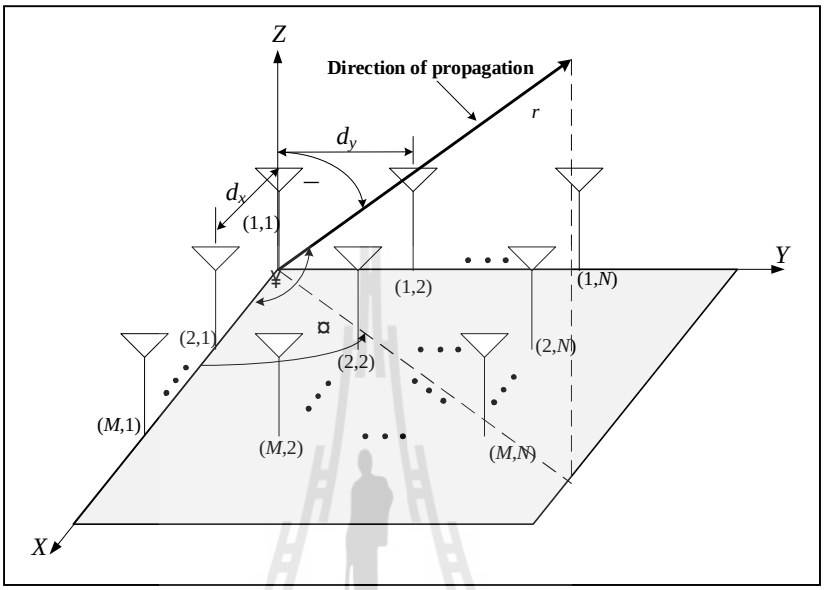

Figure 2.5 $N \times M$ rectangular planar array.

where $\hat{x}$, $\hat{y}$ and $\hat{z}$ is the unit vector in the *x*, *y* and *z* direction, respectively. The $\hat{r}$ is the unit vector in the direction of propagation, *γ* is the direction of propagation, *θ* is an angle as measured from the *z*-axis and ¤ is an angle from the *x*-axis on the *x*-*y* plan.

For this case, the array factor on the *x*-axis can be written as

$$AF_x = \sum_{m=1}^{M} I_m e^{j(m-1)(kd_x\cos\¥ + \ _x)}$$

$$= \sum_{m=1}^{M} I_m e^{j(m-1)(kd_x\sin^{-}\cos¤ + \ _x)}\,, \qquad (2.11)$$

where M is the number of antennas on the x-axis, I_{m} is the excitation coefficient of each antenna element on the x-axis as shown in Figure 2.5, d_{x} is the inter-element spacing on the x-axis, γ is the direction of propagation, k is the wave number, β_{x} is an electrical phase difference between two adjacent antennas on the x-axis, θ is an angle as measured from the z-axis and ¤ is an angle from the x-axis on the x-y plan. For this case, the array factor on the y-axis can be written as

$$AF_y = \sum_{n=1}^{N} I_n e^{j(n-1)(kd_y \sin^{-}\cos¤ + \ _y)} \tag{2.12}$$

where I_n is the excitation coefficient of each antenna element on the y-axis as shown in Figure 2.5, d_{y} is the inter-element spacing on the y-axis, k is the wave number and β_{y} is an electrical phase difference between two adjacent antennas on the y-axis. Thus, the array factor for the entire planar array can be obtained by multiplying (2.11) with (2.12) as follows.

$$AF = \sum_{n=1}^{N} I_{1n} \left[\sum_{m=1}^{M} I_{m1} e^{j(m-1)(kd_x \sin^{-}\cos¤ + \ x)} \right] e^{j(n-1)(kd_y \sin^{-}\cos¤ + \ _y)} \tag{2.13}$$

We assume that the excitation coefficient of each antenna element is equal. Thus,

$$I_{mn} = I_m I_n \tag{2.14}$$

In addition, the excitation coefficients of the entire antennas are uniform, $I_{\mathrm{mn}} = I_0$, thus (2.13) can be expressed as

$$AF = I_0 \sum_{m=1}^{M} e^{j(m-1)(kd_x \sin^{-} \cos¤ + \ x)} \sum_{n=1}^{N} e^{j(n-1)(kd_y \sin^{-} \cos¤ + \ _y)}$$

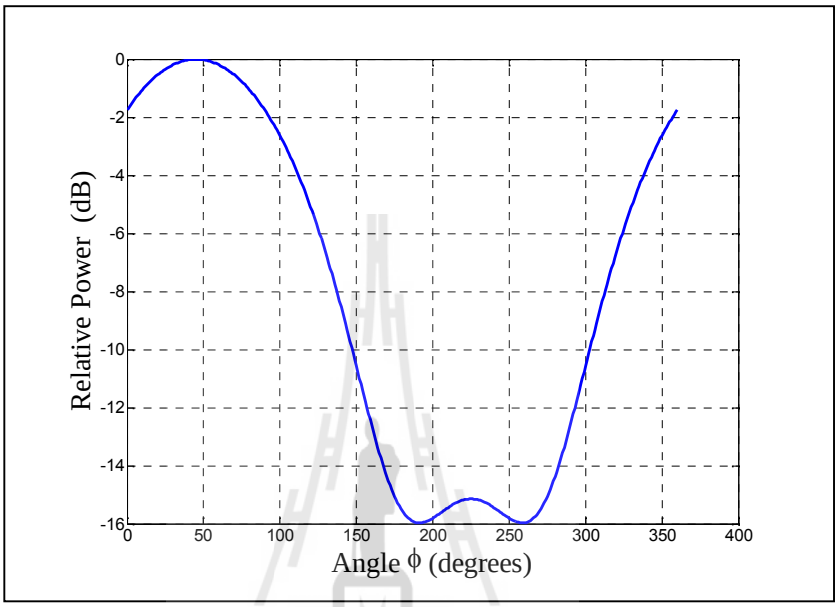

$$AF_n(\bar{}, ¤) = \left\{ \frac{1}{M} \frac{\sin\left(\frac{M}{2} \cdot \ _x\right)}{\sin\left(\frac{\cdot \ _x}{2}\right)} \right\} \left\{ \frac{1}{N} \frac{\sin\left(\frac{N}{2} \cdot \ _y\right)}{\sin\left(\frac{\cdot \ _y}{2}\right)} \right\}$$

$$\cdot \ _x = kd_x \sin^{-} \cos¤ + \ _x$$

$$\cdot_{y} = kd_{y}\sin^{-}\cos\text{¤} + \quad_{y}, \tag{2.18}$$

According to (2.16), we can simulate the radiation pattern of the 2×2 rectangular planar array as shown in Figure 2.6 where the element spacing, d_x and d_y, are both equal to $\lambda/4$. The direction of propagation as measured from the z-axis is assumed as $\theta = 90°$ and the direction of propagation as measured from the x-axis is assumed as ¤ = 45°. According to (2.17) and (2.18), the phase difference of each element is $\beta_x = kd_x\sin90°\cos45°$ and $\beta_y = -kd_y\sin90°\cos45°$. Subtracting the phase different values into the array factor (2.15), we obtain the maximum value of array factor in the direction of 45°. Therefore, the main beam can be pointed to the 45° as we can see in Figure 2.6.

2.3.3 Circular array

In circular array, the antenna elements are located in a circular ring which is shown in Figure 2.7. The N antennas are located at the radius of a with the phase angle, ¤_n, where the direction of propagation is θ. As we consider far-field conditions, the position vectors $\bar{r}$ and $\bar{r}_n$ are parallel, thus, the unit vector in the direction of propagation of each array can be calculated by

$$\text{º}_{n} = \cos\text{¤}_{n}\hat{x} + \sin\text{¤}_{n}\hat{y}. \tag{2.19}$$

The unit vector in the direction of the far-field point can be calculated by

$$\hat{r} = \sin^{-}\cos\text{¤}\,\hat{x} + \sin^{-}\sin\text{¤}\,\hat{y} + \cos^{-}\hat{z}. \tag{2.20}$$

Figure 2.7 shows that the distance $\bar{r}_n$ is less than the distance r by the scalar projection of $\hat{r}_n$. Thus,

$$r_n = r - a\hat{r}_n \cdot \hat{r}, \tag{2.21}$$

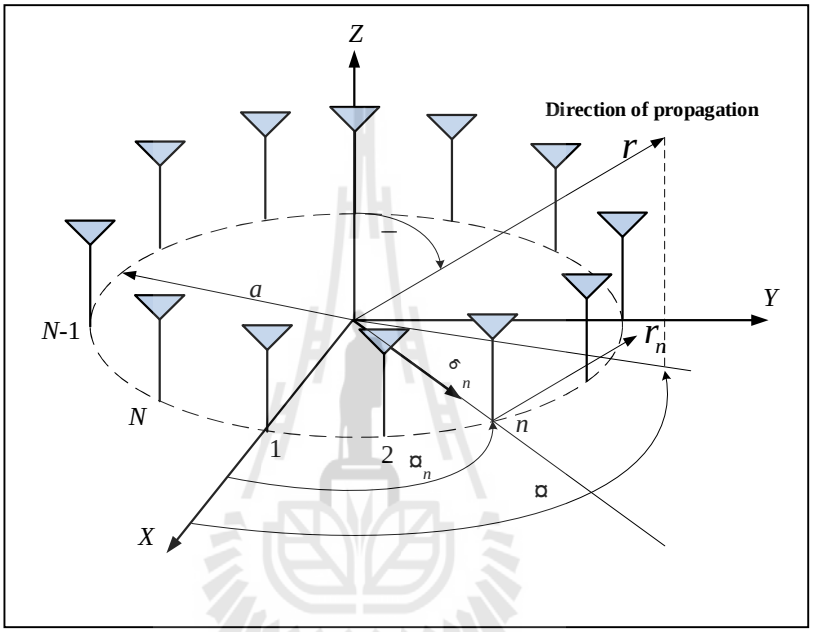

Figure 2.7 Circular array of *N*-elements.

where

$$\begin{aligned}\hat{r}_n \cdot \hat{r} &= \sin\theta\cos\phi\cos\phi_n + \sin\theta\sin\phi\sin\phi_n \\ &= \sin\theta\cos(\phi - \phi_n).\end{aligned} \tag{2.22}$$

Finally, the array factor of circular array can be calculated as follows

$$AF = \sum_{n=1}^{N} e^{-j(ka\hat{r}_n \cdot \hat{r} + \beta_n)}$$

$$= \sum_{n=1}^{N} e^{-j\left[ka\sin^{-}\cos(¤-¤_n)+¢_n\right]}$$

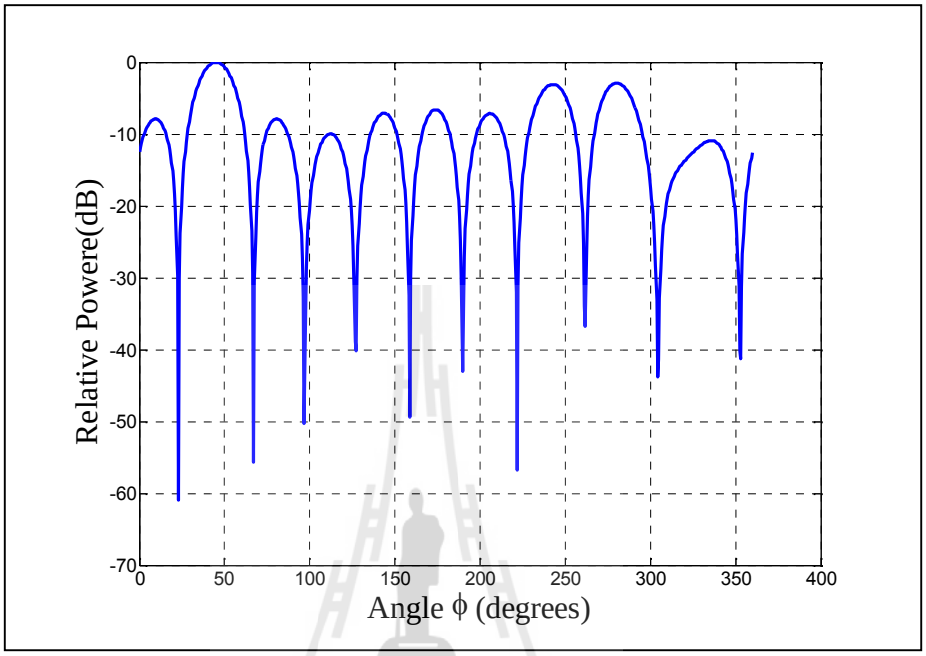

$¤_n$

$$¤_n = \frac{2®}{N}(n-1)$$

$¤_0$

$$¢_n = -ka\sin^{-}{}_0 \cos(¤_0 - ¤_n)$$

$¤_0$

$$AF = \sum_{n=1}^{N} e^{-j\{ka[\sin\theta\cos(\phi-\phi_n)-\sin\theta_0\cos(\phi_0-\phi_n)]\}} . \quad (2.25)$$

According to (2.25), we can simulate the radiation pattern of the circular array as shown in Figure 2.8 where the number of antenna elements is 10 and the radius, *a*, is λ. Also, the direction of propagation is $\theta_0 = 90°$ and $\phi_0 = 45°$. Thus, the phase difference between element is $\psi_n = 2\pi\sin 90^\circ \cos\left(45^\circ - \phi_n\right)$.

2.4 Beamforming Technique

The beamforming is the method used to create the radiation pattern of the antenna array by constructively adding the phases of the signals in the directional signal transmission or reception (Rivas M., (2010) and Gross F. (2005)). The beamforming can be used in various applications such as in mobile networks. The base station deploying beamforming can point its main beam to a desired direction and point the nulls to the interference as shown in Figure 2.9. According to this capability, beamforming has lots of advantages as follows

(i) Enhance the coverage area.

(ii) Reduce the transmitted power.

(iii) Reduce co-channel interference and multipath interference.

(iv) Provide high security.

(v) Improve system capacity.

Beamforming can be divided into two general types which are smart antennas (or conventional beamforming) and distributed beamformer (cooperative beamforming).

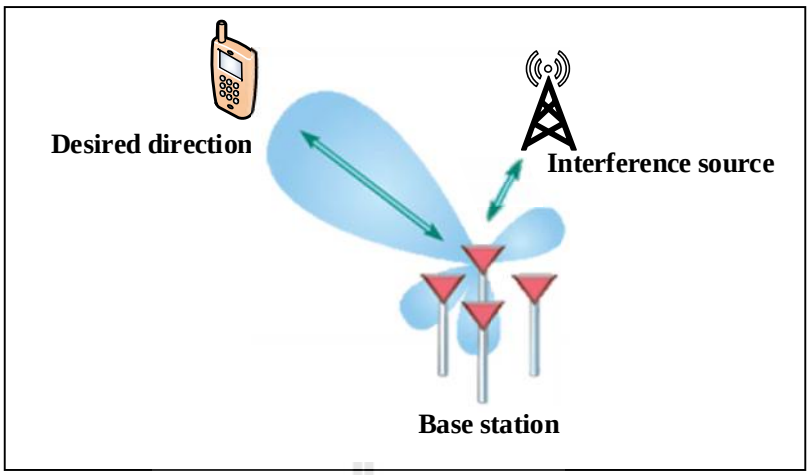

Figure 2.9 Base station in a mobile network with beamforming technique.

2.4.1 Smart antennas

The smart antennas are the systems of antenna array having smart signal processing used to calculate a beamforming algorithm (Liberti Jr. J. C., et.al. (1999)). The first smart antennas were developed in early 1980s for military communications and intelligence gathering such as radar communication. In the 1990s, smart antennas were developed for upgrading to digital radio technology in the mobile phone, indoor wireless network and satellite broadcasting.

The smart antennas consist of two major parts: array antennas and signal processing. The systems of antenna array receive/transmit the spatial signals. Then, the signal processing identifies a spatial signal signature such as the Direction of Arrival (DOA) of the signal used for calculating the beamforming vectors. The simple beamforming of two linear antenna array is shown in Figure 2.10 which can be calculated by starting the received signals as follows

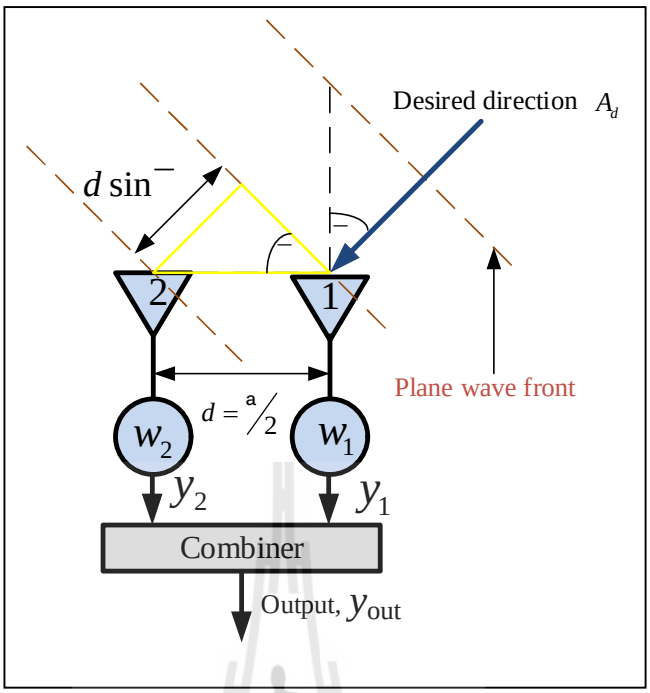

Figure 2.10 2×1 smart antenna systems.

$$y_1 = w_1 A_d e^{j(kd\sin\theta)(n-1)} = w_1 A_d \tag{2.26}$$

and

$$y_2 = w_2 A_d e^{-j(kd\sin\theta)(n-1)} = w_2 A_d e^{-j(kd\sin\theta)}, \tag{2.27}$$

where y_1 and y_2 is the received signal of antennas #1 and #2 respectively, k is the wave number, $k = 2\pi/\lambda$, θ is the direction of desired signal as measured from the z-axis, d is the distance between antenna elements and A_d is the desired signal which comes in direction of θ. Thus, the output signal, y_{out}, can be calculated by

$$y_{out} = y_1 + y_2$$

$$= w_1\left(A_d\right) + w_2\left(A_d e^{-j(kd\sin^{-})}\right)$$

$$= A_d\left(w_1 + w_2 e^{-j(kd\sin^{-})}\right), \tag{2.28}$$

We need a beamforming vector which provides the maximum beamforming gain (or combined signal). Thus, the optimum weighing coefficient for (2.28) is

$$w_1 = e^{j(0)} \tag{2.29}$$

and

$$w_2 = e^{j(kd\sin^{-})}, \tag{2.30}$$

Subtracting the weighing coefficients shown in (2.29) and (2.30) into (2.28), we obtain the maximum output signal as follows

$$y_{out} = A_d\left(e^{j(0)} + e^{-j(kd\sin^{-})}e^{j(kd\sin^{-})}\right) = 2A_d \tag{2.31}$$

This section shows that smart antennas may be employed at the mobile node in order to enhance beamforming gain. Unfortunately, the installation of multiple antenna elements on a mobile terminal is difficult due to its size and the requirement of power consumption. Therefore, a distributed beamforming has been recently proposed to handle the problem which will be discussed in next section.

2.4.2 Distributed beamforming

The distributed beamforming concept is similar to smart antennas but the position of antennas (or nodes) is not fixed. Also, it could be said that the distributed beamforming is similar to a virtual array antennas in which each node sends the same data at the same time to base station (Yao K., et.al, (1998)). The transmitting nodes have to perform the carrier phase synchronization so that the transmitted signals are constructively gained when combined at base station. Thus, the distributed beamforming requires only one antenna per node.

The average received power of the distributed beamforming can be calculated by

$$E\left[P_R\right] = 1 + \left(N - 1\right)\left(E\left[\cos ¤_n\right]\right), \tag{2.32}$$

where $E[\cdot]$ is an expectation operator, N is the number of transmitting node and $¤_n$ is the phase of received signal from the n^{th} transmitting node. The (2.32) shows that the phase synchronization is the key success for distributed beamforming networks as the phase offsets or phase errors among all transmitted signals can reduce the power of combined signal at base station.

Figure 2.11 shows the distributed beamforming networks in which the location of each transmitting node, (r_n, ψ_n) is random (Ochiai H., et.al, (2005)). The N collaborative transmitting nodes are located in (x, y) plane where n stands for node index (n = 1, …, N). The node location is uniformly distributed in a specified region. Also, node location is denoted in polar coordinate which is expressed by radius of

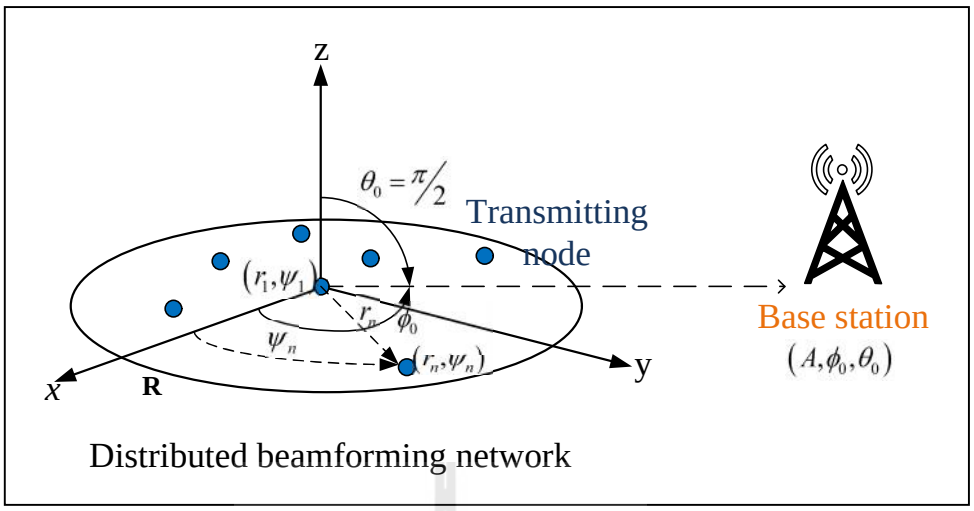

Distributed beamforming network

$r_n = \sqrt{x_n^2 + y_n^2}$ $\cdot_n = \tan^{-1}(y_n / x_n)$

$(A, ¤_0, \bar{}_0)$

$\bar{}_0 = ®/2$

$r_n \in [0, R]^N$ $\cdot_n \in [-®, ®]^N$

$d_n(¤, \bar{})$

$$d_n\left(¤,¯\right)=\sqrt{A^2+r_n^2-2r_nA\sin¯_0\cos\left(¤_0-·_n\right)}, \tag{2.33}$$

where A is distance between the center of network and base station, r_n is a position of n^{th} node in terms of radius, $·_n$ is a position of n^{th} node in terms of angle, $¯_0$ is a direction of base station as measured from the z-axis and $¤_0$ is a direction of base station as measured from the x-axis. Then, the initial phase of each transmitting node can be calculated by

$$\Psi_n=-\frac{2®}{a}d_n\left(¤_0,¯_0\right). \tag{2.34}$$

According to (2.33) and (2.34), we obtain the array factor as follows.

$$\begin{aligned}F\left(¤,¯\mid r,·\right)&=\frac{1}{N}\sum_{n=1}^{N}e^{j·_n}e^{j\frac{2®}{a}d_n\left(¤,¯\right)}\\&=\frac{1}{N}\sum_{n=1}^{N}e^{j\frac{2®}{a}\left[d_n\left(¤,¯\right)-d_n\left(¤_0,¯_0\right)\right]},\end{aligned} \tag{2.35}$$

where n is a number of node, $·_n$ is a position of n^{th} node in term of radius, d_n is distance between the n^{th} node and the base station and λ is wave length of operation frequency.

Assuming that the far-field condition when $A \gg r_n$, the (2.34) can be rewritten as

$$d_n\left(¤,¯\right)\equiv A-r_n\sin¯\cos\left(¤-·_n\right). \tag{2.36}$$

Thus, the far-field beam pattern in the case of using closed loop is approximated by

$$F\left(¤,¯ \mid r,\cdot\right) \approx \frac{1}{N}\sum_{n=1}^{N} e^{j\frac{2®}{a} r_n\left[\sin¯_0 \cos(¤_0 - \cdot_n) - \sin¯ \cos(¤ - \cdot_n)\right]}. \tag{2.37}$$

Alternatively, in the case of using open-loop reference signal, the initial phase (2.34) can be rewritten as

$$\Psi_n^{\dagger} = \frac{2®}{a} r_n \sin¯_0 \cos\left(¤_0 - \cdot_n\right). \tag{2.38}$$

Then, we obtain the array factor as

$$\begin{aligned} F^{\dagger}\left(¤,¯ \mid r,\cdot\right) &= \frac{1}{N}\sum_{n=1}^{N} e^{j\Psi_n^{\dagger}} e^{j\frac{2®}{a} d_n(¤,¯)} \\ &\approx \frac{1}{N}\sum_{n=1}^{N} e^{j\frac{2®}{a}\left[A - r_n \sin¯ \cos(¤ - \cdot_n) + r_n \sin¯_0 \cos(¤_0 - \cdot_n)\right]} \\ &= e^{j\frac{2®}{a}} A \frac{1}{N}\sum_{n=1}^{N} e^{j\frac{2®}{a} r_n\left[\sin¯_0 \cos(¤_0 - \cdot_n) - \sin¯ \cos(¤ - \cdot_n)\right]}, \end{aligned} \tag{2.39}$$

where N is the number of node, A is distance between the center of network and base station, r_n is a position of n^{th} node in terms of radius, $\cdot_n$ is a position of n^{th} node in terms of angle, $¯_0$ is a direction of base station as measured from the z-axis and $¤_0$ is a direction of base station as measured from the x-axis. Equation (2.37) and (2.39) show that the array factor of distributed beamforming resembles to the array factor of

circular array as discussed in Section 2.3.3. However, the location of each node is not fixed.

Using this assumption, the node location (r_n, ψ_n) is uniformly distributed in the radius of network R as shown in Figure 2.11. Therefore, the probability density function (pdf) of r_n and ψ_n are given by

$$f_{r_n}(r) = \frac{2r}{R^2}, \qquad 0 < r < R \tag{2.40}$$

and

$$f_{\cdot_n}(\cdot) = \frac{1}{2\pi}, \qquad -\pi < \cdot < \pi \tag{2.41}$$

As the base station is assumed at the same plane of other nodes, thus $\bar{}_0 = \pi/2$. Then, the array factor (2.39) can be rewritten as

$$\tilde{F}(\alpha \mid r, \cdot) = \frac{1}{N}\sum_{n=1}^{N} e^{j\frac{4\pi}{\lambda} r_n \sin\left(\frac{\alpha_0 - \alpha}{2}\right)\sin\left(\cdot_n - \frac{\alpha_0 + \alpha}{2}\right)}$$

$$= \frac{1}{N}\sum_{n=1}^{N} e^{j4\pi\frac{R}{\lambda}\sin\left(\frac{\alpha_0 - \alpha}{2}\right)\tilde{r}_n \sin(\tilde{\cdot}_n)}, \tag{2.42}$$

where $\tilde{r}_n = r_n/R$ and $\tilde{\cdot}_n = \cdot_n - \left((\alpha_0 + \alpha)/2\right)$. Also, the compound random variable is

$$z_n = \tilde{r}_n \sin(\tilde{\cdot}_n), \tag{2.43}$$

which has the probability density function (pdf) of

$$f_{z_n}(z) = \frac{2}{\pi}\sqrt{1-z^2}, \quad -1 \le z \le 1 \tag{2.44}$$

According to (2.42) and (2.43), we obtain the array factor as follows

$$\tilde{F}(\theta \mid z) = \frac{1}{N}\sum_{n=1}^{N} e^{j4\pi\tilde{R}\sin\left(\frac{\theta_0-\theta}{2}\right)z_n}, \tag{2.45}$$

where $\tilde{R} \approx R/\lambda$ is the radius of network which normalized by wave length and θ_0 is the direction of the base station. Finally, the far-field beam pattern can be defined as

$$\begin{aligned} P(\theta \mid z) &\approx \left|\tilde{F}(\theta \mid z)\right|^2 \\ &= \tilde{F}(\theta \mid z)\tilde{F}^*(\theta \mid z) \\ &= \frac{1}{N^2}\sum_{n=1}^{N}\sum_{l=1}^{N} e^{j4\pi\tilde{R}\sin\left(\frac{\theta_0-\theta}{2}\right)(z_n-z_l)} \\ &= \frac{1}{N} + \frac{1}{N^2}\sum_{n=1}^{N} e^{j\psi(\theta)z_n}\sum_{\substack{l=1 \\ l\neq n}}^{N} e^{-j\psi(\theta)z_l} \end{aligned} \tag{2.46}$$

where $\psi(\theta) \approx 4\pi\tilde{R}\sin\left(\frac{\theta_0-\theta}{2}\right)$.

Figure 2.12 shows the radiation pattern of the distributed beamforming with perfect phase synchronization which obtained by (2.46) where the number of transmitting node N is 16, the radius of network $\tilde{R} = 1$ and the direction of base station

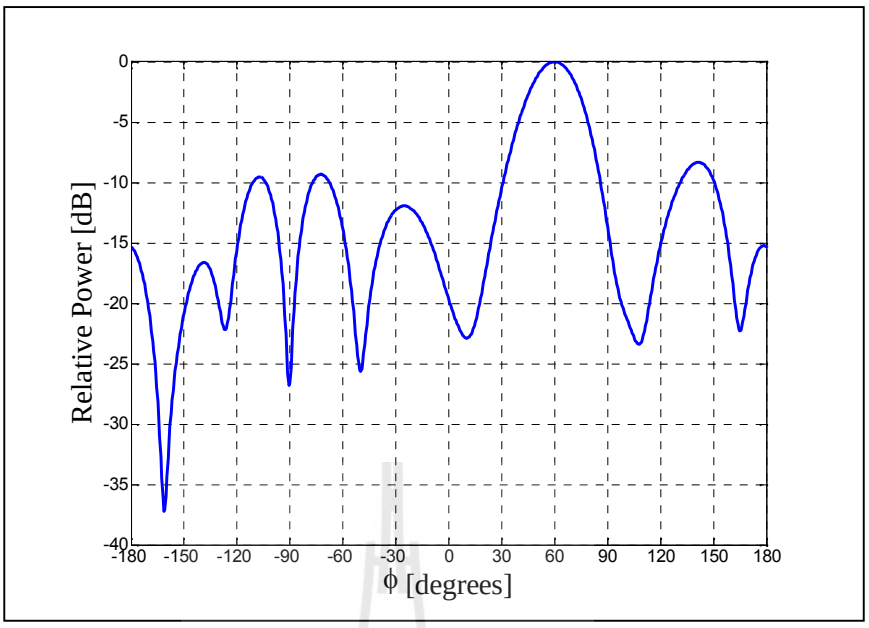

¤0

$$\hat{\Psi}_n = -\frac{2\pi}{\lambda} d_n \left(\sin\theta_0 \cos\phi_0 + \sin\theta_0 \sin\phi_0\right) + \xi_n$$

where d_n is distance between the n^{th} node and the base station and φ_n is the phase offset due to the imperfect phase synchronization. According to the phase offset is assumed as independent and identically distributed (i.i.d.) random variables. Then, from (2.35) to (2.38) and (2.45), the far-field array factor with $\theta = \theta_0 = \pi/2$ can be given by

$$\tilde{F}\left(¤ \mid z, ¨ \right) = \frac{1}{N}\sum_{n=1}^{N} e^{jz_n 4® \tilde{R} \sin\left(\frac{¤_0 - ¤}{2}\right) + ¨_n} . \tag{2.48}$$

Then, we obtain the average beam pattern as follows

$$\begin{aligned} P_{av}\left(¤\right) &= \mathrm{E}_{z,¨}\left\{P\left(¤ \mid z, ¨\right)\right\} \\ &= \frac{1}{N} + \left(1 - \frac{1}{N}\right)\left|2\frac{J_1\left(\sim\left(¤\right)\right)}{\sim\left(¤\right)}\right|^2 \left|A_¨\right|^2, \end{aligned} \tag{2.49}$$

where $\mathrm{E}_{z,¨}\left\{P\left(¤ \mid z, ¨\right)\right\}$ is the expectation of radiated power, $P\left(¤ \mid z, ¨\right)$ presented in (2.46) and £¨ is the attenuation given by phase offset, φ_n, which can be calculated by

$$£_¨ = \frac{I_1\left(\frac{1}{±_¨^2}\right)}{I_0\left(\frac{1}{±_¨^2}\right)}, \tag{2.50}$$

where $I_m(x)$ is the m^{th}-order modified Bessel function of the first kind and $±_¨^2$ is the variance of the phase noise which related to the loop Signal-to-Noise Ratio (SNR) of the Phase Lock Loop (PLL).

For the open loop case, the initial phase of n^{th} transmitting node in the case of $\theta_0 = \pi/2$ can be rewritten as follows

$$\hat{\Psi}_n^{\dagger} = \frac{2\pi}{\lambda}\left(r_n + \delta r_n\right)\cos\left(\theta_0 - \left(\phi_n + \delta\phi_n\right)\right)$$

$$= \frac{2\pi}{\lambda} r_n \cos\left(\theta_0 - \left(\phi_n + \delta\phi_n\right)\right) + \frac{2\pi}{\lambda}\delta r_n \cos\left(\theta_0 - \left(\phi_n + \delta\phi_n\right)\right), \qquad (2.51)$$

where δr_n and $\delta\psi_n$ are the random variables of estimated node location error which are assumed to be independent and identically distributed (i.i.d.), then, the far-field array factor approximation is

$$\tilde{F}^{\dagger}\left(\theta \mid r, \phi, \delta\phi, \delta r\right) = \frac{1}{N}\sum_{n=1}^{N} e^{j\Psi_n^{\dagger}} e^{j\frac{2\pi}{\lambda}d_n\left(\theta, \phi_0 = \frac{\pi}{2}\right)}$$

$$= \frac{1}{N}\sum_{n=1}^{N} e^{j\frac{2\pi}{\lambda}\left\{A - r_n\left[\cos(\theta - \phi_n) - \cos(\theta_0 - \phi_n - \delta\phi_n)\right] + \delta r_n \cos(\theta_0 - \phi_n - \delta\phi)\right\}}$$

$$= \frac{1}{N}\sum_{n=1}^{N} e^{j\left\{\frac{2\pi}{\lambda}A + \frac{4\pi}{\lambda}r_n\left[\sin\left(\phi_n - \frac{\theta_0 + \theta - \delta\phi}{2}\right)\sin\left(\frac{\theta_0 - \theta - \delta\phi}{2}\right)\right] + \frac{2\pi}{\lambda}\delta r_n \cos\left(\phi_n - (\theta_0 - \delta\phi)\right)\right\}}. \qquad (2.52)$$

Let $\hat{\phi}_n = \phi_n - \left(\theta + \theta_0 - \delta\phi\right)/2$. Thus, the right-hand side of (2.52) is given by

$$\tilde{F}^{\dagger}\left(\theta \mid r, \phi, \delta\phi, \delta r\right) = \frac{1}{N}\sum_{n=1}^{N} e^{j\left\{\frac{2\pi}{\lambda}A - \frac{4\pi}{\lambda}r_n \sin\tilde{\phi}_n \sin\left(\frac{\theta - \theta_0 - \delta\phi}{2}\right) + \frac{2\pi}{\lambda}\delta r_n \cos\left(\tilde{\phi}_n + \frac{\theta - \theta_0 + \delta\phi}{2}\right)\right\}}$$

$$= e^{\frac{2\pi}{\lambda}A}\frac{1}{N}\sum_{n=1}^{N} e^{-j\frac{4\pi}{\lambda}r_n \sin\tilde{\phi}_n \sin\left(\frac{\theta - \theta_0 - \delta\phi_n}{2}\right) + j\frac{2\pi}{\lambda}\delta r_n \cos\left(\tilde{\phi}_n + \frac{\theta - \theta_0 + \delta\phi_n}{2}\right)}. \qquad (2.53)$$

According to (2.39) and (2.53), we obtain the beam pattern as follows

$$P(\varphi \mid z, v, \phi) \approx \left|\tilde{F}(\varphi \mid z)\right|^2$$

$$= \frac{1}{N} + \frac{1}{N^2}\sum_{n=1}^{N}\sum_{\substack{l=1 \\ l\neq n}}^{N} e^{-j4\pi\tilde{R}\left\{z_n \sin\left(\frac{\varphi-\varphi_0-\phi_n}{2}\right)-z_l \sin\left(\frac{\varphi-\varphi_0-\phi_l}{2}\right)\right\}} e^{j\frac{2\pi}{\lambda}(v_n - v_l)}, \qquad (2.54)$$

where

$$z_n \approx \frac{r_n}{R}\sin\tilde{\theta}_n$$

$$= \tilde{r}_n \sin\left(\theta_n + \frac{\phi_n}{2} - \frac{\varphi+\varphi_0}{2}\right), \qquad (2.55)$$

and

$$v_n \approx \phi r_n \cos\left(\tilde{\theta}_n + \frac{\varphi+\phi_n}{2}\right)$$

$$= \phi r_n \cos\left(\theta_n + \phi_n - \varphi_0\right). \qquad (2.56)$$

According that the location of each node is uniformly distributed, the $\tilde{\theta}_n$ can be seen as a uniformly distributed random variable, thus the pdf of z_n, (2.55), corresponds to (2.44). The v is uniformly distributed over $[-\pi, \pi]$ and δr_n is uniformly distributed over $[-r_{max}, r_{max}]$. Therefore, the pdf of v_n can be given by

$$f_{v_n} = \frac{1}{\pi r_{\max}}\left[\ln\left(1+\sqrt{1-\left(\frac{v}{r_{\max}}\right)^2}\right) - \ln\frac{|v|}{r_{\max}}\right], \quad |v| \le r_{\max} \qquad (2.57)$$

According to (2.44), (2.53) and (2.57), the average beam pattern can be written as

$$P_{av}(¤) = \frac{1}{N} + \left(1 - \frac{1}{N}\right)\left|£_{.}(¤)\right|^2 \left|£_r\right|^2, \tag{2.58}$$

where $£_{.}(¤)$ is the location error in terms of phase which can be calculated by

$$£_{.}(¤) \approx \mathrm{E}_{z_n, ¢\cdot_n}\left\{ e^{j4®\tilde{R}z_n \sin\left(\frac{¤_0 + ¢\cdot_n - ¤}{2}\right)} \right\}$$

$$= \mathrm{E}_{¢\cdot_n}\left\{ \frac{J_1\left(4®\tilde{R}\sin\frac{¤ - ¢\cdot_n}{2}\right)}{2®\tilde{R}\sin\frac{¤ - ¢\cdot_n}{2}} \right\}, \tag{2.59}$$

According to $\delta\psi_n$ is uniformly distributed over $[-\psi_{max}, \psi_{max}]$ and $\sin(¤ + ¢\cdot_n) \approx ¤ + ¢\cdot_n$, the (2.59) can be rewritten as

$$£_{.}(¤) \approx \frac{1}{2}\left(1 - \frac{¤}{\cdot_{\max}}\right){}_1F_2\left(\frac{1}{2};\frac{3}{2},2;-\left(®\tilde{R}(¤ - \cdot_{\max})\right)^2\right)$$

$$+ \frac{1}{2}\left(1 + \frac{¤}{\cdot_{\max}}\right){}_1F_2\left(\frac{1}{2};\frac{3}{2},2;-\left(®\tilde{R}(¤ + \cdot_{\max})\right)^2\right) \tag{2.60}$$

where ${}_pF_q(x)$ is the generalized hypergeometric function where p is a parameter of type 1 and q is parameter of type 2 of a hypergeometric serie.

If no loss generality, $¤_0 = 0$, was assumed, the (2.60) can be rewritten as follows

$$£_{.}(¤ = 0) = {}_1F_2\left(\frac{1}{2};\frac{3}{2},2;-\left(®\frac{R\cdot_{\max}}{a}\right)^2\right). \tag{2.61}$$

From (2.58), $£_r$ is the location error in terms of radius which can be calculated by

$$£_r \approx E_{v_n}\left\{e^{j\frac{2®}{a}v_n}\right\}$$

$$= \frac{2}{®}\int_0^1 \cos\left(\frac{2®}{a}r_{\max}t\right)\ln\frac{1+\sqrt{1-t^2}}{t}dt$$

$$= {}_1F_2\left(\frac{1}{2};1,\frac{3}{2};-\left(®\frac{r_{\max}}{a}\right)^2\right), \qquad (2.62)$$

Figure 2.13 shows the average beam pattern which affected by the estimated radius error, δr_n, obtained using (2.58) and (2.62). For this case, the system is assumed to have an errors free in phase estimation while estimation error in network having radius r_n is assumed as $r_{\max}/a = 0.1$, $r_{\max}/a = 0.5$ and $r_{\max}/a = 1.0$. The obtained results show that the main beam's gain is extremely degraded when error in radius estimation is occurred. The main beam's gain is degraded by 6%, 81% and 98% when the estimation error in network radius is $r_{\max}/a = 0.1$, $r_{\max}/a = 0.5$ and $r_{\max}/a = 1.0$ respectively. This is how to calculate the percentage degradation. For example in case of having $r_{\max}/a = 0.5$, the ratio of main beam is approximately 0.19 or 19%. Thus, the degradation of main beam's gain is 100-19 = 81% or 0.8.

Furthermore, some examples showing an effect of estimation error in phase are shown in Figure 2.14. For this case, the estimation of nodes location in terms of radius r_n is assumed to be perfect. Also, the estimation error in phase $\delta\psi_n$ is assumed as $R\cdot_{\max}/a = 0.1$, $R\cdot_{\max}/a = 0.5$ and $R\cdot_{\max}/a = 1.0$. The obtained

results show that the directions of obtained main beams deviate from the direction of destination

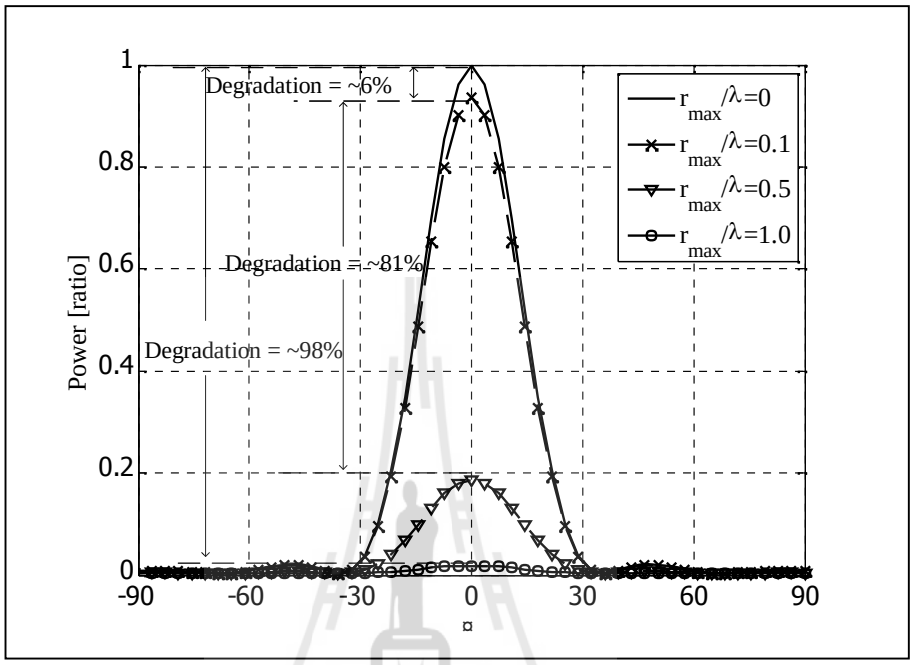

Figure 2.13 Average beam pattern with imperfection in network radius estimation, r_n.

($¤_0$ = 0°). The deviated main beams are approximately at 3°, 15° and 30°. Thus, the main beam's gain is degraded by 2%, 48% and 96% respectively comparing to the optimum beamforming. This is how to calculate the percentage degradation. For example in case of having $R \cdot_{\max} / ª = 0.1$, the ratio of main beam is approximately 0.02 or 2%. Note that the maximum normalized power of main beam is denoted as 1.0 or 100%. For the case of $R \cdot_{\max} / ª = 0.5$, the ratio of main beam in direction of destination is approximately 0.52 or 52%. Thus, the degradation of main beam's gain is 100-52 = 48% or 0.48. Regarding these simulation results, we can conclude that the

imperfection in network radius estimation degrades main beam's gain while the imperfection of phase estimation deviates the direction of main beam.

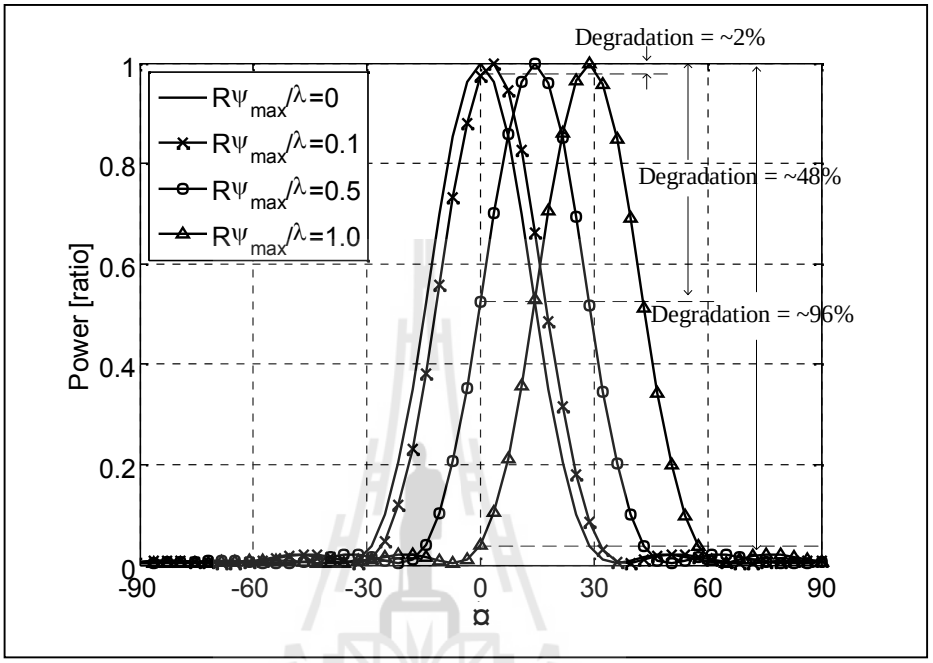

Figure 2.14 Average beam pattern with imperfection in phase estimation, ψ_n.

For the case when both of estimated radius and phase are imperfect. Figure 2.15 shows the contour plot of degradation of main beam's gain when the imperfection of estimated radius $r_{\max}/a$ and estimated phase $R\cdot_{\max}/a$ is assumed. This figure is obtained using (2.58), (2.61) and (2.62). From the figure, we can allow the imperfection of estimated radius and phase not lower than 0.2 and 0.4 in order to limit the degradation within half-power beam width.

The results in this section present that the estimated node location error or phase synchronization error can degrade the beamforming gain. Therefore, phase

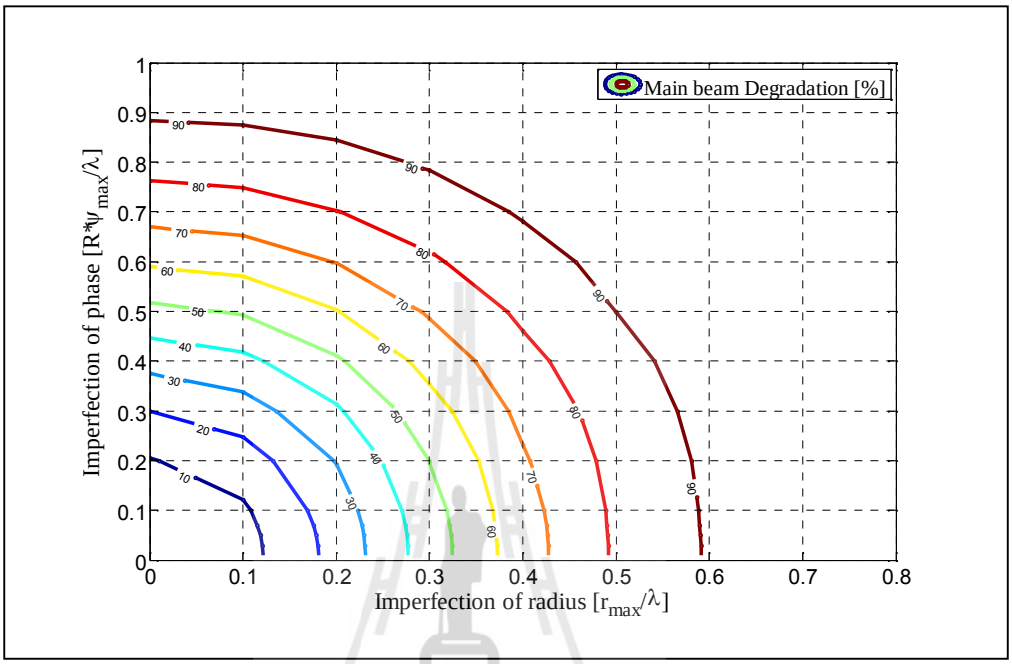
Main beam Degradation [%]
Imperfection of phase [R*ψmax/λ]
Imperfection of radius [rmax/λ]
0
0.1
0.2
0.3
0.4
0.5
0.6
0.7
0.8
0.9
1
90
80
70
60
50
40
30
20
10

capacity and reduce the transmitted power. The beamforming can be divided into two general types which are smart antennas and distributed beamforming. However, the distributed beamforming is more interesting as it requires only one individual antenna element at a transmitting node to perform beamforming. Thus, the distributed beamforming is suitable for a mobile node or terminal. In the distributed beamforming networks, each transmitting node sends the same data at the same time to base station. The transmitting nodes have to perform the carrier phase synchronization so that the transmitted signals are constructively gained when combined at base station. Otherwise, the phase offsets or phase errors among all transmitted signals would reduce the power of combined signal at base station. Section 2.4.2 presents the performance of distributed beamforming with imperfect phase synchronization. The results show that the main beam's gain is extremely degraded when error in radius estimation is occurred. The directions of obtained main beam deviate from the direction of destination ($¤_0 = 0°$) when the error in phase estimation is occurred. Therefore, phase synchronization is the key success for distributed beamforming networks. The major phase synchronization techniques will be discussed in next chapter.

CHAPTER III

PHASE SYNCHRONIZATION FOR DISTRIBUTED BEAMFORMING

3.1 Introduction

As phase synchronization is the key success for distributed beamforming networks, lots of phase synchronization techniques have been proposed so far. These techniques can be divided into two general types which are closed loop and open loop synchronization techniques (Mudumbai R., et,al., (2009)). The closed-loop technique needs feedback signals from base station to adjust phase offsets among the transmitting nodes. The open loop technique needs the interaction among nodes with only a minimal feedback signaling from base station. The base station may simply transmit an unmodulated sinusoidal beacon to the transmitting nodes. Then, the transmitting nodes use the received beacon signal to achieve an appropriate phase compensation for beam formation. Figure 3.1 demonstrates a route map of this chapter. Section 3.1 is an introduction of this chapter which presents the categories of synchronization techniques. A closed-loop phase synchronization called one-bit feedback technique is presented in the Sections 3.2. The open loop phase synchronization called master-slave and round-trip techniques are presented in Sections 3.3 and 3.4, respectively. The section 3.5 presents a zero-feedback phase synchronization technique which does not require any feedback signal from base station. Finally, Section 3.6 points out the advantages and disadvantages of the mentioned phase synchronization techniques. Note that some symbols appeared in the

Sections 3.2 to 3.4 are changed from the literatures for the sake of continuation for this thesis.

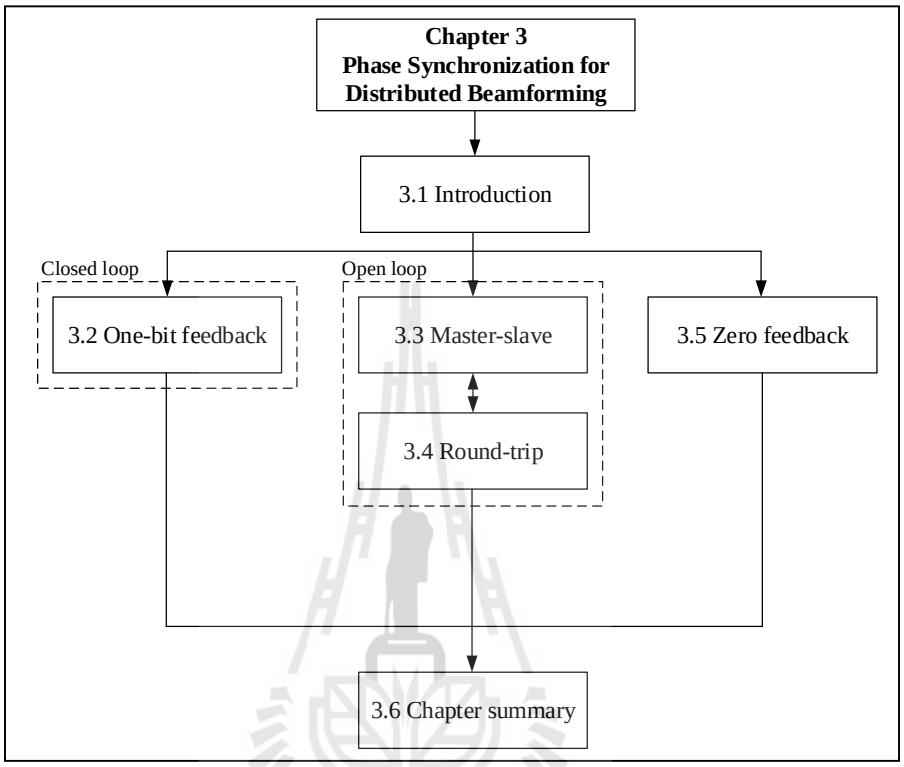

Figure 3.1 Route map of organization in Chapter III.

3.2 One-Bit Feedback Phase Synchronization

A one-bit feedback is one of the best techniques for closed-loop phase synchronization (Mudumbai R., et.al, (2005); Mudumbai R., (2010) and Rahman M. M, at.al, (2012)).The one-bit feedback technique can be considered as a distributed version of a stochastic approximation algorithm. Figure 3.2 shows a configuration of distributed nodes having a number of transmitting nodes employing the one-bit feedback phase synchronization technique. For this technique, each node transmits the

same signal with individual random phase to base station. The transmitting signal can be written as

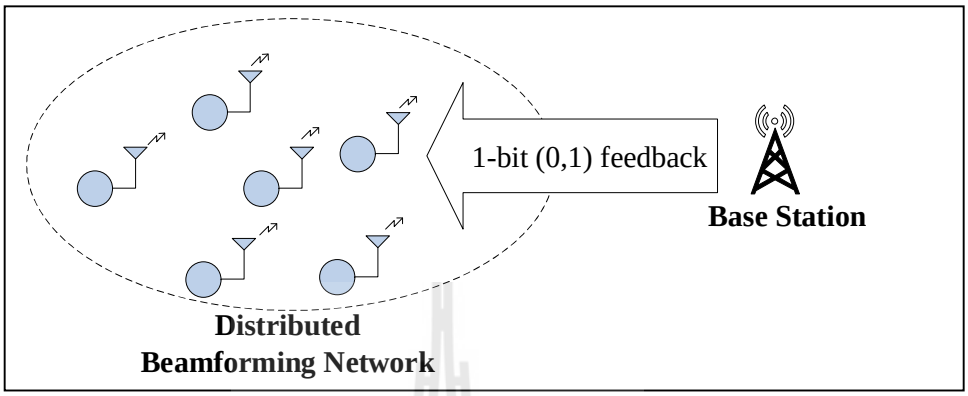

Figure 3.2. Configuration of distributed nodes employing the one-bit feedback phase synchronization technique (Mudumbai R., (2010)).

$$s_n(t) = Ax(t)e^{j(\mu_c t + \theta_n)} \tag{3.1}$$

where $\mu_c = 2\pi f_c$ is a carrier frequency, A is carrier amplitude normalized to unity, A = 1, for all transmitting nodes, $x(t)$ is the data message and θ_n is the initial phase of n^{th} transmitting node. Then, the received signal at the base station is

$$Y = x(t)\sum_{n=1}^{N} \alpha_n A e^{j(\mu t + \theta_n + \varphi_n + \gamma_n)} \tag{3.2}$$

where N is the number of transmitting nodes, α_n is the attenuation in channel between n^{th} node and base station where $\alpha_n \geq 0$, γ_n is an unknown phase offsets from different local oscillators and φ_n is the phase offset affected by the channel. According to (3.2),

the beamforming gain depends on the phase alignment of $\bar{}_n + ¥_n + ¨_n$. Thus, the objective of this technique is to align the phase of all transmitting nodes using one-bit feedback signal. The received signal at i^{th} retransmission can be written as

$$Y_i = x(t)\sum_{n=1}^{N} \sim_n A e^{j(\mu_c t + \Phi_n)} e^{j¢_{i,n}} \tag{3.3}$$

where $\Phi_n = \bar{}_n + ¥_n + ¨_n$ is the phase at the receiver corresponding to the signal from n^{th} transmitting node and $¢_{n,i}$ is the random phase perturbation for an appropriate phase compensation of n^{th} transmitting node and i^{th} retransmission.

After the base station receives the combined signal, Y_1, for the 1st time (n = 1) as shown in (3.3), the base station records the received SNR of Y_1. Then, all transmitting nodes retransmit signal Y_2 with a new random weighting coefficient, $¢_{n,i+1}$. After the SNR of the received signal is estimated at base station, one bit (0 or 1) is fed back to all transmitting nodes. The bit "0" means that SNR is worse than before so that each node has to randomly adjust their phases again. While bit "1" means that SNR is better so that all nodes have to update their latest phase adjustment. Otherwise all nodes do this closed-loop procedure again in order to update the best phase adjustment. Thus, the best known phases at the transmitting nodes are updated as follows

$$\_{}_{n,i+1} = \begin{cases} \bar{}_{n,i} + ¢_{n,i}, & Y_i > Y\_best_i \\ \_{}_{n,i}, & \text{otherwise} \end{cases} \tag{3.4}$$

where Y_best_i is the highest indicated signal strength which can be denoted by

$$Y\_best_i = \max_{n<i} Y_n \tag{3.5}$$

Simultaneously, the base station also updates its record of the highest received signal strength as follows

$$Y\_best_{i+1} = \max_{n<i} \left(Y\_best_i, Y_i \right) \tag{3.6}$$

Therefore, we can summarize the basic concept of the one-bit feedback technique for one iteration as follows.

(i) Each transmitting node adjusts its carrier phase randomly.

(ii) All transmitting nodes simultaneously transmit their signals to the base station as a distributed beamformer.

(iii) Base station estimates the SNR of the received signal.

(iv) Base station broadcasts one bit back to the transmitting nodes indicating whether its SNR is better or worse than before so that the transmitting nodes can properly adjust their phases. If it is better, all nodes keep their latest phase adjustments, otherwise all transmitting nodes undo their latest phase adjustments and retransmit signal with a new random weighting coefficient.

Figure 3.3 shows the convergence behavior of the phase angles in a simulation of the 1-bit feedback algorithm with 10 transmitting nodes (Mudumbai R., (2010)). As we can see, the 500-iteration provides the phase of each nodes within 45° to 60°. That means the phase offset among the transmitting nodes is 0° to 15° which provides the beamforming gain at 97% of maximum value. The beamforming gain can be calculated utilizing the (2.32) as $E\left[P_R\right] = 1 + \left(N-1\right)\left(E\left[\cos ¤_n\right]\right)$ where $¤_n$ is the phase

$¤_n = 0^\circ$

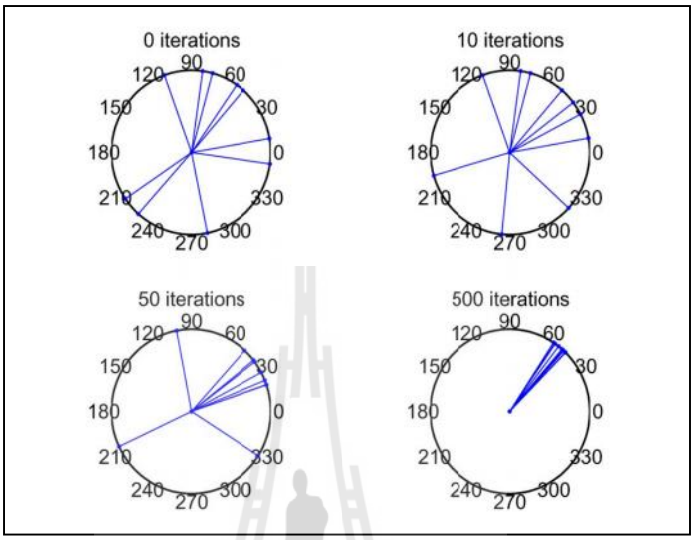

$$h_i(y) = \pm_{\Re}[i]\, l\left(\frac{y(1-x_i)}{\pm_{\Re}[i]}\right)$$

$\pm_{\Re}[i]$

$$\pm^2_{\Re}[i] = \frac{1}{2N^2}\sum_{n=1}^{N} \sim^2_n \left(1 - x_i^2 - °_i E_{y,i}\left[\cos\left(2¤_n[i]\right)\right]\right)$$

where α_n is the attenuation by channel, $x_i = E\left[\cos\left(¢_{n,i}[i]\right)\right]$ and $°_i = x_i^2 - E\left[\cos\left(2¢_{n,i}[i]\right)\right]$. The $l\left(y\left(1-x_i\right)/±_{ℜ}[i]\right)$ in (3.7) can be calculated as follows.

$$l(x) = \frac{1}{\sqrt{2®}} e^{-\frac{x^2}{2}} - xQ(x) \tag{3.9}$$

where $Q(x)$ denote the complementary comparative distribution function of a standard Gaussian random variable which can be calculated by

$$Q(x) = \int_x^{\infty} \frac{1}{\sqrt{2®}} e^{-\frac{t^2}{2}} dt \tag{3.10}$$

Figure 3.4 (a) shows the beamforming gain $y[i]$ with a several number of iteration, i, which obtained using (3.7) and Monte Carlo simulation where N = 10 transmitting nodes and the phase perturbation, $¢_{n,k}$, is distributed over the range from -31.6° to 31.6 °. Note that the dot line denotes the standard deviation of $\left[Y\_best_i\right]/N$ which converges to zero as N increases. The results present that the one-bit feedback technique requires at least 100 iterations in order to achieve 90% guarantee of perfect or maximum beamforming gain. Figure 3.4 (b) shows the beamforming gain $y[i]$ where N = 100 transmitting nodes and the phase perturbation, $¢_{n,i}$ is distributed over -10° to 10°. The simulated results present that the one-bit feedback technique requires at least 1,000 iterations in order to achieve 90% guarantee of perfect or maximum beamforming gain. In addition, the system requires at least 10,000 iteration when the

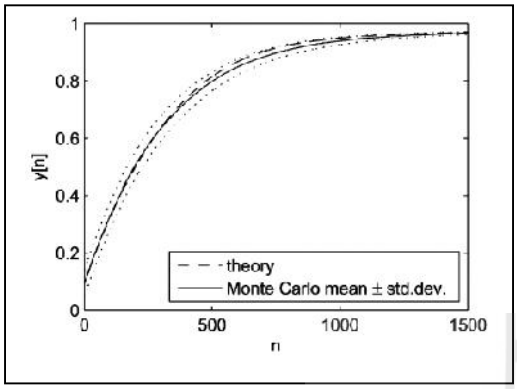

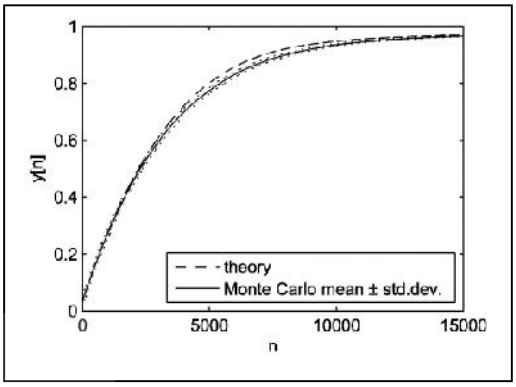

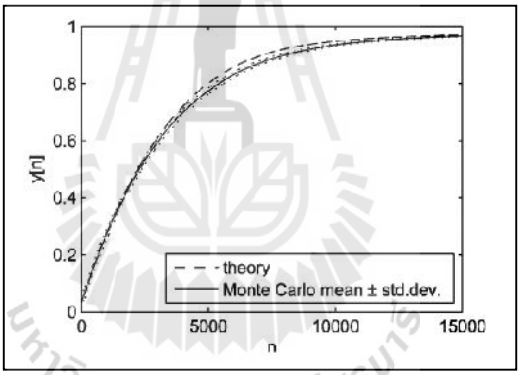

may be unreliable as the communication channel between base station and nodes is usually unstable.

In order to overcome the mentioned problems, two open-loop phase synchronization techniques have been proposed to reduce interaction between base station and nodes: master-slave and time-slot round-trip techniques. The master-slave open-loop phase synchronization technique is presented in the Section 3.3 and the time-slot round-trip open-loop phase synchronization technique is presented in the Section 3.4.

3.3 Master-Slave Phase Synchronization

Figure 3.5 shows the configuration of nodes employing a master-slave phase synchronization technique. A node in the networks is selected as a master node while all remaining nodes are assigned as slave nodes. The phase synchronization is achieved by sending the reference signals between master and slave nodes (Mudumbai R., (2007)). The algorithm of the master-slave technique can be written as follows.

Step 1: The master node has a local oscillator which generates a sinusoid signal to all slave nodes as shown in Figure 3.6. The transmitted sinusoid signal can be written as follows

$$c_0(t) = \Re\left(\tilde{c}_0(t)\right) \tag{3.11}$$

where $\tilde{c}_0(t) = e^{j(\mu_c t + \¥_0)}$, $\mu_c = 2® f_c$ and γ_0 is the (reference) phase of master node. The authors simply sets the constant γ_0 to zero for simplicity. They have also assumed that

the local communication channel between master and slave node has a large SNR and ignored a receiver noise in the channel.

Step 2: The n^{th} slave node receives the signal transmitted by master node as

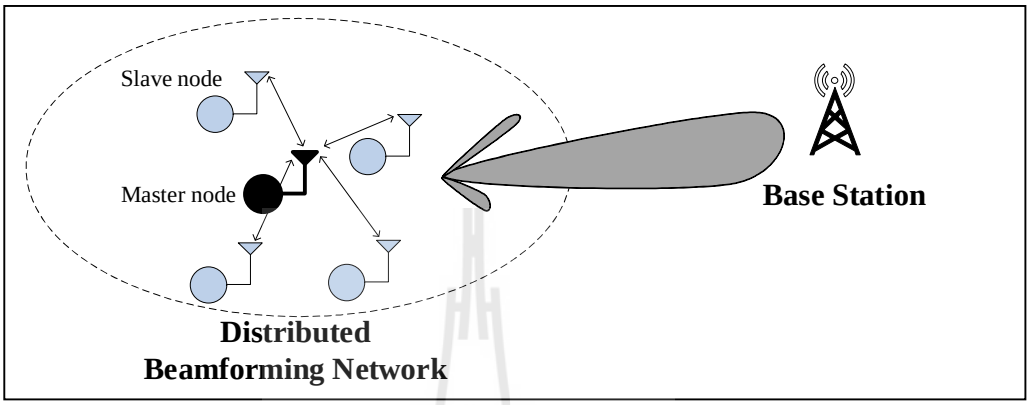

Figure 3.5 Configuration of distributed nodes employing a master-slave phase synchronization technique.

$$c_{n,0}(t) = \Re\left(\tilde{c}_{n,o}(t)\right)$$
$$= \Re\left(A_{n,0}e^{j(\mu_c t+¥_0-¥_n)}\right) \quad (3.12)$$

where γ_n is the phase offset between the master and n^{th} slave node. $A_{n,0}$ is the amplitude of the received signal form n^{th} slave node which was set to be unity for simplicity. The n^{th} slave node uses the signal (3.12) as an input to a second-order phase locked-loop. Thus, the steady-state Voltage-Controlled Oscillator (VCO) output can be used as a carrier signal consistent across all nodes as presented in Figure 3.6. This signal provides the information of phase offset between the master and n^{th} slave node, γ_n.

Step 3: The n^{th} slave node transmits the (uncompensated) VCO signal (3.12) back to the master node. The summary of the forward and reverse master-slave channels imply that the signal at master node can be written as

$$c_{i,1}(t) = A_{i,1}\Re\left(A_{i,0}e^{j(\mu_c t + \varphi_0 - 2\varphi_i)}\right) \tag{3.13}$$

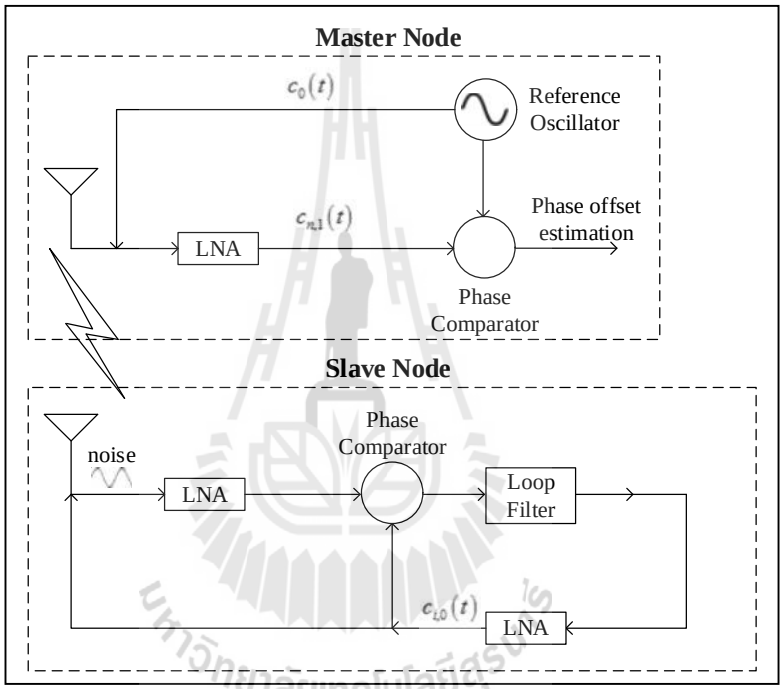

Figure 3.6 Round-trip phase calibration for master-slave technique (Mudumbai R., (2007)).

where $A_{n,1}$ is the received signal amplitude at the master node, $A_{n,1}$ was set to be unity for simplicity.

Step 4: The master node estimates the phase difference between the received signal from slave nodes (3.13) and the transmitting sinusoid signal (3.11) as

$$\Delta\text{¤}_n = \left(2\text{¥}_n \bmod 2\text{®}\right) \tag{3.14}$$

where mod means the modulo operation. Thus, the estimated value of the offset, γ_n, can be written as

$$\text{¥}_n = \frac{\Delta\text{¤}_n}{2} \tag{3.15}$$

Step 5: After the offset, γ_n, is estimated, the master node transmits this information back to all slave nodes. Then, the n^{th} slave node has calibrated carrier signal, $c_n(t)$, which uses to perform channel estimation and beamforming as

$$\begin{aligned} c_n(t) &= \Re\left(\tilde{c}_n(t)\right) \\ &= \Re\left(\tilde{c}_{n,0}(t)e^{j\text{¥}_n}\right) \\ &= e^{j\left(\mu_c t+\text{¤}_n^e\right)} \end{aligned} \tag{3.16}$$

where ¤_n^e is the estimation error in the phase calibration which obtained by the (3.12) and (3.13), $\text{¤}_n^e = \text{¥}_n - \text{¥}_n$.

Step 6: In order for the transmitting nodes are able to beam towards the base station, the information about the direction of the base station is required. Using channel reciprocity allows the network to achieve this information. Thus, the base station transmits an unmodulated carrier signal as

$$g(t) = \Re\left(\tilde{g}(t)\right) = \Re\left(e^{j(\mu_c t+\text{¤}_0)}\right) \tag{3.17}$$

where $\mu_c = 2\pi f_c$ and ϕ_n is phase of unmodulated carrier signal which is just a constant scaling term and adds no relative phase errors between sensors.

Step 7: Each transmitting node independently demodulates its received signal appeared in (3.17) using $c_n(t)$ which obtained by (3.16) to get an estimated $\hat{h}_n$ of its own complex channel gain as

$$\hat{h}_n = h_n e^{j\left(-\phi_n^e + \phi_n^h\right)} \tag{3.18}$$

where ϕ_n^h is an effective phase noise.

Then, the transmitting nodes use the synchronized carrier signal (3.16) and the channel estimate (3.18) to modulate the transmitting signal for beamforming. The slave nodes obtain their carrier signal from the VCO that is synchronized to the reference signal from the master node. However, it is not possible for the slave nodes to receive a synchronization signal from the master node while they are transmitting. Therefore, the VCOs of the slave nodes need to operate in an open-loop mode as shown in Figure 3.7. In the open-loop operation, the slave's carrier signals obtained from the VCO undergoes uncompensated a phase drift because of internal oscillator noise and overtime. Thus, the different slave carriers drift out of phase. This motivates the time-division duplex mode as shown in Figure 3.8, where the master node periodically transmits a reference carrier signal to resynchronize the slave carriers in order to keep the total phase error bounded. The noisy carrier signal used by the n^{th} slave node for modulation can be written as

$$c_n^o(t) = \Re\left(\tilde{c}_n^o(t)\right)$$

$$= \Re\left(\tilde{c}_n(t)e^{j\phi_n^d(t)}\right)$$

$$= \Re\left(e^{j\left(\mu_c t+\phi_n^e+\phi_n^d(t)\right)}\right) \quad (3.19)$$

where $\phi_n^d(t)$ is the phase drift of n^{th} slave which occurs from the uncompensated VCO. Figure 3.9 shows the simulation of oscillator phase drift where N_p is the phase noise

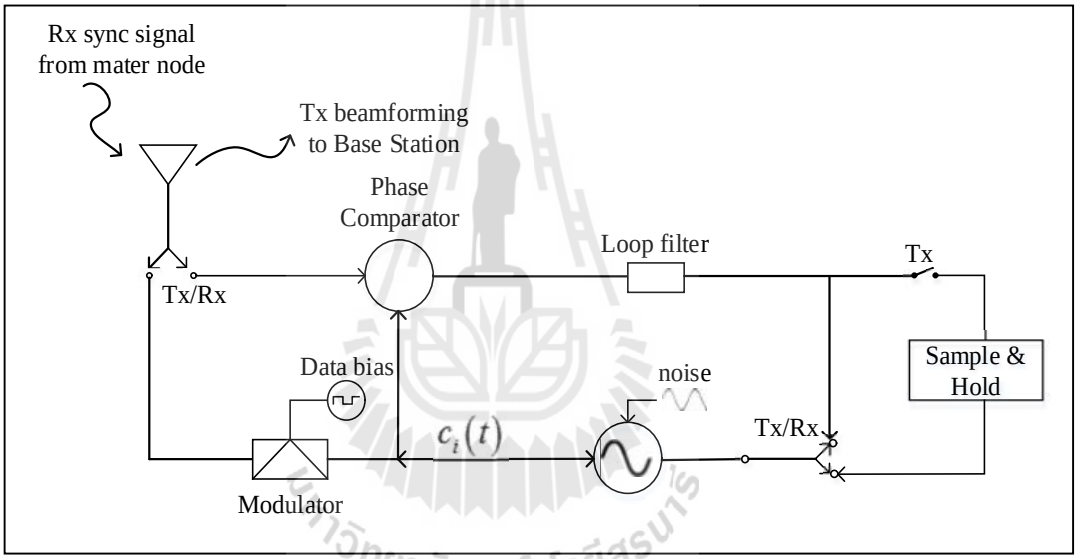

Figure 3.7 Schematic of a slave node for master-slave technique (Mudumbai R., (2007)).

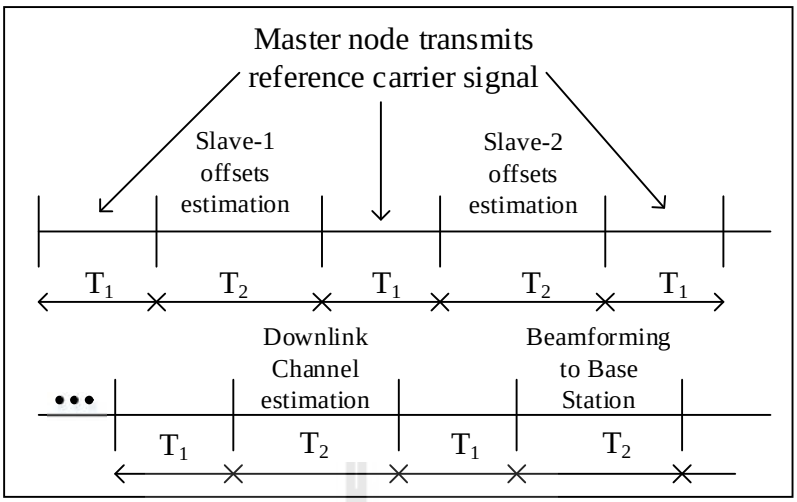
Master node transmits
reference carrier signal
Slave-1
offsets
estimation
Slave-2
offsets
estimation
T1
T2
T1
T2
T1
Downlink
Channel
estimation
Beamforming
to Base
Station
T1
T2
T1
T2

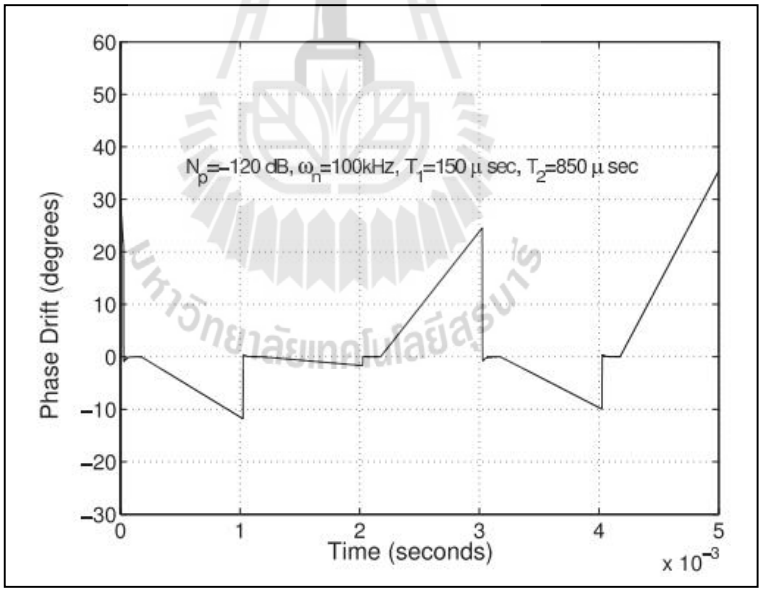
Np=-120 dB, ωn=100kHz, T1=150 μ sec, T2=850 μ sec
Phase Drift (degrees)
Time (seconds)
x 10-3
60
50
40
30
20
10
0
-10
-20
-30
0
1
2
3
4
5

power, T_1 and T_2 are time-slot duration as shown in Figure 3.8 and ω_n is the natural frequency. The result shows that the phase drift can be 35° at the time of 5×10^{-3} seconds. This parameter can degrade the beamforming gain.

Step 8: After modulation by carrier signal (3.19), n^{th} slave node applies a complex amplification (3.18) to compensate the channel and transmits the fallowing signal

$$\begin{aligned} s_n(t) &= \Re\left(\tilde{s}_n(t)\right) \\ &= \Re\left(\hat{h}_n^* m(t)\tilde{c}_n(t)\right) \end{aligned} \tag{3.20}$$

Then, the received signal at the base station is given by

$$\begin{aligned} r(t) &= \Re\left(\sum_{n=1}^{N} h_n \tilde{s}_n(t) + n(t)\right) \\ &= \Re\left(m(t)\sum_{n=1}^{N} h_n \hat{h}_n^* \tilde{c}_n(t)\right) \\ &= \Re\left(m(t)\sum_{n=1}^{N} |h_n|^2 e^{j\left(\mu_c t - \¤_n^h + 2\¤_n^e + \¤_n^d(t)\right)}\right) \end{aligned} \tag{3.21}$$

where h_n is the complex channel gain, N is the number of transmitting nodes, n = 1, 2, 3, …, N, $m(t)$ is the transmitting message, $\¤_n^d(t)$ is the uncompensated VCO phase drift of slave n^{th} is transmitting, $\¤_n^h$ is an effective phase noise and $\¤_n^e$ is the estimation error in the phase calibration.

The (3.21) presents that the master-slave technique can remove the phase offset between node, ¥$_n$. However, the estimation error in the phase calibration, $\¤_n^e$,

$¤_n^h$ $¤_n^d(t)$

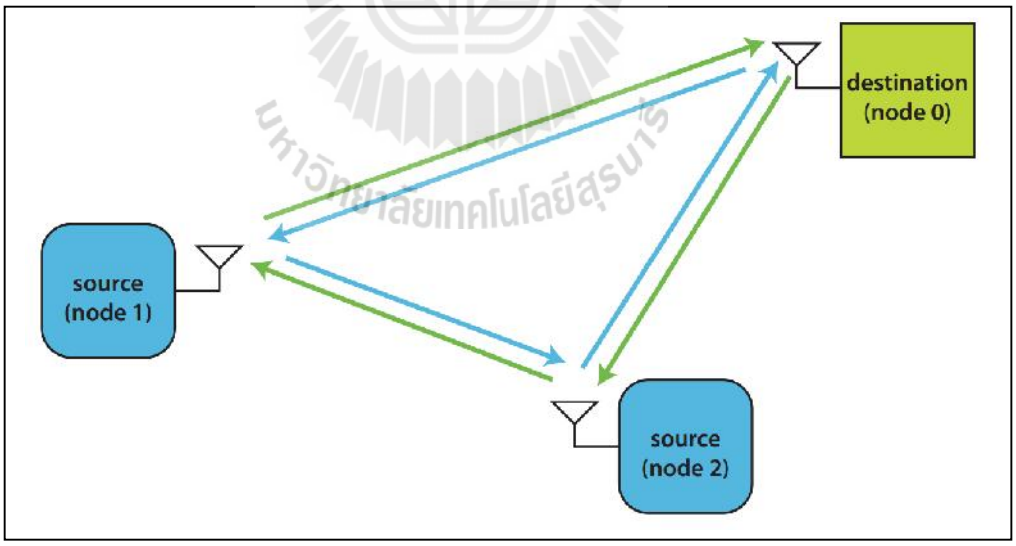

destination is receiving the sum of two carriers, modulated by the common message, after they have propagated through circuits with identical phase shifts.

For clarity of exposition, the protocol for the case with two transmitting source nodes is assumed. In this case, the time-slotted round-trip carrier synchronization protocol has a total of four timeslots.

For time slot 0 (TS 0): The destination transmits the sinusoidal primary beacon to both sources. Both sources generate phase and frequency estimation from their local observations. The transmitting beacon signal can be written as follows

$$x_0(t) = \cos\left(\mu(t - t_0) + \alpha_0\right) \qquad t \in [t_0, t_0 + T_0] \tag{3.22}$$

where T_0 is a duration of transmitting beacon from the destination to both sources. Then, the received signal at each source node can be written as

$$y_{0n} = \beta_{0n} \cos\left(\mu\left(t - \left(t_0 + \tau_{0n}\right)\right) + \alpha_0\right) + \eta_{0n}(t) \tag{3.23}$$

for $t \in [t_0 + \tau_{0n}, t_0 + \tau_{0n} + T_0]$ where $\eta_{0n}(t)$ is noise in the channel between destination and n^{th} source nodes. τ_{0n} is the time delay while transmitting signal from destination to n^{th} source and β_{0n} is the attenuation between destination and n^{th} source. Each source tracks the primary beacon from the destination using its first phase PLL. Prior to the conclusion of the primary beacon, each source stops tracking and enters holdover mode on its PLL. If the PLLs are designed correctly, the transient response of the PLL will complete prior to entering holdover. This results in local frequency and phase estimation at each source, denoted by $\hat{\mu}_{0n}$ and $\hat{\alpha}_{0n}$ respectively, for $n \in \{1, 2\}$.

For time slot 1 (TS 1): The 1st source node (S_1) uses its first PLL (running in holdover mode) to transmit a sinusoidal secondary beacon to the 2nd source node (S_2) that is a periodic extension of $y_{01}(t)$ as shown in (3.23). The secondary beacon transmitted by S_1 can be written as

$$x_{12}(t) = a_{12}\cos\left(\hat{\mu}_{01}(t-t_1)+\hat{\alpha}_1\right) \qquad t \in [t_1, t_1+T_1] \tag{3.24}$$

where a_{12} is the received signal strength at the S_2 and $\hat{\alpha}_1$ is the extrapolated phase of the first PLL at S_1 (time t_1) which can be written as

$$\hat{\alpha}_1 = \hat{\alpha}_{01} + \hat{\mu}_{01}\left(t-\left(t_0-\tau_{01}\right)\right) = \hat{\alpha}_{01} + \hat{\mu}_{01}T_0 \tag{3.25}$$

where $\hat{\alpha}_{01}$ and $\hat{\mu}_{01}$ are estimated phase and frequency of the channel between destination and the S_1, τ_{01} is the time delay while transmitting signal from destination to S_1 and T_0 is a duration of transmitting beacon from the destination to both sources. Then, the secondary beacon is received by S_2 as

$$y_{12}(t) = \sim_{12} a_{12}\cos\left(\hat{\mu}_{01}\left(t-\left(t_1+\tau_{12}\right)\right)+\hat{\alpha}_1\right)+\eta_{12}(t) \tag{3.26}$$

for $t \in [t_1+\tau_{12}, t_1+\tau_{12}+T_1]$ where $\eta_{12}(t)$ denotes the noise in the $S_1 \rightarrow S_2$ channel. τ_{12} is the time delay while transmitting signal from the S_1 to S_2, T_1 is a duration of transmitting beacon between the S_1 and S_2, α_{12} is the attenuation between the S_1 and S_2, and a_{12} is the received signal strength of S_2. The S_2 uses its second PLL to track this beacon and enters holdover on the second PLL prior to the conclusion of this

beacon. The frequency and phase estimation of the second PLL at S_2 are denoted by $\hat{\mu}_{12}$ and $\hat{\alpha}_{12}$ respectively.

For time slot 2 (TS 2): The S_2 uses its first PLL to transmit a secondary sinusoid to S_1. Then, the secondary beacon transmitted by S_2 can be written as

$$x_{21}(t) = a_{21}\cos\left(\hat{\mu}_{02}(t-t_2)+\hat{\alpha}_2\right) \qquad t \in [t_2, t_2+T_2] \tag{3.27}$$

where

$$\begin{aligned}\hat{\alpha}_2 &= \hat{\alpha}_{02} + \hat{\mu}_{02}\left(t_2 - \left(t_0 + \tau_{02}\right)\right) \\ &= \hat{\alpha}_{02} + \hat{\mu}_{02}\left(\tau_{01} + \tau_{12} - \tau_{02} + T_0 + T_1\right)\end{aligned} \tag{3.28}$$

which is the extrapolated phase of the first PLL at S_2 at the time t_2. α_{21} is the attenuation between the S_2 and S_1, $\hat{\alpha}_{02}$ and $\hat{\mu}_{02}$ are estimated phase and frequency of the channel between destination and S_2, τ_{01} is the time delay while transmitting signal from destination to S_1, τ_{02} is the time delay while transmitting signal from destination to S_2, τ_{12} is the time delay while transmitting signal from the S_1 and S_2, T_0 is a duration of transmitting beacon from the destination to both sources and T_1 is a duration of transmitting beacon between the S_1 and S_2

After propagating through the $S_2 \rightarrow S_1$ channel, this secondary beacon is received by S_1 as

$$y_{21}(t) = \sim_{21} a_{21}\cos\left(\hat{\mu}_{02}\left(t-\left(t_2+\tau_{12}\right)\right)+\hat{\alpha}_2\right) + \dagger_{21}(t) \tag{3.29}$$

for $t \in \left[t_2 + \tau_{12}, t_2 + \tau_{12} + T_2\right]$ where $\eta_{21}(t)$ denotes the noise in the $S_2 \rightarrow S_1$ channel, α_{21} is the attenuation between the S_2 and S_1, a_{21} is the received signal strength of S_1. This work has used the fact that $\tau_{21} = \tau_{12}$ and $\omega_{21} = \omega_{12}$. The S_1 uses its second PLL to track this beacon and enters holdover on the second PLL prior to the conclusion of this beacon. The frequency and phase estimation of the second PLL at S_1 are denoted by $\hat{\mu}_{21}$ and $\hat{\theta}_{21}$ respectively.

For time slot 3 (TS 3): Each S_1 and S_2 transmit to the destination as a distributed beamformer by using the phase estimation from the second PLL (running in holdover mode). The carrier at each source is transmitted as a periodic extension of the secondary beacons received at each source. Since the performance of the distributed beamformer is primarily affected by the phase offset between the carriers at the destination. We can write the transmissions of S_1 and S_2 as unmodulated carriers which can be written as

$$x_{10}(t) = a_{10} \cos\left(\hat{\mu}_1 (t - t_{31}) + \hat{\theta}_{31}\right) \quad t \in \left[t_{31}, t_{31} + T_3\right] \tag{3.30}$$

where

$$\hat{\theta}_{31} = \hat{\theta}_{21} + \hat{\mu}_{21}\left(t_{31} - \left(t_2 + \tau_{12}\right)\right) \tag{3.31}$$

and

$$\hat{\theta}_{32} = \hat{\theta}_{12} + \hat{\mu}_{12}\left(t_{32} - \left(t_1 + \tau_{12}\right)\right) \tag{3.32}$$

which are the extrapolated phases of the second PLLs at S_1 and S_2 at time t_3 respectively.

Therefore, the received signal at the base station can be written as

$$y_0(t) = \sum_{n=1}^{2} \sim_{0n} a_{n0} \cos\left(\hat{\mu}_{mn}(t - t_3) + \hat{\alpha}_{3i}\right) + \dagger_0(t) \tag{3.33}$$

for $m \neq n$, $t \in [t_3, t_3 + T_3]$ and $t_3 = t_{31} + \delta_{01} = t_{32} + \delta_{02}$ where α_{0n} is the attenuation between destination and n^{th} source, a_{n0} is the received signal strength at the destination which transmitted from n^{th} source, $\hat{\alpha}_{3n}$ and $\hat{\mu}_{mn}$ are estimated phase and frequency of the third PLL at the destination and $\dagger_0(t)$ is noise at the destination. The $\delta_{0n} = \delta_{n0}$ and $\sim_{0n} = \sim_{n0}$ for $n \in \{1, 2\}$ are also assumed.

Figure 3.11 summarizes the time-slotted round-trip carrier synchronization protocol and shows how the protocol is repeated in order to avoid unacceptable phase drift between the sources during beamforming.

In a distributed beamforming system with $N > 2$ sources as shown in Figure 3.12, the time-slotted round-trip carrier synchronization protocol has a total of $2N$ timeslots denoted as TS(0) ,... , TS($2N-1$) where N is the number of transmitting nodes. The activity in each timeslot is summarized as follows:

(i) In TS(0), the destination transmits the sinusoidal primary beacon to all N sources. Each source generates local phase and frequency estimation from its observation.

(ii) In TS(n) for $n = 1, \ldots, N-1$, the S_n transmits a sinusoidal secondary beacon to the S_{n+1}. The secondary beacon transmitted by the S_n in TS(n) is a periodic extension of the beacon received in TS($n-1$). The S_{n+1} generates local phase and frequency estimation from this observation.

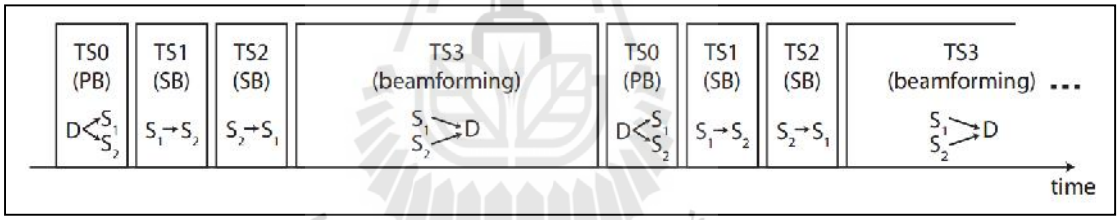
TS0
(PB)
TS1
(SB)
TS2
(SB)
TS3
(beamforming)
TS0
(PB)
TS1
(SB)
TS2
(SB)
TS3
(beamforming)
...
time

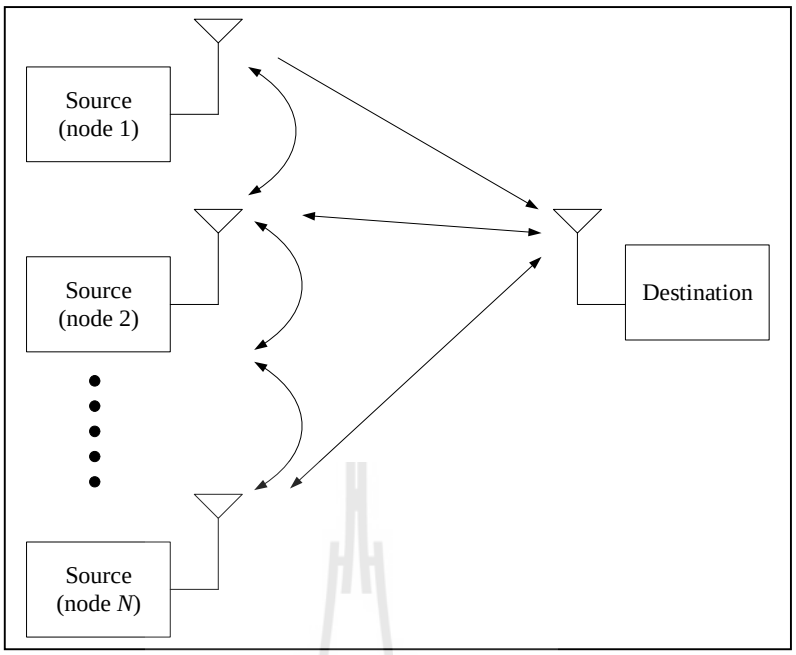

Figure 3.12 *M*-source round-trip distributed beamforming system (Brown D.R., et.al, (2010)).

(v) In TS(2N−1), all N sources simultaneously transmit to the destination as a distributed beamformer. The frequency and initial phase of the carrier transmitted by each source is based only on the local phase and frequency estimation obtained in the prior timeslots.

These procedure is similar to the two-source case, the total phase shift of the D → S_1 → S_2 → ⋯ → S_M → D and the D → S_M → S_{M-1} ⋯→ S_1 → D circuits are identical where D means destination.

The round-trip technique can synchronize the phase of each transmitting node by using the equivalence of round-trip transmission delays through a multi-hop chain between transmitting nodes and base station. However, the round-trip technique requires some feedbacks from base station. The interaction between nodes increases

complexity for all transmitting nodes. In addition, nodes require a special hardware such as PLL to obtain a reference signal when performing open-loop in order to achieve phase synchronization.

3.5 Zero-Feedback Synchronization

A zero-feedback technique for phase synchronization has been lately proposed (Bletsas A., et.al, (2010) and Sklivanitis G., et.al, (2011)). This technique does not require any feedback signal from base station. Also all transmitting nodes are assumed as the conventional radio transceivers employing no special hardware. The technique employs a carrier frequency offset between all transmitting nodes for the phase synchronization.

Denoting the complex channel gain from N transmitters $n \in \{1, 2, ..., N\}$ to destination as h_n ($|h_n| = A_n$) and symbol duration as T_s, the received baseband signal of b^{th} symbol at the destination can be expressed as

$$y[b] = \sum_{n=1}^{N} h_n e^{\{j2\pi\Delta f_n b T_s + \phi_n\}} x[b] + w[b]$$

$$= \underbrace{x[b] \sum_{n=1}^{N} A_n \exp\{j(2\pi\Delta f_n b T_s + \phi_n)\}}_{\tilde{x}[b]} + w[b]$$

$$= \tilde{x}[b] + w[b] \tag{3.34}$$

where N is the number of transmitting nodes. Δf_n is the carrier frequency offset from nominal carrier frequency, f_c, A_n is the amplitude for n^{th} transmitter, ϕ_i is the phase offset for n^{th} transmitter and $w[b]$ is the additive noise at the destination which has an

average power per symbol as $\mathbf{E}\{w[b]w[b]^*\} = W_0$. It is assumed that $\mathbf{E}\{\Delta f_n\} = 0$ and $\mathbf{E}\{\Delta f_b{}^2\} = \sigma^2$. The carrier frequency offset is due to manufacturing errors of the local oscillator crystal and varies slowly with time due to environmental conditions (e.g. temperature). The standard deviation is given by $\sigma = \sqrt{\mathbf{E}\{\Delta f_i^2\}} = f_c \times$ ppm, where ppm is the frequency skew of the clock crystals with typical values of 1 − 20 parts per million (ppm). For example, clock crystals of 20 ppm provides the carrier frequency offsets of 2.4 GHz × 20 × 10^{-6} = 48 kHz.

The parameters A_n and ¤$_n$ depend on the relative mobility between n^{th} transmitter and receiver. This work also assumes that the time symbols, τ_c, remain constant corresponding to channel coherence time, T_s. Therefore, the received signal power per symbol, for any $b \in [1, \tau_c]$, can be written as follows

$$\left|\tilde{x}[b]\right|^2 = x[b]^2 \left\{ \sum_{n=1}^{N} A_n^2 + 2\sum_{n\neq m} A_n A_m \cos\left(\underbrace{2®\Delta f_n bT_s + ¤_n}_{\tilde{¤}_k[b]} - 2®\Delta f_m bT_s - ¤_m \right) \right\}$$

$$= x[b]^2 \left\{ \sum_{n=1}^{N} A_n^2 + 2\sum_{n\neq m} A_n A_m \cos\left(\tilde{¤}_n[b] - \tilde{¤}_n[b] \right) \right\} \qquad (3.35)$$

where $x[b]$ is the transmitting message, A_n ad A_m are the received signal amplitude of the n^{th} and m^{th} node respectively, Δf_n and Δf_m are the carrier frequency offset of the n^{th} and m^{th} node respectively, T_s is the time symbol, ¤$_n$ and ¤$_m$ is the phase offset of the n^{th} and m^{th} node respectively. The second sum in (3.35) includes $\binom{N}{2} = \frac{N!/(N-2)!}{2!}$, corresponding to all possible pairs among the N transmitters. This work assumes an energy constellation to be equal and also denotes the

$$\mathrm{SNR}[b] = \frac{\mathrm{E}\left\{\left|\tilde{x}[b]\right|^2\right\}}{\mathrm{E}\left\{\left|w[b]\right|^2\right\}}$$

$$= \frac{P_T}{W_0}\left\{\sum_{n=1}^{N} A_k^2 + 2\sum_{n\neq m} A_n A_m \cos\left(\tilde{¤}_n[b] - \tilde{¤}_m[b]\right)\right\}$$

$$= \frac{P_T}{W_0}\left\{\sum_{n=1}^{N} A_n^2 + 2\sum_{n\neq m} A_n A_m \cos\left(2® \left(\Delta f_n - \Delta f_m\right) b T_s + ¤_n - ¤_m\right)\right\}$$

$$= \frac{P_T}{W_0}\mathrm{L}_{\mathrm{BF}}[b]$$

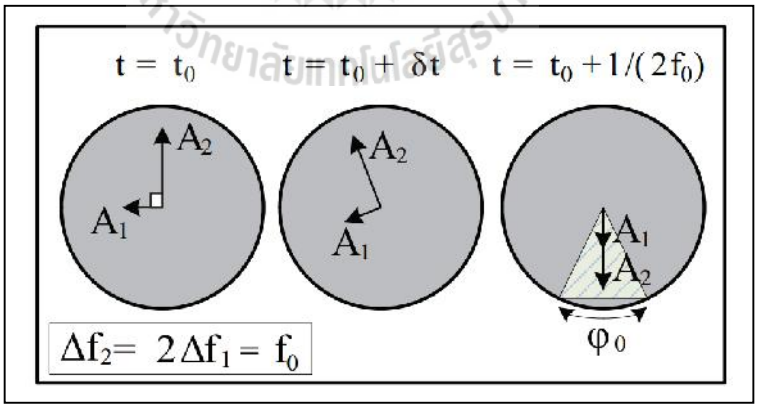

positive or negative depending on the symbol, b, the phase offsets $\{¤_n\}$,as well as the distribution of the carrier frequency offsets $\{\Delta f_n\}$ $n \in \{1, 2, \ldots, N\}$. Figure 3.13 shows the special case of two distributed transmitters ($N = 2$) with carrier frequency offsets of

$\Delta f_2 = 2\Delta f_1 = f_0$; their signals arrive at the destination with phase difference $\pi/2$ at time instant $t = t_0$. The two signals align at $t = t_0 + 0.5/f_0$, providing constructive addition at the destination (beamforming gain).

This work has studied the general-N signal alignment case for any carrier frequency offset distribution $p_{\Delta f}(\Delta f)$ and carrier phases at the destination $\bar{\phi} = [\phi_1, ¤_2, \ldots, ¤_M]^T$. Specifically, this work defines an alignment parameter, a, with $0 < a \leq 1$. The alignment parameter, a, can be described as follows: if $\cos\left(\tilde{¤}_n[b] - \tilde{¤}_m[b]\right) \geq a$ for all pairs $\{n, m\}$, $n \neq m$ and $n, m \in \{1, 2, \ldots, N\}$. The cosines in the beamforming factor become strictly positive and all N-transmitted signals align constructively, without any type of feedback from the destination. In mathematical notation, the alignment event is defined as

$$\text{Align}[b, a, N] = \bigcap_{N \neq m} \left\{\cos\left(\tilde{¤}_N[b] - \tilde{¤}_m[b]\right) \geq a\right\} \tag{3.37}$$

where $n \neq m, \forall n, n \in \{1, 2, \ldots, N\}$. According to (3.36) and (3.37), the $L_{BF}[b]$ can be rewritten as

$$L_{BF}[b] \geq \left\{\sum_{n=1}^{N} A_n^2 + 2a\sum_{n \neq m} A_n A_m\right\} = 10\log_{10}\left(N + 2a\binom{N}{2}\right)$$

$$= 10\log_{10}\left(N\left[1+a\left(N-1\right)\right]\right) \tag{3.38}$$

The (3.38) shows that the beamforming gain, $\mathrm{L}_{\mathrm{BF}}[b]$, is optimum when phase is aligned or a = 1. Thus, the maximum beam forming gain is $\mathrm{L}_{\mathrm{BF}}[b] = 10\log_{10}\left(N^2\right)$ dB. Furthermore, define the following indicator random variable as

$$_b[a,N] = \begin{cases} 1, & \text{with prob. Pr}\left\{\text{Align}[b,a,N]\right\} \\ 0, & \text{with prob. 1-Pr}\left\{\text{Align}[b,a,N]\right\} \end{cases} \tag{3.39}$$

Then, the N-distributed nodes repeatedly transmit the same unsynchronized carrier for $B \le \tau_c$ symbols where B is a number of symbol. Thus, the random variable (3.39) can be rewritten as

$$(N) = {}_1[a,N] + {}_2[a,N] + \ldots + {}_{2_c}[a,N] \tag{3.40}$$

The (3.40) denotes the number of symbols where the N-signals align with beamforming factor $\mathrm{L}_{\mathrm{BF}}[n]$ which at least equals to

$$\mathrm{L}_{\mathrm{BF}}[b] \ge \left\{\sum_{n=1}^{N} A_n^2 + 2a\sum_{n\neq m} A_n A_m\right\} = \mathrm{L}_0\left(N\right) \tag{3.41}$$

Therefore, the average number of symbols in [1, N] with minimum beamforming factor $\mathrm{L}_0(N)$ becomes

$$\mathrm{E}\left\{\ (N)\right\} = \sum_{n=1}^{B\le 2_c} \Pr\left\{\text{Align}[\mathrm{b},a,N]\right\} \tag{3.42}$$

$$\Pr\left\{\text{Align}\left[b,a,N\right]\right\} \geq \int_{y=0}^{2®}\int_{x=y}^{\min\left\{y+¤_0,2®\right\}} p_{y,x}\left(y,x\right)dxdy$$

$$p_{y,x}\left(y=\min_{n\in\{1,2,\ldots N\}}\left\{\breve{¤}_n\right\}, y=\max_{n\in\{1,2,\ldots N\}}\left\{\breve{¤}_n\right\}\right)$$

$$\breve{¤}_n\left(b\right)=\tilde{¤}_n\left(b\right)\bmod 2® = \left(2®bT_s\Delta f_n + ¤_n\right)\bmod 2®$$

$$\breve{¤}_n \in \left[0,2®\right) \quad n\in\left\{1,2,\ldots,N\right\}$$

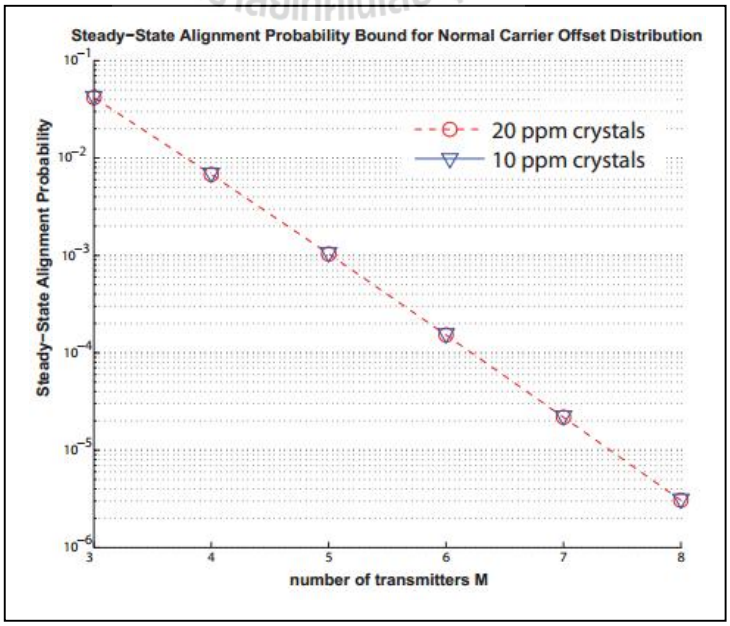

$$a = \cos\left(¤_0\right) = \cos\left(\tilde{¤}_n\left[b\right] - \tilde{¤}_m\left[n\right]b\right)$$

$\mathrm{E}\{\ \ (N)\}$

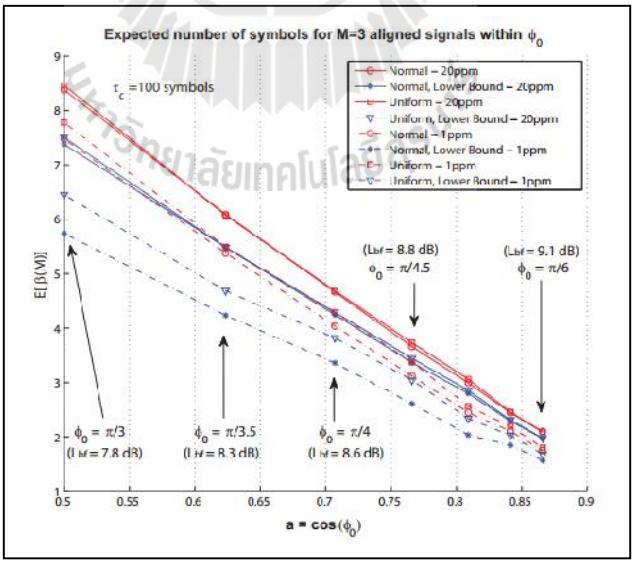

$¤_0$ $¤_1$ $¤_2$ $¤_3$

the alignment delay by approximately 50%, since now 50 symbols must be repeatedly transmitted in order to achieve alignment at one symbol on average (as opposed to 25

symbols for the case of $a = \cos(\pi/4)$). The last observation highlights the fundamental communication tradeoff between beamforming factor and the number of symbols as the transmitting signals need to be repeatedly transmitted to ensure signal alignment.

3.6 Chapter Summary

This chapter has presented the literatures survey proposed in literatures which can be summarized as follows.

(i) **One-bit feedback technique** : Every transmitting node adjusts its carrier phase randomly. Then, all nodes transmit the same data to base station. After the SNR of received signal is estimated at the base station. Then, the base station broadcasts one bit (0 or 1) of feedback to the nodes indicating whether its SNR is better or worse than before the nodes adjusted their phases. If it is better, all nodes keep their latest phase adjustment; otherwise, all nodes undo their latest phase adjustments. This technique requires a large number of retransmissions (or feedback signal) from nodes to base station to ensure the phase alignment.

(ii) **Master-slave technique** : A node in the networks is selected as a master node while all remaining nodes are assigned as slave nodes. The phase synchronization is achieved by sending the reference signals between master and slave nodes.

(iii) **Time-slot round-trip technique** : phase synchronization among nodes is obtained by sending a reference data round between nodes. The idea is based on the equivalence of round-trip transmission delays through a multi-hop chain between transmitting nodes and base station. However, both master-slave and round-trip techniques require some feedbacks from base station. Moreover, the interaction among nodes increases complexity for transmitting nodes.

(iv) **Zero-feedback technique** : This technique does not require any feedback signal from base station. All transmitting nodes are assumed as the conventional radio transceivers employing no special hardware. This technique employs a carrier frequency offset between transmitting nodes for the phase synchronization. However, the zero-feedback technique requires the large number of packet retransmissions.

Table 3.1 Disadvantages of existing phase synchronization techniques from literatures.

	Requirement		
Technique	**Feedback signal from the base station**	**Large number of retransmissions**	**Reference signal among nodes**
One-bit feedback	✓	✓	
Master-Slave	✓		✓
Round-Trip	✓		✓
Zero-feedback		✓	

From above literatures, the major disadvantage of existing phase synchronization techniques, one-bit feedback and zero-feedback, is that they require a

large number of retransmissions. This requirement reduces the battery-lifetime of transmitting nodes or mobile terminals. Also, the master-slave and round-trip techniques require the transmitting reference signal among nodes which increases complexity to all transmitting nodes. Therefore, the disadvantage of existing phase synchronization techniques can be summarized in Table 3.1.

To overcome these limitations, a non-feedback distributed beamforming technique is proposed in this thesis which will be discussed in the next chapter. The proposed technique does not require any feedback signal from base station or interaction between nodes. Only a few number of retransmissions from nodes, which is only the same as the number of beamforming nodes. This number is relatively small comparing to the one employed for one-bit feedback and zero-feedback techniques.

CHAPTER IV

NON-FEEDBACK DISTRIBUTED BEAMFORMING

4.1 Introduction

To overcome the limitations of the major phase synchronization technique as discussed in the Chapter 3, a non-feedback distributed beamforming technique is proposed in this thesis. The proposed technique employs an inverse matrix to extract the combined signal at a base station. The concept of extraction is based on solving a linear equation using inverse matrix method (Kreyszig E., (1999)), which is suitable for solving a system involving *v*-linear equations in *v*-unknown variables. After performing a signal extraction, each extracted signal is weighted for phase synchronization at the base station. Finally, the base station obtains a combined signal with maximum beamforming gain. However, the retransmitted signals may be distorted due to phase variations when travelling through the communication channel. To investigate into the mentioned effect the phase variation in real circumstance is taken into account in this Section 4.3. Figure 4.1 demonstrates a route map of this chapter. Section 4.1 is an introduction of this chapter which presents a background concept of the proposed non-feedback technique. Sections 4.2 presents the three major parts of proposed technique including 4.2.1 RF front end receiver operation, 4.2.2 spatial-temporal extraction operation and 4.2.3 optimum weight. Section 4.3 presents the performance of proposed technique under the phase variation. Section 4.4 presents the comparison performance between the proposed technique and literatures which discussed in Chapter 3. Finally, Section 4.5 concludes the chapter.

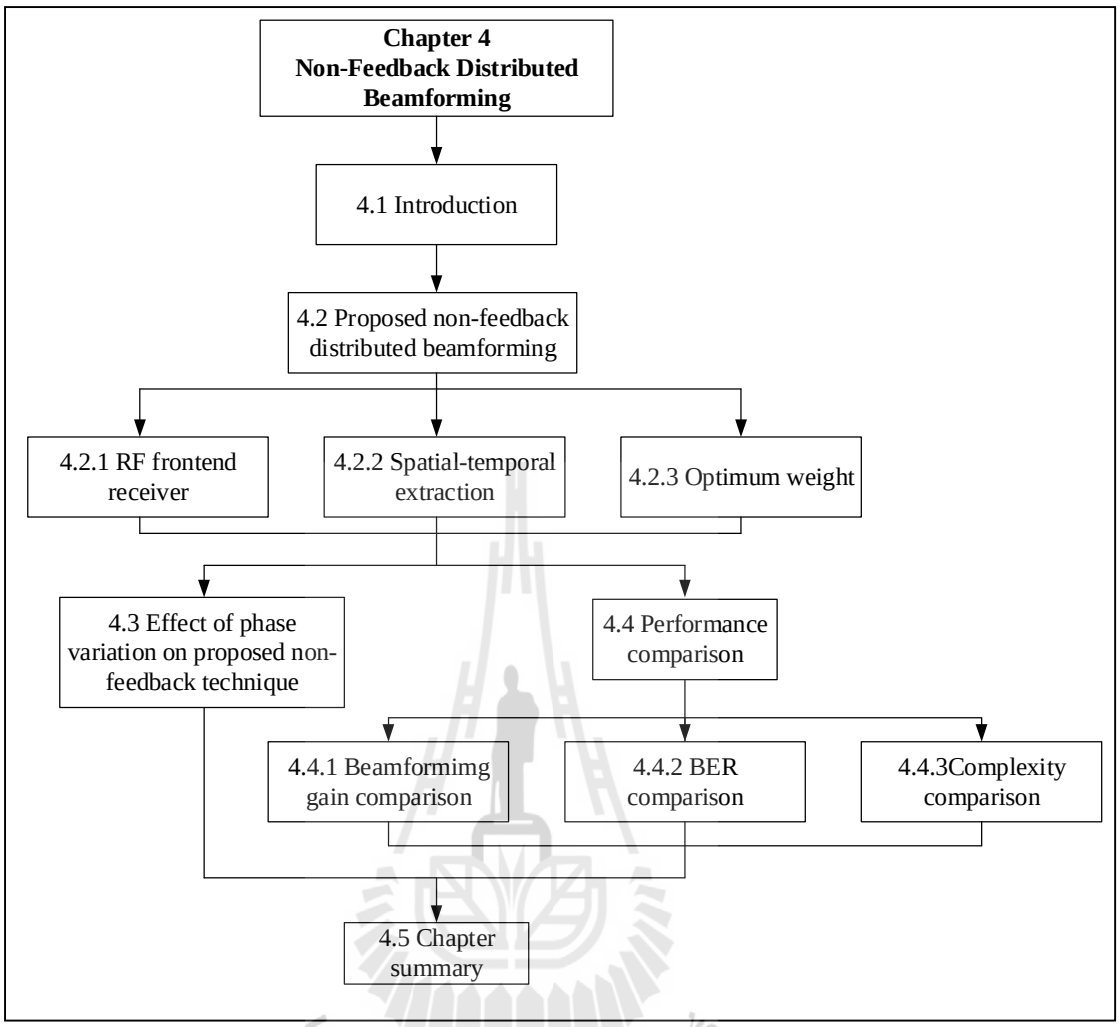

Figure 4.1 Route map of study in Chapter IV.

4.2 Proposed Non-Feedback Distributed Beamforming

This thesis proposes a non-feedback distributed beamforming which does not require any interaction between nodes and feedback signals. The model consists of three major parts: 4.2.1 RF Front End Receiver Operation which converts the RF signals to the baseband signals, 4.2.2 Spatial-Temporal Extraction which performs the signal extraction and phase synchronization at base station and 4.2.3 Optimum

Weight which synchronizes the phase of the extracted signal. All three parts will be detailed as follows.

4.2.1 RF Front End Receiver Operation

For simplicity, each received signal amplitude, A_n, is assumed to be 1. Thus, the received signals which come from all transmitting nodes can be written as

$$\begin{aligned} Y_R(t) &= \Re\left\{\sum_{n=1}^{N} y_n(t) + W_{PB}(t)\right\} \\ &= \Re\left\{x(t)\sum_{n=1}^{N} h_n e^{j(\mu_n t+\phi_n)} + W_{PB}(t)\right\} \\ &= x(t)\sum_{n=1}^{N}\left[h_n\cos(\mu_n t+\phi_n)\right] + \underbrace{w_I(t)\cos(\mu_c t) - w_Q(t)\sin(\mu_c t)}_{\Re\{W_{PB}(t)\}} \end{aligned} \tag{4.1}$$

where N is the number of transmitting nodes. $y_n(t)$ is a signal from the n^{th} node, ω_n = $\omega_c + \Delta\omega_n$ where ω_c is a carrier frequency and $\Delta\omega_n$ is a frequency offset, $\phi_n = \phi_0 + \Delta\phi_n$ where ϕ_0 is the nominal phase and $\Delta\phi_n$ is a phase offset. Also, $W_{PB}(t)$ is pass-band AWGN which consists of in-phase $w_I(t)$ and quadrature $w_Q(t)$ components. Then, the received signal appeared in (4.1) is demodulated and a lower frequency part is obtained as

$$\begin{aligned} Y_{de}(t) &= Y_R(t)\cos(\mu_{LO}t) \\ &= x(t)\sum_{n=1}^{N}\left[h_n\cos(\mu_n t+\phi_n)\right]\cos(\mu_{LO}t) + w_I(t)\cos(\mu_c t)\cos(\mu_{LO}t) \\ &\quad - w_Q(t)\sin(\mu_c t)\cos(\mu_{LO}t) \end{aligned}$$

$$= x(t)\sum_{n=1}^{N}\left\{\frac{h_n}{2}\left[\cos\left(\mu_n t+\mu_{LO}t+¤_n\right)+\cos\left(\mu_n t-\mu_{LO}t+¤_n\right)\right]\right\}$$

$$+\frac{w_I(t)}{2}\left[\cos\left(\mu_c t+\mu_{LO}t\right)+\cos\left(\mu_c t-\mu_{LO}t\right)\right]$$

$$-\frac{w_Q(t)}{2}\left[\sin\left(\mu_c t+\mu_{LO}t\right)+\sin\left(\mu_c t-\mu_{LO}t\right)\right] \qquad (4.2)$$

where μ_{LO} is a Local Oscillating (LO) frequency. Therefore, an intermediate frequency (IF) is $\Delta\mu_{IF}=\mu_n-\mu_{LO}$ and $\Delta\mu_{IF}=\mu_c-\mu_{LO}$. After the band-pass filter in RF modulator with a gain of G = 2 is used for the signal component of μ_{IF}, the output signal of the filter is given as

$$Y_{BPF}(t)=2\cdot\frac{1}{2}x(t)\sum_{n=1}^{N}h_n\left[\cos\left(\mu_n t-\mu_{LO}t+¤_n\right)\right]+2\cdot\frac{1}{2}w_I(t)\cos\left(\mu_c-\mu_{LO}\right)t$$
$$+2\cdot\frac{1}{2}w_I(t)\cos\left(\mu_c-\mu_{LO}\right)t$$

$$= x(t)\sum_{n=1}^{N}\left[h_n\cos\left(\Delta\mu_{IF}t+¤_n\right)\right]+w_I(t)\cos\left(\mu_{IF}t\right)-w_Q(t)\sin\left(\mu_{IF}t\right) \qquad (4.3)$$

After the received signal was modulated to be an intermediate frequency (IF), an Analog-to-Digital Converter (ADC) with sampling rate T_s is used to convert the RF received signal to a digital signal expressed as

$$Y_{ADC}(s)=x(s)\sum_{n=1}^{N}h_n\cos\left(\Delta\Omega_{IF}s+\Phi_n\right)$$

$$+w_I(s)\cos\left(\Omega_{IF}s\right)-w_Q(k)\sin\left(\Omega_{IF}s\right) \qquad (4.4)$$

where s is the sampling time variable, $\Delta\Omega_n$ is the frequency offset and Φ_n is the phase offset at the sampling time, s. Then, the RF received signal is converted to digital domain. The Digital Down-Converter (DDC) shifts down the frequency of received signal by multiplying the received signal with a sinusoidal signal and a 90° phase-shifted version of the sinusoidal signal. The output signal from DDC is performed in $I(s)$ and $Q(s)$ which can be calculated using

$$I(s)=Y_{ADC}(s)\cos(\Omega_{DLO}s) \tag{4.5}$$

and

$$Q(s)=Y_{ADC}(s)\sin(\Omega_{DLO}s) \tag{4.6}$$

where Ω_{DLO} is a digital local oscillator frequency. The digital signals shown in (4.5) and (4.6) can be expressed as

$$I(s)=\frac{x(s)}{2}\sum_{n=1}^{N}\left\{h_n\left[\cos(\Delta\Omega_{IF}s+\Omega_{DLO}s+\Phi_n)+\cos(\Delta\Omega_{IF}s-\Omega_{DLO}s+\Phi_n)\right]\right\}$$

$$+\frac{w_I(s)}{2}\left[\cos(\Omega_{IF}+\Omega_{DLO})s+\cos(\Omega_{IF}-\Omega_{DLO})s\right]$$

$$-\frac{w_Q(s)}{2}\left[\sin(\Omega_{IF}-\Omega_{DLO})s+\sin(\Omega_{IF}+\Omega_{DLO})s\right] \tag{4.7}$$

and

$$Q(s)=\frac{x(s)}{2}\sum_{n=1}^{N}\left\{h_n\left[\sin(\Delta\Omega_{IF}s+\Omega_{DLO}s+\Phi_n)+\sin(\Delta\Omega_{IF}s-\Omega_{DLO}s+\Phi_n)\right]\right\}$$

$$+\frac{w_I(s)}{2}\left[\sin(\Omega_{IF}+\Omega_{DLO})s+\sin(\Omega_{IF}-\Omega_{DLO})s\right]$$

$$-\frac{w_Q(s)}{2}\left[\cos(\Omega_{IF}-\Omega_{DLO})s-\cos(\Omega_{IF}+\Omega_{DLO})s\right] \tag{4.8}$$

If the digital local oscillator frequency equals to the intermediate frequency i.e., $\Omega_{DLO} = \Omega_{IF}$, then the Low-Pass Filter (LPF) with a gain of $G = 2$ can be used to filter out the intermediate frequency, $\Omega_{DLO} + \Omega_{IF} = 2\Omega_{IF}$. The output signals of each LPF are obtained as

$$I_{LPF}(s) = x(s)\sum_{n=1}^{N} h_n \cos(\Delta\Omega_{IF}s - \Omega_{DLO}s + \Phi_n) + w_I(s) \tag{4.9}$$

and

$$Q_{LPF}(s) = x(s)\sum_{n=1}^{N} h_n \sin(\Delta\Omega_{IF}s - \Omega_{DLO}s + \Phi_n) + w_Q(s) \tag{4.10}$$

The received signal is modulated and down converted using RF modulator and digital down converter, respectively. Finally, the base station obtains the digital base-band signal as follows

$$\begin{aligned} Y(s) &= \sum_{n=1}^{N}\left[I_{LPF}(s) - jQ_{LPF}(s)\right] \\ &= x(s)\sum_{n=1}^{N}\left\{\left[\cos(\Delta\Omega_{IF}s-\Omega_{DLO}s+\Phi_n)-j\sin(\Delta\Omega_{IF}s-\Omega_{DLO}s+\Phi_n)\right]\right\} \\ &\quad + w_I(s) + jw_Q(s) \\ &= x(s)\sum_{n=1}^{N} h_n e^{-j\left((\Delta\Omega_{IF}-\Omega_{DLO})s+\Phi_n\right)} + W_{BB}(s) \end{aligned} \tag{4.11}$$

where $W_{BB}(\varsigma)$ is a base-band additive white Gaussian noise, $W_{BB}(\mathrm{s}) = w_I(\mathrm{s}) + jw_Q(\mathrm{s})$. According to $\Omega_{DLO} = \Omega_{IF} = \Omega_c - \Omega_{LO}$, $\Omega_n = \Omega_c + \Delta\Omega_n$ and $\Delta\Omega_{IF} = \Omega_n - \Omega_{LO}$. Then, (4.11) can be rewritten as follows

$$Y(\mathrm{s}) = x(\mathrm{s})\sum_{n=1}^{N} h_n e^{-j(\Delta\Omega_n \mathrm{s} + \Phi_n)} + W_{BB}(\mathrm{s}) \tag{4.12}$$

where $W_{BB}(\mathrm{s})$ is a baseband AWGN, $W_{BB}(\mathrm{s}) = w_I(\mathrm{s}) + jw_Q(\mathrm{s})$. The summarized detail of the RF front end receiver is presented in Figure. 4.2.

According to (4.12), the digital base-band signal is distorted by the phase offset, Φ_n. Thus, the proposed technique is proposed to eliminate the phase offset in the two next operations.

4.2.2 Spatial-Temporal Extraction Operation

The proposed technique consists of two major operations: 4.2.2 Spatial-Temporal Extraction and 4.2.3 Optimum Weighting, as shown in Figure 4.3. In the “Spatial-Temporal Extraction”, the proposed technique uses an inverse matrix to achieve the extracted signals. The concept of extraction is based on solving a linear equation using inverse matrix method. Then, the extracted signals are transmitted to “Optimum Weighting” in order to find the optimum weights of signal. Finally, the base station obtains a gainfully signal.

In the Spatial-Temporal Extraction, the combined signal (4.12) is extracted. The concept of extraction is that the all transmitting nodes in the networks

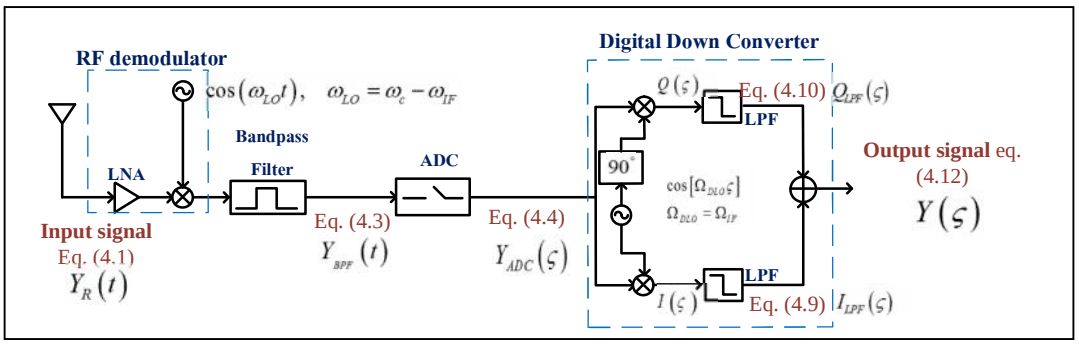

Figure 4.2 Block diagram of the RF front end receiver.

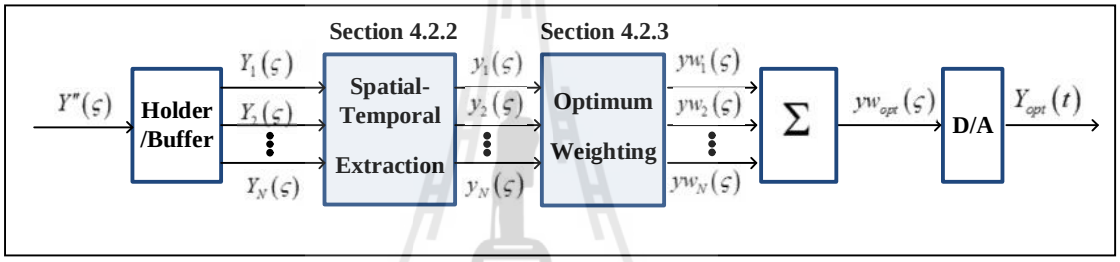

Figure 4.3. Block diagram of the proposed non-feedback technique.

transmit the same message to the base station at the same time. The nodes transmit signal repeatedly for *N* times which equals to the number of the transmitting nodes.

For each retransmission, the transmitting nodes adjust their phases according to proposed phase adjustment pattern matrix, $\mathbf{A}_{NN}$ which can be achieved by following algorithm.

(i) At 1st symbol period, all transmitting nodes send the signal without any phase adjustment.

(ii) At the n^{th} symbol period where n = 2, 3, …, N, only the $(n-1)^{th}$ transmitting node shifts its phase by 180°. For example, at the 2nd

symbol period, the 1st node shifts its phase by 180° and at the 3rd symbol period,

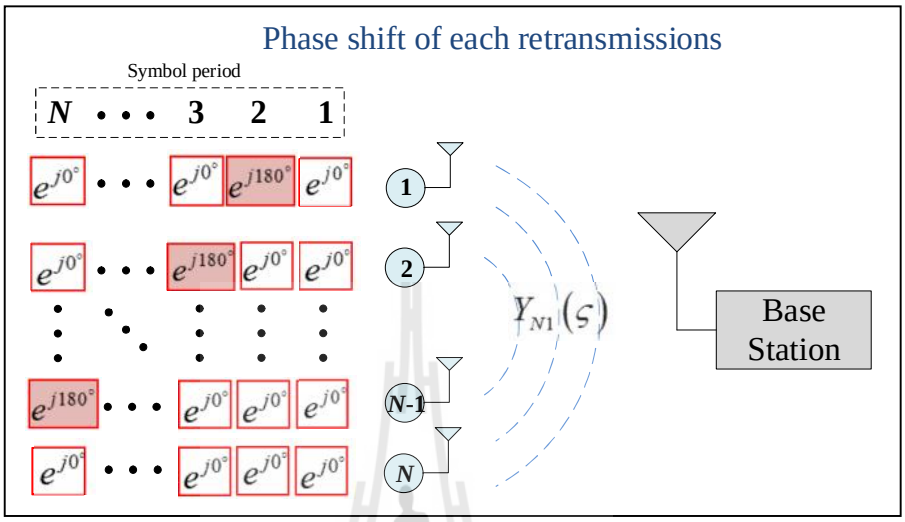

Figure 4.4. Proposed phase shifting pattern.

the 2nd node shifts its phase by 180° as seen in Figure 4.4 which shows the summary of proposed phase adjustment pattern.

(iii) Repeat the phase shifting pattern for N symbol periods. According to the proposed phase adjustment pattern as presented above, we obtain the fixed coefficient matrix $\mathbf{A}_{NN}$ by retransmitting signal for N times as shown in the following equations.

$$\mathbf{A}_{NN} = \begin{bmatrix} 1 & 1 & \cdots & 1 & 1 \\ e^{j180^\circ} & 1 & \cdots & 1 & 1 \\ 1 & e^{j180^\circ} & \cdots & 1 & 1 \\ \vdots & \vdots & \ddots & \vdots & \vdots \\ 1 & 1 & \cdots & e^{j180^\circ} & 1 \end{bmatrix} \tag{4.13}$$

After having completed N retransmissions with the algorithm, all received signals are simultaneously arranged to form the vector $\mathbf{Y}_N(\mathsf{s})$ as

$$\mathbf{Y}_N(\mathsf{s}) = \mathbf{A}_{NN}\mathbf{y}_N(\mathsf{s}) + \mathbf{W}_{BB,N}(\mathsf{s}) \tag{4.14}$$

or

$$\begin{bmatrix} Y_1(\mathsf{s}) \\ Y_2(\mathsf{s}) \\ Y_3(\mathsf{s}) \\ \vdots \\ Y_N(\mathsf{s}) \end{bmatrix} = \underbrace{\begin{bmatrix} 1 & 1 & \cdots & 1 & 1 \\ e^{j180^\circ} & 1 & \cdots & 1 & 1 \\ 1 & e^{j180^\circ} & \cdots & 1 & 1 \\ \vdots & \vdots & \ddots & \vdots & \vdots \\ 1 & 1 & \cdots & e^{j180^\circ} & 1 \end{bmatrix}}_{\mathbf{A}_{NN}} \begin{bmatrix} y_1(\mathsf{s}) \\ y_2(\mathsf{s}) \\ y_3(\mathsf{s}) \\ \vdots \\ y_N(\mathsf{s}) \end{bmatrix} + \begin{bmatrix} W_{BB,1}(\mathsf{s}) \\ W_{BB,2}(\mathsf{s}) \\ W_{BB,3}(\mathsf{s}) \\ \vdots \\ W_{BB,N}(\mathsf{s}) \end{bmatrix} \tag{4.15}$$

where $\mathbf{Y}_N(\mathsf{s})$ is the vector of combined received signals obtained by retransmitting the signal N times where the each retransmitting signal has the phase adjustment in order to create the coefficient matrix $\mathbf{A}_{NN}$. The $\mathbf{y}_N(\mathsf{s})$ is the vector of transmitted message from all transmitting nodes and $W_{BB,N}(\mathsf{s})$ is the vector of baseband AWGN where N is the number of transmitting nodes. Equation (4.15) confirms that the retransmitting signal of $\mathbf{Y}_N(\mathsf{s})$ provides the coefficient matrix $\mathbf{A}_{NN}$.

As the combined signal vector appeared in (4.14), $\mathbf{Y}''_N(\mathsf{s})$ can be extracted by applying the inverse matrix that is used to solve the system of simultaneous linear equations. Thus, we can extract the combined signal by utilizing the inverse matrix as

$$\mathbf{A}_{NN}^{-1}\mathbf{Y}_N(\mathsf{s}) = \mathbf{A}_{NN}^{-1}\mathbf{A}_{NN}\mathbf{y}_N(\mathsf{s}) + \mathbf{A}_{NN}^{-1}\mathbf{W}_{BB,N}(\mathsf{s}) \tag{4.16}$$

Then, expressing $\mathbf{y}_N(\mathsf{s})$ in (4.14) as

$$\mathbf{y}_N(s)+\mathbf{A}_{NN}^{-1}\mathbf{W}_{BB,N}(s)=\mathbf{A}_{NN}^{-1}\mathbf{Y}_N(s) \tag{4.17}$$

Equatiob (4.17) represents the noisy signal from each node which can be extracted by applying the proposed $\mathbf{A}_{NN}^{-1}$.

The proposed technique will be demonstrated on an example of a beamforming network that is composed of four collaborative nodes, i.e., N = 4. Each transmitting node and base station equips with a single antenna element. All nodes are stationary. The operation frequency is 2.45 GHz. The received signals at base station are assumed to be equal and have SNR of 20 dB, which is referred to the minimum SNR of Wi−Fi network. This confirms the feasibility of proposed concept when operated in real circumstances having high noise signal. The phase offset is Gaussian distributed over $-\pi$ to π. The frequency offset refers to typical frequency offset of the clock crystals which is 1−20 ppm (Bletsas A., et.al, (2010)). As the operating frequency is 2.45 GHz, the maximum possible frequency offset is 2.45 GHz × 20 × 10^{-6} = 49 kHz and the minimum frequency offset can be calculated as 2.45 GHz × 1 × 10^{-6} = 2.45 kHz. Thus, the frequency offset is Gaussian distributed over -49 kHz to 49 kHz. As the systems are stationary, the effect of fading channel is now neglected. Thus, the received signal amplitude from all nodes is equal to 1. As this thesis focuses on the phase synchronization, the perfect timing synchronization across all nodes is assumed in this system.

In the case of N = 4, the expressions (4.14) can be re-written as follows.

$$\mathbf{Y}_4''(s)=\mathbf{A}_{44}\mathbf{y}_4(s)+\mathbf{W}_{BB,4}(s) \tag{4.18}$$

or

$$\begin{bmatrix} Y_1''(s) \\ Y_2''(s) \\ Y_3''(s) \\ Y_4''(s) \end{bmatrix} = \underbrace{\begin{bmatrix} 1 & 1 & 1 & 1 \\ e^{j180^\circ} & 1 & 1 & 1 \\ 1 & e^{j180^\circ} & 1 & 1 \\ 1 & 1 & e^{j180^\circ} & 1 \end{bmatrix}}_{\mathbf{A}_{44}} \begin{bmatrix} y_1(s) \\ y_2(s) \\ y_3(s) \\ y_4(s) \end{bmatrix} + \begin{bmatrix} W_{BB,1}(s) \\ W_{BB,2}(s) \\ W_{BB,3}(s) \\ W_{BB,4}(s) \end{bmatrix} \tag{4.19}$$

where $Y_1(s)$, $Y_2(s)$, $Y_2(s)$ and $Y_4(s)$ are the received signal from retransmissions for the first, second, third and fourth time respectively. Also, $y_1(s)$, $y_2(s)$, $y_3(s)$ and $y_4(s)$ are the transmitting signal and $W_{BB,1}(s)$, $W_{BB,2}(s)$, $W_{BB,3}(s)$ and $W_{BB,4}(s)$ are baseband AWGN. Then, we can extract the original signal by utilizing the inverse matrix, $\mathbf{A}_{44}^{-1}$ as

$$\mathbf{y}_4(s) + \mathbf{A}_{44}^{-1}\mathbf{W}_{BB,4}(s) = \mathbf{A}_{44}^{-1}\mathbf{Y}_4(s) \tag{4.20}$$

or

$$\begin{bmatrix} y_1(s) \\ y_2(s) \\ y_3(s) \\ y_4(s) \end{bmatrix} + \underbrace{\begin{bmatrix} 0.5 & -0.5 & 0 & 0 \\ 0.5 & 0 & -0.5 & 0 \\ 0.5 & 0 & 0 & -0.5 \\ -0.5 & 0.5 & 0.5 & 0 \end{bmatrix}}_{\mathbf{A}_{44}^{-1}} \begin{bmatrix} W_{BB,1}(s) \\ W_{BB,2}(s) \\ W_{BB,3}(s) \\ W_{BB,4}(s) \end{bmatrix} = \underbrace{\begin{bmatrix} 0.5 & -0.5 & 0 & 0 \\ 0.5 & 0 & -0.5 & 0 \\ 0.5 & 0 & 0 & -0.5 \\ -0.5 & 0.5 & 0.5 & 0 \end{bmatrix}}_{\mathbf{A}_{44}^{-1}} \begin{bmatrix} Y_1(s) \\ Y_2(s) \\ Y_3(s) \\ Y_4(s) \end{bmatrix} \tag{4.21}$$

Figure 4.5 shows the original signals of 4 transmitting nodes which are separately sent to the base station, $y_1(s)$, $y_2(s)$, $y_3(s)$ and $y_4(s)$. The initial phase of each

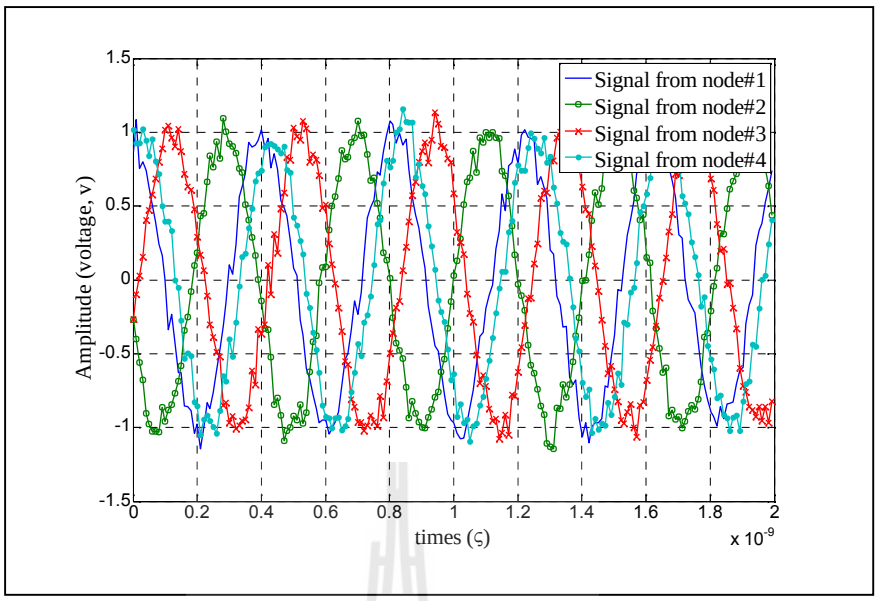

$Y_1(s)$ $Y_2(s)$ $Y_2(s)$ $Y_4(s)$

$\mathbf{y}_4(s)+\mathbf{A}_{44}^{-1}\mathbf{W}_{BB,4}(s)$

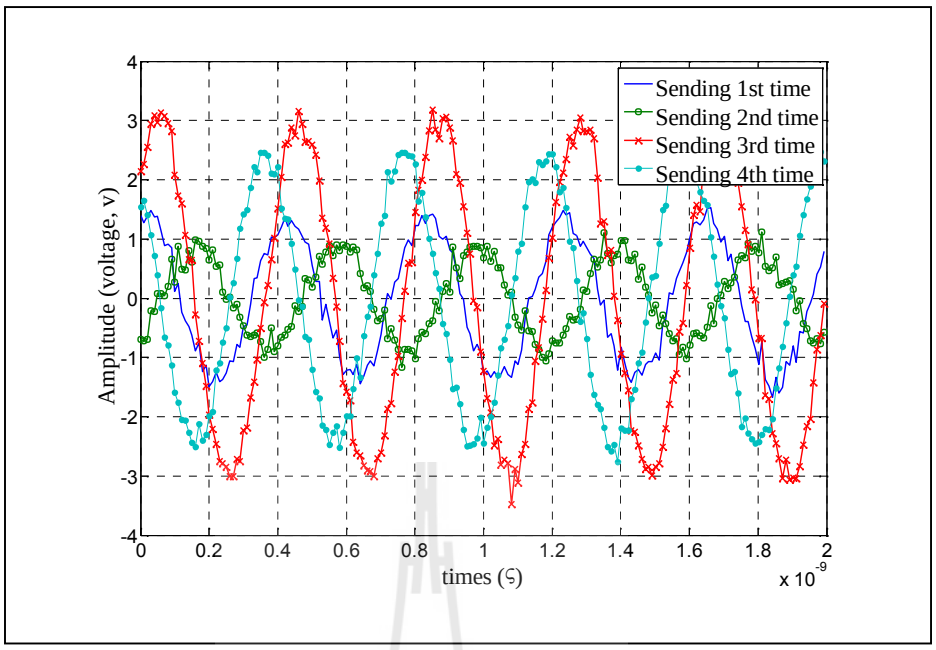

$Y_1(s)$ $Y_2(s)$ $Y_2(s)$ $Y_4(s)$

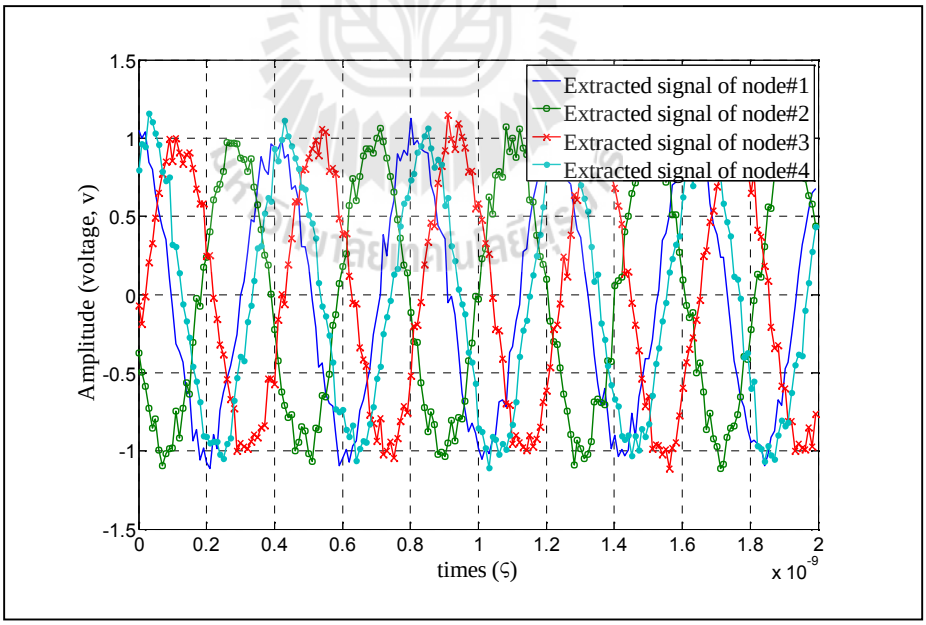

4.2.3 Optimum Weighting Operation

After we obtain the extracted signals as pointed out in the previous step, the signals are sent to the phase weighting block as shown in Figure 4.3. In this block, the phases of extracted signals will be synchronized by utilizing a simple algorithm. The concept behind this synchronization technique is as follows.

(i) The transmitted signal from the 1st node is given to be a reference signal.

(ii) Then, signals from remaining nodes $y_n(s)$ will be weighted by shifting their phases from 0° to 360° in order to find the best weighting coefficients which provide the highest combined signal strength between the reference node $y_1(s)$ and the remaining nodes $y_n(s)$ where n = 2, 3, … , N. As a result, the phase of synchronized signals equal to the chosen reference signal.

Figure 4.8 presents the flow chart of the proposed phase synchronization concept. In the process of finding the best weighting coefficients, we can use a weighting step size which is larger than 1° to reduce the processing time. Figure 4.9 shows a normalized beamforming gain when employing several weighting steps varied from 1° to 100°. In this simulation, we assume that the received signal amplitude from all nodes is equal to 1 having SNR = 20 dB, the number of nodes is 20 and the phase offset is uniformly distributed over 0° to 360°. As we can see in Figure 4.9, a larger weighting step provides lower beamforming gain. This is because a large weighting step may skip the optimum weighting coefficient. However, the weighting step of about 10° provides a similar beam-forming gain as employing a

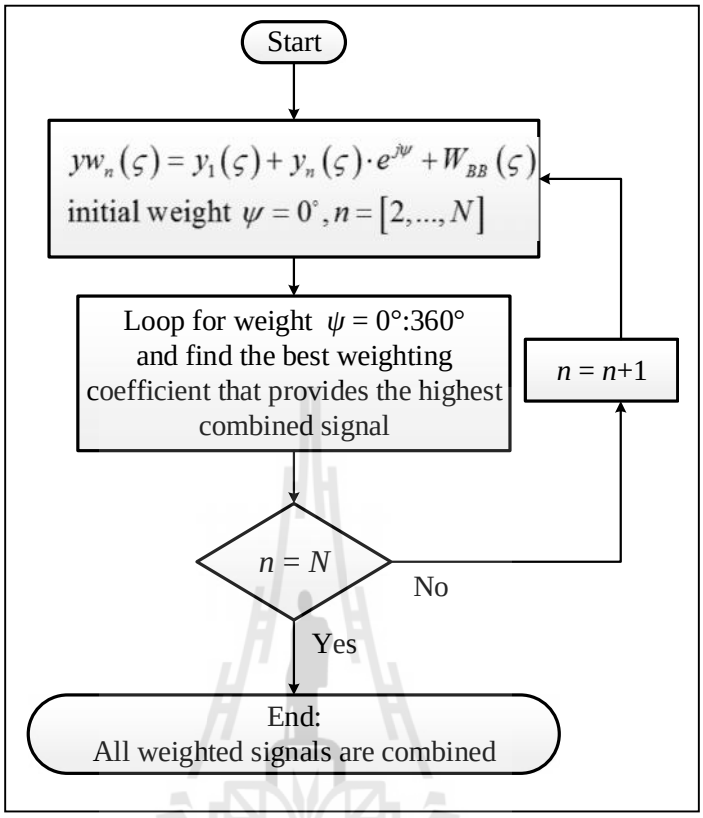
Start
$yw_n(\varsigma) = y_1(\varsigma) + y_n(\varsigma) \cdot e^{j\psi} + W_{BB}(\varsigma)$
initial weight $\psi = 0^\circ, n = [2,...,N]$
Loop for weight ψ = 0°:360° and find the best weighting coefficient that provides the highest combined signal
$n = n+1$
$n = N$
No
Yes
End:
All weighted signals are combined

$Y_{opt}(s)$

$y_1(s)$

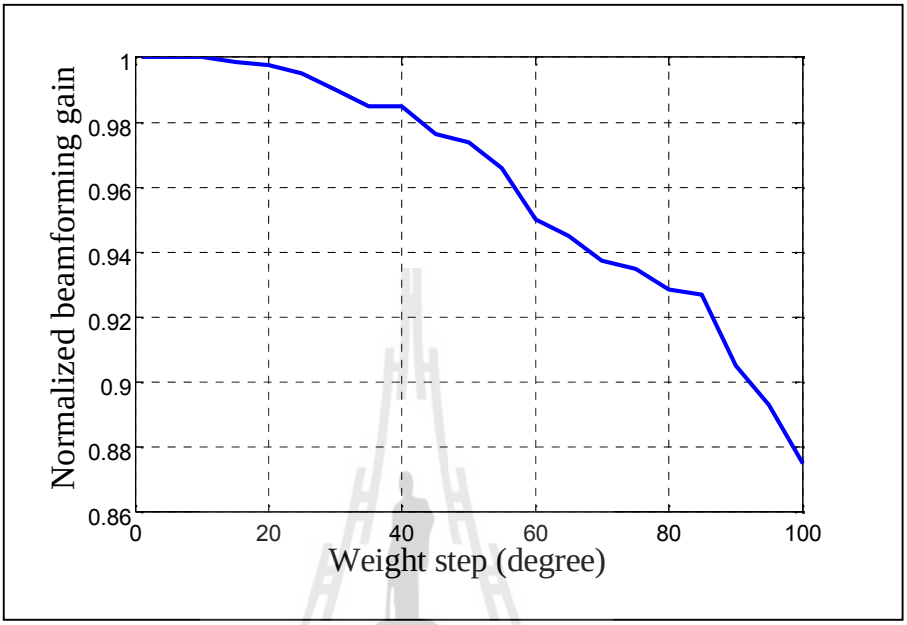
Normalized beamforming gain
1
0.98
0.96
0.94
0.92
0.9
0.88
0.86
0
20
40
60
80
100
Weight step (degree)

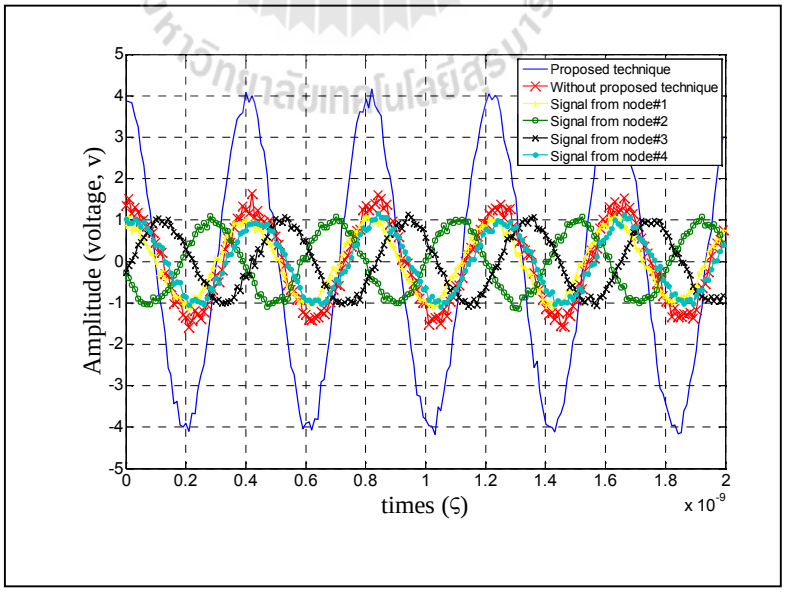
Proposed technique
Without proposed technique
Signal from node#1
Signal from node#2
Signal from node#3
Signal from node#4
Amplitude (voltage, v)
5
4
3
2
1
0
-1
-2
-3
-4
-5
0
0.2
0.4
0.6
0.8
1
1.2
1.4
1.6
1.8
2
times (ς)
x 10^-9

The simulation results in this section also reveal that the proposed non-feedback technique has efficiency over the one-bit feedback and zero-feedback techniques as the proposed technique requires a lower number of retransmissions comparing to the one-bit feedback and zero-feedback techniques. In practical, the proposed non-feedback technique provides $N^2/N = N$ beamforming gain per transmission while the work presented in (Mudumbai R., et,al., (2009)) has stated that the one-bit feedback offers $N^2/5N = N/5$ beamforming gain per transmission with the requirement of at least $5N$ retransmissions in order to achieve 75% guarantee of maximum beamforming gain. For examples, consider employing 3 nodes in the network, the proposed technique and one-bit feedback offer gain per transmission of $3^2/3 = 3$ and $3/5 = 0.6$, respectively. In addition, from (Bletsas A., et.al, (2010) and Sklivanitis G., et.al, (2011)) in case of having 3 transmitting nodes, the zero-feedback technique provides $3^2/50 = 0.18$ beamforming gain per transmission and requires at least 50 retransmissions in order to achieve ≈95% guarantee of maximum beamforming gain. As we can see, the proposed concept offers a higher beamforming gain per one transmission compared to other techniques.

The proposed technique also requires a lower power consumption for phase synchronization than the one-bit feedback and zero-feedback techniques as the proposed technique requires a lower number of retransmissions. For example, the 3 transmitting nodes ($N = 3$) are computer laptops and the typical Wireless LAN transmission power in laptops are 32 mW (milliwatts). Therefore, the proposed technique e. g., one-bit feedback and zero-feedback techniques require the power consumption of $N\times32 = 96$ mW, $5N\times32 = 480$ mW and $50N\times32 = 4{,}800$ mW, respectively.

4.3 Effect of Phase Variation on Proposed Phase Synchronization

According to the proposed non-feedback technique described in previous section, the retransmission signals may be distorted when being transmitted through the channel. Therefore, we further investigate into the effect of phase variation on the proposed non-feedback technique.

We assume that underlying fading channel is Rayleigh flat fading channel and the phase variations are random on Gaussian distribution. The Gaussian distribution generally defines the random behavior of amplitudes and phases of the arriving multipath signals (Gross F. (2005)). The Gaussian probability density function (pdf) is defined as

$$p(\varphi) = \frac{1}{\sqrt{2\pi\sigma^2}} e^{-\frac{(\varphi-\varphi_0)^2}{2\sigma^2}} \quad ; -\pi \le \varphi \le \pi \tag{4.22}$$

where φ is the measured phase value, φ_0 is the mean of phase values and σ is the standard deviation of phase values.

In order to take into account the random phase variations, the received signal (4.15) can be revised as

$$\begin{bmatrix} Y_1(s) \\ Y_2(s) \\ Y_3(s) \\ \vdots \\ Y_N(s) \end{bmatrix} = \underbrace{\begin{bmatrix} 1 & 1 & \cdots & 1 & 1 \\ e^{j(180^\circ+\Delta\varphi_{1,2})} & e^{j(\Delta\varphi_{2,2})} & \cdots & e^{j(\Delta\varphi_{N-1,2})} & e^{j(\Delta\varphi_{N,2})} \\ e^{j(\Delta\varphi_{1,3})} & e^{j(180^\circ+\Delta\varphi_{2,3})} & \cdots & e^{j(\Delta\varphi_{N-1,3})} & e^{j(\Delta\varphi_{N,3})} \\ \vdots & \vdots & \ddots & \vdots & \vdots \\ e^{j(\Delta\varphi_{1,N})} & e^{j(\Delta\varphi_{2,N})} & \cdots & e^{j(180^\circ+\Delta\varphi_{N-1,N})} & e^{j(\Delta\varphi_{N,N})} \end{bmatrix}}_{\Delta\mathbf{A}_{NN}} \times \begin{bmatrix} y(s) \\ y_2(s) \\ y_3(s) \\ \vdots \\ y_N(s) \end{bmatrix} + \begin{bmatrix} W_{BB,1}(s) \\ W_{BB,2}(s) \\ W_{BB,3}(s) \\ \vdots \\ W_{BB,N}(s) \end{bmatrix} \tag{4.23}$$

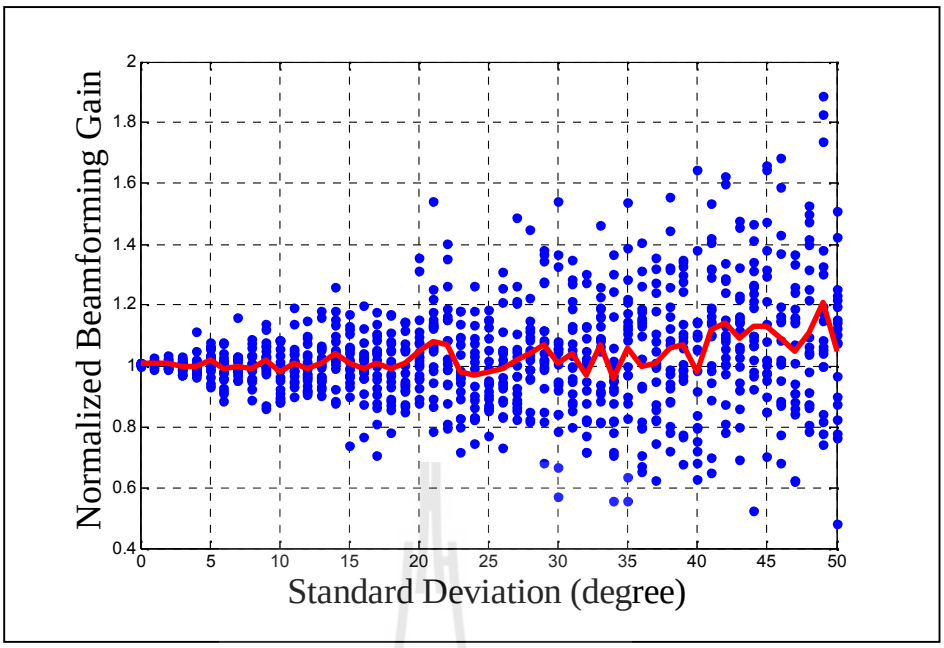

$\Delta\mathbf{A}_{NN}$

$\Delta\mathbf{A}_{NN} \neq \mathbf{A}_{NN}$ $\mathbf{A}_{NN}$

$\mathbf{A}_{NN}^{-1}\Delta\mathbf{A}_{NN} \neq I_{NN}$

$$\mathbf{y}_N(\mathrm{s}) + \mathbf{A}_{NN}^{-1}\mathbf{W}_{BB,N}(\mathrm{s}) = \mathbf{A}_{NN}^{-1}\mathbf{Y}_N(\mathrm{s})$$

$$\mathbf{y}_N(\mathrm{s}) = \left[\mathbf{A}_{NN}^{-1}\Delta\mathbf{A}_{NN}\right] y_N(\mathrm{s})$$

extracted signals in which $\mathbf{y}_N(\mathrm{s})$ depends on the size of phase variation, $\Delta\mathbf{A}_{NN}$. Figure 4.11 shows the normalized beamforming gain of the proposed technique for different standard deviations of phase variation, σ. Note that the number of iterations for the simulation is 20. The solid line represents the average values of all simulations. The simulation results show that the beamforming gain strongly deviates from the correct value of 1 when standard deviation increases. This indicates that the phase of each retransmission is affected by the communication channel.

Moreover, we present an investigation into the phase variation in real environment. The only phase values are measured by a network analyzer. The measured phase values are taken into the (4.12) and (4.24) for the simulation. The simulation model is similar to the model presented in the Section 4.2. The experiment was performed at the telecommunication laboratory, Suranaree University of Technology, Thailand. The floor plan of laboratory is shown in Figure 4.12. The circular markers refer to the measuring locations. There are four measuring locations as follows: location 1 represents the case of near Line-of-Sight (near LOS); location 2 is set up for far LOS; location 3 shows the case of near Non Line-of-Sight (near NLOS); and finally, location 4 is set up for the case of far NLOS. The distances between measuring locations and network analyzer for those 4 cases are 4, 7, 6 and 10 meters, respectively. The configuration of measurement set up is shown in Figure 4.13. The measurement systems consist of a transmitting antenna, receiving antenna, Power Amplifier (PA), Low Noise Amplifier (LNA) and network analyzer. A transmitting signal is generated by network analyzer. Then, the generated signal is amplified by PA before transmitting

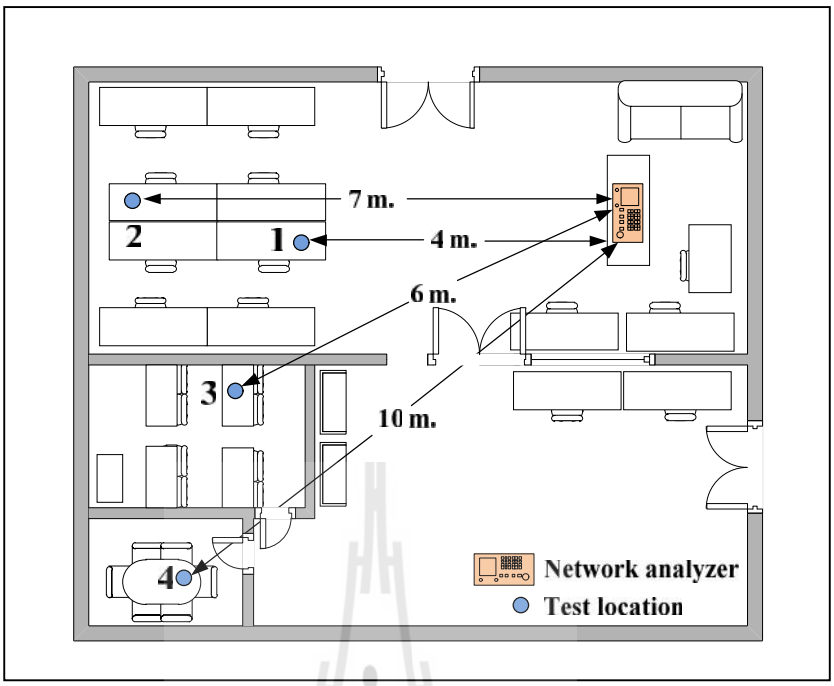
7 m.
4 m.
6 m.
10 m.
1
2
3
4
Network analyzer
Test location

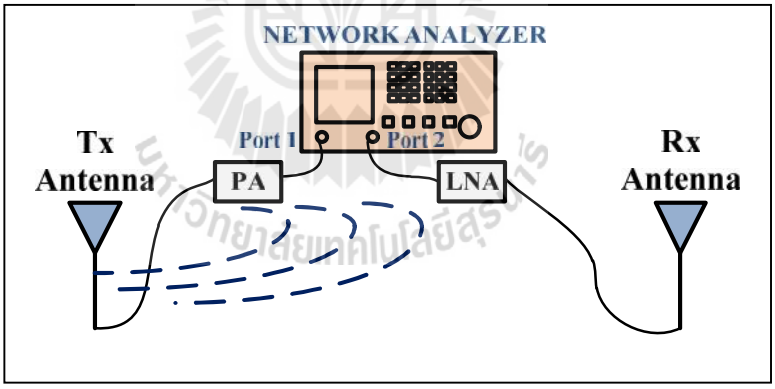
NETWORK ANALYZER
Port 1
Port 2
Tx
Antenna
PA
LNA
Rx
Antenna

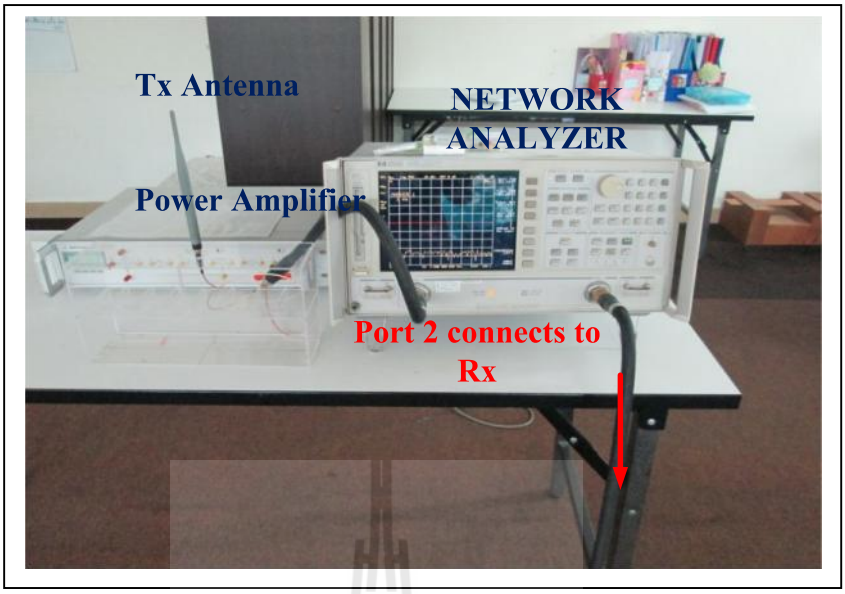
Tx Antenna
NETWORK ANALYZER
Power Amplifier
Port 2 connects to Rx

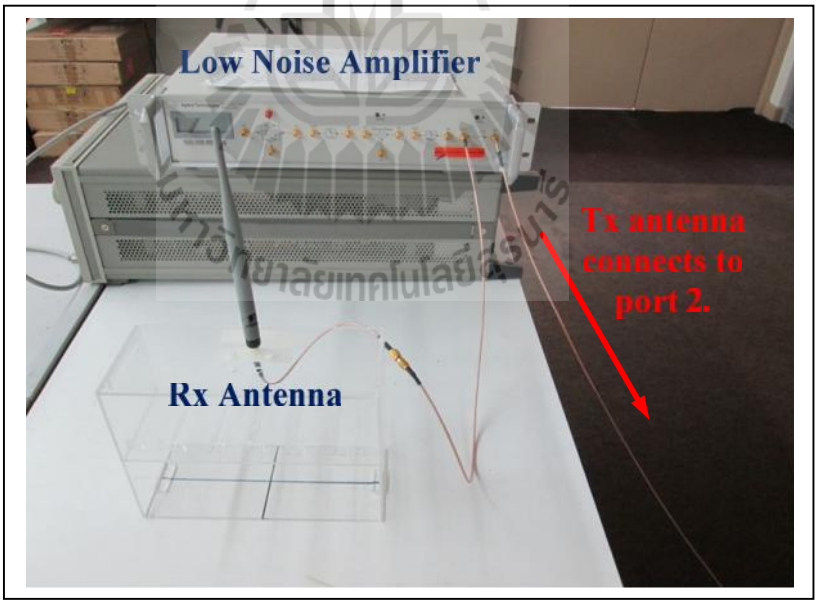
Low Noise Amplifier
Tx antenna connects to port 2.
Rx Antenna

phase is measured by network analyzer. The receiver set up is shown in Figure 4.15. Note that all transmission cables are calibrated before performing measurement.

For off-line processing, we collect the phase of 100 values for each measuring location. Figures 16, 17, 18 and 19 show the phase distribution measured from location 1, 2, 3 and 4, respectively. The histograms show the frequencies of phase value in an instant time. The measured results show that in real environment the size of phase variation or standard deviation is about only 3° to 6° which is shown in Table 4.1. In this case, the proposed non-feedback technique provides average normalized beamforming error as 1.7%, 2.4%, 3.6% and 4.4% when standard deviation is 3°, 4°, 5° and 6°, respectively. Note that the normalized beamforming error is defined by the beamforming gain value with respect to the correct value of 1. For example, the normalized beamforming gain is 1.02 then the average normalized beamforming error is $(0.98 - 1)\times 100 = 2\%$. For the worst case when the standard deviation is 6°, the beamforming error is only 4.4%.

This error has slightly impacted on beamforming gain as shown in Figure 4.20. This figure shows the combined signal for 4 extracted signals which are obtained using proposed non-feedback technique. The standard deviation of phase variation is 6° (worst case). Also, the phase offset and frequency offset are Gaussian distributed in which the phase offset is random over $-\pi$ to π and the frequency offset is random over –49 kHz to 49 kHz. The results show that the combined signal amplitude is ~3.9 (5.9 dB) from the maximum amplitude at 4 (6 dB). Thus, the beamforming error is $(0.1/4) \times 100 = 2.5\%$. However, the phase of combined signal is slightly offset as the phase of reference node, node 1 is −98.9° while the phase of combined signal which provided

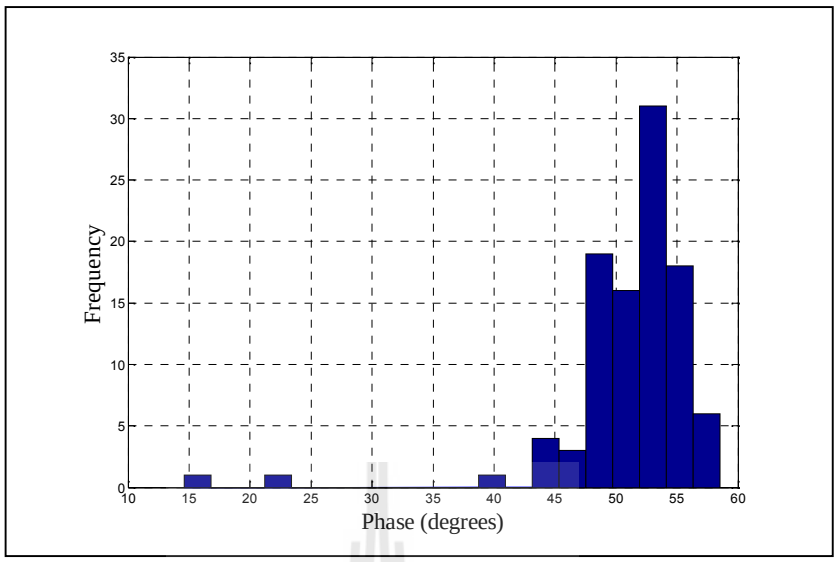
Frequency
Phase (degrees)
0
5
10
15
20
25
30
35
10
15
20
25
30
35
40
45
50
55
60

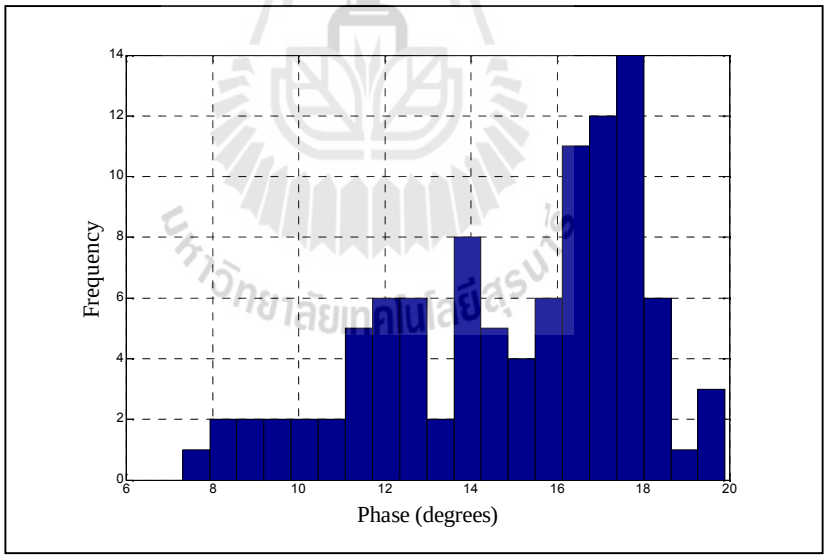
Frequency
Phase (degrees)
0
2
4
6
8
10
12
14
6
8
10
12
14
16
18
20

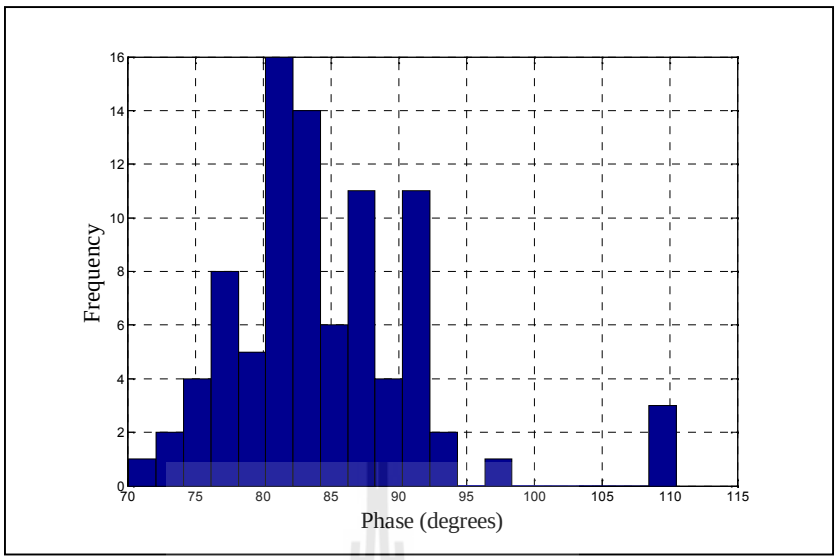
Frequency
Phase (degrees)
0
2
4
6
8
10
12
14
16
70
75
80
85
90
95
100
105
110
115

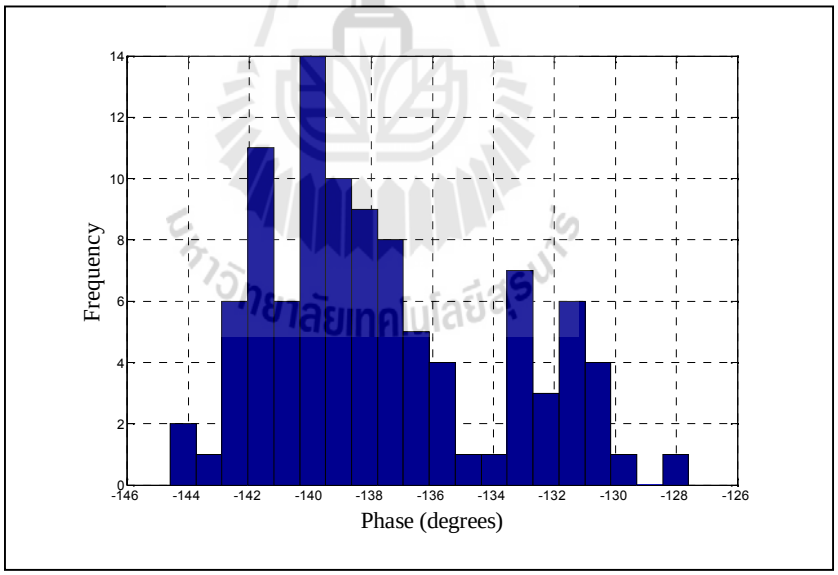
Frequency
Phase (degrees)
0
2
4
6
8
10
12
14
-146
-144
-142
-140
-138
-136
-134
-132
-130
-128
-126

Table 4.1 Mean and standard deviation of measured phase.

Test Locations	Mean	σ
Location 1 near-LOS	51.2°	5.8°
Location 2 far-LOS	14.9°	2.9°
Location 3 near- NLOS	83.5°	5.5°
Location 4 far-NLOS	-137.7	3.8°

by using the proposed technique is −83.2°. Thus, the phase error is (15.7°/98.9°)×100 = 16%. Figure 4.21 shows the average beamforming gain (dB) of the proposed technique which is affected by the worst case phase variation (standard deviation is 6°). Note that the number of simulation for an average value is 50 times. The proposed beamforming gain of proposed non-feedback technique is comparable to a perfect phase synchronization at every number of nodes. Therefore, in real environment where the phase changes by time, the proposed non-feedback technique still works very well.

4.4 Performance Comparison

In this section, the performance in terms of beamforming gain, BER and complexity of literatures (in Chapter 3) and proposed one is compared. In the simulation, the received signals at base station have unit amplitudes, $A_n = 1$. The random initial phase of each node is uniformly distributed over $-\pi$ to π. The effects of fading channel and Doppler are neglected. According to a performance comparison results focused on the phase synchronization, the perfect timing and frequency synchronizations across nodes are assumed.

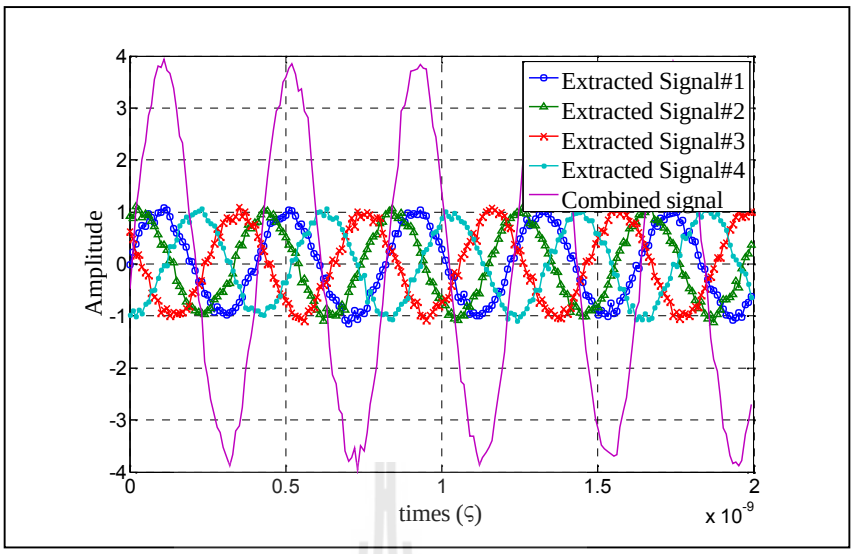
Extracted Signal#1
Extracted Signal#2
Extracted Signal#3
Extracted Signal#4
Combined signal
Amplitude
times (s)
x 10^-9

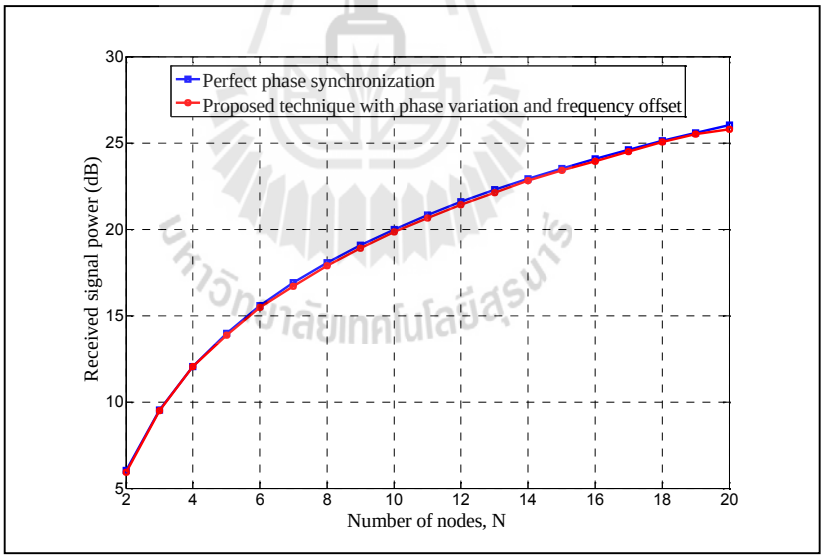
Perfect phase synchronization
Proposed technique with phase variation and frequency offset
Received signal power (dB)
Number of nodes, N

4.4.1 Beamforming Gain Comparison

Figure 4.22 shows the average gains for the cases of proposed non-feedback and time-slot round-trip are equal to the case of perfect phase synchronization where the number of transmitting nodes is varied from 2 to 10 nodes and SNR of 20 dB. The weighting step of 10° is used. Note that the reason of choosing the weighting step of 10° has been mentioned earlier. The results show that the non-feedback and time-slot round-trip techniques are comparable in terms of beamforming gain. However, the proposed non-feedback technique is preferable as it does not require any feedback from the base station while the time-slot round-trip technique requires a reference signal transmitted back from the base station. Moreover, the proposed non-feedback technique does not require any interaction between nodes while time-slot round-trip technique does. Although, the master-slave technique also does not require any feedback from the base station but it requires an interaction between transmitting nodes. This introduces a complexity to the systems. Moreover, the beamforming gain of the master-slave technique may be distorted by an uncompensated VCO phase drift. This phase drift is occurred by the internal oscillator noise and over time of phase compensation in the open loop mode, while the slave nodes are transmitting. Thus, the slave's carrier signals can be drifted out of phase (Mudumbai R., (2007)).

According to the number of retransmissions is limited to 50, the one-bit feedback and zero feedback techniques provide lower beamforming gain compared with the proposed one. This is because the one-bit feedback and zero feedback technique require a large number of retransmissions to achieve the maximum

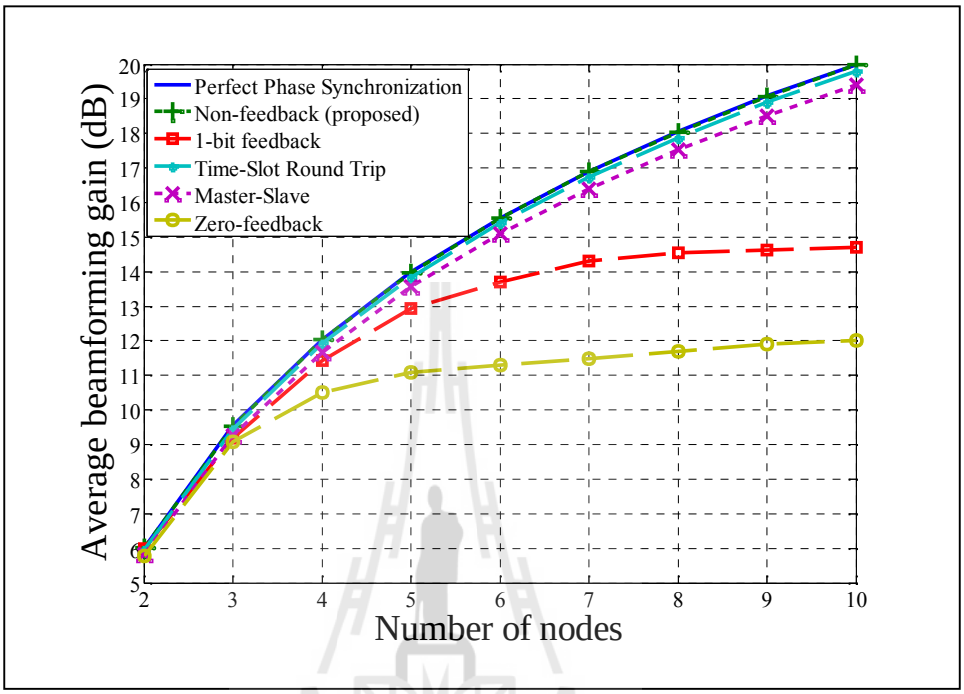
Perfect Phase Synchronization
Non-feedback (proposed)
1-bit feedback
Time-Slot Round Trip
Master-Slave
Zero-feedback
Average beamforming gain (dB)
Number of nodes
20
19
18
17
16
15
14
13
12
11
10
9
8
7
6
5
2
3
4
5
6
7
8
9
10

of the maximum beamforming gain when having 3 and 4 transmitting nodes respectively (Bletsas A., et.al, (2010)). That means only 50 retransmissions is not enough to archive the maximum beamforming gain when $N \geq 3$. Therefore, the proposed non-feedback technique has the following advantages over other phase synchronization techniques: higher effective gain with lower number of retransmissions. Also, it avoids interactions between transmitting nodes and also does not require any feedback signal from the base station.

4.4.2 BER Comparison

We assume that the number of transmitting node is 10. Figure 4.23 shows the BER comparison where the number of retransmissions is not limited. The results show that the BER of proposed technique and the literatures are comparable with the perfect phase synchronization. Because, the one-bit feedback and zero-feedback techniques have enough the number of feedback or retransmission signal to perform the optimum phase synchronization. Master-slave and round-trip technique do not require the large number of retransmissions signal to perform the phase synchronization. Thus, the BER of master-slave and round-trip technique is comparable with the perfect phase synchronization. However the beamforming gain of the master-slave technique may be distorted by an uncompensated VCO phase drift (Mudumbai R., (2007)). However, the unlimited retransmission signal may be impractical as the battery life of transmitting nodes is very limited. Therefore, Figure 4.24 shows the BER comparison where the number of retransmissions are limited for 50 times. The results show that the BER of one-bit feedback is degraded as it requires the number of retransmissions signal at least $10N$ in order to achieve 90% guarantee of perfect or maximum beamforming gain (Mudumbai R., (2010)). Thus, in the case

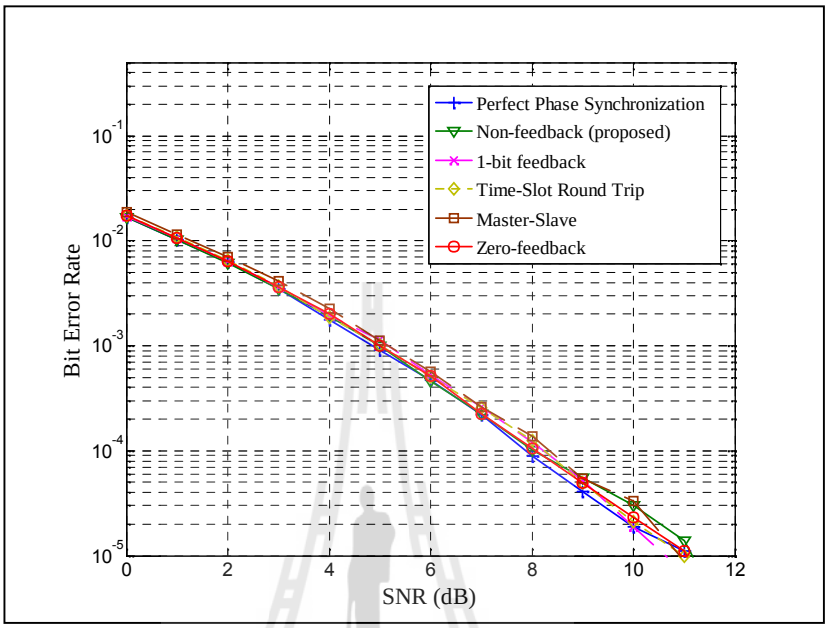
Perfect Phase Synchronization
Non-feedback (proposed)
1-bit feedback
Time-Slot Round Trip
Master-Slave
Zero-feedback
Bit Error Rate
SNR (dB)

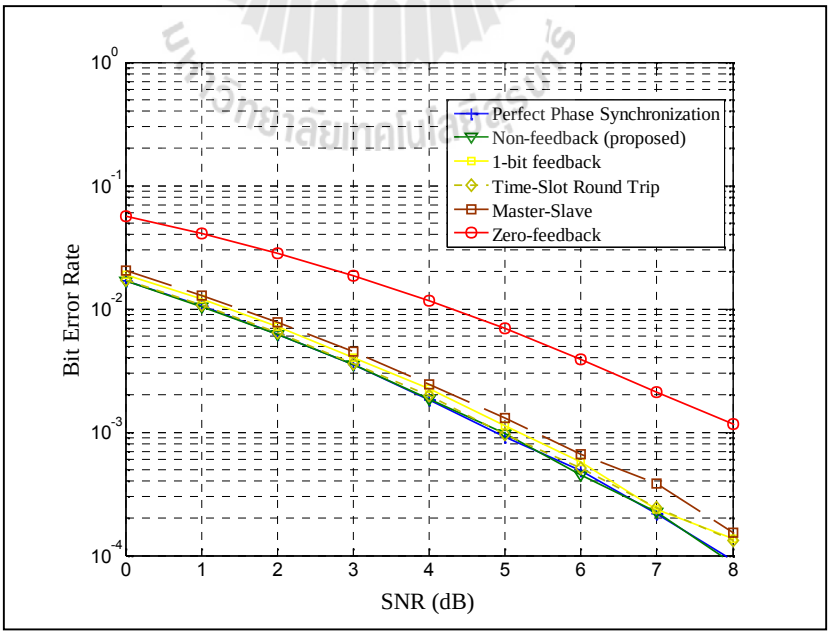
Perfect Phase Synchronization
Non-feedback (proposed)
1-bit feedback
Time-Slot Round Trip
Master-Slave
Zero-feedback
Bit Error Rate
SNR (dB)

the BER compared to perfect phase synchronization. The zero feedback also has the similar problem with one-bit feedback technique. The zero-feedback require the number of retransmissions signal larger than 700,000 times where number of node is 10 as discussed in the Figure 3.14. BER of maser-slave technique can be degraded by the phase drift as presented in Figure 3.9.

4.4.3 Complexity Comparison

The complexity of literatures and proposed technique are investigate by using FLoating-point Operations Per Second (FLOPS) which can indicate the complexity of calculation (Golub G. H., et.al., (1991)). The number of FLOPS increase as a complexity of algorithm increases. Table 4.2 shows the number of FLOPS of the basic mathematical operation (Uthansakul P., (2009)). Note that the procedure of each literatures which use for calculation FLOPS are presented earlier in Chapter 3. Table 4.3 shows the FLOPS calculation of the one-bit feedback technique where N is the number of nodes and I is the number of retransmissions signal. According to the master-

slave and round-trip technique utilize the PLLs to estimate the phase of the pilot signals, the Table 4.4 shows the FLOPS calculation of PLL where $s = j2\pi f$, C_p is the magnitude of the phase step in radians, H is the product of the individual feedback transfer function, f_{out} is the output frequency and f_{ref} is the reference frequency (Nash G., (2006)). Table 4.5 and 4.6 shows the FLOPS calculation of the master-slave and round-trip technique respectively where N is the number of the transmitting nodes and

V is the number of iteration in PLL. Table 4.7 shows the FLOPS calculation of the zero- feedback technique where N is the number of the transmitting nodes and I is the

number of retransmissions signal. Table 4.8 shows the FLOPS calculation of the proposed non-

Table 4.2 Number of FLOPS of the basic mathematical operation.

Operation	**FLOPS**
$a + b$	1
$a \cdot b$	1
$(a + jb) + (c + jd)$	2
$(a + jb) \cdot (c + jd)$	6
$\lvert a + jb \rvert^2$	3
$\sin(a),\ \ln(a),\ \log_2(a)$	0

Table 4.3 FLOPS calculation of the one-bit feedback technique.

Algorithm	**FLOPS**
Initial transmitting signal $Y = x(t)\sum_{n=1}^{N} \sim_n A e^{j(\mu t + \_n + ¥_n + \cdot\cdot_n)}$	$2(N-1)$
Base station estimate a received signal. $\_{}_{n,i+1} = \begin{cases} \_{}_{n,i} + ¢_{n,i}, & Y_i > Y\_best_i \\ \_{}_{n,i}, & \text{otherwise} \end{cases}$	1
Transmitting nodes adjust their phase and retransmissions. $Y_i = x(t)\sum_{n=1}^{N} \sim_n A e^{j(\mu_c t + \Phi_n)} e^{j¢_{n,i}}$	$6N + 2(N-1)$
Number of retransmissions	I

Total	$8NI - I + 2N - 2$

Table 4.4 FLOPS calculation of PLL.

Algorithm	**FLOPS**
Phase estimation $\bar{}_e(s) = \frac{(s+a)C_p}{(s^2+as+H)}$	11
Number of loops iteration in PLL f_{out}/f_{ref}	V
Total	$11V$

Table 4.5 FLOPS calculation of the master-slave technique.

Algorithm	**FLOPS**
Master node transmits a pilot signal to slaves. $c_{n,0}(t) = \Re\left(A_{n,0}e^{j(\mu_c t + ¥_0 - ¥_n)}\right)$	1
Slave nodes estimate the phase of the pilot signal by using PLL.	$11V(N-1)$
Slave nodes bounce a signal back to the master node. $c_{n,1}(t) = A_{n,1}\Re\left(A_{n,0}e^{j(\mu_c t + ¥_0 - 2¥_n)}\right)$	$(N-1)$
Master node estimates the phase of received signal. $\Delta¤_n = (2¥_n \bmod 2®)$	$2(N-1)$
Slave nodes estimate the phase of the pilot signal by using PLL	$11V(N-1)$
Base station transmits a beacon signal to all nodes. $g(t) = \Re\left(e^{j(\mu_c t + ¤_0)}\right)$	1
All nodes estimate the phase of received signal by using PLL.	$11V(N-1)$
Slave nodes mod the estimated signal. $c_n^o(t) = \Re\left(e^{j\left(\mu_c t + ¤_n^e + ¤_n^d(t)\right)}\right)$	$(N-1)$
All nodes transmit signal to the base station $r(t) = \Re\left(m(t)\sum_{n=1}^{N}\lvert h_n\rvert^2 e^{j\left(\mu_c t - ¤_n^h + 2¤_n^e + ¤_n^d(t)\right)}\right)$	$2(N-1)$
Total	$4N + 3VN - 4$

Table 4.6 FLOPS calculation of the round-trip technique.

Algorithm	FLOPS
TS 0: The destination transmits the sinusoidal primary beacon to both sources	$V \cdot N$
TS 1: S_1 transmits a sinusoidal beacon to S_2.	$V \cdot (N-1)$
TS 2: S_2 transmits a sinusoidal beacon to S_1.	$V \cdot (N-1)$
TS 3: Both sources transmit simultaneously to the destination as a distributed beamformer.	N
Total	$3VN - 2V + 3N - 1$

Table 4.7 FLOPS calculation of the zero-feedback technique.

Algorithm	FLOPS
Base station estimate a received signal. $y[b] = \sum_{n=1}^{N} h_n e^{\{j2\pi\Delta f_n b T_s + \theta_n\}} x[b] + w[b]$	$2(N-1)$
Number of retransmissions.	I
Total	$2I(N-1)$

Table 4.8 FLOPS calculation of the proposed non-feedback technique.

Algorithm	FLOPS
Phase adjustment at all nodes	$6(N-1)$
Number of retransmissions.	N
Inverse matrix calculation, $\mathbf{A}_{NN}^{-1}$	$\frac{1}{3}N^3 + \frac{2}{3}N$
Extraction signal. $\mathbf{y}_N(s) + \mathbf{A}_{NN}^{-1}\mathbf{W}_{BB,N}(s) = \mathbf{A}_{NN}^{-1}\mathbf{Y}_N''(s)$	$2N^2 - N$
Weighting the extracted signals. $yw_n(s) = y_1(s) + y_n(s) \cdot e^{j\cdot} + W_{BB}(s)$	$8(N-1)$
Weighting step 0° to 360°	U
Combing signal	$2(N-1)$
Total	$\frac{1}{3}N^3 + 2N^2 + 8K + 8UN + \frac{2}{3}N - 8U - 8$

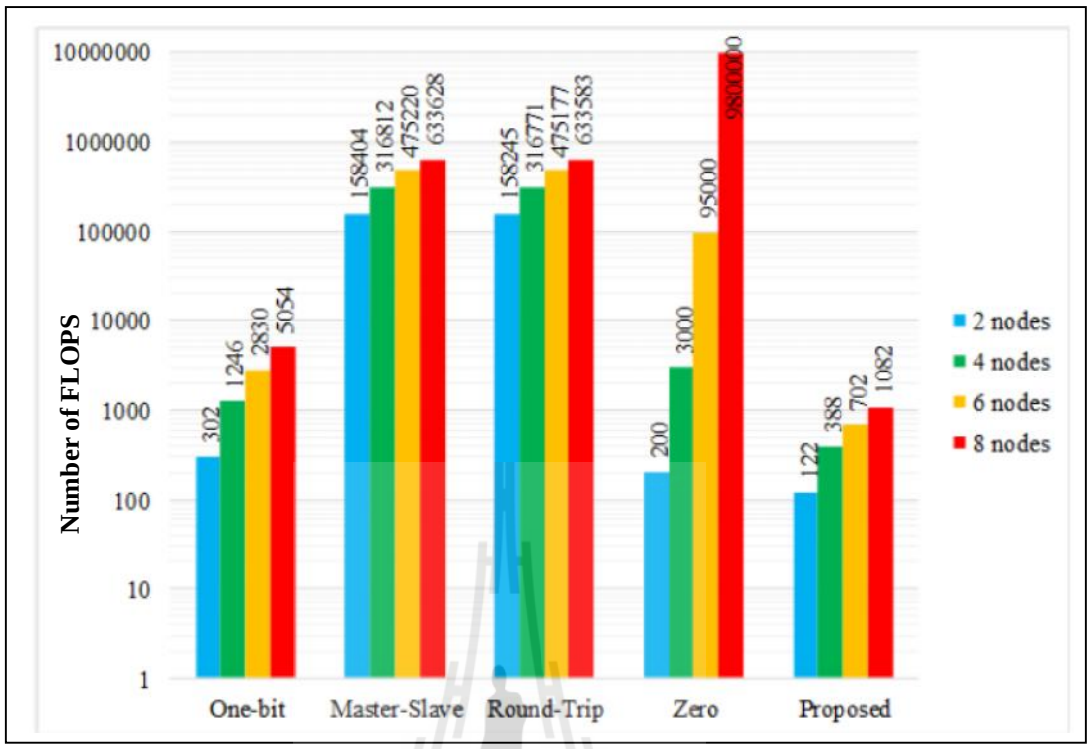

Figure 4.25. FLOPS comparison of proposed non-feedback technique vs. existing techniques.

feedback technique which discussed in Section 4.2 where N is the number of the transmitting nodes and U is the number of iteration in the optimum weighting operation.

Figure 4.25 shows FLOPS comparison where number of the transmitting nodes is 10 nodes, $N = 10$. For one-bit feedback technique, the number of retransmissions of $10N$ iterations (in order to achieve 90% guarantee of maximum beamforming gain) is assumed. For master-slave and round-trip technique, the output frequency and reference frequency for PLL are defined as, f_{out} = 480 MHz and f_{ref} = 200 kHz (Nash G., (2006)). Thus, number of loop in PLL, V, is 2,400. For zero-feedback technique, the number of iteration is referred by Figure 3.14. For proposed

non-feedback technique the weighting step as 30° is used, U = 13. The results in Figure 4.25 shows that the proposed non-feedback technique has a lowest complexity as it requires a lower number of retransmissions from nodes, which is only the same as the number of transmitting nodes, N. However, the one-bit feedback and zero feedback technique have higher complexity than the proposed technique as they require the large number of transmissions in order to archive the optimum beamforming gain. The master-slave and round-trip also have higher complexity as they have phase estimation in the PLL which requires a large number of iteration.

4.5 Chapter Summary

This chapter has proposed an alternative phase synchronization technique, so called non-feedback distributed beamforming technique. The algorithm of proposed non-feedback is presented in Section 4.2. Using the proposed technique, phase synchronization can be accomplished at base station instead of mobile terminals. The proposed technique requires a lower number of retransmissions comparing to one-bit feedback and zero-feedback techniques. Also, the proposed non-feedback technique does not require any feedback signal and interaction between transmitting nodes. Table 4.9 summarizes the requirement comparison between proposed non-feedback and literatures. Moreover, the proposed non-feedback technique is analyzed under the real environment having random phase variation of the transmitted signal as presented in Section 4.3. The obtained results prove that the proposed technique is stable in a real environment. From the simulation results in Section 4.4, the proposed non-feedback technique provides a high beamforming gain compared with the literatures.

Moreover, the proposed technique provides lower complexity and BER than the literatures.

Table 4.9 Requirement comparison between proposed non-feedback and literatures.

	Requirement		
Technique	**Feedback signal from the base station**	**Large number of retransmissions**	**Reference signal among nodes**
One-bit	✓	✓	
Master-Slave	✓		✓
Round-Trip	✓		✓
Zero-feedback		✓	
Non-feedback			

CHAPTER V

AN EXPERIMENTAL STUDY OF NON-FEEDBACK DISTRIBUTED BEAMFORMING

5.1 Introduction

In a real circumstance, the proposed non-feedback distributed beamforming can be affected by characteristic of communication channel such as phase variation or fading. Therefore, the experimental study of proposed techniques is considered in order to validate the proposed technique. A testbed consisting of two transmitting nodes and one base station was developed under SDR technology. The testbed utilizes a Universal Software Radio Peripheral (USRP) as it provides high speed ADCs, DACs, FPGA and USB interface support (Clark C. (2008)). This chapter consists of five section as presented in Figure 5.1. The Section 5.1 is an introduction of the chapter. Section 5.2 discusses the Software-defined radio (SDR) which utilized as a testbed. The experiments are separated into two parts : Section 5.3 is an experiment on received signal power and Section 5.4 is an experiment on BER. The first one presents the proposed technique provides a gainfully combined signal at base station while the latter presents the enhancement of system performance in terms of BER. Finally, the chapter is concluded in Section 5.5.

5.2 Software-Defined Radio

Software-defined radio (SDR) is a radio communication technology based on software defined wireless communication protocols instead of hardware (e.g. mixers,

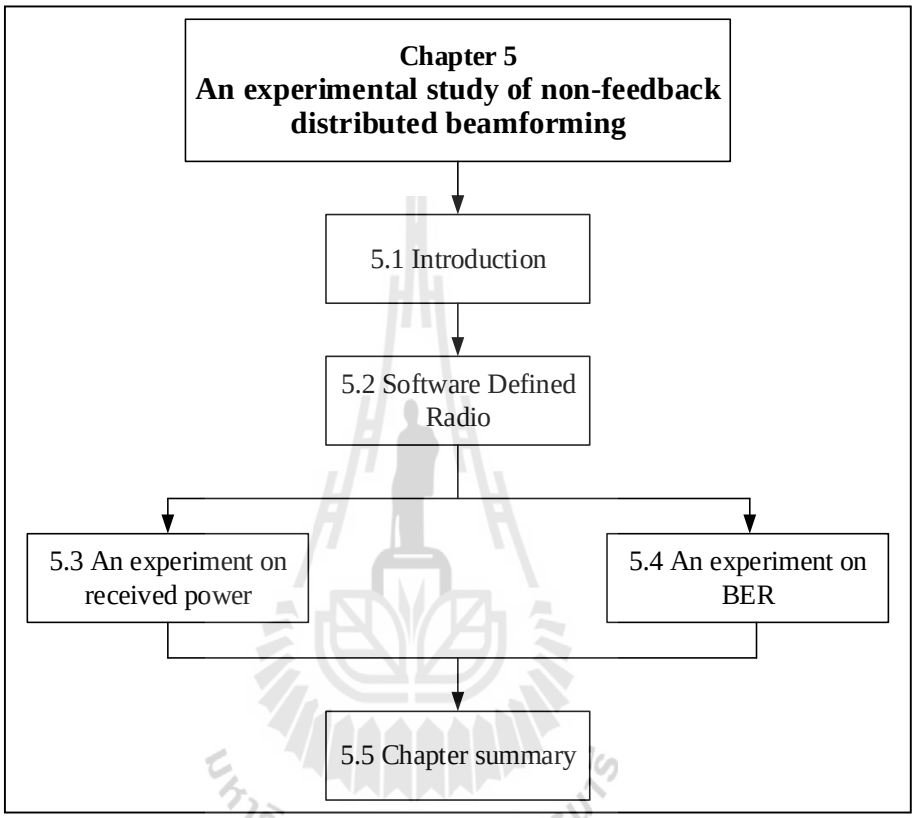

Figure 5.1 Route map of study in Chapter V.

filters, amplifiers, modulators/demodulators, detectors, etc.) (Clark C. (2008)). Thus, SDR reduces the component cost because hardware specific components are replaced by DSPs and FPGAs. The basic ideal of SDR is presented in Figure 5.2. The ideal receiver attaches an analog-to-digital converter to an antenna. A digital signal processor reads the converter and then its software transforms the stream of data from the converter to any other forms the application require. The ideal transmitter is similar to the receiver. A digital signal processor generates a stream of digital data

(usually binary). These data are sent to a digital-to-analog converter in order to converts digital

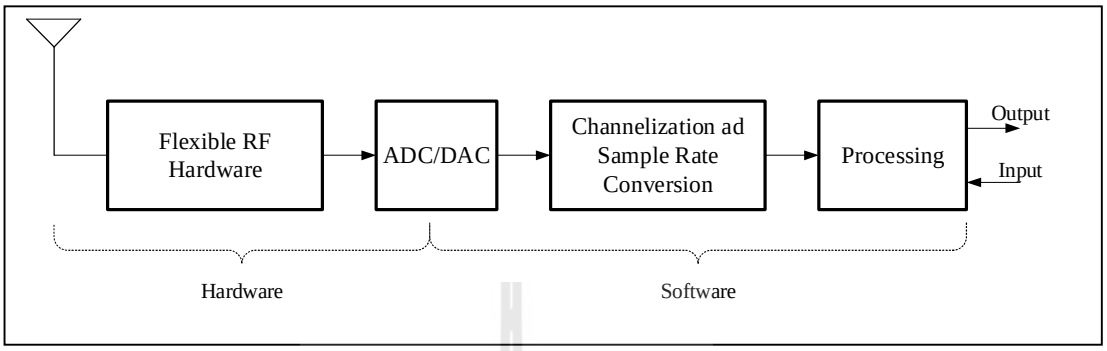

Figure 5.2 Configuration of SDR.

data into an analog signal which is amplified by RF hardware. Then, the amplified analog signal is transmitted by a radio antenna.

5.2.1 Equipment List

For this thesis, the USRP1, USRP B100, XCVR2450 and SBX daughter boards (or RF broads) were equipped in the testbed. These equipment is provided by Ettus Research.

A USRP1 is the original hardware of the USRP (Universal Software Radio Peripheral) family of products, which enables engineers to rapidly design and implement powerful, flexible software radio systems (Ettus, (2015)). Figure 5.3 shows a USRP1 module. The USRP1 has the features as follows.

- Altera Cyclone FPGA
- Two dual 64 MS/s, 12-bit ADC's
- Two dual 128 MS/s, 14-bit DAC's
- DDC/DUC with 15 mHz resolution

- Up to 16 MS/s USB 2.0 streaming
- Auxiliary digital and analog I/O
- 25 ppm frequency accuracy reference

A USRP B100 is an ideal model for users that require an entry-level software defined radio device for cost-sensitive applications (Ettus, (2015)). The B100 hardware provides low-cost RF processing capability. Figure 5.4 shows the USRP B100 module. The B100 has the features as follows

- Spartan 3A-1400 FPGA
- Two dual 64 MS/s, 12-bit ADC's
- Two dual 128 MS/s, 14-bit DAC's
- DDC/DUC with 15 mHz resolution
- Up to 16 MS/s USB 2.0 streaming
- Auxiliary digital and analog I/O
- 2.5 ppm frequency accuracy reference

Ettus research offers many daughter boards with differing features. The daughter boards are easily installed and available for almost any project. In this thesis, the XCVR2450 and SBX daughterboard are utilized for the USRP1 and B100 respectively. Figure 5.5 and 5.6 shows the XCVR2450 and SBX daughterboard modules respectively. A XCVR2450 daughterboard has the features as follows

- Support dual band: 2.4-2.5GHz, 4.9-5.9GHz
- The typical power output of the XCVR2450 is 100 mW.

A SBX daughterboard has the features as follows.


Ettus
Research
USRP
Universal Software Radio Peripheral


Ettus Research
USRP B100

- A typical noise figure is 5 dB.

In this work, a VERT2450 antenna shown in Figure 5.7 is used. The VERT2450 antenna has the features as follows.

- Omni-directional vertical antenna
- Support dual band: 2.4 to 2.48 GHz and 4.9 to 5.9 GHz.
- Provides 3dBi Gain.

5.2.2 GNU Radio Companion

In this experiment, the proposed non-feedback technique is developed by utilizing the USRP family of boards with the GNU Radio Companion (GRC). The GRC is an open-source software development toolkit which contains the signal processing blocks used for implementing SDR (Clark C. (2008)). The GRC provides a graphic user interface of GNU Radio and the signal processing blocks, allowing a system to be quickly constructed. The signal processing blocks of GRC are primarily written using the Python programming language, while the performance-critical signal processing path is implemented in C++ using processor floating point extensions. Thus, the developer is able to implement real-time, high-throughput radio systems in a simple-to-use and rapid-application-development environment. Therefore, GRC enables the user a wide range of flexibility such as smart antennas and wireless sensor networks.

5.3 An Experiment on Received Signal Power

Figure 5.8 shows the configuration of experiment setup to measure the received signal power including two USRP1. A cosine wave is transmitted using the

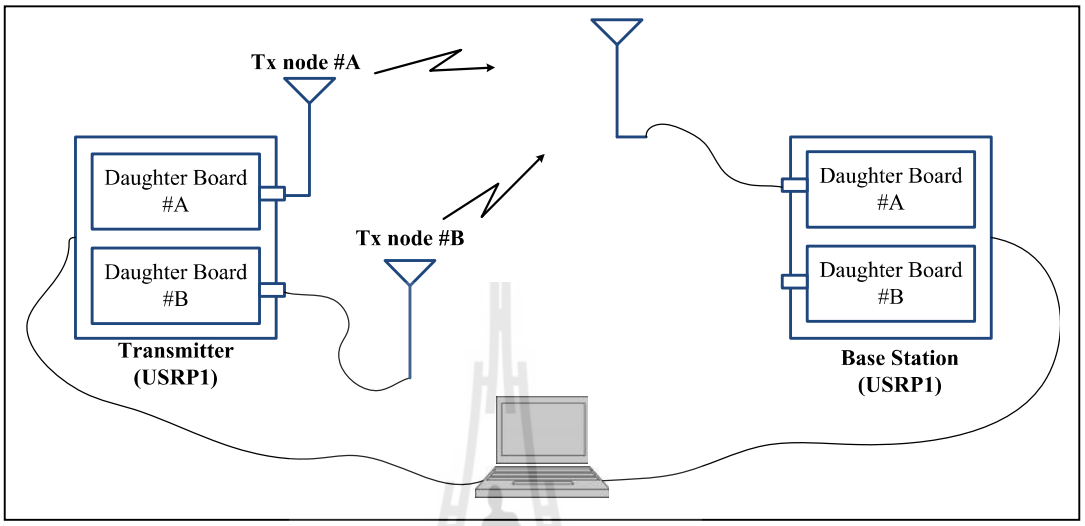
Tx node #A
Tx node #B
Daughter Board #A
Daughter Board #B
Transmitter (USRP1)
Daughter Board #A
Daughter Board #B
Base Station (USRP1)

USRP1 by utilizing a network analyzer. Figure 5.11 presents a calibrated power in which the optimum programming gain is 29 dB which provides a transmitting gain of 24.8 dB.

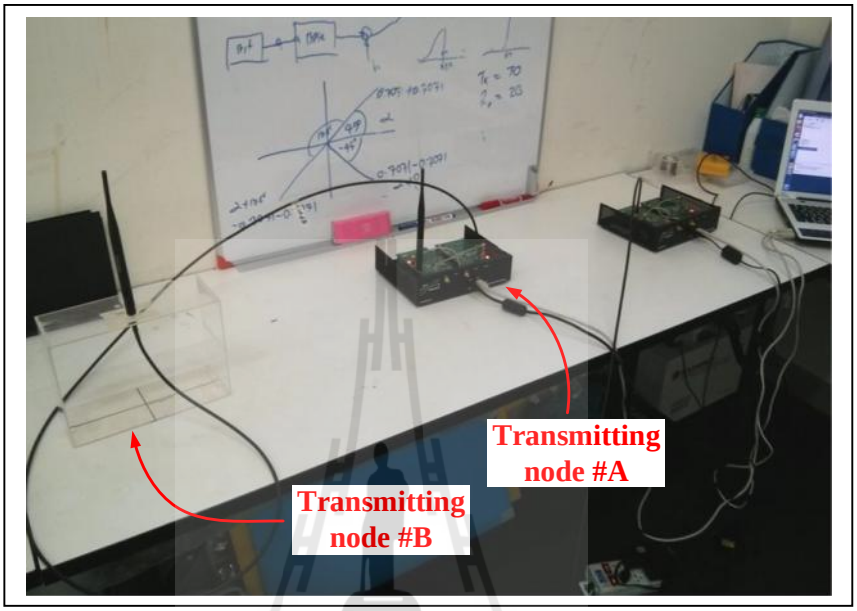

Figure 5.9 Configuration of the two transmitting nodes on received signal power.

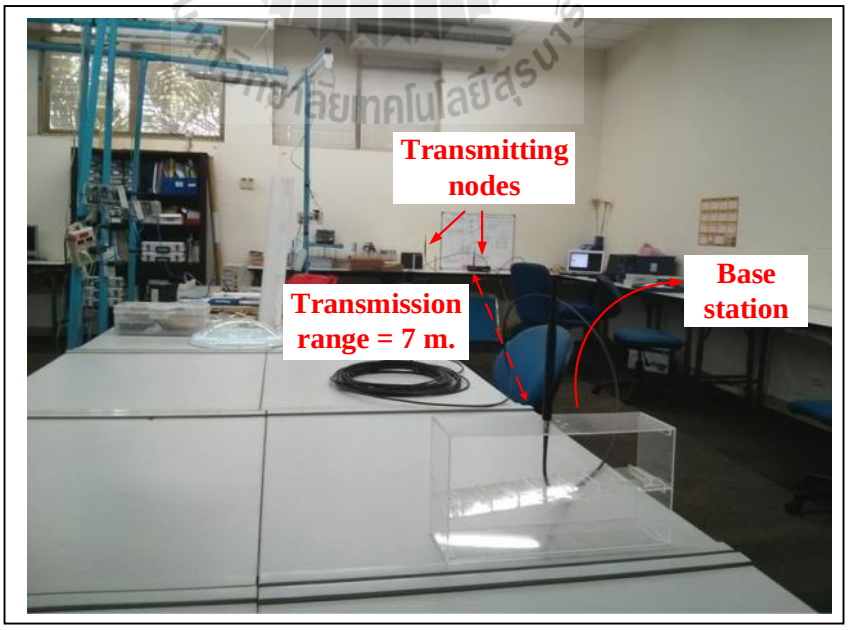

Figure 5.10 Configuration of the base station on received signal power.

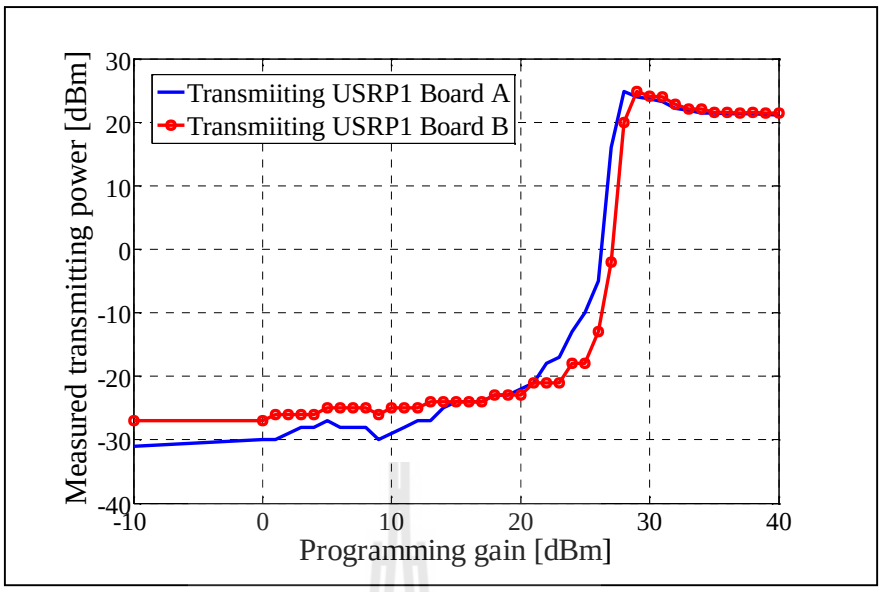
Transmiiting USRP1 Board A
Transmiiting USRP1 Board B
Measured transmitting power [dBm]
Programming gain [dBm]
30
20
10
0
-10
-20
-30
-40
-10
0
10
20
30
40

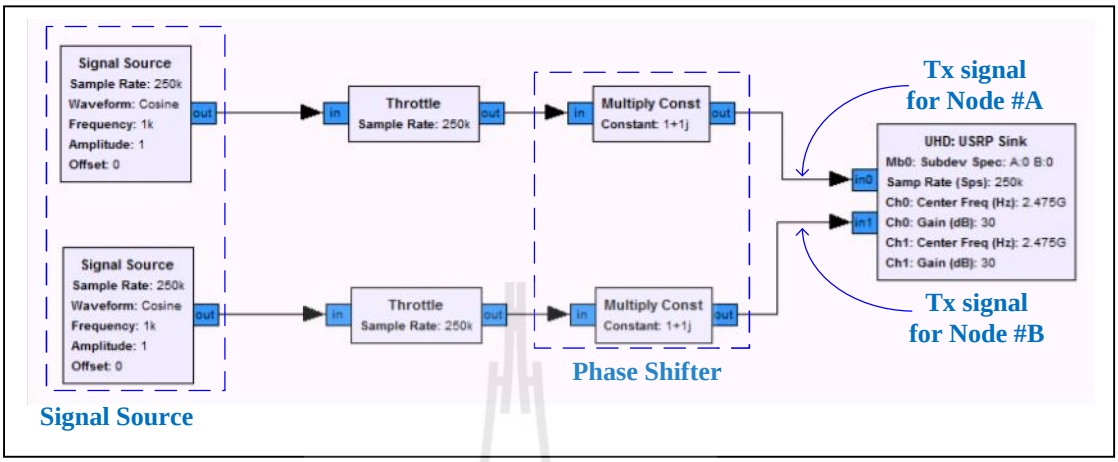
Signal Source
Sample Rate: 250k
Waveform: Cosine
Frequency: 1k
Amplitude: 1
Offset: 0
Signal Source
Sample Rate: 250k
Waveform: Cosine
Frequency: 1k
Amplitude: 1
Offset: 0
Throttle
Sample Rate: 250k
Throttle
Sample Rate: 250k
Multiply Const
Constant: 1+1j
Multiply Const
Constant: 1+1j
UHD: USRP Sink
Mb0: Subdev Spec: A:0 B:0
Samp Rate (Sps): 250k
Ch0: Center Freq (Hz): 2.475G
Ch0: Gain (dB): 30
Ch1: Center Freq (Hz): 2.475G
Ch1: Gain (dB): 30
Tx signal for Node #A
Tx signal for Node #B
Phase Shifter
Signal Source

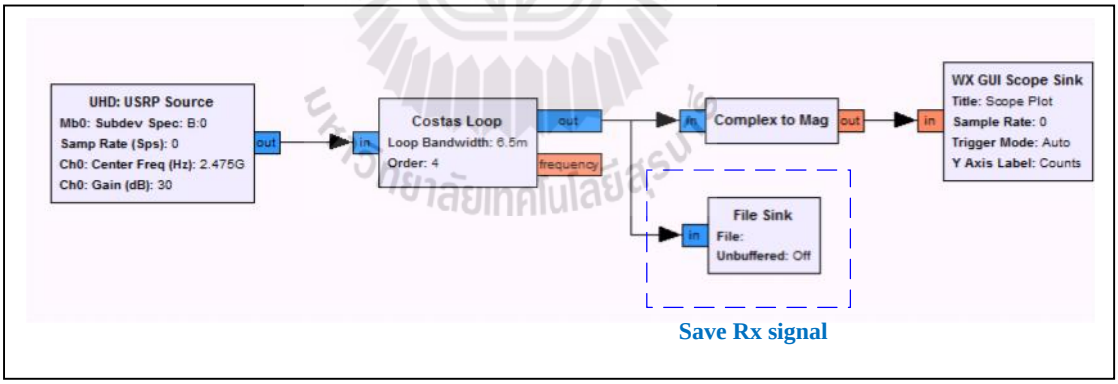
UHD: USRP Source
Mb0: Subdev Spec: B:0
Samp Rate (Sps): 0
Ch0: Center Freq (Hz): 2.475G
Ch0: Gain (dB): 30
Costas Loop
Loop Bandwidth: 6.5m
Order: 4
frequency
Complex to Mag
WX GUI Scope Sink
Title: Scope Plot
Sample Rate: 0
Trigger Mode: Auto
Y Axis Label: Counts
File Sink
File:
Unbuffered: Off
Save Rx signal

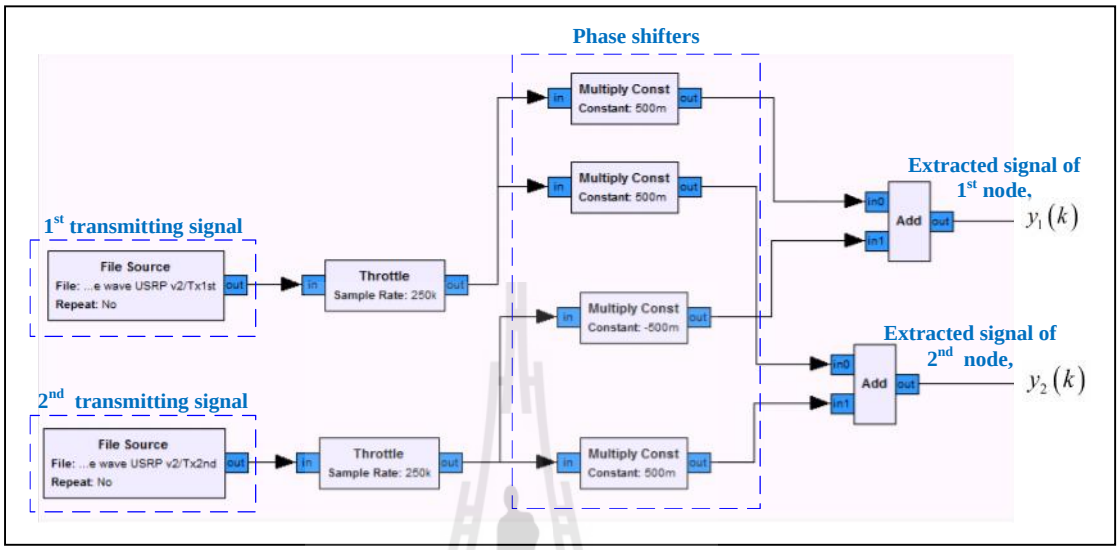
Phase shifters
1st transmitting signal
File Source
File: ...e wave USRP v2/Tx1st
Repeat: No
Throttle
Sample Rate: 250k
Multiply Const
Constant: 500m
Multiply Const
Constant: 500m
Multiply Const
Constant: -500m
Multiply Const
Constant: 500m
Add
Extracted signal of 1st node, $y_1(k)$
Add
Extracted signal of 2nd node, $y_2(k)$
2nd transmitting signal
File Source
File: ...e wave USRP v2/Tx2nd
Repeat: No
Throttle
Sample Rate: 250k

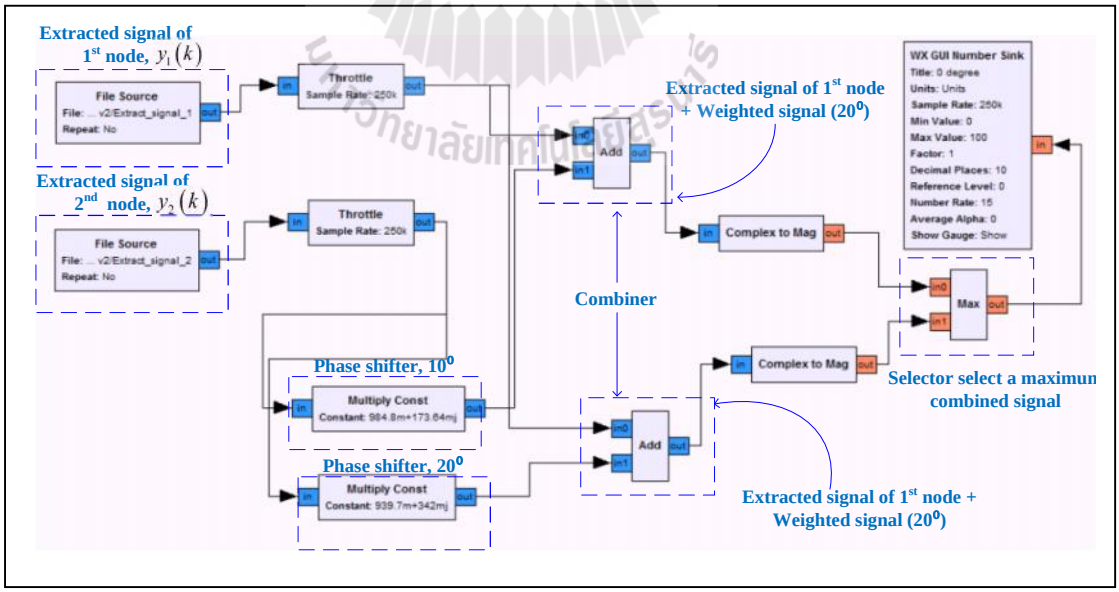
Extracted signal of 1st node, $y_1(k)$
File Source
File: ... v2/Extract_signal_1
Repeat: No
Throttle
Sample Rate: 250k
Extracted signal of 2nd node, $y_2(k)$
File Source
File: ... v2/Extract_signal_2
Repeat: No
Throttle
Sample Rate: 250k
Add
Extracted signal of 1st node + Weighted signal (20^0)
Complex to Mag
WX GUI Number Sink
Title: 0 degree
Units: Units
Sample Rate: 250k
Min Value: 0
Max Value: 100
Factor: 1
Decimal Places: 10
Reference Level: 0
Number Rate: 15
Average Alpha: 0
Show Gauge: Show
Max
Combiner
Phase shifter, 10^0
Multiply Const
Constant: 984.8m+173.64mj
Phase shifter, 20^0
Multiply Const
Constant: 939.7m+342mj
Add
Complex to Mag
Selector select a maximun combined signal
Extracted signal of 1st node + Weighted signal (20^0)

the two extracted signal which related to the signal transmitted from node #A and #B. Figure 5.15 presents the programming block diagram of the weighting and combining signal. The two extracted signal are weighted and combined according to proposed weighting algorithm discussed in Chapter IV. Finally, the base station obtains the maximum combined signal using a selector.

The measured results are presented in a histogram of average combined magnitude at base station. Note that this magnitude is average from 100-time of data recording. Figure 5.16 shows the results in the case of only a single node (node #A) transmits a cosine wave to base station while Figure 5.17 is for the case when only node #B transmits a cosine wave to base station. Figures 5.18 and Figures 5.19 show the average of combined magnitude when both nodes #A and #B transmit a signal for the 1^{st} time and 2^{nd} time, respectively. Then, Figure 5.20 shows the output of combined signal when the proposed beamforming scheme has been performed. However, the proposed scheme is off (without phase synchronization), the combined signal turns to be lower as shown in Figure 5.21. As a 100-time of experiments is recorded, Table 5.1 shows a mean value and standard deviation of all cases. The results present that the proposed technique provides an optimum gain as 0.038 volt with respect to the optimum beamforming gain. Note that the optimum gain can be calculated by summation of the received signal power from node #A and #B (0.012 + 0.026 = 0.038). Thus, the gain of proposed technique is significantly better than without phase synchronization which provides a signal gain as only 0.026 volt. Moreover, a standard deviation in case of proposed technique (σ = 0.0051) is lower than the case when the proposed scheme is off (σ = 0.0078). This implies that the proposed technique provides higher stability in terms of received signal power.

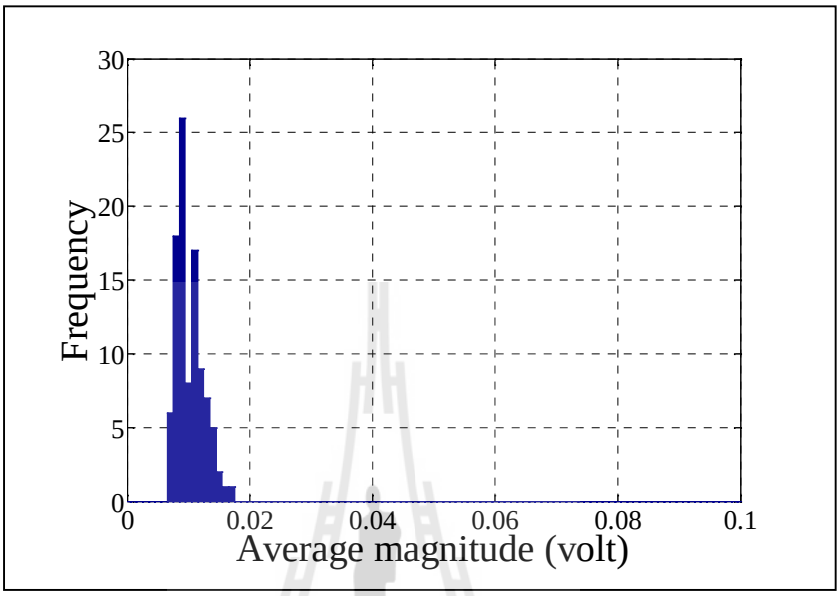
Frequency
30
25
20
15
10
5
0
0
0.02
0.04
0.06
0.08
0.1
Average magnitude (volt)

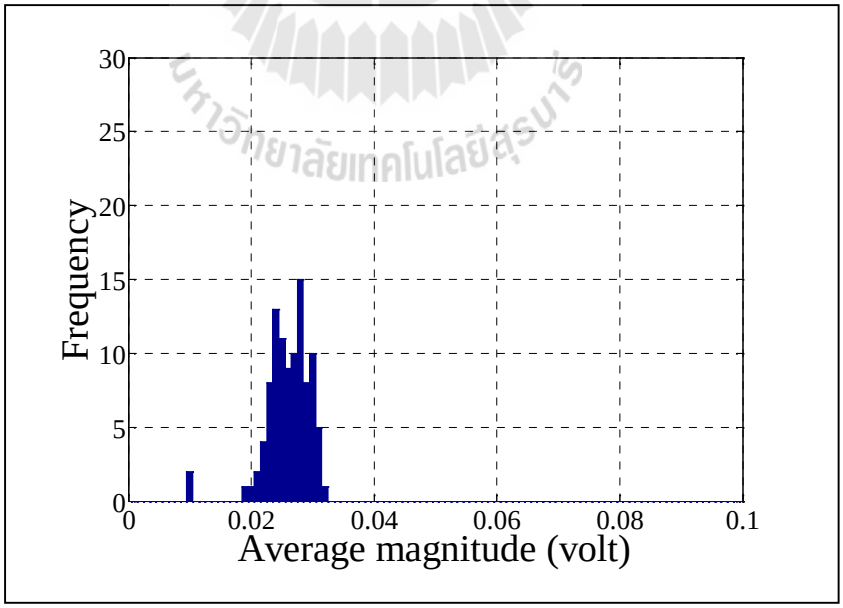
Frequency
30
25
20
15
10
5
0
0
0.02
0.04
0.06
0.08
0.1
Average magnitude (volt)

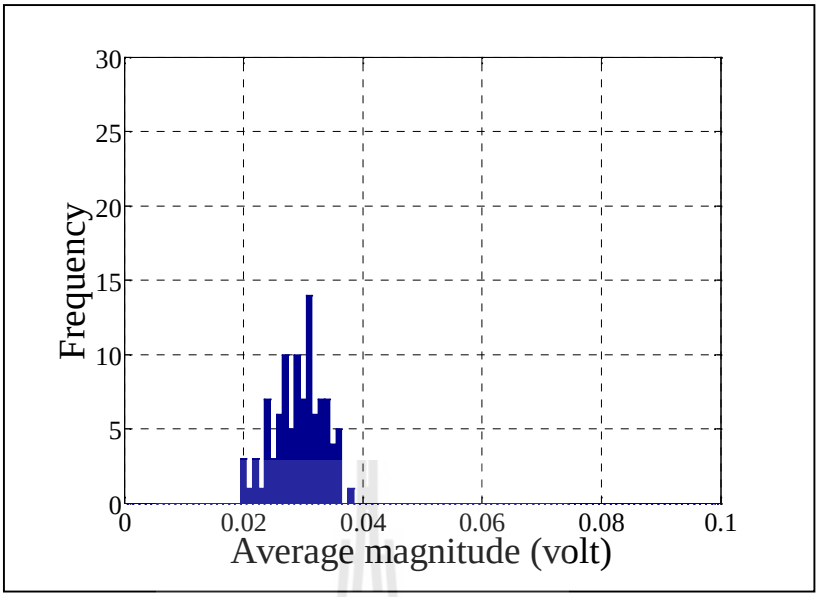
Frequency
30
25
20
15
10
5
0
0
0.02
0.04
0.06
0.08
0.1
Average magnitude (volt)

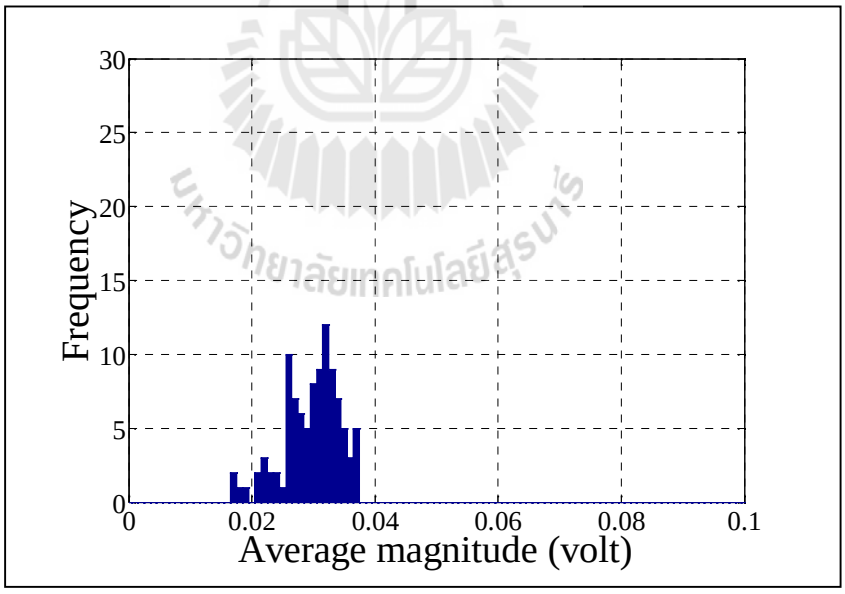
Frequency
30
25
20
15
10
5
0
0
0.02
0.04
0.06
0.08
0.1
Average magnitude (volt)

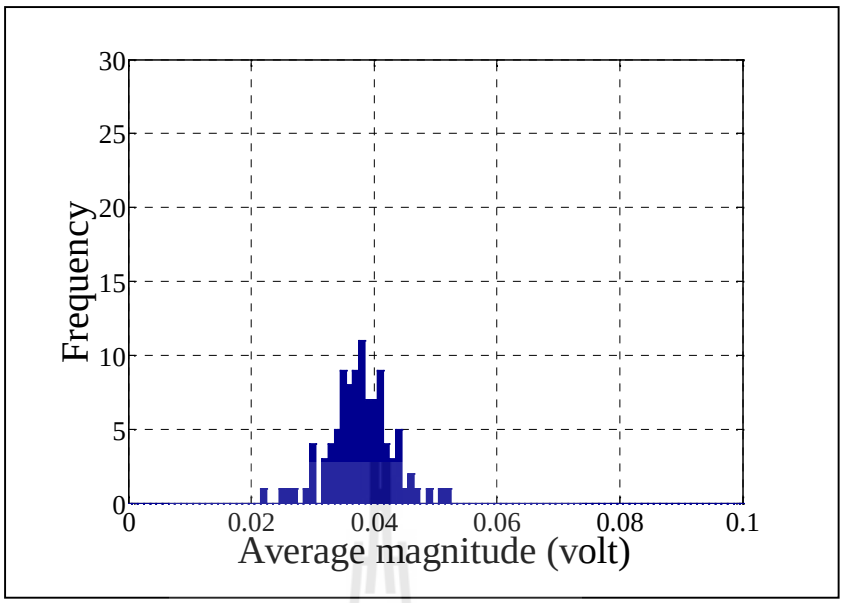
Frequency
30
25
20
15
10
5
0
0
0.02
0.04
0.06
0.08
0.1
Average magnitude (volt)

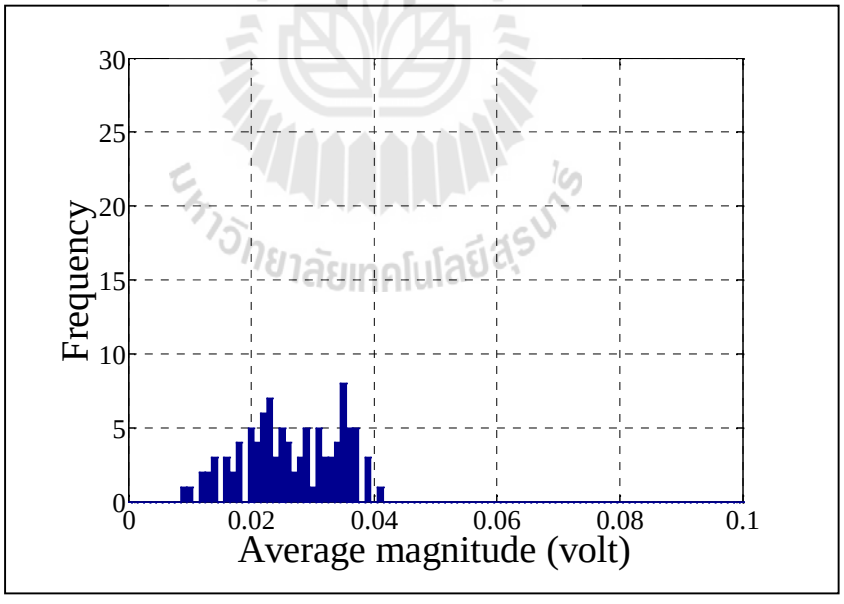
Frequency
30
25
20
15
10
5
0
0
0.02
0.04
0.06
0.08
0.1
Average magnitude (volt)

Table 5.1 Mean and standard deviation of measured average magnitude

	1×1 A	**1×1 B**	**2×1 1st**	**2×1 2nd**	**2×1 on**	**2×1 off**
Mean (v)	0.012	0.026	0.030	0.030	0.038	0.026
Standard deviation (v)	0.0022	0.0037	0.0042	0.0046	0.0051	0.0078

signal cannot totally guarantee the quality of the received data. This is because the received signal can be affected by transmission channel such as fading, noise and interference Therefore, the candidate further investigates into the BER in the next section.

5.4 An Experiment on Bit Error Rate

A testbed for BER measurement is shown in Figure 5.22. In this experiment, transmitting nodes transmit the random binary bits to a base station. The number of transmitting bits is 1 million which has a carrier frequency at 2.45 GHz. The USRP is employed at base station and two USRPB100s are employed as the transmitting nodes, nodes #A and #B. A SBX-120 is used as the daughter boards for USRP B100. All USRPs are connected to a laptop for signal processing and recording. The two transmitting nodes are placed at the sidewall as shown in Figure 5.23. The configuration of the base station is the same as the one for previous experiment shown in Figure 5.10. Also, all losses in transmission line have been calibrated before performing the measurement. According to a transmitting power of USRP B100 is not calibrated. Thus, the candidate calibrates the transmitting power of USRP B100 by utilizing a network analyzer. A calibrated power of USRP B100 is presented in Figure 5.24. The measured results show that the optimum programming gain is 31 dB which provides a transmitting gain of 25 dB.

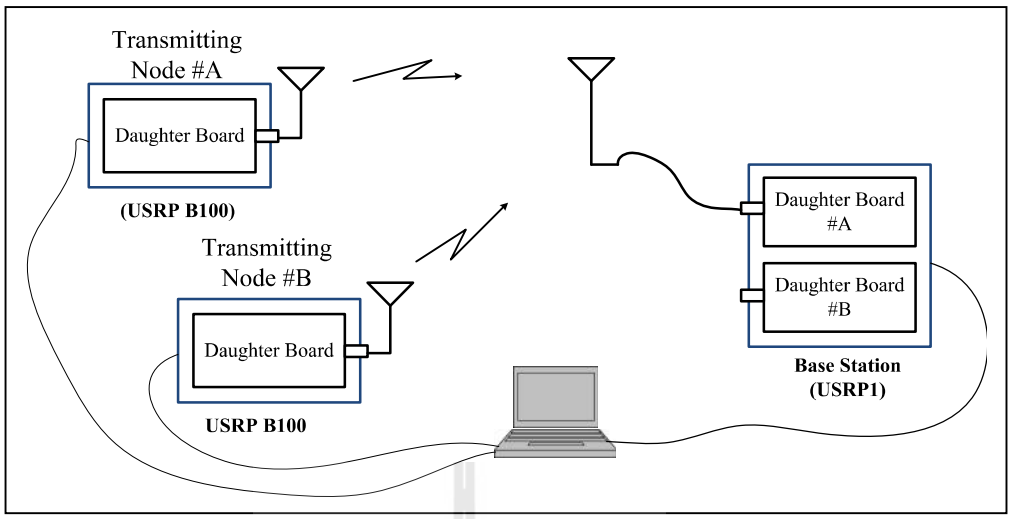
Transmitting
Node #A
Daughter Board
(USRP B100)
Transmitting
Node #B
Daughter Board
USRP B100
Daughter Board
#A
Daughter Board
#B
Base Station
(USRP1)

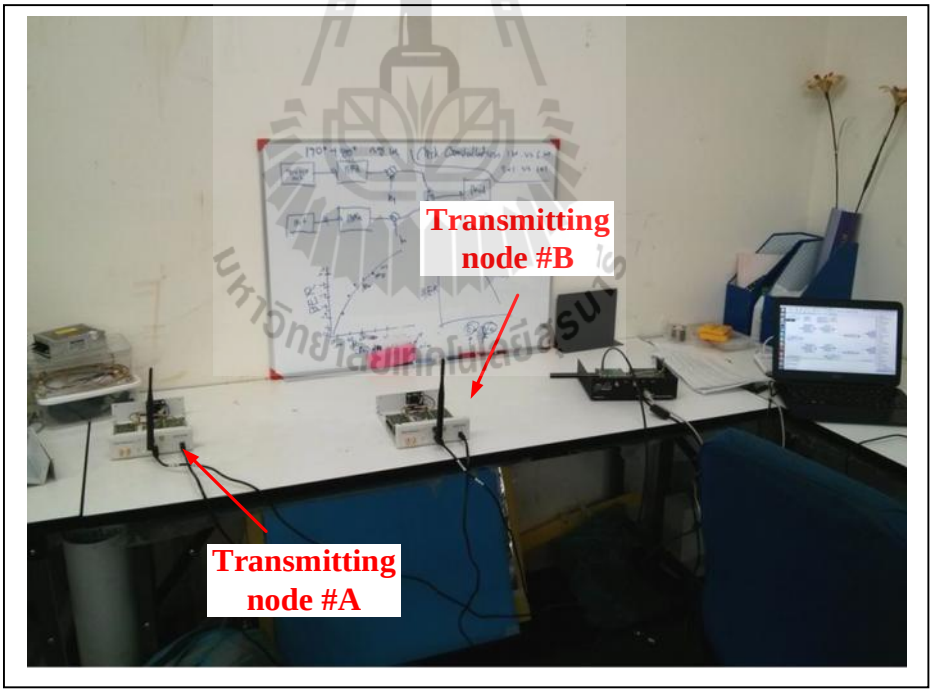
Transmitting
node #B
Transmitting
node #A

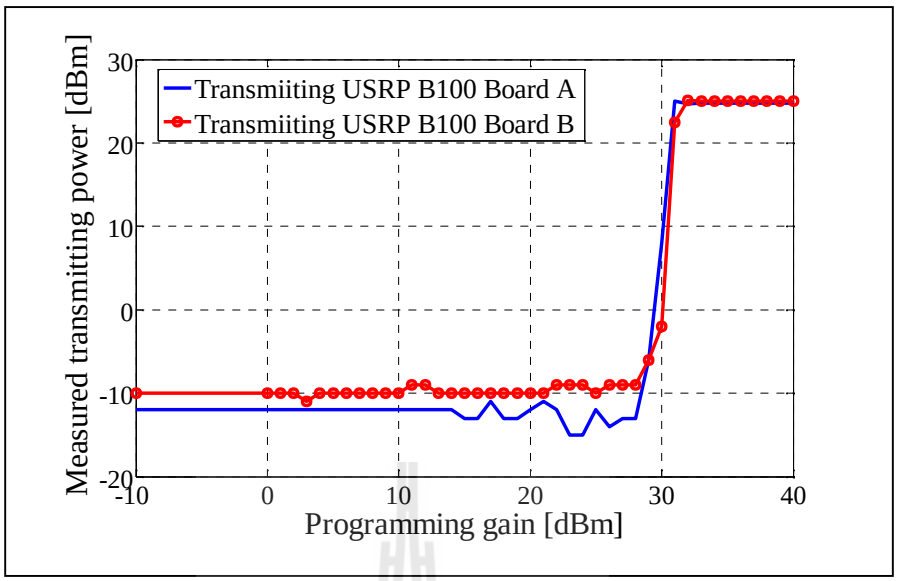
Transmiiting USRP B100 Board A
Transmiiting USRP B100 Board B
Measured transmitting power [dBm]
Programming gain [dBm]
30
20
10
0
-10
-20
-10
0
10
20
30
40

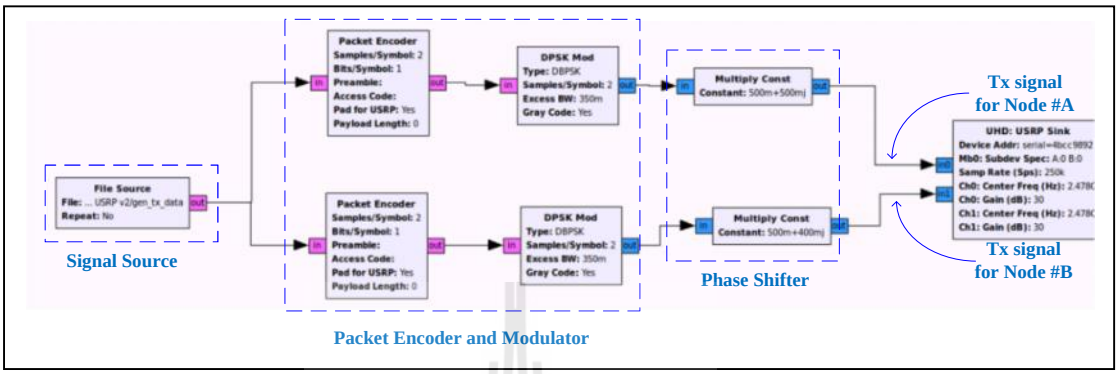

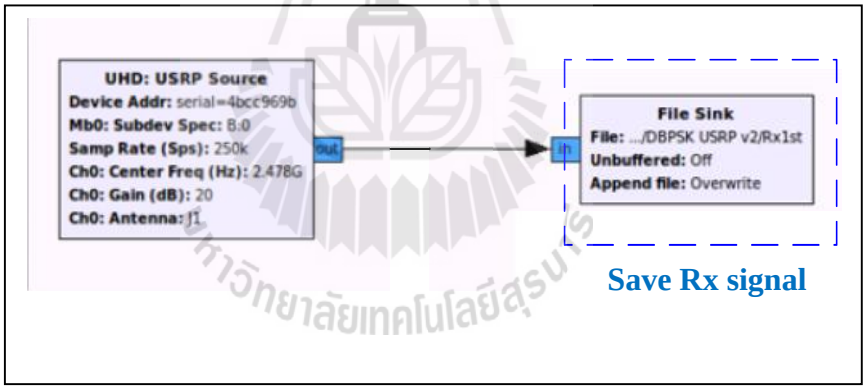

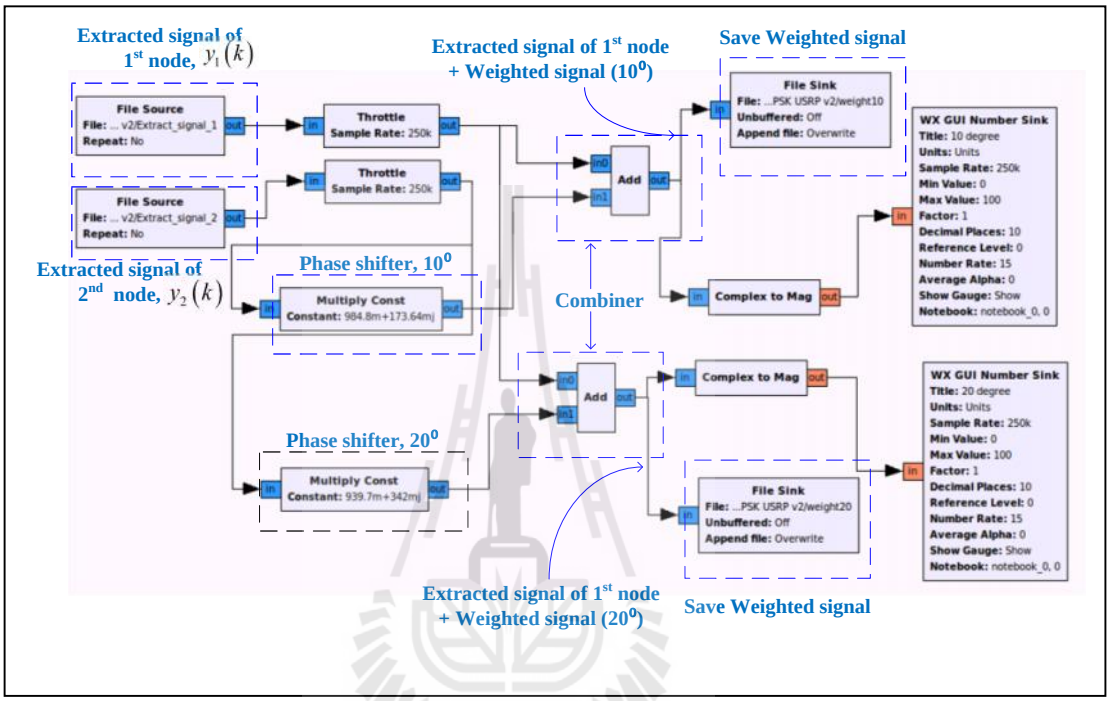

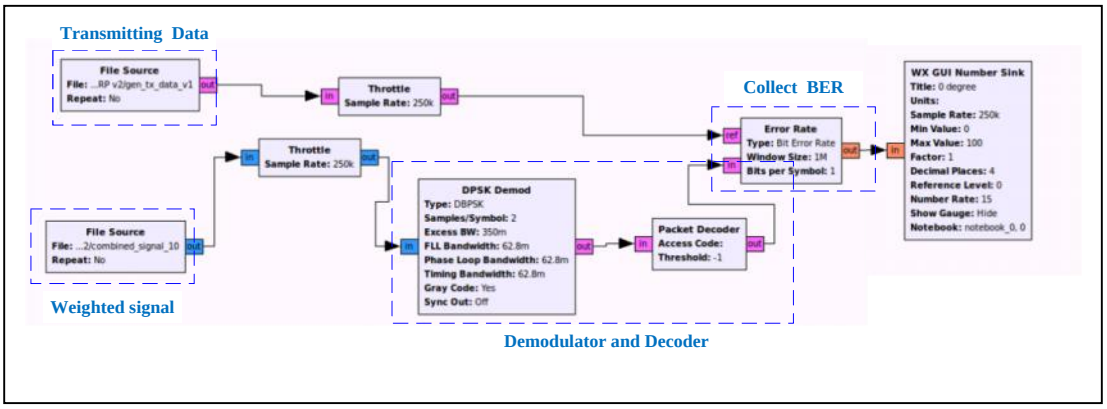

Gray code is enabled. Then, a demodulated signal is decoded by “Packet Decoder”. Finally, the decoded signal is used to collect a BER.

The measurement results are presented in a histogram of BER where 100-time of recorded data has been average. Note that the measured BER employing USRP is relatively sensitive with noise. Thus, the major portion of measured BER is the optimum case as 0.0 or the worst case as 0.5. Note that BER = 0.0 means that there is no bit error at all, while BER = 0.5 means that bit error turns out be a half of transmitted bits, e.g. bit error is 500,000 when transmitting 1 million bits. Figure 5.29 presents the BER in the case of transmitting data from only node #A while Figure 5.30 presents the case when only Node #B transmits the data. The results show that transmitting data from only a single node provides a low performance in terms of BER: the portion of BER = 0.0 which is only 11/100 in the case of only node #A and the portion of BER = 0.0 which is only 22/100 in the case of only node #B. Then, the proposed technique is applied in order to enhance the BER. Figures 5.31 and 5.32 show the BER at the base station when the two nodes transmit data at the 1^{st} and 2^{nd} time, respectively. Figure 5.33 shows the BER of combined signal at base station when the proposed technique has been applied. Figure 5.34 shows the BER for the case without the proposed technique. The results present that the proposed technique provides a lower BER than the case when transmitting signal from a single node and when the proposed technique is not applied. The portion of BER = 0.0 in case of using the proposed technique is 45/100. The portion of BER = 0.0 in case of 1^{st} and 2^{nd} retransmission and without phase synchronization is only 25/100, 17/100 and 14/100 respectively. Table 5.2 shows a mean and standard deviation BER of all cases as the experiments have been recorded for 100 times. The results in this table confirm

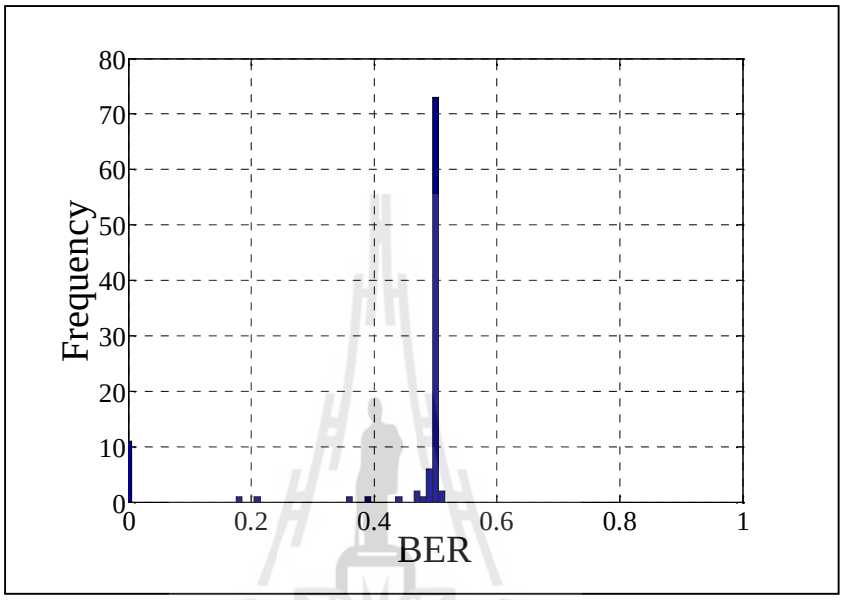
Frequency
BER
0
10
20
30
40
50
60
70
80
0
0.2
0.4
0.6
0.8
1

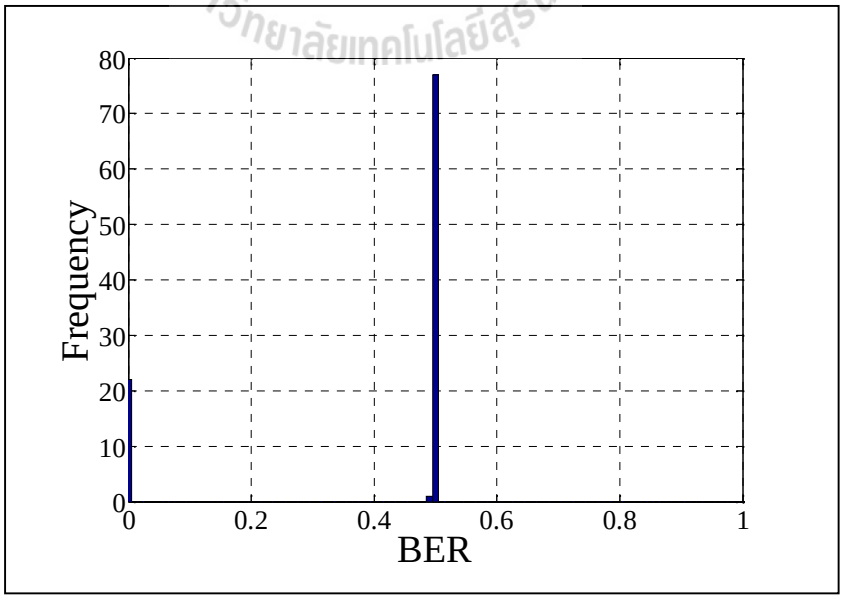
Frequency
BER
0
10
20
30
40
50
60
70
80
0
0.2
0.4
0.6
0.8
1

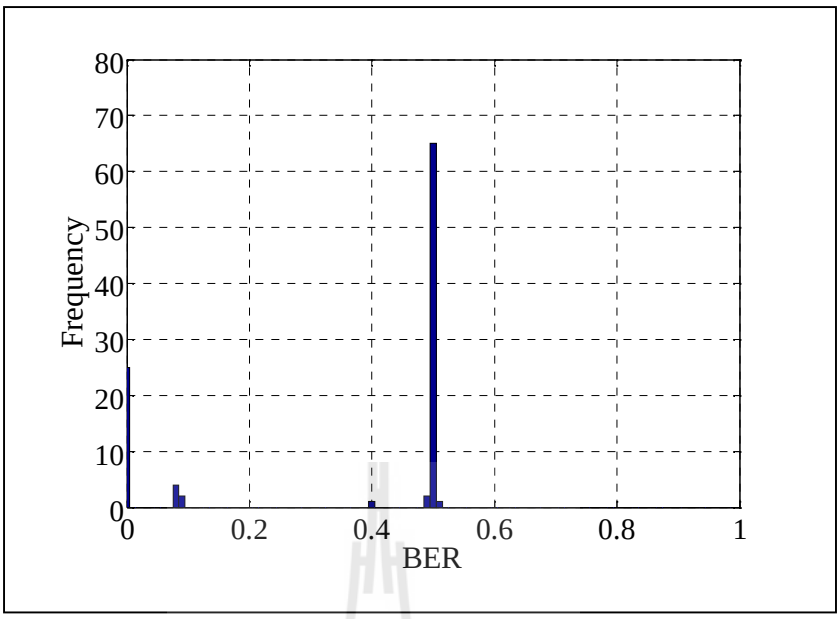
Frequency
BER
0
10
20
30
40
50
60
70
80
0
0.2
0.4
0.6
0.8
1

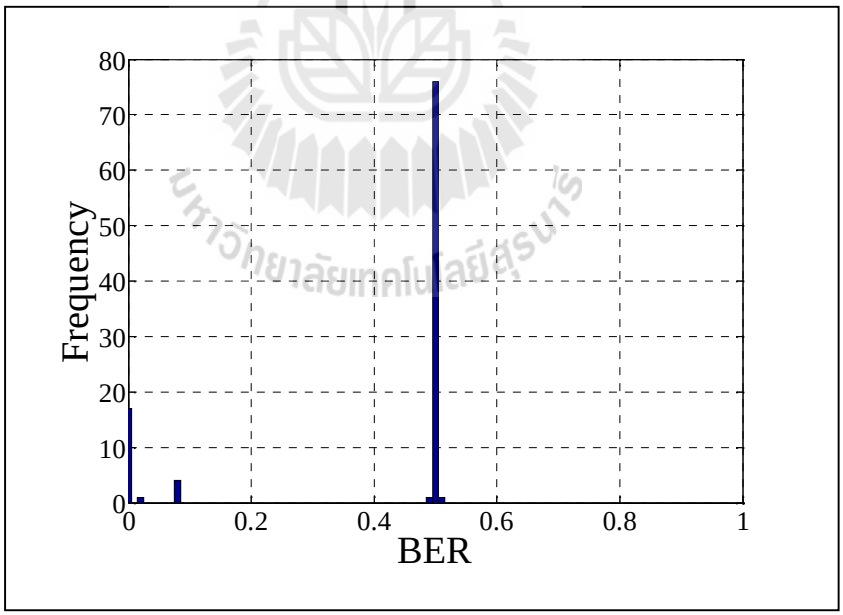
Frequency
BER
0
10
20
30
40
50
60
70
80
0
0.2
0.4
0.6
0.8
1

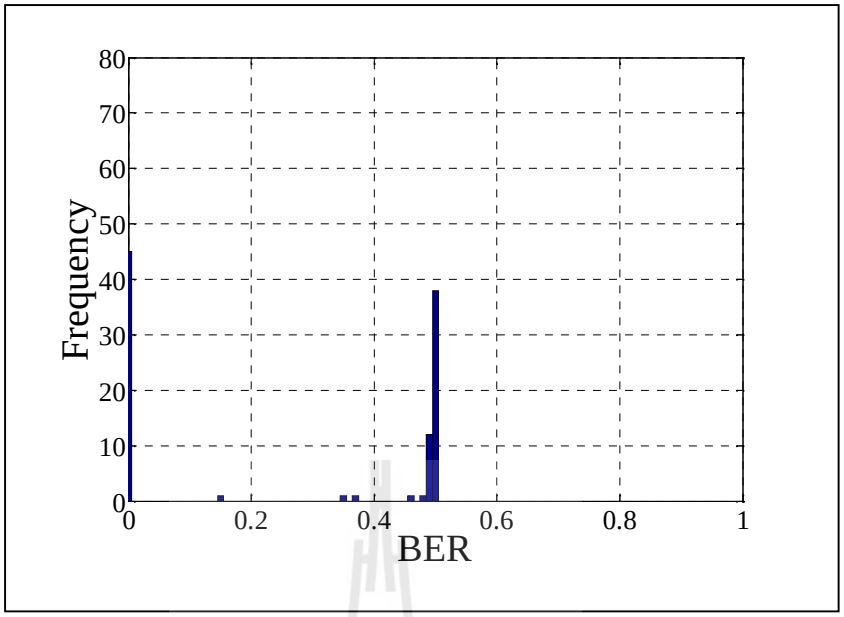
Frequency
BER
0
10
20
30
40
50
60
70
80
0
0.2
0.4
0.6
0.8
1

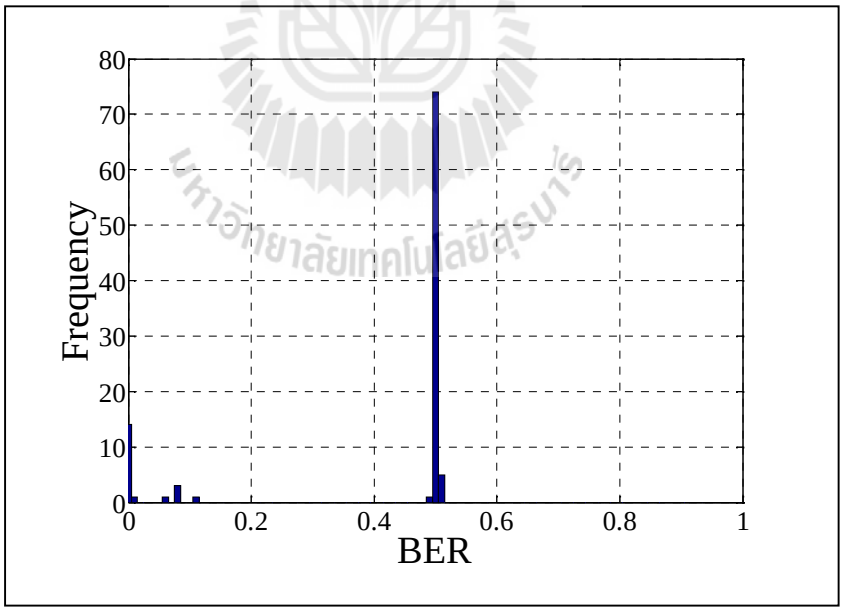
Frequency
BER
0
10
20
30
40
50
60
70
80
0
0.2
0.4
0.6
0.8
1

Table 5.2 Mean and standard deviation of measured BER.

	1×1 A	**1×1 B**	**2×1 1st**	**2×1 2nd**	**2×1 on**	**2×1 off**
Mean (v)	0.43	0.39	0.35	0.39	0.27	0.40
Standard deviation (v)	0.16	0.21	0.22	0.20	0.25	0.19

#A and #B is 0.43 and 0.39, respectively. The mean BER in case of retransmission and without phase synchronization is 0.35, 0.39 and 0.40, respectively. Therefore, the experimental results in this section validate the proposed technique that it can be utilized to realize for a distributed beamforming network with an optimum gain and lower BER.

5.5 Chapter Summary

The proposed non-feedback technique has been analyzed under real indoor environment. The SDR is utilized as a testbed. The measured results have revealed that the proposed technique provides the optimum beamforming gain. Also, it can enhance the system performance by lowing a BER comparing to the case when the phase synchronization is not applied.

CHAPTER VI

THESIS CONCLUSION

6.1 Conclusion

So far, major phase-synchronization techniques for distributed beamforming suffer from the problem related to the feedback procedure as base station sends feedback reference signals back to the transmitting nodes. A one-bit feedback procedure requires a large number of retransmissions which degrades the battery lifetime of mobile terminals (Mudumbai R., (2010)). Moreover, the transmission of feedback signal from base station to distributed collaborative nodes may be not reliable when the communication channel between base station and nodes is weak. A master-slave and time-slot round-trip utilize reference signal between transmitting collaborative nodes ((Mudumbai R., (2007) and Brown D.R., et.al, (2010)). This requirement gives rise to complexity at transmitting nodes. Alternatively, a zero feedback technique does not require any reference signal between nodes but requires a large number of retransmissions (Bletsas A., et.al, (2010)). In this thesis, a new technique handles a non-feedback beamforming employing an operation in both space and time domains. The proposed non-feedback beamforming performs an extraction of combined signal at base station which means the transmitting nodes do not need to deal with phase synchronization anymore, hence they can save energy and also battery life. The concept of extraction is based on a classical equation solving using inverse matrix. This procedure requires a few retransmission from nodes. After performing a signal extraction, each extracted signal is properly weighted to obtain an

appropriate phase alignment at base station. Finally, the base station obtains a combined signal with maximum beamforming gain. According to the proposed concept, all transmitting nodes do not require any feedback or reference signals. The number of retransmissions are less comparing to the one-bit feedback and zero feedback techniques. Therefore, the transmitting nodes are of low complexity and also low power consumption.

The simulation results reveal that the proposed non-feedback technique provides a high beamforming gain compared with the ones presented in literatures. Moreover, the proposed technique provides lower BER. With respect to the existing methods in the literatures, the proposed non-feedback technique is low of complexity comparing to one-bit feedback, zero-feedback master-slave and time-slot round-trip techniques.

For the experiment, this thesis has shown the design and construction of proposed non-feedback distributed beamformer. The testbed consisting of two transmitting nodes and one base station was developed under SDR technology by using USRP. The measured results have revealed that the proposed technique provides the optimum beamforming gain. Also, it can enhance the system performance by lowing a Bit Error Rate (BER) comparing to the case when the phase synchronization is not applied.

6.2 Future studies

Based on the knowledge learned and acquired over this research, some recommendations for future wireless communication design should be presented. According to the proposed non-feedback technique requires the number of

retransmissions of N when N is the number of transmitting nodes, the non-feedback technique requires a large number of retransmissions when the number of transmitting nodes is large. This may be extremely reduces the battery life at transmitting nodes. Therefore, a few general and useful formulas or coding techniques should be reviewed in order to reduce the number of retransmissions.

REFERENCES

Amini S., Na D. J., Choi K. (2014). **Performance comparison between distributed beamforming and clustered beamforming**. IEEE Conferance Information Technology: New Generations (ITNG), 11th, Apr. 7-9, 2014, pp. 174 – 179.

Balanis C. A. (1997). **Antenna Theory: Analysis and Design 2nd ed**. John John Wiley & Son, LTD, ch. 6.

Bletsas A., Lippman A., and Sahalos J. N. (2010). **Simple zero-feedback distributed beamforming with unsynchronized carriers.** IEEE Journal Selection Areas Communication, vol. 28, no. 7, Sept. 2010, pp. 1046-1054.

Brown D.R. and Poor H.V. (2008). **Time-slotted round-Trip carrier synchronization for distributed beamforming**. IEEE Transaction Signal Processing, vol. 56, 2008, pp. 5630 – 5643.

Brown D.R., Boyang Z., Svirchuck B. and Min N. (2010). **An experimental study of acoustic distributed beamforming using round-trip carrier synchronization**. IEEE Conferance Phased Array Systems and Technology (ARRAY), 12-15 Oct. 2010, pp. 316 -323

Bunsanit C., Uthansakul P. and Uthansakul M. (2012) **Refinement method for weighting scheme of fully spatial beamformer**. International Journal of Antennas and Propagation, vol. 2012, no. 359847.

Dohler M. and Li. Y. (2010). **Cooperative Communications: Hardware, Channel & PHY**. John Wiley & Son, LTD, ch. 1.

Ettus Research Company. **Supplier of software defined radio platforms**. April 2015, http://www.ettus.com/

Golub G. H. and Van Loan C.F . **Matrix Computations**. Johns Hopkins University Press, 1991.

Gross F. (2005). **Smart Antennas for Wireless Communication**. Mc Graw Hill, ch. 2.

Hwang K. S., Ko Y. C., and Alouini M. S. (2008). **Outage Probability of Cooperative Diversity System with Opportunistic Relaying Based on Decode-and-Forward**. IEEE Transaction in Wireless Communication, vol. 7 no. 12, Dec. 2008, pp. 51-57.

Innok A., Uthansakul P. and Uthansakul M. (2012). **Angular beamforming technique for MIMO beamforming system**. International Journal of Antennas and Propagation, vol. 2012, no. 638150.

Issariyakul T. and Krishnamurthy V. (2009). **Amplify-and-Forward Cooperative Diversity Wireless Networks: Model, Analysis, and Monotonicity Properties.** IEEE/ACM Transaction Network in Communication, vol. 17 no. 1, Feb 2009, pp.225-238.

Kaiser T. (2005). **When will smart antennas be ready for the market? Part I.** IEEE Signal Processing Magazine, vol. 22, no. 2, Mar. 2005, pp. 87-92.

Kreyszig E. (1999). **Advanced Engineering Mathematics 10th ed**. John Wiley & Sons, Ltd. Ch. 7.

Kosanovic M. and Stojcev M. (2012). **Sensor node lifetime prolonging**. Telecommunications Forum (TELFOR), 2012 20th, pp. 178 -181.

Liberti Jr. J. C. and Rappaport T. S. (1999). **Smart Antennas for Wireless Communications: IS-95 and Third Generation CDMA Applications**, Prentice Hall PTR, NJ, ch. 2.

Meerasri P., Uthansakul P. and Uthansakul M. (2014). **Self-interference cancellation-based mutual-coupling model for full-duplex single-channel MIMO systems**. International Journal of Antennas and Propagation, vol. 2014, no. 405487.

Mudumbai R., et.al (2013). **A Scalable Architecture for Distributed Transmit Beamforming with Commodity Radios: Design and Proof of Concept**. IEEE Transaction on Wireless Communication, Vol. 12, March 2013, pp. 1418 – 1428.

Mudumbai R., et.al (2005). **Scalable feedback control for distributed beamforming in sensor networks**. IEEE Conference Information Theory (ISIT), Australia, Sept. 2005, pp. 137–41.

Mudumbai R., Brown D.R., Madhow U. and Poor H.V. (2009). **Distributed transmit beamforming: challenges and recent progress**. IEEE Communication. Magazine, vol. 47, no. 2, Feb. 2009, pp. 102-110.

Mudumbai R., Barriac G., and Madhow U. (2007). **On the feasibility of distributed beamforming in wireless networks**. IEEE Transaction Wireless Communication, vol. 6, May 2007, pp. 1754–63.

Mudumbai R. (2010). **Distributed transmit beamforming using feedback control**. IEEE Transaction Information Theory, vol. 56, no. 1, Jan. 2010, pp. 411–426.

Nash G. **Phase-Locked Loop Design Fundamentals**. Freescale Semiconductor, Document Number: AN535, Rev. 1.0, Feb. 2006.

Ochiai H., Mitran P., Poor H.V., Tarokh V. (2005). **Collaborative beamforming for distributed wireless ad hoc sensor networks**. IEEE Transaction and Signal Processing, vol.53, no. 11, Nov. 2005, pp. 4110-4124.

Ozil I. and Brown D.R. (2007). **Time-Slotted Round-Trip Carrier Synchronization**. IEEE Conference on Asilomar Signals, Systems and Computers (ACSSC 2007), 4-7 Nov. 2007, pp. 1781 -1785.

Rahman M. M., Baidoo-Williams H. E., Mudumbai R. and Dasgupta S. (2012). **Fully wireless implementation of distributed beamforming on a software-defined radio platform**. IEEE conferance Information Processing in Sensor Networks (IPSN), 2012, Beijing, April 16-20, 2012, pp. 305–315.

Rayal F. (2005). **Why have smart antennas not yet gained traction with wireless network operators?**. IEEE Antennas Propagation Magazine, vol. 47, no. 46, Dec 2005, pp. 124 – 126.

Rivas M. (2010). **A Review of Adaptive Beamforming Techniques for Wideband Smart Antennas**. IEEE Conference WiCOM 2010, 23-25 Sept. 2010, pp. 1-5.

Sklivanitis G. and Bletsas A. (2011). **Testing zero-feedback distributed beamforming with a low-cost SDR testbed**. 2011 IEEE Conference Signals, Systems and Computers (ASILOMAR), 6-9 Nov. 2011, pp. 104 -108

Sriploy P., Uthansakul P. and Uthansakul M. (2013.) **Effect of path loss on the distributed beamforming for wireless sensor networks**. 2013 IEEE International Conference on ECTI-CON 2013, May 14-17, 2013, pp. 1–4.

Uthansakul M., Bialkowski M.E. (2005). **Investigations into a wideband spatial beamformer employing a rectangular array of planar monopoles**. IEEE Antennas Propagation Magazine, vol. 47, no. 5, pp. 91-99.

Uthansakul P., Innok A. and Uthansakul M. (2011). **Open-loop beamforming technique for MIMO system and its practical realization**. International Journal of Antennas and Propagation, vol. 2011, no. 723719, 2011.

Uthansakul P., Adaptive **MIMO Systems Explorations for Indoor Wireless Communications**. Appendix D, 2009.

Yao K., Hudson R. E., C. W. Reed C. Daching, et.al (1998). **Blind beamforming on a randomly distributed sensor array system**. IEEE Journal Selection Areas Communication, vol. 16, no. 8, Oct. 1998, pp. 1555 – 1567.

Yang L., Quraqe K. A., Serpedin E. and Alouini M. (2013). **Performance analysis of distributed beamforming in a spectrum sharing system**. IEEE Transaction on Vehicular Technology, vol. 62, no. 4, May 2013, pp. 1655 – 1666.

Lo Y. T. (1964). **A mathematical theory of antenna arrays with randomly spaced elements**. IRE Transaction Antenna Propagation, vol. AP-12, May 1964, pp. 257-268.

APPENDIX A

PUBLICATIONS

List of Publications

National Conference Paper

Sriploy P., Uthansakul P. and Uthansakul M., (2013). ผลกระทบของการสูญเสียเชิงวิถีต่อเทคนิคการก่อลำคลื่นแบบกระจายสำหรับเครือข่ายเซ็นเซอร์ไร้สายในพื้นที่อาคาร. ECTI-Conference on Application Research and Development 2013 (ECTI-CARD 2013). May 2013, no. 1098, 6 pages.

International Conference Paper

Sriploy P., Uthansakul P. and Uthansakul M., (2012). **An effect of imperfection in node location estimation on distributed beamforming**. 2012 9th International Conference on Electrical Engineering/Electronics, Computer, Telecommunications and Information Technology (ECTI-CON), 16-18 May 2012, pp 1-4, 4 pages.

Sriploy P., Uthansakul P. and Uthansakul M., (2013). **Effect of path loss on the distributed beamforming for Wireless Sensor Networks**. 2013 10th International Conference on Electrical Engineering/Electronics, Computer, Telecommunications and Information Technology (ECTI-CON), 15-17 May 2013, pp 1-4, 4 pages.

International Journal Paper

Sriploy P., Uthansakul P. and Uthansakul M., (2014). **The Optimum Number of Nodes and Radius for Distributed Beamforming Networks**. ECTI TRANSACTIONS ON ELECTRICAL ENGINEERING, ELECTRONICS, AND COMMUNICATIONS (ECTI-EEC), Vol 12, No 2, Aug. 2014, 13 pages (Scopus Indexing).

Sriploy P., Uthansakul P. and Uthansakul M., (2016). **Nonfeedback Distributed Beamforming Using Spatial-Temporal Extraction**. International Journal of Antennas and Propagation, Volume 2016, Article ID 7086234, 16 pages. (ISI Impact factor 0.660)

ผลกระทบของการสูญเสียเชิงวิถีต่อเทคนิคการก่อลำคลื่นแบบกระจายสำหรับเครือข่ายเซ็นเซอร์ไร้สายในพื้นที่อาคาร

นาย พงษ์นรินทร์ ศรีพลอย[1], ผศ. ดร. พีระพงษ์ อุทารสกุล[2] และ ผศ. ดร. มนต์ทิพย์ภา อุทารสกุล[3]
สาขาวิชาวิศวกรรมโทรคมนาคม ม.เทคโนโลยีสุรนารี อ.เมือง จ. นครราชสีมา ประเทศไทย 30000
[1]d5440054@g.sut.ac.th [2]uthansakul@sut.ac.th [3]mtp@sut.ac.th

บทคัดย่อ

จากการศึกษาปริทรรศน์วรรณกรรมที่ผ่านมาพบว่าการสูญเสียจากผลกระทบเชิงวิถีไม่ได้ถูกนำมาพิจารณาในระบบการก่อรูปลำคลื่นแบบกระจายสำหรับระบบเครือข่ายเซนเซอร์ไร้สาย ดังนั้นงานวิจัยชิ้นนี้จึงได้พิจารณาถึงผลกระทบจากการสูญเสียเชิงวิถีที่มีต่อการก่อรูปลำคลื่นแบบกระจาย ผลจากงานวิจัยชิ้นนี้ได้แสดงให้เห็นว่าผลกระทบเชิงวิถีสามารถลดทอนประสิทธิภาพหรืออัตราขยายของการก่อรูปลำคลื่นในเทคนิคการก่อรูลำคลื่นแบบกระจายอย่างมาก

Abstract

From literatures, path loss effect has not been taken into account when analyzing beamforming performance of distributed or cooperative beamforming networks such as Wireless Sensor Networks (WSNs). Therefore, this paper investigates in to the mentioned effect on beamforming performance of WSNs through computer simulation. The obtained results indicate that the path loss occurring between the networks and destination extremely degrades beam pattern and beamforming gain.

คำสำคัญ

Beampattern, Distributed beamforming, Free-Space Path loss, Wireless sensor networks

1. บทนำ

ในปัจจุบันระบบเครือข่ายเซ็นเซอร์ไร้สาย (Wireless Sensor Networks: WSNs) ได้ถูกนำมาใช้ในงานหลายประเภทเช่นใช้ในการตรวจสภาพแวดล้อม ในทางการแพทย์ หรือทางการทหาร เนื่องมาจากข้อดีที่เซนเซอร์โนดมีความสามารถในการส่งข้อมูลที่ความเร็วสูงและมีขนาดเล็กและสามารถเคลื่อนที่ได้ทำให้มีความยืดหยุ่นในการติดตั้ง อย่างไรก็ตามเซ็นเซอร์โนดมีข้อจำกัดที่มีกำลังส่งสัญญาณที่ต่ำเนื่องจากแบตเตอรี่ที่ติดตั้งส่วนใหญ่มีขนาดเล็กและตัวเซนเซอร์เองมักถูกติดตั้งอยู่บริเวณที่เข้าถึงได้ยากเช่นบนหลังคา พื้นที่อันตรายหรือบริเวณเครื่องจักรทำให้การเข้าไปเปลี่ยนแบตเตอรี่บ่อยๆนั้นทำได้ยากระบบเซนเซอร์โนดจึงมักใช้วิถีส่งแบบแอดฮอก (ad-hoc networks) แต่ในบางกรณีเช่นเวลาเครือข่ายเซนเซอร์โนดอยู่ห่างจากปลายทางมากๆ ตัวเซนเซอร์จำเป็นต้องส่งสัญญาณที่มีกำลังสูงซึ่งส่งผลให้พลังงานของแบตเตอรี่ลดลงอย่างรวดเร็ว ซึ่งปัญหานี้อาจแก้ได้โดยติดตั้งสายอากาศแบบแถวลำดับให้กับตัวโนดเพื่อเพิ่มอัตราขยายให้กับโนด แต่วิถีดังกล่าวต้องการค่าอุปกรณ์และค่าการติดตั้งที่เพิ่มขึ้นและต้องการพื้นที่ในการติดตั้งมากขึ้นซึ่งไม่เหมาะสมกับระบบเครือข่ายเซ็นเซอร์ไร้สายทำให้ข้อดีของระบบลดลง ดังนั้นเทคนิคการก่อลำคลื่นแบบกระจาย (Distributed Beamforming) จึงถูกนำมาประยุกต์ใช้กับระบบเครือข่ายเซ็นเซอร์ไร้สาย เนื่องจากเทคนิคการก่อลำคลื่นแบบกระจายสามารถเพิ่มอัตราส่วนสัญญาณต่อสัญญาณรบกวน (Signal-to-Interference Ratio: SINR) ให้กับระบบได้โดยที่ไม่ต้องติดตั้งสายอากาศเพิ่ม [1] โดยสามารถขยายได้มากถึง N^2 เท่าเมื่อ N คือจำนวนโนดในระบบ เทคนิคการก่อลำคลื่นแบบกระจายมีพื้นฐานมาจากเทคนิคสายอากาศแถวลำดับแบบสุ่ม (random antenna array) โดยตำแหน่งของโนดจะกระจายตัวแบบสุ่มและแต่ละโนดจะมีการกระจายข้อมูลแก่กันและทำการเข้ากันได้ของข้อมูลแล้วช่วยกันส่งข้อมูลไปปลายทางในรูปแบบเดียวกับสายอากาศแบบแถวลำดับ ดังนั้นข้อมูลที่ถูกส่งไปจะถูกขยายโดยการรวมกันของข้อมูลที่ปลายทาง [2]

เป็นที่ทราบกันดีว่าการสูญเสียเชิงวิถี (path loss) สามารลดทอนสัญญาณในระบบสื่อสารไร้สาย งานวิจัย [3] ได้แสดงให้เห็นว่าการ

สูญเสียเชิงวิถีสามารถลดทอนกำลังของสัญญาณส่งในระบบเครือข่ายเซ็นเซอร์ไร้สาย นอกจากนี้งานวิจัยยังแสดงให้เห็นว่าการเพิ่มจำนวนโนดในระบบสามารถเพิ่มประสิทธิภาพให้กับระบบได้ งานวิจัย [4] ได้แสดงให้เห็นว่าการสูญเสียเชิงวิถียังส่งผลต่อการหาตำแหน่งของโนดในระบบเครือข่ายไร้สายซึ่งจะส่งผลต่อการเข้ากันได้ของสัญญาณ (synchronization) สำหรับเทคนิคการก่อลำคลื่นแบบกระจาย อย่างไรก็ตามจากการศึกษาปริทรรศน์วรรณกรรมที่เกี่ยวข้องกับเทคนิคการก่อลำคลื่นแบบกระจายสำหรับระบบเครือข่ายเซ็นเซอร์ไร้สายพบว่าไม่มีการนำเอาการสูญเสียเชิงวิถีมาพิจารณา ยกตัวอย่างเช่นงานวิจัย [5] ได้ศึกษาถึงเทคนิคการก่อลำคลื่นแบบกระจายสำหรับระบบเครือข่ายเซ็นเซอร์ไร้สายแบบแอดฮอค (wireless ad hoc sensor networks) และงานวิจัย [6] ได้ศึกษาเทคนิคการก่อลำคลื่นแบบกระจายที่มีการกระจายตัวของโนดแบบเกาส์ โดยงานวิจัยทั้งสองไม่ได้พิจารณาถึงผลกระทบจากการสูญเสียเชิงวิถี ถึงแม้ว่างานวิจัย [7] ได้กล่าวว่าเราไม่จำเป็นต้องพิจารณาถึงการสูญเสียเชิงวิถีก็ได้เนื่องจากเราสามารถชดเชยการสูญเสียเชิงวิถีได้โดยการเพิ่มจำนวนโนด เพิ่มกำลังส่งหรือชดเชยการลดทอนที่ปลายทาง แต่การเพิ่มจำนวนโนดนั้นปฏิบัติจริงได้ยากเนื่องจากข้อจำกัดของระบบ ส่วนการเพิ่มกำลังส่งก็เป็นการลดอายุการใช้งานของโนดลงและการชดเชยสัญญาณก็ยากที่จะชดเชยการลดทอนจากการสูญเสียเชิงวิถีได้ทั้งหมด

ดังนั้นงานวิจัยชิ้นนี้จึงได้ศึกษาถึงผลกระทบของการสูญเสียเชิงวิถีที่มีผลต่อเทคนิคการก่อลำคลื่นแบบกระจายสำหรับระบบเครือข่ายเซ็นเซอร์ไร้สายในพื้นที่ในอาคาร โดยผลจากการศึกษาได้แสดงให้เห็นว่าการลดทอนจากการสูญเสียเชิงวิถีมีผลต่อประสิทธิภาพของเทคนิคการก่อลำคลื่นอย่างมากโดยเฉพาะในกรณีที่ระยะทางระหว่างระบบเครือข่ายเซ็นเซอร์ไร้สายกับสถานีปลายทางมีระยะห่างกันมากๆ สถานีปลายทางจะไม่สามารถรับข้อมูลได้เนื่องจากกำลังของสัญญาณที่รับได้มีค่าต่ำกว่าค่าความไว (sensitivity) ของภาครับ ดังนั้นเราจึงควรพิจารณาการสูญเสียเชิงวิถีในเทคนิคการก่อลำคลื่นแบบกระจาย

งานวิจัยชิ้นนี้ประกอบด้วยสี่บทโดยในบทแรกจะกล่าวถึงบทนำที่มาและแรงจูงใจของงานวิจัยนี้ บทที่สองจะอธิบายถึงทฤษฎีเทคนิคการก่อรูปลำคลื่นแบบกระจายและการสูญเสียเชิงวิถี ส่วนบทที่สามจะแสดงถึงผลการทดลองที่ได้จากการจำลองแบบทางคอมพิวเตอร์ และบทสุดจะกล่าวถึงการสรุปผลของงานวิจัยชิ้นนี้

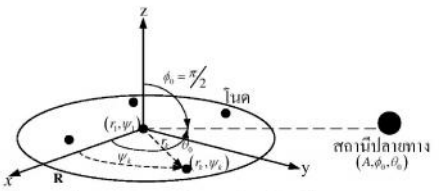

รูปที่ 1. แบบจำลองระบบเทคนิคการก่อรูปลำคลื่นแบบกระจายสำหรับเครือข่ายเซ็นเซอร์ไร้สาย

2. เทคนิคการก่อลำคลื่นแบบกระจายและการสูญเสียเชิงวิถี

2.1 ทฤษฎีการก่อรูปลำคลื่น

แบบจำลองระบบเทคนิคการก่อรูปลำคลื่นแบบกระจายสำหรับเครือข่ายเซ็นเซอร์ไร้สายได้ถูกแสดงในรูปที่ 1 โดยอ้างอิงมาจากงานวิจัย [5] ตำแหน่งของเซนเซอร์โนดจำนวน N ($k = 1,\ldots, N$) จะถูกสุ่มแบบสม่ำเสมออยู่บนระนาบ (x, y) และตำแหน่งของโนดจะถูกอ้างอิงอยู่ในรูปเชิงขั้ว (r_k, ψ_k) โดยที่ $r_k = \sqrt{x_k^2 + y_k^2}$ และ $\psi_k = \tan^{-1}(y_k/x_k)$ ขณะที่ตำแหน่งของสถานีปลายทางอ้างอิงในรูปของเชิงทรงกลม $(A, \emptyset_0, \theta_0)$ ในงานวิจัยนี้เรากำหนดให้ปลายทางอยู่บนระนาบเดียวกันกับโนดดังนั้น $\theta_0 = \pi/2$ นอกจากนี้ยังกำหนดให้โนดแต่ละโนดติดตั้งสายอากาศแบบไอโซทรอปิกจำนวน 1 ต้น

ในการวิเคราะห์ถึงแบบรูปลำคลื่นของเทคนิคการก่อรูปลำคลื่นแบบกระจายจะเริ่มที่การหาค่าเฟสของแต่ละโนด โดยเฟสเริ่มต้นของแต่ละโนดในกรณีที่การเข้าสัญญาณเป็นแบบเปิดคือ

$$\psi_k = \frac{2\pi}{\lambda} r_k \sin\theta_0 \cos(\phi_0 - \psi_k) \quad (1)$$

ดังนั้นตัวประกอบแถวลำดับที่สนามระยะไกลของสายอากาศแต่ละโนดคือ

$$F(\phi, \theta: r_k, \psi_k) \approx \frac{1}{N}\sum_{k=1}^{N} e^{j\frac{2\pi}{\lambda} r_k [\sin\theta_0 \cos(\phi_0 - \psi_k) - \sin\theta \cos(\phi - \psi_k)]} \quad (2)$$

จากที่เรากำหนดให้สถานีปลายทางอยู่บนระนาบเดียวกันกับโนด $\theta = \theta_0 = \pi/2$ ดังนั้นสมการที่ (2) จึงสามารถจัดรูปได้ดังนี้

$$F(\phi: r_k, \psi_k) = \frac{1}{N}\sum_{k=1}^{N} e^{j\frac{4\pi}{\lambda} r_k \sin\left(\frac{\phi_0-\phi}{2}\right)\sin\left(\varphi_k - \frac{\phi_0+\phi}{2}\right)}$$
$$= \frac{1}{N}\sum_{k=1}^{N} e^{j\frac{4\pi R}{\lambda}\sin\left(\frac{\phi_0-\phi}{2}\right)\left(\frac{r_k}{R}\right)\sin\left(\varphi_k - \frac{\phi_0+\phi}{2}\right)} \quad (3)$$

นอกจากนี้เรายังกำหนดให้ทิศทางของปลายทางคือ $\phi_0 = 0$ ดังนั้นสมการที่ (3) จึงสามารถจัดรูปได้เป็น

$$F(\phi: z_k) \approx \frac{1}{N}\sum_{k=1}^{N} e^{-j4\pi\hat{R}\sin\left(\frac{\phi}{2}\right)z_k} \quad (4)$$

เมื่อ $\hat{R} = R/\lambda$ และ

$$z_k(\phi: r_k, \psi_k) = \left(\frac{r_k}{R}\right)\sin\left(\psi_k - \left(\frac{(\phi_0+\phi)}{2}\right)\right) \quad (5)$$

โดย z_k มีค่าฟังก์ชันความหนาแน่นความน่าจะเป็น (probability density function) เท่ากับ

$$f_{z_k} = \left(\frac{r_k}{R}\right)\sqrt{1-z^2}, \quad -1 \le z \le 1 \quad (6)$$

จากสมการที่ (4) เราสามารถหาแบบรูปการแผ่พลังงานของระบบเครือข่ายเซ็นเซอร์ไร้สายได้ดังนี้

$$P(\phi: z_k) = |F(\phi: z_k)|^2 = F(\phi: z_k)F^*(\phi: z_k)$$
$$= \frac{1}{N^2}\sum_{k=1}^{N}\sum_{l=1}^{N} e^{-j4\pi\hat{R}\sin\left(\frac{\phi}{2}\right)(z_k - z_l)}$$
$$= \frac{1}{N} + \frac{1}{N^2}\sum_{k=1}^{N} e^{-j\beta z_k}\sum_{l=1, l\neq k}^{N} e^{-j\beta z_k} \quad (7)$$

เมื่อ $\beta = 4\pi\hat{R}\sin(\phi/2)$

ตามที่เราไม่สามารถทราบถึงตำแหน่งที่แน่นอนของโนดเนื่องจากโนดมีการกระจายตัวแบบสุ่มหรือเคลื่อนที่ไปเรื่อยๆ ดังนั้นแบบรูปการแผ่พลังงานของระบบจึงไม่คงที่ ดังนั้นในงานวิจัยนี้เราจึงพิจารณาแบบรูปการแผ่พลังงานในรูปของค่าเฉลี่ยดังนี้

$$P_{av}(\phi) = E_z\{P(\phi: z_k)\} \quad (8)$$

เมื่อ $E_x\{\cdot\}$ คือการหาค่าเฉลี่ยและจากสมาการที่ (6) และ (7) เราจะได้

$$P_{av}(\phi, \beta) = \frac{1}{N} + \left(1 - \frac{1}{N}\right)\left|2\frac{J_1(4\pi\hat{R}\sin(\phi/2))}{4\pi\hat{R}\sin(\phi/2)}\right|^2 \quad (9)$$

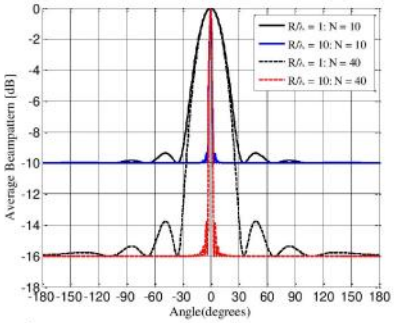

รูปที่ 2. แบบรูปการแผ่พลังงานเฉลี่ยของเทคนิคการก่อรูปลำคลื่นแบบกระจาย

เมื่อ $J_1(\cdot)$ คือฟังก์ชันเบสเซลลำดับที่หนึ่ง

จากสมการที่ (9) ขนาดของพูข้างจะขึ้นอยู่กับเทอมแรกของสมการซึ่งจะเห็นว่ายิ่งเราเพิ่มจำนวนโนดขนาดของพูข้างจะลดลง ขณะที่พูหลักจะขึ้นกับเทอมที่สองของสมการซึ่งสมพันธ์กับขนาดของระบบ, $\hat{R}$ โดยยิ่งระบบมีขนาดใหญ่พูหลักจะยิ่งแคบตามที่ได้แสดงในรูปที่ 2 ขณะที่สมการสภาพเจาะจงทิศทางของเทคนิคการก่อรูปลำคลื่นแบบกระจายคือ

$$D = \frac{N}{1+0.0933Z\frac{N}{R}} \quad (10)$$

โดยสภาพเจาะจงทิศทางของระบบจะสามารถแสดงให้เห็นถึงประสิทธิภาพหรืออัตราขยายของเทคนิคการก่อรูปลำคลื่นแบบกระจาย จากสมการที่ (10) จะเห็นได้ว่าสภาพเจาะจงทิศทางมีความสัมพันธ์กันกับจำนวนโนดและรัศมีของระบบ โดยยิ่งจำนวนโนดและรัศมีเพิ่มขึ้นค่าสภาพเจาะจงทิศทางก็จะเพิ่มขึ้นตาม เนื่องมาจากการเพิ่มรัศมีทำให้พูหลักแคบลงขณะที่การเพิ่มจำนวนโนดทำให้พูข้างลดลงตามที่ได้อธิบายในสามการที่ (9)

2.2 การสูญเสียเชิงวิถี

ในงานวิจัยนี้เรากำหนดให้เครือข่ายเซ็นเซอร์ไร้สายถูกติดตั้งในพื้นที่ปิดเช่นในโรงงานหรืออาคารสำนักงานเป็นต้น ดังนั้นเราจึงพิจารณาถึงการสูญเสียเชิงวิถีในพื้นที่ปิดตามสามการต่อไปนี้

ตารางที่ 1. ค่าสัมประสิทธิ์การสูญเสียเชิงวิถี, N

Frequency [GHz]	Environment		
	Resident	Office	Commercial
0.9	-	3.3	2.0
1.2-1.3	-	3.2	2.2
1.8-2.0	2.8	3.0	2.2
4.0	-	2.8	2.2
60.0	-	2.0	1.7

ตารางที่ 2. ค่าสัมประสิทธิ์การทะลุผ่าน, $L_f(n_f)$

Frequency [GHz]	Environment		
	Resident	Office	Commercial
0.9	-	9 (1floor)	-
	-	19 (2floor)	-
	-	24 (3floor)	-
1.8-2.0	$4n_f$	$15+4(n_f-1)$	$6+3(n_f-1)$

$$\gamma_k(dB) = 20log_{10}(f) + 10nlog_{10}(d_k) + L_f(n_f) - 28 \quad (11)$$

เมื่อ n คือค่าสัมประสิทธิ์การสูญเสียเชิงวิถี (path loss exponent) และ $L_f(n_f)$ คือค่าสัมประสิทธิ์การทะลุผ่าน (floor penetration factor) ตัวอย่างค่าสัมประสิทธิ์การสูญเสียเชิงวิถีและค่าสัมประสิทธิ์การทะลุผ่านได้แสดงไว้ในตารางที่ 1 และ 2 ตามลำดับ ขณะที่ d_k คือระยะห่างระหว่าโนดแต่ละตัวกับสถานีปลายทางซึ่งมีค่าเท่ากับ

$$d_k(\phi,\theta) \approx A - r_k \sin\theta \cos(\phi - \psi_k) \quad (12)$$

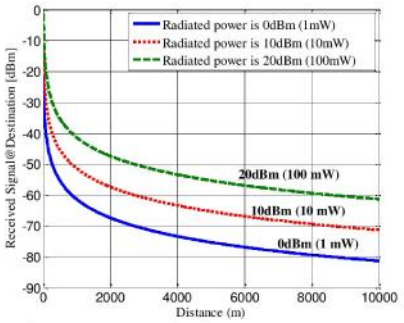

รูปที่ 3. กำลังสัญญาณที่ได้ที่สถานีปลายทาง ณ ระยะห่างระหว่างโนดกับปลายทางต่างๆ

เมื่อ A คือระยะห่างระหว่างจุดศูนย์กลางของระบบกับปลายทางตามที่ได้แสดงในรูปที่ 1 ดังนั้นกำลังสัญญาณที่สถานีปลายทางรับได้จะเท่ากับ

$$R_{x,i} = 10\log\left(\frac{N}{1+\mu\frac{N}{R}}\right) + G_t + G_r + P_t - \gamma_k \quad (13)$$

เมื่อ $\mu = 0.09332$, G_t คืออัตราขยายของสายอากาศภาคส่ง G_r คืออัตราขยายของสายอากาศภาครับและ P_t คือกำลังส่งสัญญาณของโนดทั้งหมดมีหน่วยเป็นเดซิเบล

รูปที่ 3 แสดงถึงกำลังของสัญญาณที่สถานีปลายทางสามารถรับได้ ณ ระยะห่างระหว่างโนดกับสถานีปลายทางตามสมการที่ (13) จากรูปจะเห็นว่าสัญญาณจะถูกลดทอนลดลงอย่างรวดเร็วและลดลงอย่างมากในกรณีที่สถานีปลายทางอยู่ห่างจากโนดมากๆ ยกตัวอย่างเช่นที่ระยะ 1000 ม. สถานีปลายทางรับสัญญาณได้ -61 dBm, -71 dBm และ -81 dBm เมื่อกำลังส่งสัญญาณเท่ากับ 0 dBm, 10 dBm และ 20 dBm ตามลำดับ

ตารางที่ 1 ค่าพารามิเตอร์ที่ใช้ในการจำลองแบบ

ความถี่ปฏิบัติการ	915 MHz
จำนวนโนด (N)	30 Nodes
รูปแบบการกระจายตัวของโนด	Uniform
รัศมีของระบบ ($\hat{R} = R/\lambda$)	5
ระยะการส่งสัญญาณ	<300m. (pico cell)
กำลังส่งสัญญาณของโนด	30 dBm
ค่าความไวของสถานีปลายทาง	-110 dBm
อัตราขยายของสายอากาศภาคส่ง	2.5 dBi
อัตราขยายของสายอากาศภาครับ	5 dBi
ค่าสัมประสิทธิ์การสูญเสียเชิงวิถี, n	3.3 (office)
ค่าสัมประสิทธิ์การทะลุผ่าน, $L_f(n_f)$	9 (1 floor, office)

3. ผลจากการจำลองแบบและวิเคราะห์ผล

สำหรับงานวิจัยนี้เราใช้โปรแกรมแมทแลบ (MATLAB) ในการสร้างแบบจำลองโดยค่าพารามิเตอร์ที่ใช้ในแบบจำลองตามที่ได้แสดงไว้ในตารางที่ 3 เราได้อ้างอิงมาจากงานวิจัย [8] โดยงานนี้ได้พัฒนาระบบเครือข่ายเซ็นเซอร์ไร้สายสำหรับความบันเทิงภายในบ้านโดยระบบต้องการส่งข้อมูลปริมาณมากและมีความเร็วสูง งานวิจัยดังกล่าวได้ออกแบบระบบบนมาตรฐาน MICA และ MICA2 โดยติดตั้งอยู่บนบอร์ด Chipcon CC100 และปฏิบัติการอยู่บนย่านความถี่ 925 MHz

รูปที่ 4 แสดงแบบรูปการแผ่พลังงานเฉลี่ยของเทคนิคการก่อรูปลำคลื่นแบบกระจายในเครือข่ายเซนเซอร์ไร้สาย จะเห็นว่าการลดทอนจากการสูญเสียเชิงวิถีสามารถลดอัตราขยายของการก่อรูปลำคลื่นแบบกระจายได้อย่างมาก โดยอัตราขยายลดลง -47 dBm, -57 dBm และ -67 dBm เมื่อระยะห่างระหว่างโนดเท่ากับสถานีปลายทางเท่ากับ 100 ม. 200 ม. และ 300 ม. ตามลำดับ ที่เป็นเช่นนี้เพราะยิ่งระยะห่างระหว่างโนดกับสถานีปลายทาง (A) มีระยะที่ห่างกันมากขึ้นการลดทอนก็จะเพิ่มขึ้นตามที่แสดงไว้ในสมการที่ (11) และ (12) และถ้ายิ่งระยะห่างระหว่างโนดกับสถานีปลายทาง

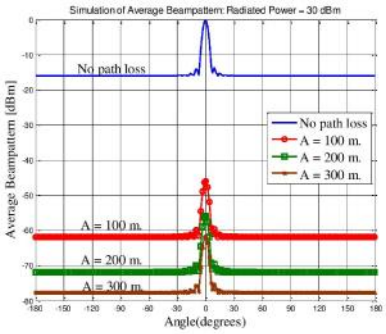

รูปที่ 4. แบบรูปการแผ่พลังงานเฉลี่ยที่ระยะห่างระหว่างโนดกับสถานีปลายทาง 100 ม. 200 ม. และ 300 ม.

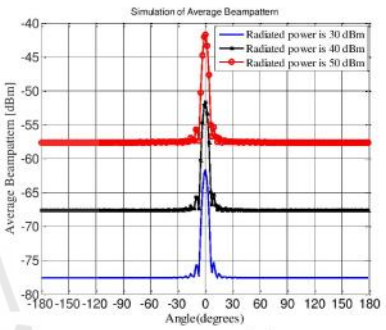

รูปที่ 5. แบบรูปการแผ่พลังงานเฉลี่ยที่มีกำลังส่งสัญญาณเท่ากับ 30 dBm, 40 dBm และ 50 dBm ที่ระยะ A=1000 ม.

มากๆ ก็อาจจะส่งผลให้สัญญาณที่รับได้ที่ปลายทางต่ำกว่าค่าความไวที่ -110 dBm ซึ่งส่งผลให้ปลายทางจะไม่สามารถรับข้อมูลได้

ขณะที่การเพิ่มกำลังส่งนอกจากจะลดอายุการใช้งานของโนดลงแล้วยังไม่สามารถที่จะชดเชยการลดทอนได้ทั้งหมดตามที่ได้แสดงในรูปที่ 5 จะเห็นว่าถึงจะเพิ่มกำลังส่งจาก 30 dBm เป็น 40 dBm และ 50 dBm สัญญาณที่รับได้ยังคงถูกลดทอนไปถึง -32 dBm และ -22 dBm ตามลำดับ เหตุที่ว่าเป็นการยากที่เราจะสามารถจะชดเชยการลดทอนจากการสูญเสียเชิงวิถีเพราะว่าการลดทอนจากการสูญเสียเชิงวิถีนั้นจะมีค่าการการลดทอนที่สูงมากโดยเฉพาะเมื่อระยะห่าง

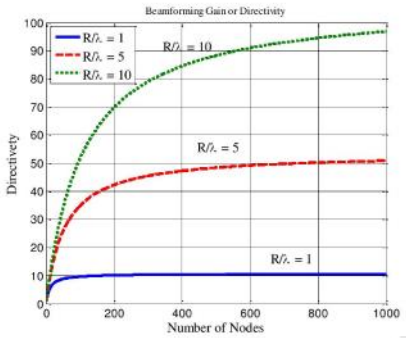

รูปที่ 6. กำลังสัญญาณที่ได้ที่สถานีปลายทาง ณ ระยะห่างระหว่างโนดกับปลายทางต่างๆ

ระหว่างโนดกับสถานีปลายทางนั้นไกลกันมากๆ ยิ่งกว่านั้นการที่เพิ่มกำลังส่งสัญญาณยังลดอายุการใช้งานของโนดลงอีกด้วย

งานวิจัย [7] ได้นำเสนอว่าเราสามารถเพิ่มอัตราขยายการส่งเพื่อขดเชยการลดทอนได้โดยการเพิ่มจำนวนโนด แต่ข้อเสนอนี้ก็มีข้อจำกัด รูปที่ 6 แสดงค่าสภาพเจาะจงทิศทางเทียบกับจำนวนโนดในรัศมีของระบบต่างๆ จากรูปจะเห็นว่าเราสภาพเจาะจงทิศทางจะเพิ่มขึ้นถ้าเราเพิ่มจำนวนโนดและรัศมี ทั้งนี้เพราะสภาพเจาะจงทิศทางจะขึ้นอยู่กับความหนาแน่น N/R ในระบบตามที่แสดงไว้ในสมการที่ (10) โดยยิ่งความหนาแน่นของโนดน้อยลงสภาพเจาะจงทิศทางจะมากขึ้น แต่สภาพเจาะจงทิศทางจะเริ่มเข้าสู่ค่าคงที่หรือเพิ่มน้อยลงทั้งนี้เพราะการเพิ่มจำนวนโนดโดยไม่เพิ่มรัศมีของระบบจะทำให้ความหนาแน่นของโนดมากส่งผลให้สภาพเจาะจงทิศทางน้อยลง จะเห็นได้จากถ้าจำนวนโนดเท่ากันที่ $R = 1$ สภาพเจาะจงทิศทางจะเพิ่มน้อยที่สุดเมื่อเทียบกับระบบที่มีรัศมีมากว่า อย่างไรก็ตามก็ตามการเพิ่มจำนวนโนดนั้นมีข้อจำกัดที่จำนวนช่องสัญญาณของระบบเช่นถ้าระบบรองรับได้ 40 ช่องสัญญาณเราก็จะไม่สามารถใช้งานโนดได้เกิน 40 โนด ยิ่งไปกว่านั้นการเพิ่มรัศมีของระบบอาจมีข้อจำกัดที่ขนาดของพื้นที่ที่นำไปติดตั้งหรือพื้นที่ที่ไม่เอื้ออำนวย

4. บทสรุป

งานวิจัยชิ้นนี้ได้ศึกษาถึงผลกระบบของการสูญเสียเชิงวิถีว่ามีผลต่อเทคนิคการก่อลำคลื่นแบบกระจายสำหรับระบบเครือข่ายเซ็นเซอร์ไร้สายอย่างไร ด้วยเหตุที่ว่างานวิจัยที่ศึกษาถึงเทคนิคการก่อลำคลื่นแบบกระจายมักจะละเลยผลกระทบจากการสูญเสียเชิงวิถี จากผลการวิจัยพบว่าการสูญเสียเชิงวิถีส่งผลต่อประสิทธิภาพของเทคนิคการก่อลำคลื่นแบบกระจายอย่างมากโดยเฉพาะในกรณีที่ระยะห่างระหว่างโนดกับปลายทางไกลกันมากๆ นอกจากนี้การขดเชยการลดทอนด้วยการเพิ่มกำลังส่งนั้นยากที่จะขดเชยการลดทอนได้ทั้งหมดอีกทั้งยังเป็นการลดอายุการใช้งานของโนดลงและการเพิ่มสภาพเจาะจงทิศทางด้วยการเพิ่มจำนวนโนดนั้นก็มีข้อจำกัดที่ขนาดของระบบและช่องสัญญาณ ดังนั้นเราจึงสามารถสรุปได้ว่าในการศึกษาเทคนิคการก่อรูปลำคลื่นแบบกระจายไม่ควรละเลยการลดทอนจากการสูญเสียเชิงวิถี

5. กิตติกรรมประกาศ

ผู้วิจัยขอขอบคุณโครงการปริญญาเอกกาญจนาภิเษกและมหาวิทยาลัยเทคโนโลยีสุรนารีสำหรับการสนับสนุนในงานทำวิจัยฉบับนี้

6. เอกสารอ้างอิง

[1] R. Mudumbai, D.R. Brown, U. Madhow, H.V. Poor, "*Distributed transmit beamforming: challenges and recent progress*," *IEEE Comm. Mag.*, Vol. 47, issue 2, pp. 102-110, Feb. 2009.

[2] Y. T. Lo, "*A mathematical theory of antenna arrays with randomly spaced elements*," *IRE Trans. Antenna Prog.*, vol. AP-12, pp. 257-268, May 1964.

[3] S. Sfar, G.J. Foschini, R.A. Valenzuela, L. Mailaender, D. Chizhik, K. Karakayali and R.S. Blum, "*Is relayed collaborative communication worth it?*" *IEEE ACSSC 2008*, , pp. 146 – 150, Oct 2008.

[4] A.N. Bishop and P.N. Pathirana, "*On the Effect of Path Loss Rates on the Optimal Receiver Position in Sensor Networks*" *IEEE ICIA 2006*, pp. 126 – 128, Dec 2006.

[5] H. Ochiai, P. Mitran, H.V. Poor, V. Tarokh, "*Collaborative beamforming for distributed wireless ad hoc sensor networks*," *IEEE Trans., Signal processing*, vol.53, issue 11, pp. 4110-4124, Nov. 2005.

[6] M.F.A. Ahmed and S.A. Vorobyov, "*Collaborative beamforming for wireless sensor networks with Gaussian distributed sensor nodes*," *IEEE Trans., Wireless Communications*, vol. 8, issue 2, pp. 638 – 643, Feb 2009.

[7] M.F.A. Ahmed, and S.A. Vorobyov, "*Sidelobe Control in Collaborative Beamforming via Node Selection* ", *IEEE Trans. Signal Processing*, vol. 58, issue 12, pp. 6168 - 6180, Dec 2010.

[8] H. Abrach, S. Bhatti, J. Carlson, et al., "*MANTIS: system sup-port for MultimodAl NeTworks of In-situ Sensors*," inProc. 2nd ACM International Workshop on Wireless Sensor Networks and Applications (WSNA '03), pp. 50–59, San Diego, Calif, USA, September 2003.

An Effect of Imperfection in Node Location Estimation on Distributed Beamforming

Pongnarin Sriploy[1], Peerapong Uthansakul[2], and Monthippa Uthansakul[3]
School of Telecommunication Engineering, Suranaree University of Technology
111, Mahawittayalai Road, Muang, Nakhon Ratchasima, Thailand 3000
[1]psriploy@hotmail.com [2]uthansakul@sut.ac.th [3]mtp@sut.ac.th

***Abstract*- Distributed beamforming technique has been introduced in the wireless sensor network (WANs) in order to increase the transmission range and signal strength of sensor node. The identical data is transmitted to the destination by all nodes which have timing and carrier synchronously. Then, the data transmissions are combined gainfully at the destination. Thus accuracy of reference signal for synchronization is extremely significant. Synchronization among nodes can achieve by utilizing the reference signals from Global Position System (GPS). This paper investigates into the effect of inaccuracy of the reference signals from GPS in term of node location (radii and phase of each node) on the beamforming performance. The simulation results show that a slightly imperfection of estimated node location can tremendously affect to the beamforming performance.**

***Index Terms*- Wireless sensor networks, beam pattern, GPS, distributed beamforming.**

I. INTRODUCTION

One of the major problems in wireless communication networks is occurred when direct transmission from mobile terminal or sensor node to destination (i.e. access point and base station) is very long distance. This tremendously affects the signal loss at destination [1]. Therefore, we often require higher amount of energy to default attenuation, which is considerably not practical. To recover this issue, a source node may be implemented with multiple antennas which can achieve sufficiently transmission power. The power gain is extended with a help of a number of antenna elements, so called antenna array [2]. Nevertheless, in many practical situations, employing antenna array has limitation in cost and size. Therefore, the distributed beamforming or collaborative beamforming technique has recently been proposed due to the advantage of dramatic increase in range, energy efficiency, data rate or Signal-to-Noise Ratio (SNR) [3 and 4]. The increasing scale of SNR in distributed beamforming is N^2, when N is number of collaborative nodes in the networks. The distributed beamforming is based on the random antenna array theory in which each node broadcasts its data to collaborative nodes in the networks [5, 6, and 7]. Then the same data is transmitted to destination by all nodes which have timing and carrier synchronously. Therefore, the transmitted data are gainfully combined at the destination. For the mention procedure, the synchronization is a key success for distributed transmission beamforming.

The synchronization can be divided into two scenarios: closed-loop and open-loop [8, 9, 10 and 11]. The closed-loop has the feedback from destination which requires knowledge of the distance, relative to the wavelength between each node and the destination. While the open-loop requires only the node locations which may be achieved by utilizing of reference signals from the Global Position System (GPS), whereas GPS can achieve a reference signal by locate a node position [12]. Therefore, the open-loop concept is more interesting as it does not require any feedback from destination. However, according to GPS Performance Standards and Specifications indicating a 95% error bound [13], using reference signal from GPS is not perfect accurate. The mentioned error in GPS may come from several causes such as: satellite geometry, satellite orbit, multipath effect and atmospheric effects. The affection of inaccuracy of GPS is approximate values such as: an ionosphere effect of ± 5 meters, Multipath effect of ± 1 meters and shifts in the satellite orbits of ± 2.5 meters [14]. An inaccuracy in position of GPS can lead to degradation in beamforming. Therefore, this paper investigates into the effect of such an imperfection of GPS accuracy in term of node location on the beamforming performance for the distributed beamforming technique when open-loop synchronization is assumed. The node locations are estimated in term of a range between sensor node and collaborative node k, radii r_k and phase of k^{th} node, ψ_k. The obtaining results provide relation between the imperfection of estimated node locations and degradation of mainbeam's gain. Note that the node locations in wireless sensor networks are randomly accordingly to probability distribution. Thus we consider the beamforming performance in term of average beamforming. The computer simulation shows that there is some error in node estimation which results in degradation of beamforming. This information can be helpful to the distributed beamforming designers who choose an open-loop scenario for network synchronization.

The remainder of this paper is organized as follows. Following introduction, a brief discussion of distributed beamforming system model and average far-field beam pattern are shown in Section II. Then, we discuss the estimated of node locations in average beam pattern in Section III. Afterwards, the simulation model and results are revealed in Section IV. Finally, Section V concludes the paper.

II. System Model and Avereage Far-Field Beam pattern

The distributed beamforming geometrical model is shown in Fig. 1, which is referred to [15]. The N sensor nodes are located in (x, y) plane where $k = 1, \dots, N$, which are random according to uniform distribution. Each node location is denoted in polar coordinates expressing by $r_k = \sqrt{x_k^2 + y_k^2}$, $\psi_k = \tan^{-1}(y_k / x_k)$. Location of the destination is denoted in spherical coordinates by $(A, \emptyset_0, \theta_0)$. In this paper, the destination node is assumed to be at the same plane as other nodes. Therefore, we assume $\theta_0 = \pi/2$. Introducing the node location vectors as $r = [r_1, r_2, \dots, r_N,] \in [0, R]^N$ and $\psi = [\psi_1, \psi_2, \dots, \psi_N,] \in [-\pi, \pi]^N$ for randomly located sensor nodes. We also assume that each node is equipped with a single isotropic antenna and the mutual coupling effects between nodes are negligible because they are sufficiently separated.

Accordingly to [15], the distance between the k^{th} nodes and destination is

$$d_k(\emptyset, \theta) \approx A - r_k \sin\theta \cos(\phi - \psi_k) \quad (1)$$

The initial phase in case of using open-loop is

$$\psi_k = \frac{2\pi}{\lambda} r_k \sin\theta_0 \cos(\phi_0 - \psi_k) \quad (2)$$

The array factor of far-field can be by

$$F \approx \frac{1}{N}\sum_{k=1}^{N} e^{j\frac{2\pi}{\lambda} r_k [\sin\theta_0 \cos(\phi_0 - \psi_k) - \sin\theta \cos(\phi - \psi_k)]} \quad (3)$$

As we assume that $\theta = \theta_0 = \pi/2$, then

$$F \approx \frac{1}{N}\sum_{k=1}^{N} e^{j\frac{4\pi}{\lambda} r_k \sin\left(\frac{\phi_0 - \phi}{2}\right) \sin\left(\varphi_k - \frac{\phi_0 + \phi}{2}\right)} \quad (4)$$

The array factor from (4) can be minimized to

$$F \approx \frac{1}{N}\sum_{k=1}^{N} e^{-j4\pi\hat{R}\sin\left(\frac{\phi}{2}\right) z_k} \quad (5)$$

where $\hat{R} = R/\lambda$ and

$$Z_k = \left(\frac{r_k}{R}\right) \sin\left(\frac{\psi_k - (\phi_0 + \phi)}{2}\right) \quad (6)$$

This has the probability density function (pdf) as

$$f_{Z_k} = \left(\frac{r_k}{R}\right)\sqrt{1 - z^2}, \quad -1 \le z \le 1 \quad (7)$$

Then, the far-field beam pattern is characterized as

$$P = |F| = FF^* = \frac{1}{N^2}\sum_{k=1}^{N}\sum_{l=1}^{N} e^{-j4\pi\hat{R}\sin\left(\frac{\phi}{2}\right)(z_k - z_l)}$$

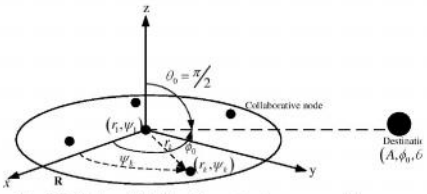

Fig. 1. Definition of distributed beamforming system model.

$$= \frac{1}{N} + \frac{1}{N^2}\sum_{k=1}^{N} e^{-j\alpha z_k}\sum_{l=1, l\neq k}^{N} e^{-j\alpha z_k} \quad (8)$$

where $\alpha = 4\pi\hat{R}\sin(\phi/2)$. As the location of each node in the systems is not known, a set of nodes are acted as a random antenna array. For this work, we assume the distribution as uniform. Hence, we investigate the beamforming performance in term of average beamforming. The average beam pattern is expressed as the expectation of the far-field beam pattern presented in (8) by

$$P_{av}(\phi) = E_z\{P\} \quad (9)$$

where $E_x\{\cdot\}$ is expectation operator. Accordingly, (7) and (8) we obtain

$$P_{av}(\phi) = \frac{1}{N} + \left(1 - \frac{1}{N}\right)\left|2\frac{J_1(\alpha)}{\alpha}\right|^2 \quad (10)$$

where $J_1(x)$ is the first-order of Bessel function.

III. Avereage Far-Field Beam pattern with Imperfect Estimated Node Location

In the open-loop scenario, an imperfection of estimated node location affects the initial phase presented in (2) as

$$\hat{\psi}_k = \frac{2\pi}{\lambda}(r_k + \Delta r_k)\cos\left(\phi_0 - (\psi_k + \Delta\psi_k)\right)$$
$$= \frac{2\pi}{\lambda} r_k \cos\left(\phi_0 - (\psi_k + \Delta\psi_k)\right) + \frac{2\pi}{\lambda}\Delta r_k \cos\left(\phi_0 - (\psi_k + \Delta\psi_k)\right) \quad (11)$$

where Δr_k and $\Delta\psi_k$ are the imperfection of estimated radii and phase, respectively. Similarity to (8), the beam pattern is expressed as

$$\hat{P} = \frac{1}{N} + \frac{1}{N^2} \times \sum_{k=1}^{N}\sum_{l=1, l\neq k}^{N} e^{-j4\pi\hat{R}\left\{z_k \sin\left(\frac{\phi - \phi_0 - \Delta\psi_k}{2}\right) - z_l \sin\left(\frac{\phi - \phi_0 - \Delta\psi_l}{2}\right)\right\}} \times e^{j\frac{2\pi}{\lambda}(v_k - v_l)} \quad (12)$$

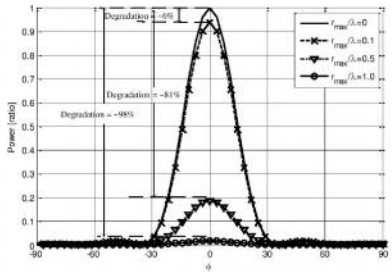

Fig. 2. Average beam pattern with imperfection of estimated radii, r_k.

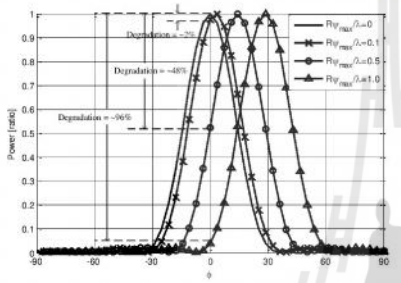

Fig. 3. Average beam pattern with imperfection of estimated phase, ψ_k.

where

$$z_k = \frac{r_k}{R}\sin\left(\psi_k + \frac{\Delta\psi_k}{2} - \frac{\phi+\phi_0}{2}\right) \quad (13)$$

$$v_k = \Delta r_k \cos(\psi_k + \Delta\psi_k - \phi_0) \quad (14)$$

We assumed that the imperfection of estimated radii Δr_k are uniformly distributed over rang of $[-r_{max}, r_{max}]$. While the imperfection of estimated phase $\Delta\psi_k$ are uniformly over $[-\psi_{max}, \psi_{max}]$ in constraint of 0 to 2π. The pdf of v_k can be expressed by

$$f_{v_k} = \frac{1}{\pi r_{max}}\left[\ln\left(1+\sqrt{1-\left(\frac{v}{r_{max}}\right)^2}\right) - \ln\frac{|v|}{r_{max}}\right] \quad \text{for } |v| \le r_{max} \quad (15)$$

Finally, the average beam pattern is expressed as

$$P_{av}(\phi) = \frac{1}{N} + \left(1-\frac{1}{N}\right)|A_\psi(\phi)|^2|A_r|^2 \quad (16)$$

where

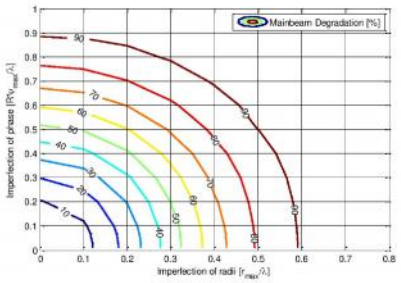

Fig. 4. Plot of mainbeam's gain degradation with respect to imperfection of estimated node location (radii and phase).

$$A_r = E_{v_k}\left\{e^{j\frac{4\pi}{\lambda}v_k}\right\}$$

$$= \frac{2}{\pi}\int_0^1 \cos\left(\frac{2\pi}{\lambda}r_{max}t\right)\ln\frac{1+\sqrt{1-t^2}}{t}dt$$

$$= {}_1F_2\left(\frac{1}{2};1,\frac{3}{2};-\left(\pi\frac{r_{max}}{\lambda}\right)^2\right) \quad (17)$$

$$A_\varphi(\phi) = E_{z_k\Delta\psi_k}\left\{e^{j4\pi R z_k \sin\left(\frac{\phi_0+\Delta\psi_k-\phi}{2}\right)}\right\}$$

$$= E_{\Delta\psi_k}\left\{\frac{J_1\left(4\pi R\sin\left(\frac{\phi-\Delta\psi_k}{2}\right)\right)}{2\pi R\sin\left(\frac{\phi-\Delta\psi_k}{2}\right)}\right\} \quad (18)$$

In next section, we investigate into how such an error caused by inaccuracy of GPS affect the beamforming performance of distributed beamforming. Moreover, the degradation of mainbeam's gain is also taken into account.

IV. Simulation Results

For simplicity to simulation, we assume that the normalized radii of network with wavelength $R = R/\lambda$ are 1 [15]. The node location is random over the networks as shown in Fig. 1 with a uniform distribution. We also assume that all nodes have identical transmitted power. The path losses are not considered. The number of sensor nodes in the simulation is 256. The destination is assumed to be located at $\phi_0 = 0°$.

Accordingly to (16) and (17), we investigate into the performance of beamforming when imperfections of estimated radii r_k are taken into account. As shown in Fig. 2, we set estimation of phase ψ_k as an error free while the imperfection of estimated radii r_k are assumed as $r_{max}/\lambda = 0.1$, $r_{max}/\lambda = 0.5$ and $r_{max}/\lambda = 1.0$. The results show that the mainbeam's gain is extremely degraded when imperfection of estimated radii r_k are occurred. The mainbeam's gain is degraded as about 6%, 81% and 98%

when $r_{max}/\lambda = 0.1$, $r_{max}/\lambda = 0.5$ and $r_{max}/\lambda = 1.0$, respectively. This is how to calculate the percentage degradation. For example for the case having $r_{max}/\lambda = 0.5$, the ratio of mainbeam is approximately 0.19 or 19%. Thus, the degradation of mainbeam's gain is 100-19 = 81% or 0.8.

In order to investigate the imperfection of estimated phase ψ_k, we utilize (16) and (18) in the simulation. According to Fig. 3, we set estimation of radii r_k to be perfect. While the imperfection of estimated phases ψ_k are assumed as $R\psi_{max}/\lambda = 0.1$, $R\psi_{max}/\lambda = 0.5$ and $R\psi_{max}/\lambda = 1.0$. The results show that the direction of obtained mainbeam are deviated from the direction of destination ($\phi_0 = 0°$.), deviated mainbeam are about 3°, 15° and 30°, thus the mainbeam's gain is degraded as about 2%, 48% and 96%,respectively. When they are compared to the optimum beamforming which has deviated direcetion is 0°, ratio of mainbeam power is 1.0 or 100%. Example to case of $R\psi_{max}/\lambda = 0.5$, the ratio of mainbeam in direction of destination is approximately 0.52 or 52%. Thus, the degradation of mainbeam's gain is 100-52=48% or 0.48. Regarding this simulation results we can conclude that the imperfection of estimated radii degrades the mainbeam's gain while the imperfection of estimated phase deviate the direction of mainbeam.

In the case when both of estimated radii and phase are imperfect. The Fig. 4 shows the contour plot of degradation of mainbeam's gain when the imperfection of estimated radii r_{max}/λ and the imperfection of estimated phase $R\psi_{max}/\lambda$ are assumed. From the figure, we can allow the imperfection of estimated radii and phase not lower than 0.2 and 0.4 in order to limit the degradation within half-power beamwidth.

Regarding the GPS issue, the authors of the work presented in [16] have tested Samsung's Galaxy S phones which have fairly serious GPS implementation issues. The authors have used Google Earth to determine the location on the linear sidewalk with the distance 333 meters. The results have revealed that the mean error in location estimation is 3.0 meters with a standard deviation of 2.0 meters when the worst-case is 8.6 meters approximately. According to this information, the imperfection of estimated radii $r_{max}/\lambda = \sim 0.3$ when assuming no error in phase, ψ_k, estimation $R\psi_{max}/\lambda = 0$. As a result, the degradation of mainbeam's gain is 40-50%, according the information from Fig. 4. Therefore, the network designer should aware of such a huge degradation when employing estimation from GPS.

V. Conclusion

This paper has revealed that the accuracy of GPS is extremely significant for distributed beamforming technique as it requires an accurate reference signal from GPS. An inaccuracy of GPS can affect a performance of beamforming. The simulation results have showed that the imperfection of estimated radii degrades the gain of mainbeam while the imperfection of estimated phase deviate the direction of mainbeam. To limit the mainbeam deviation within half-power beamwidth, the imperfection of estimated radii may be lower than 0.2 while the imperfection of estimated phase may be lower than 0.4.

Acknowledgment

The authors acknowledge the financial support from The Royal Golden Jubilee Ph.d Program (RGJ-Ph.D) 1.Q.TS/52/B.1.B.XX and Suranaree University of Technology, Thailand

References

[1] S. Sfar, G.J. Foschini, R.A. Valenzuela, L. Mailaender, D. Chizhik, K. Karakayali and R.S. Blum, "Is relayed collaborative communication worth it?" *IEEE ASILOMARSSC 2008*, pp. 146 – 150, Oct 2008.

[2] C. A. Balanis, *Antenna Theory: Analysis and Design*, 2nd ed. John Wiley, 1997.

[3] R. Mudumbai, G. Barriac, U. Madhow, "On the Feasibility of Distributed Beamforming in Wireless Networks," *IEEE Trans., Wireless Comm.*, vol. 6, issue 5, pp. 1754-1763, 2007.

[4] D. Mischa and L. Yonghui, "Cooperative Communications: Hardware, Channel&PHY", AJohn Wiley and Son, Ltd., Pub., 2010

[5] Y. T. Lo, "A mathematical theory of antenna arrays with randomly spaced elements," *IRE Trans. Antenna Prog.*, vol. AP-12, pp. 257-268, May 1964.

[6] H. Unz, "Linear arrays with arbitrarily distributed elements", *IRE Trans. Anten. Propag.*, vol. 8, no. 2, pp. 222–223. 1960.

[7] A. Ishimaru, "Theory of unequally-spaced arrays", *IRE Trans. Anten. Propag.*, vol. 10, no. 6, pp. 691–702, 1962.

[8] R. Mudumbai, D.R. Brown, U. Madhow, H.V. Poor, "Distributed transmit beamforming: challenges and recent progress," *IEEE Comm. Mag.*, Vol. 47, issue 2, pp. 102-110, Feb. 2009.

[9] D. Brown, G. Prince, and J. McNeill, "A method for carrier frequency and phase synchronization of two autonomous cooperative transmitters", *Proc. IEEE 6th Worksh. Sig. Proces. Adv. Wir. Commun.*, New York, USA, pp. 260–264, 2005.

[10] I. Ozil and D. Brown, "Time-slotted round-trip carrier synchronization", *ACSSC 2007*, Pacific Grove, USA, pp. 1781–1785, 2007.

[11] P. Jeevan, S. Pollin, A Bahai, and P Varaiya, "Pairwise algorithm for distributed transmit beamforming", *IEEE. ICC'08*, Beijing, China, pp. 4245–4249, 2008.

[12] G. Xu, *GPS : theory, algorithms, and applications* 2nd. New York : Springer, c2007.

[13] "GPS Performance Standards & Specifications" available: http://www.gps.gov/technical/ps/

[14] "Sources of Errors in GPS" available: http://www.kowoma.de/en/gps/errors.htm

[15] H. Ochiai, P. Mitran, H.V. Poor, V. Tarokh, "Collaborative beamforming for distributed wireless ad hoc sensor networks," *IEEE Trans., Signal processing*, vol.53, issue 11, pp. 4110-4124, Nov. 2005.

[16] "Samsung Epic 4G GPS walking test" available: http://www.paleotechnologist.net/?p=409

Effect of Path Loss on the Distributed Beamforming for Wireless Sensor Networks

Pongnarin Sriploy[1], Peerapong Uthansakul[2], and Monthippa Uthansakul[3]
School of Telecommunication Engineering, Suranaree University of Technology
111, Mahawittayalai Road, Muang, NakhonRatchasima, Thailand 3000
[1]d5440054@g.sut.ac.th [2]uthansakul@sut.ac.th [3]mtp@sut.ac.th

***Abstract*—From literatures, path loss effect has not been taken into account when analyzing beamforming performance of distributed or cooperative beamforming networks such as Wireless Sensor Networks (WSNs). Therefore, this paper investigates into the mentioned effect on beamforming performance of WSNs through computer simulation. The obtained results indicate that the path loss occurring between the networks and destination extremely degrades beam pattern and beamforming gain.**

***Keywords*—Beam pattern, Distributed beamforming, Free-Space Path loss, Wireless sensor networks**

I. INTRODUCTION

Recently, Wireless Sensor Networks (WSNs) have gained lot of consideration into several monitoring applications in various areas. This is because WSNs have an advantage in term of flexibility as its sensor nodes are scalable and movable. However, WSNs have a major limitation in term of energy efficiency and battery lifetime. As the sensor nodes are small of size, carrying long-life battery having large dimension is impractical. Moreover, sometimes the sensor networks are installed in some inaccessible places such as roof of building, forest or river. This results in difficulty for battery replacement. Thus, WSNs minimize their energy consumption by utilizing techniques such as ad hoc protocol, low-power processing or data collision reduction. However, in some situations, extra power is still needed e.g. when the distance between sensor nodes and destination is long. This introduces signal loss at destination. To avoid the mention impairments, sensor networks have to boost up the transmitted power. However, this is considerably not practical as battery lifetime is shortened. Recently, utilizing multiple antenna elements at individual sensor nodes have been considered as the transmitted power can be gained depending on a number of antenna elements, so called antenna array [1].Nevertheless, installing antenna array has limitation in cost and size. Therefore, a distributed beamforming or collaborative beamforming technique has recently been considered to WSNs due to the advantage of dramatic increase in range, energy efficiency, data rate or Signal-to-Noise Ratio (SNR)[2]. The increasing scale of SNR in distributed beamforming is N^2, when N is number of collaborative wireless sensor nodes in the networks. The distributed beamforming is based on random array theory as a number and position of sensor nodes in WSNs are often random. A sensor node distributes its data among neighboring nodes then all nodes transmit the same data to destination with time and carrier synchronization [3]. Therefore, the transmitted data are gainfully combined at the destination.

As known that attenuation in free-space path loss degrades wireless communication performance. The authors of the work presented in [4] have shown that path loss degrade the transmitted signal strength in WSNs. They have also recommended that a higher number of nodes is required to improve the system performance. The work presented in [5] has studied some problems in finding an optimal position for a sensor node. The authors have revealed that signal path loss tremendously affects the topology of sensor networks. However, most of literatures dealing with distributed beamforming on WSNs have not taken into account the effect of signal path loss. For example, the work presented in [6] has studied performance of distributed beamforming for wireless ad hoc sensor networks in which the distributions of nodes are uniform. The authors have shown the system performance in the term of average far-field beam pattern, 3-dB beamwidth and directivity with respect to several numbers of nodes and network radius. Also, the authors of the work presented in [7] have revealed the distributed beamforming performance when all nodes are distributed with Gaussian manner. Both works appeared in [6-7] and also in [8-10] have not considered the effect of path loss which probably alters the system performance. However, the work presented in [11] has mentioned that signal path loss is negligible when increasing number of collaborative nodes, gaining transmitted power or compensating received signal at destination. An increase in a number of sensor nodes is considerably not practical as this can result in budget limitation. Also, gaining transmitted power is unreasonable because of battery-lifetime constraint. In addition, compensating signal at destination is not possible when path loss is severe as the margin between desired and undesired signal is low [12]. Moreover, this also increases the network complexity [13].

Therefore this paper investigates a path loss effect on distributed beamforming for WSNs. The obtained results show that the free space path loss has extremely effected on distributed WSNs beamforming. This is because the destination cannot receive a transmitted signal as it is lower than signal sensitivity.

The remainder of this paper is organized as follows. Following introduction, a brief discussion of distributed beamforming and path loss effect is shown in Section II. Afterwards, the simulation and results are revealed in Section III. Finally, Section IV concludes the paper.

978-1-4799-0545-4/13/S31.00 ©2013 IEEE

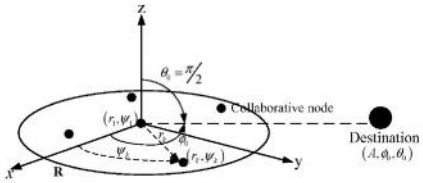

Fig. 1.Definition of distributed beamforming system model.

II. Path loss Model and Average Far-Field Beampattern

A. System Model of Distributed beamforming and Path Loss

The distributed beamforming geometrical model is shown in Fig. 1, which is referred to the work presented in [6]. The N sensor nodes are located in (x, y) plane where $k = 1, \ldots, N$. This k parameter is random according to uniform distribution. Each node location is denoted in polar coordinates expressed by $r_k = \sqrt{x_k^2 + y_k^2}$ and $\psi_k = \tan^{-1}(y_k/x_k)$. Location of the destination is denoted in spherical coordinates denoted by$(A, \emptyset_0, \theta_0)$. In this work, the destination (base station or access point) is assumed to be located at the same plane as other nodes are. As a result, we assume that$\theta_0 = \pi/2$. The node location vectors are $r = [r_1, r_2, \ldots, r_N,] \in [0, R]^N$ and $\psi = [\psi_1, \psi_2, \ldots, \psi_N,] \in [-\pi, \pi]^N$ which are randomly located. We also assume that each node is equipped with a single isotropic antenna and the mutual coupling effects between nodes are negligible because they are sufficiently separated.

The initial phase of each sensor node in the case of open-loop synchronization (referred to x-axis) is

$$\psi_k = \frac{2\pi}{\lambda} r_k \sin\theta_0 \cos(\phi_0 - \psi_k) \tag{1}$$

We assume that each sensor node is located in polar coordinates. As we can see in Fig. 1, sensor node geometry is appeared as circular antenna array as the location of nodes are randomly $r_k$and ψ_k. Therefore the far-field array factor of distributed beamforming for wireless sensor can be written by

$$F(\phi, \theta: r_k, \psi_k) \approx \frac{1}{N}\sum_{k=1}^{N} e^{j\frac{2\pi}{\lambda} r_k[\sin\theta_0 \cos(\phi_0 - \psi_k) - \sin\theta\cos(\phi - \psi_k)]} \tag{2}$$

Note that the destination is located on the same plane as sensor nodes, $\theta = \theta_0 = \pi/2$. Then (2) can be minimized to

$$F(\phi: r_k, \psi_k) = \frac{1}{N}\sum_{k=1}^{N} e^{j\frac{4\pi}{\lambda} r_k \sin\left(\frac{\phi_0 - \phi}{2}\right)\sin\left(\varphi_k - \frac{\phi_0 + \phi}{2}\right)} = \frac{1}{N}\sum_{k=1}^{N} e^{j\frac{4\pi R}{\lambda}\sin\left(\frac{\phi_0 - \phi}{2}\right)\left(\frac{r_k}{R}\right)\sin\left(\varphi_k - \frac{\phi_0 + \phi}{2}\right)} \tag{3}$$

Moreover we assumed that the direction of the destination is denoted as $\phi_0 = 0$. Thus, the position of destination is $(A, \phi_0 = 0, \theta_0 = \pi/2)$. Therefore, the array factor from (3) can be minimized to be

$$F(\phi: z_k) \approx \frac{1}{N}\sum_{k=1}^{N} e^{-j4\pi\hat{R}\sin\left(\frac{\phi}{2}\right) z_k} \tag{4}$$

where $\hat{R} = R/\lambda$ representing the normalized network radius with lambda. Then, corresponding z_k is

$$z_k(\phi: r_k, \psi_k) = \left(\frac{r_k}{R}\right)\sin\left(\psi_k - \left(\frac{(\phi_0 + \phi)}{2}\right)\right) \tag{5}$$

This z_k has the probability density function (pdf) as

$$f_{z_k} = \left(\frac{r_k}{R}\right)\sqrt{1 - z^2}, \quad -1 \le z \le 1 \tag{6}$$

We can estimate the radiation pattern by taking absolute array factor of (4). Then the far-field radiation pattern is characterized as

$$P(\phi: z_k) = |F(\phi: z_k)|^2 = F(\phi: z_k)F^*(\phi: z_k) = \frac{1}{N^2}\sum_{k=1}^{N}\sum_{l=1}^{N} e^{-j4\pi\hat{R}\sin\left(\frac{\phi}{2}\right)(z_k - z_l)} = \frac{1}{N} + \frac{1}{N^2}\sum_{k=1}^{N} e^{-j\beta z_k}\sum_{l=1, l\neq k}^{N} e^{-j\beta z_k} \tag{7}$$

where $\beta = 4\pi\hat{R}\sin(\phi/2)$.

As a set of nodes are acted similar to a random antenna array. For this paper, we assume that positions of nodes are uniform. Next, we investigate the beamforming performance in term of average beam pattern. The average beam pattern is expressed as the expectation of the far-field beam pattern presented as

$$P_{av}(\phi) = E_z\{P(\phi: z_k)\} \tag{8}$$

where $E_x\{\cdot\}$ is expectation operator. According to (6) and (7), we obtain

$$P_{av}(\phi, \beta) = \frac{1}{N} + \left(1 - \frac{1}{N}\right)\left|2\frac{J_1(4\pi\hat{R}\sin(\phi/2))}{4\pi\hat{R}\sin(\phi/2)}\right|^2 \tag{9}$$

where $J_1(\cdot)$ is first-order Bessel function and N is number of nodes.

Equation (9) reflects the figure of average beam pattern in which the first term is related to side lobe level. As we can see, lower side lobe level can be obtained when increasing number of N. The second term appeared in (9) is related to beamwidth of main lobe which can be controlled by $\hat{R}$. As a result, the factors N and $\hat{R}$ appeared in (9) control beamforming gain or directivity of distributed beamforming.

The mentioned directivity of sensor node can be expressed by

$$D = \frac{U}{U_0} = \frac{\int_{-\pi}^{\pi} P(0)d\phi}{\int_{-\pi}^{\pi} P(\phi)d\phi} = \frac{2\pi}{\int_{-\pi}^{\pi} P(\phi)d\phi} \tag{10}$$

When U is the radiation intensity (W/unit solid angle), U_0 is the radiation intensity of isotropic antenna (W/unit solid angle) and $P(\phi)$ is the radiation intensity in direction of ϕ.

TABLE I
SIMULATION PARAMETERS FOR OUTDOOR SCENARIO

Operation Frequency	ISM band, 902-928 MHz
Number Nodes (N)	40 Nodes
Node Distribution	Uniform
Radius of Network	5
Transmission Range	<10 km. (macro cell)
Radiated Power	0 dBm, 10 dBm, 20 dBm
Signal Sensitivity	-106 dBm
Transmitted Antenna Gain	2.5 dBi
Received Antenna Gain	5 dBi

The work presented in [6] has shown the close-form formula for distributed beamforming as

$$D = \frac{N}{1+0.09332\frac{N}{R}} \quad (11)$$

B. Path loss Channel Model

In this paper, we assume that WSNs is considered in outdoor condition as the most WSNs are utilized. For this case, we adopt a simple Free-Space Path Loss (FSPL) model is expressed by

$$\alpha_k(dB) = 20log_{10}(d_k) + 20log_{10}(f) - 27.55 \quad (12)$$

where d_k is a distance between sensor node k^{th} and destination (meters) and f is an operating frequency (megahertz).

We utilize Euclidean estimation for approximating the distance between the k^{th} node and destination which is expressed as

$$d_k(\phi,\theta) = \sqrt{A^2 + r_k^2 - 2r_k A\sin\theta\cos(\phi-\psi_k)} \quad (13)$$

where A is the distance between center of network and the destination as shown in Fig 1.while$r_k$is the location of sensor nodes referred to the network center.

Analyzing a radiation pattern are commonly considered in far-field region which has very long distance between sensor nodes and destination, $A \gg r_k$. Then, (12) can be minimized to

$$d_k(\phi,\theta) \approx A - r_k\sin\theta\cos(\phi-\psi_k) \quad (14)$$

When the size of network is not large, we may estimate $d_k(\phi,\theta) \approx A$ which is represented to all node's distance.

III. SIMULATION RESULTS AND DISCUSSIONS

This section reveals the effect of path loss on the beamforming performance of distributed beamforming for WSNs. Some utilized parameters appeared from [14] are adopted in which the authors have developed WSNs for area monitoring and integrated vehicle health management having several nodes distance. The utilized parameters for the simulation in this paper are shown in Table 1. Note that each node is equipped with a single isotropic antenna which has identical radiated power.

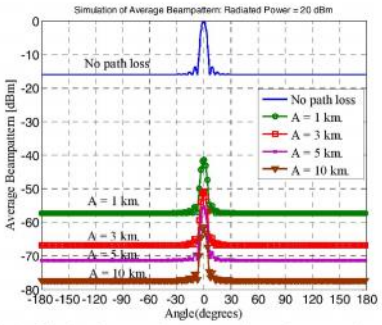

Fig. 2. Simulated average beam pattern in outdoor scenario with several A when number of collaborative nodes (N) is 40 nodes and radiated power is 20 dBm.

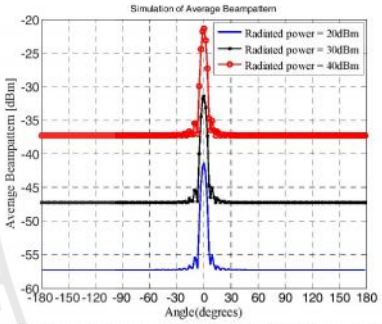

Fig. 3. Simulated average beam pattern in outdoor scenario with several radiated power when number of collaborative nodes (N) is 40 nodes and A is 1000 m.

Fig. 2 shows the average beam pattern of distributed beamforming for outdoor scenario when the 40 sensor nodes are randomly located in the networks. Please note that this number is referred to the number of channel. As we can see, the effect of path loss is more pronounced when distance between the network and destination increases. At A = 1 km, the average beam pattern is dropped to -40 dBm. At longer distance, the beam pattern gain is dropped to -50 dBm, -57 dBm and -62 dBm when A = 3 km, 5 km and 10 km respectively. This is because that path loss effect is more pronounced when distance between transmitter and receiver increases according to (12) and (13).

Fig. 3 shows the average beam pattern of distributed beamforming when the radiated power is given as: 20 dBm, 30 dBm and 40 dBm. The beamforming gain is also degraded with respect to a decrease in radiated power. As we can see in the figure, beamforming gain is of -43 dBm, -33 dBm and -23 dBm when the radiated power is 20 dBm, 30 dBm and 40 dBm respectively. These results have revealed that radiated

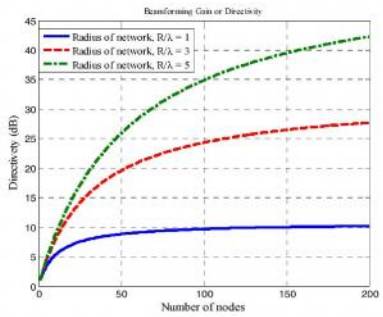

Fig. 4.Number of nodes vs. beamforming gain.

power can be pushed up in order to compensate the path loss between the network and destination. Note that the mentioned compensation is not practical when the transmitter is situated at very far away from receiver. Moreover, this is considerably not practical as the battery-lifetime of sensor networks is very limited. Nevertheless, some researchers have proposed the idea of increasing the number of nodes to tackle the mentioned problem. As we can see in Fig. 4, this figure presents that beamforming gain or directivity can be increased when utilizing more number of sensor nodes. This is because the beamforming gain or directivity is related to the nodes density $N/\hat{R}$ as shown in (11). However, the directivity is stable at higher number of nodes. Referring to (11), the directivity depends on only $\hat{R}$ at high number of nodes, which has been constantly given at the beginning. Also, as seen in Fig. 4, the higher $\hat{R}/\lambda$ is given, the higher directivity can be obtained. The reason is that directivity is reverse to the network radii as shown in (11).

At this point, path loss extremely affects the beamforming performance of distributed beamforming systems. There are several remedies such as increasing of the network radii or number of utilized nodes. However, these are considerably not practical. Firstly, utilizing higher number nodes introduces an increased budget. Also, adding more number of nodes is not possible e.g., the work presented in [14] has utilized only 40 channels. This means that maximum number of node which can operate at the same time is only 40.Moreover, an increase in network radii may be limited by the size of implemented area or environment.

IV. Conclusion

This paper has studies the effect of path loss on beamforming performance of distributed WSNs. The reason is that most of literatures have neglected this impairment. From running some simulations, we can see that path loss extremely effect on beam pattern in the way of decreasing beamforming gain. In addition, at long distance between the networks and destination, the beamforming is failed. However, some simulations have revealed that increasing number of nodes or radiated power helps boosting up the beamforming gain. Nevertheless, this is considerably not practical because increasing number of nodes has impact to the system budget. In addition, the number of utilized nodes is limited according to available channels of the systems. In summary, the path loss effect is one important factor that should not be ignored when designing a distributed or cooperative beamforming networks.

Acknowledgment

The authors acknowledge the financial support from The Royal Golden Jubilee Ph.d Program (RGJ-Ph.D) 1.Q.TS/52/B.1.B.XX and Suranaree University of Technology, Thailand.

References

[1] C. A. Balanis, *Antenna Theory: Analysis and Design*, 2nd ed. John Wiley, 1997.

[2] R. Mudumbai, G. Barriac,U. Madhow, "On the Feasibility of Distributed Beamforming in Wireless Networks," *IEEE Trans., Wireless Comm.*, vol. 6, issue 5, pp. 1754-1763, 2007.

[3] Y. T. Lo, "A mathematical theory of antenna arrays with randomly spaced elements," *IRE Trans. Antenna Prog.*, vol. AP-12, pp. 257-268, May 1964.

[4] S. Sfar, G.J. Foschini, R.A. Valenzuela, L. Mailaender, D. Chizhik, K. Karakayali and R.S.Blum, "Is relayed collaborative communication worth it?" *IEEE ACSSC 2008*, , pp. 146 – 150, Oct 2008.

[5] A.N. Bishop and P.N. Pathirana, "On the Effect of Path Loss Rates on the Optimal Receiver Position in Sensor Networks" *IEEE ICIA 2006*, pp. 126 – 128, Dec 2006.

[6] H. Ochiai,P. Mitran,H.V. Poor,V. Tarokh, "Collaborative beamforming for distributed wireless ad hoc sensor networks,"*IEEE Trans., Signal processing*, vol.53, issue 11, pp. 4110-4124, Nov. 2005.

[7] M.F.A. Ahmed and S.A. Vorobyov, "Collaborative beamforming for wireless sensor networks with Gaussian distributed sensor nodes," *IEEE Trans., Wireless Communications*, vol. 8, issue 2, pp. 638 – 643, Feb 2009.

[8] M. Ahmed and S. Vorobyov, "Node selection for sidelobe control in collaborative beamforming for wireless sensor networks", *Proc. IEEE 10th Worksh. Sig. Proces. Adv. Wir. Commun. SPAWC'09*, Perugia, Italy, pp. 519–52, 2009.

[9] K. Zarifi, A. Ghrayeb, and S. Affes, "Distributed Beamforming for Wireless Sensor Networks With Improved Graph Connectivity and Energy Efficiency ", *IEEE Trans. Signal Processing*, vol. 58, issue 3, pp. 1904 – 1921, March 2010.

[10] W. Lintz, J. McEachen, and M. Tummala, "Sensor beamforming with distributed mobile elements in a wireless sensor network",*in Proc. Canadian Conf. Elec. Comp. Eng. CCECE'09*, St. John's, Newfoun-land and Labrada, Canada, 2009, pp. 323–328.

[11] M.F.A. Ahmed, and S.A. Vorobyov, "Sidelobe Control in Collaborative Beamforming via Node Selection", *IEEE Trans. Signal Processing*, vol. 58, issue 12, pp. 6168 - 6180, Dec 2010.

[12] S. Ahmed, and H. Arslan, "Evaluation and compensation of frequency dependent path loss over OFDM subcarriers in UAC", *IEEE Conf. OCEANS 2009*, 26-29 Oct. 2009, pp. 1-5.

[13] R.G. Mazzolin, "Technology challenges in adapting commercial wireless technology to military applications", IEEE Antennas and Prop. for Wireless Com., 2000, pp. 161-164.

[14] H. O. Marcy, J. R. Agre, C. Chien, L. P. Clare, N. Romanov, andA. Twarowski, "Wireless sensor networks for area monitoring and integrted vehicle health management applications," *Proc. AIAA Guidance, Navigation, and Control Conference and Exhibit*, Portland, Orc, USA, vol. 1, 1999.

The Optimum Number of Nodes and Radius for Distributed Beamforming Networks

Pongnarin Sriploy[*1],
Peerapong Uthansakul[*2], and **Monthippa Uthansakul**[*3], Non-members

ABSTRACT

This paper presents a ready-made formula to calculate the number of node and network radius for distributed beamforming networks. The calculation is based on guarantee of received signal at destination to be higher than received sensitivity. The proposed calculation model already includes path loss and also imperfection in node location estimation, which can be applied for both indoor and outdoor scenarios.

Keywords: Array signal processing, Distributed beamforming, Path loss, Phase synchronization and Wireless communications.

1. INTRODUCTION

As a rapid increase in data rate transmission in wireless communication is needed, distributed beamforming networks are currently considered as one solution for the next generation of wireless communication systems. The distributed beamforming is based on a random antenna array theory in which all user terminals in the network transmit their same signal at same time to destination or base station [1]. Then, the received signal at destination can be gained when the phase of transmitted signal are aligned following some phase synchronization techniques. According to this concept, the received signal at destination can be gained by $10log_{10}N$, where N stands for the number of collaborative user terminals in the networks. If all user terminals transmit collaborative signal without phase synchronization, the received signal at destination may be not gained as the received signal's phases are off-set. Therefore, phase synchronization is a relatively significant key to obtain maximum beamforming gain. Generally, phase synchronization can be divided into two scenarios according to interaction between nodes and destination: closed-loop and open-loop [2]. For the first concept, destination directly controls the node's phase adjustment by transmitting feedback signal from destination to nodes in which knowledge of distance relative to wavelength between each node and destination is required. According to this, nodes in the networks are able to compensate own phase off-set following the feedback reference signals. Some examples of the mentioned concept have been shown in [3, 4], which are full-feedback closed-loop and one-bit feedback closed-loop synchronization, respectively. For the later concept, the information of node location is required, which can be usually obtained from Global Position System (GPS). Then, nodes in the networks are able to compensate individual phase off-set according to node location information. Some examples of open-loop phase synchronization are master-slave and round-trip open-loop synchronizations as shown in [5, 6]. Comparing between these two scenarios, the open-loop synchronization is more interesting as it does not require any feedback from destination. Unfortunately, utilizing synchronization technique such as one-bit feedback or master-slave gives rise to system complexity at nodes and destination. However, as mentioned before, we can reduce this complexity by utilization of GPS at individual nodes. Then the information of node location can be obtained from GPS directly. Thus, nodes in the networks compensate own phase off-set according to node location information instead of employing phase compensating message though the open-loop concept [7]. However, from literatures, GPS performance standards and specifications indicate an error in location estimation at bound of 95% [8]. As a result, using reference signal from GPS is not a perfect choice. The mentioned error in GPS may come from several causes such as: satellite geometry, satellite orbit, multipath effect or atmospheric effects [9]. Our previous work [10] has shown that the imperfection in node location estimation in terms of radius degrades the gain in the direction of main beam. Also, imperfection in terms of phase makes some changes in main beam direction. However, phase synchronizing error is not the only one factor that affects beamforming performance, but also the path-loss between nodes and destination. The authors of the work presented in [11] have shown that path loss degrades the transmitted signal strength in distributed networks. They have also recommended that an increase in the number of nodes is required to improve the system performance. In addition, the work presented in [12] has also revealed that signal path loss tremendously affects the topology of the networks. Moreover, from

Manuscript received on July 31, 2014 ; revised on December 11, 2014.

* The authors are with Department of School of Telecommunication Engineering, Suranaree University of Technology 111, Mahawittayalai Road, Muang, Nakhon Ratchasima, Thailand 3000 Email: 1D5440054@g.sut.ac.th[1], uthansakul@sut.ac.th[2], mtp@sut.ac.th[3]

our previous work [13], path loss extremely affects beam pattern as it degrades the beamforming gain. At this point, it can be said that phase synchronization and path-loss extremely involve in evaluating the performance of distributed beamforming networks. According to the degradation mentioned above, some researchers have proposed an increase in the number of collaborative nodes and radius of the networks [14, 15]. The reason is that increasing number of collaborative nodes and network radius provides higher beamforming gain. The results have indicated that side lobe level can be reduced when increasing the number of nodes and main beam width is reduced as network radius increases. Unfortunately, an increase in the number of nodes is relatively limited by communication channel and also this introduces an increased budget. Also, the concept of allowing longer network radius may be limited by available space. However, gaining transmitted power is an alternative choice. Still, increasing power in transmitter is also relatively limited because of battery-lifetime constraint. Therefore in this paper, we propose an idea to choose an optimum number of collaborative nodes and network radius for distributed beamforming. The effect of phase synchronizing error and path loos are included to the model. The outcome of study is a ready-made formula to calculate the appropriate number of node and network radius with respect to received sensitivity.

The remainder of this paper is organized as follows. Following introduction, a brief discussion of distributed beamforming and path loss model are shown in Section 2 and 3 respectively. Moreover, the effect of phase synchronizing error in distributed beamforming is discussed in Section 4. Afterwards, the proposed concept for optimum selection of the number of nodes and network radius is presented in Section 5. Finally, Section 6 concludes the paper.

2. DISTRIBUTED BEAMFORMING WITH PERFECT PHASE SYNCHRONIZATION

The distributed beamforming geometry is shown in Fig. 1 which refers to the work presented in [7]. The N collaborative nodes are located in (x, y) plane where k stands for node index ($k = 1, , N$). The node location is uniformly distributed in a specified region. Also, node location is denoted in polar coordinate which is expressed by $r_k = \sqrt{x_k^2 + y_k^2}$ and $\psi_k = tan^{-1}(y_k/x_k)$. Also, destination position is denoted in spherical coordinates by (A, ϕ_0, θ_0). In this work, destination (base station or access point) is assumed at the same plane of other nodes, $\theta_0 = \pi/2$. The node location vectors are $r_k \in [-\pi, \pi]^N$ and $\psi_k \in [-\pi, \pi]^N$. We also assume that each node is equipped with a single isotropic antenna. Also, the mutual coupling effects between nodes are negligible because they are sufficiently separated.

The initial phase of individual node in case of open-loop synchronization referred to x-axis is expressed by

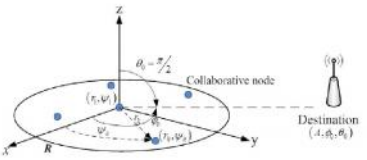

Fig.1: *Definition of distributed beamforming systems.*

$$\Psi_k = \frac{2\pi}{\lambda} r_k \sin\theta_0 \cos(\phi_0 - \psi_k) \tag{1}$$

where λ is the wavelength, r_k is distance between k_{th} node and network center. Also, θ_0 and ϕ_0 are direction angles of destination referred to x-axis and z-axis respectively as seen in Fig. 1 while ψ_k is direction angle of k_{th} node referred to x-axis. As considered in far-field region, we assume that each node is located in polar coordinates. Thus, sensor node geometry looks like circular array but location of nodes are random with parameters r_k and ψ_k. Therefore, the far-field array factor of distributed sensor or user terminals can be written as

$$F(\phi, \theta | r, \psi) \approx \frac{1}{N} \sum_{k=1}^{N} e^{j\frac{2\pi}{\lambda} r_k [\sin\theta_0 \cos(\phi_0 - \psi_k) - \sin\theta\cos(\phi - \psi_k)]} \tag{2}$$

where N is the number of nodes. As we can see in (2), it is similar to circular array factor equation while the node location (r_k, ψ_k) is random. We has previously denoted that destination is located on the same plane with nodes, $\theta = \theta_0 = \pi/2$. Then, (2) can be minimized to

$$\begin{aligned} \bar{F}(\phi | r, \psi) &= \frac{1}{N} \sum_{k=1}^{N} e^{j\frac{4\pi}{\lambda} r_k \sin\left(\frac{\phi_0 - \phi}{2}\right) \sin\left(\psi_k - \frac{\phi_0 + \phi}{2}\right)} \\ &= \frac{1}{N} \sum_{k=1}^{N} e^{j4\pi\frac{R}{\lambda} \sin\left(\frac{\phi_0 - \phi}{2}\right) \bar{r}_k \sin\left(\tilde{\psi}_k\right)} \end{aligned} \tag{3}$$

where R is network radius, $\bar{r}_k = r_k/R$ and $\tilde{\psi}_k = \psi_k - ((\phi_0 + \phi)/2)$. If network model is a symmetrical circular respected to azimuth angle ϕ, then its array factor does not relate to ϕ_0. To ease the calculation, we also assume that destination direction is at bore sight direction, $\phi_0 = 0°$. Thus, the position of destination is $A, \phi_0 = 0°, \theta_0 = \pi/2$, note that $-\pi \le \phi \le \pi$. Then the distributed beamforming array factor from (3) can be minimized to

$$\bar{F}(\phi | z) = \frac{1}{N} \sum_{k=1}^{N} e^{-j4\pi\bar{R}\sin\left(\frac{\phi}{2}\right) z_k} \tag{4}$$

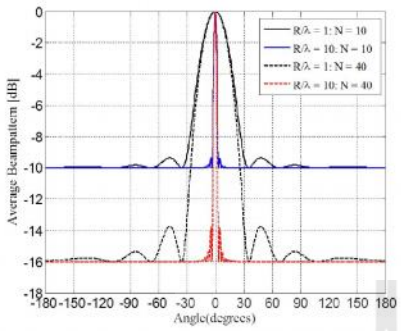

Fig.2: *Average beampattern of distributed beamforming networks with various N and $\tilde{R}$.*

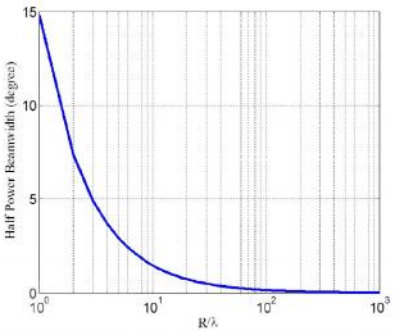

Fig.3: *Half-power beam width of distributed beamforming networks with various network radius $\tilde{R}$.*

where $\tilde{R} = R/\lambda$ is a normalized network radius and corresponding z_k is defined by

$$z_k = \tilde{r}_k \sin\left(\tilde{\psi}_k\right) \tag{5}$$

This z_k has the probability density function (pdf) as follow:

$$f_{z_k}(z) = \frac{2}{\pi}\sqrt{1-z^2}, \qquad -1 \le z \le 1 \tag{6}$$

We can estimate the radiation pattern by taking magnitude of the array factor shown in (4). Then, the far-field radiation pattern is characterized by

$$\begin{aligned} P(\phi|z) &\triangleq \left|\tilde{F}(\phi|z)\right|^2 = \tilde{F}(\phi|z)\,\tilde{F}^*(\phi|z) \\ &= \frac{1}{N^2}\sum_{k=1}^{N}\sum_{l=1}^{N} e^{j4\pi\tilde{R}\sin\left(\frac{\phi_0-\phi}{2}\right)(z_k-z_l)} \\ &= \frac{1}{N} + \frac{1}{N^2}\sum_{k=1}^{N} e^{j\alpha(\phi)z_k}\sum_{\substack{l=1\\ l\neq k}}^{N} e^{-j\alpha(\phi)z_l} \end{aligned} \tag{7}$$

where $\alpha(\phi) = 4\pi\tilde{R}\sin\left((\phi_0-\phi)/2\right)$ and ϕ is destination direction in azimuth, within $-\pi \le \phi \le \pi$.

In this paper, nodes positions are assumed to have uniformly random distribution. Thus, we investigate the beamforming performance in terms of average beam- pattern. The average beampattern is expressed by the expectation of far-field beam pattern as follow:

$$P_{av}(\phi) = \mathrm{E}_z\left\{P(\phi|z)\right\} \tag{8}$$

where $E_z\{.\}$ is expectation operator. According to (6) and (7), we obtain average beampattern as

$$P_{av}(\phi) = \frac{1}{N} + \left(1-\frac{1}{N}\right)\left|2\frac{J_1(\alpha(\phi))}{\alpha(\phi)}\right|^2 \tag{9}$$

where $J_1(.)$ is first-order Bessel function, N is the number of nodes,$\tilde{R} = R/\lambda$ is normalized network radius and ϕ is destination direction in azimuth. The (9) informs the behavior of average beampattern when the first term of this expression $1/N$ relates to side lobe level. As we can see in Fig. 2, side lobe level becomes lower as the number of nodes N increases. This is because increasing N makes the term of $1/N$ smaller. According to this, side lobe level is only related to the number of nodes while main beam width is related to network radius $\tilde{R}$ in which narrower beam width can be achieved when increasing network radius. This is because main beam width correlates with the second term of (9) or $(1-(1/N))\left|2J_1(\alpha(\phi))/\alpha(\phi)\right|^2$. When the number of node is very large thus the second term of (9) can be minimized to $\left|2J_1(\alpha(\phi))/\alpha(\phi)\right|^2$. Therefore, $\lim_{\alpha(\phi)\to+\infty}\left|2J_1(\alpha(\phi))/\alpha(\phi)\right|^2 \approx 0$. Also in (7), $\alpha(\phi)$ is related to network radius . Thus, main beam width can be decreased by increasing network radius $\tilde{R}$. In conclusion, factors N and $\tilde{R}$ appeared in (9) directly relate to beamforming gain of distributed beamforming.

Half-power beam width (HPBW) or 3-dB beam width is the angular separation between the half-power points (or 3-dB) on the antenna radiation pattern, referred to the maximum value of main beam gain. The HPBW of distributed beamforming relates to network radius of collaborative node as discussed before. The HPBW of average beampattern for distributed beamforming can be achieved by numerical solving as shown in (10).

$$\begin{aligned} &\phi_{av}^{3dB} = 2\sin^{-1}\left(\frac{0.1286}{\tilde{R}}\right) \\ &or \quad \phi_{av}^{3dB} = \frac{0.26}{\tilde{R}} \quad when \quad \tilde{R} \gg 1 \end{aligned} \tag{10}$$

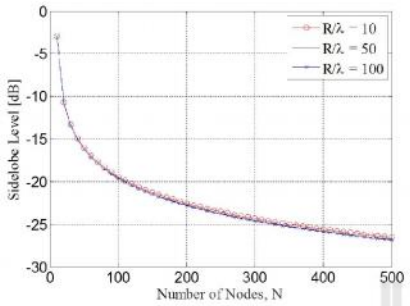

Fig.4: *Side lobe level of distributed beamforming networks with various the numbers of nodes.*

The (10) describes that main beam width inversely depend on network radius. This means that its HPBW can be decreased as network radius increases. This behavior is shown in Fig. 3. On the other hand, increasing network radius is involved side lobe level. Fig. 4 shows simulation result regarding the effect of changing network radius on side lobe level. As we can see, side lobe level of beamforming pattern becomes lower when increasing the number of nodes.

Another important parameter of beampattern is directivity. The directivity informs radiated gain in desired direction referred to single isotropic antenna. The definition of directivity is as follow:

$$D = \frac{U}{U_0} = \frac{\int_{-\pi}^{\pi} P(0)\, d\phi}{\int_{-\pi}^{\pi} P(\phi)\, d\phi} = \frac{2\pi}{\int_{-\pi}^{\pi} P(\phi)\, d\phi} \quad (11)$$

when U is radiation intensity (W/unit solid angle), U_0 is radiation intensity of isotropic antenna (W/unit solid angle) and $P(\phi)$ is radiation intensity in direction of ϕ. A summary equation of directivity from the work presented in [7] is adopted in this paper as follow:

$$D_{av} \geq \frac{N}{1 + 0.09332\frac{N}{\tilde{R}}} \quad (12)$$

Fig. 5 shows the directivity with respect to various the number of nodes and network radius, N and $\tilde{R}$ respectively. As we can see in this figure, directivity is gained as N and $\tilde{R}$ increase. This is because increasing N provides lower side lobe level and increasing $\tilde{R}$ makes its main beam narrower as described in (9). The directivity of distributed beamforming is a parameter to compensate the degradation caused by path loss which will be discussed in next section.

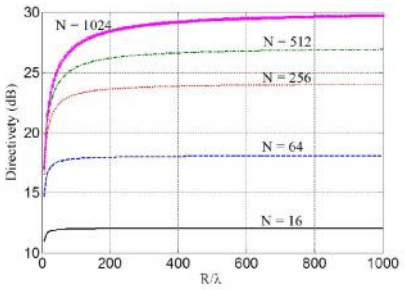

Fig.5: *Directivity of distributed beamforming networks with various N and $\tilde{R}$.*

3. PATH LOSS CHANNEL MODEL

Path loss between user terminals and destination is one significant factor to indicate true performance of the networks. In this paper, we consider path loss for both outdoor and indoor conditions. For outdoor scenario, we assume that transmission between user terminals and destination has no any obstacle causing some scattering or reflecting to the signal. Therefore, we adopt a simple Free-Space Path Loss (FSPL) model presented in [16] which can be expressed by

$$\alpha_k\,(dB) = 20\log_{10}(d_k) + 20\log_{10}(f) - 27.55 \quad (13)$$

where d_k is distance between k^{th} node and destination (meters) and f is operating frequency (megahertz).

We utilize Euclidean estimation for approximating the distance between the k^{th} node and destination, which can be expressed by

$$d_k(\phi,\theta) = \sqrt{A^2 + r_k^2 - 2r_k A\sin\theta\cos(\phi - \psi_k)} \quad (14)$$

where A is distance between network center and destination as shown in Fig. 1, r_k is node location referred to the network center while θ_0 and ϕ_0 are direction angles of destination referred to x-axis and z-axis respectively and ψ_k is direction angle of k^{th} node referred to x-axis as shown in Fig. 1.

When analysing its radiation pattern in far-field region, we usually assume that distance between node and destination is relatively long, $A \gg r_k$. Then, (12) can be minimized to

$$d_k(\phi,\theta) \approx A - r_k\sin\theta\cos(\phi - \psi_k) \quad (15)$$

When the network size is not large, we can estimate that of $d_k(\phi,\theta) \approx A$ which is represented to all node's distance.

In case of indoor condition, we adopt indoor path loss model presented in [17] which has been defined by

$$\gamma_k\,(dB) = 20\log_{10}(f) + 10n\log_{10}(d_k) + L_f(n_f) - 28 \quad (16)$$

Table 1: *Path Loss Exponential, n.*

Frequency [GHz]	Environment		
	Resident	Office	Commercial
0.9	-	3.3	2.0
1.2-1.3	-	3.2	2.2
1.8-2.0	2.8	3.0	2.2
4.0	-	2.8	2.2
60.0	-	2.0	1.7

Table 2: *Floor Penetration Factor, $L_f(n_f)$.*

Frequency [GHz]	Environment		
	Resident	Office	Commercial
0.9	-	9(1floor)	-
	-	19(2floor)	-
	-	24(3floor)	-
1.8-2.8	$4n_f$	15+4(n_f-1)	6+3(n_f-1)

where n is path loss exponent and $L_f(n_f)$ is floor penetration factors. The n and $L_f(n_f)$ can be selected from Tables 1 and Tables 2, respectively.

According to the path-loss model mentioned above, the received signal at destination for outdoor condition can be expressed by

$$R_x = 10\log\left(\frac{N}{1+0.09332}\right) + G_t + G_r + P_t - \alpha_k \qquad (17)$$

when the first term represents distributed beamforming gain (dB), G_t stands for transmitted antenna gain (dB), G_r is received antenna gain (dB), P_t is radiated power (dB) and α_k is path loss in case of outdoor scenario.

Also similar to (17), the received signal at destination for indoor scenario can be expressed by

$$R_x = 10\log\left(\frac{N}{1+0.09332}\right) + G_t + G_r + P_t - \gamma_k \qquad (18)$$

when γ_k is path loss of indoor condition.

Fig. 6 shows degradation in signal strength in case of outdoor and indoor when $n = 3.3$ and $L_f(n_f) = 9$. Please note that both transmitter and receiver are located on same floor. The figure shows that path loss in indoor scenario is more pronounced comparing with the case of outdoor environment. This is because there are many obstacles in indoor environment. This effect has an influence to the performance of distributed beamforming networks. Therefore, the received signal at destination is degraded as revealed in Fig. 7. This figure shows various radiated power levels adopted from [18] including outdoor path-loss effect. As we can see in the figure, received signal strength for all cases is extremely dropped with an increase in distance between destination and nodes. Also, at $A = 1000$ m, received signal strength is approximately -61.3 dBm, -51.3 dBm and -41.3 dBm when radiated power is 0 dBm, 10 dBm and 20 dBm,

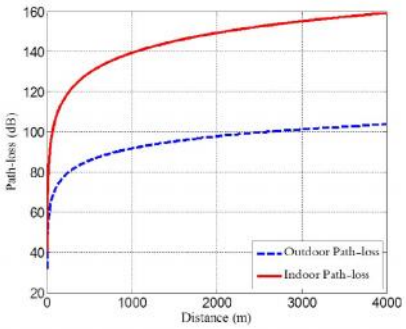

Fig.6: *FSPL (outdoor and indoor) vs. distance between transmitter and receiver.*

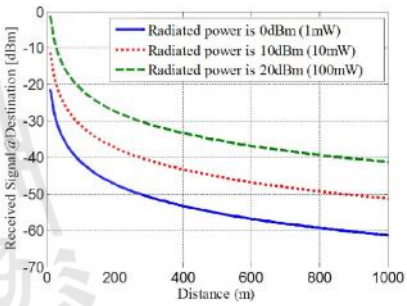

Fig.7: *Received signal strength at destination in outdoor scenario vs. distance between transmitter and receiver.*

respectively. Next, we further investigate into the effect of path loss on the beamforming performance of distributed beamforming networks.

For outdoor condition, we reveal the effect of path loss on the beamforming performance of distributed beamforming for WSNs. Some utilized parameters appeared from Rochwell Science Center [18] have been adopted. The authors of [18] have developed WSNs for area monitoring and integrated vehicle health management which has several nodes distance. We utilize some parameters from this work as shown in Table 3. Note that all nodes are individually equipped with a single isotropic antenna having identical radiated power.

Fig. 8 shows average beampattern of distributed beamforming networks for outdoor scenario when 40 sensor nodes are randomly located in the networks. Please note that this number is referred to the number

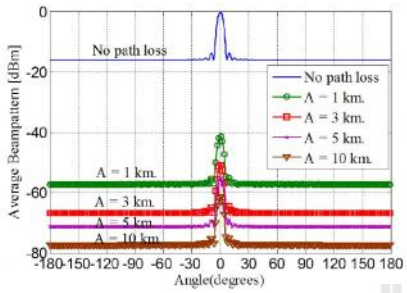

Fig.8: *Average beam pattern in outdoor scenario with several A when number of collaborative nodes (N) is 40 nodes and radiated power is 20 dBm.*

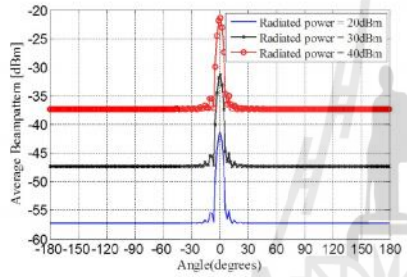

Fig.9: *Simulated average beam pattern in outdoor scenario with several radiated power when number of collaborative nodes (N) is 40 nodes and A is 1000 m.*

of communication channel. As we can see, the effect of path loss is more pronounced when distance (A) between the networks and destination increases. At A = 1 km, the average beampattern is dropped to -40 dBm. At longer distance, the beampattern gain is dropped to -50 dBm, -57 dBm and -62 dBm when A = 3 km, 5 km and 10 km respectively. This is because that path loss effect is more pronounced when distance between transmitter and receiver increases according to (13) and (14).

Fig. 9 shows the average beampattern of distributed beamforming networks when radiated power is given as: 20 dBm, 30 dBm and 40 dBm. The beamforming gain is also degraded with respect to the change of radiated power. As we can see in the figure, beamforming gain is of -43 dBm, -33 dBm and -23 dBm when radiated power is 20 dBm, 30 dBm and 40 dBm, respectively. These results have revealed that path loss effect can be eased by increasing radiated power at transmitter. However, this compensation is

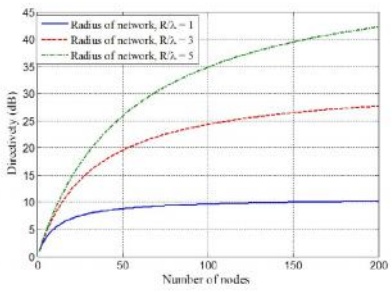

Fig.10: *Beamforming gain vs. the number of collaborative nodes, N.*

not practical when transmitter is far away from receiver. Moreover, this is considerably not practical as the battery-lifetime of sensor nodes is very limited. Nevertheless, some researchers have proposed the idea of increasing the number of nodes to tackle the mentioned problem [12, 14]. Fig. 10 presents that beamforming gain or directivity can be increased when utilizing the higher number of nodes. This is because the beamforming gain or directivity is related to nodes density $N/\bar{R}$ as shown in (12). However, the obtained directivity is stable when using a large number of nodes. Referring to (12), directivity depends on only $\bar{R}$ at a large number of nodes, which has been constantly given at the beginning. Also, as seen in Fig. 10, the higher $\bar{R}/\lambda$ is given then the higher directivity can be obtained. The reason is that directivity reverses to the network radius as shown in (12).

For indoor condition, we adopt simulation model and some parameters from the work presented in [19] which are shown in Table 4. The author of [19] have developed WSNs for home entertainment which is able to send a large data with high speed transmission. The authors have provided a new multithreaded embedded operating system which is integrated with a general purpose single-board hardware platform to enable flexible and rapid prototyping of WSNs.

The results in case of indoor condition look similar to the ones from outdoor condition. As we can see in Fig. 11, the beamforming gain is also extremely dropped by path loss effect especially when distance between WSNs and destination is very far. The beampattern gain is dropped to -47 dBm, -57 dBm and -67 dBm when A = 100 m, 200 m and 300 m respectively. In Fig. 12, radiated power is gained from 30 dBm to 40 dBm and 50 dBm. However, beam pattern gain is still degraded to -32 dBm and -22 dBm, respectively. This seems that gaining transmitted power in indoor cannot overcome the

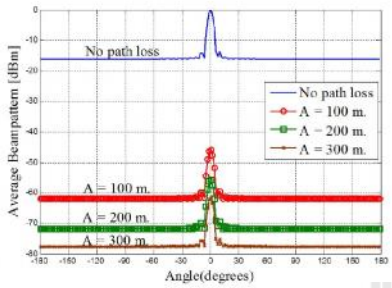

Fig.11: *Average beampattern for indoor scenario with several A when the number of collaborative nodes (N) is 30 nodes and radiated power is 30 dBm.*

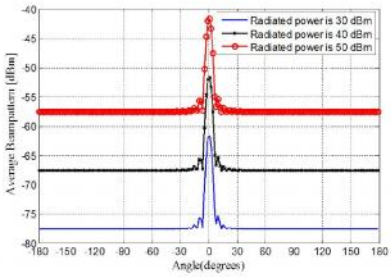

Fig.12: *Average beampattern for indoor scenario with several radiated power when the number of collaborative nodes (N) is 30 nodes and A is 300 m.*

degradation caused by path loss.

From all obtained simulation results, we can conclude that path loss extremely affects the beamforming performance of distributed beamforming systems. There are several remedies such as increasing of network radius or the number of utilized nodes. However, these are considerably not practical. Utilizing more collaborative nodes introduces an increased budget. Also, adding more nodes is not possible for some cases. For example, the work presented in [18] has utilized only 40 nodes operating at the same time as the limitation of available channels. Moreover, an increase in network radius may be limited by the size of available space or environment. However, the path loss is not the only one factor that affects beamforming performance, but also the phase synchronization error or imperfections in node location estimation degrades the beamforming performance. Therefore we step on to discuss an effect of imperfection in node location estimation on distributed beamforming in next section.

4. DISTRIBUTED BEAMFORMING MODEL WITH IMPERFECT PHASE SYNCHRONIZATION

In this work, we focus on open-loop synchronization as it avoids any feedback (or reference) signal from destination. For open-loop scenario, imperfect synchronization due to an error in node-location estimation affects the initial phase presented in (2) as follows:

$$\begin{aligned}\tilde{\Psi}_k^{\dagger} &= \frac{2\pi}{\lambda}\left(r_k+\delta r_k\right)\cos\left(\phi_0-\left(\psi_k+\delta\psi_k\right)\right)\\ &= \frac{2\pi}{\lambda}r_k\cos\left(\phi_0-\left(\psi_k+\delta\psi_k\right)\right)\\ &\quad+\frac{2\pi}{\lambda}\delta r_k\cos\left(\phi_0-\left(\psi_k+\delta\psi_k\right)\right)\end{aligned} \tag{19}$$

where δr_k and $\delta\psi_k$ are estimation error of node location in terms of network radius and angle, respectively. The δr_k and $\delta\psi_k$ are corresponding error random variables where both δr_k and $\delta\psi_k$ are assumed to be independent and identically distributed as well as r_k and ψ_k described in (1). Similar to (7), the beampattern can be expressed by

$$\begin{aligned}P\left(\phi|z,v,\delta\psi\right) &= \left|\tilde{F}\left(\phi|z\right)\right|^2\\ &= \frac{1}{K}+\frac{1}{K^2}\sum_{k=1}^{K}\sum_{\substack{l=1\\ l\neq k}}^{K}\\ &\quad e^{-j4\pi\tilde{R}\left\{z_k\sin\left(\frac{\phi-\phi_0-\delta\psi_k}{2}\right)-z_l\sin\left(\frac{\phi-\phi_0-\delta\psi_l}{2}\right)\right\}}\times\\ &\quad e^{j\frac{2\pi}{\lambda}\left(v_k-v_l\right)}\end{aligned} \tag{20}$$

where

$$z_k = r_k\sin\left(\psi_k+\frac{\delta\psi_k}{2}-\frac{\phi+\phi_0}{2}\right) \tag{21}$$

$$v_k = \delta r_k\cos\left(\psi_k+\delta\psi_k-\phi_0\right) \tag{22}$$

We assume that estimation error in network radius δr_k is uniformly distributed over range of $[-r_{max}, r_{max}]$. In addition, estimation error in phase $\delta\psi_k$ is uniformly distributed over range of $[-\psi_{max}, \psi_{max}]$ in constraint between 0 to 2π. The pdf of v_k can be expressed by

$$f_{v_k} = \frac{1}{\pi r_{\max}}\left[\ln\left(1+\sqrt{1-\left(\frac{v}{r_{\max}}\right)^2}\right)-\ln\frac{|v|}{r_{\max}}\right] \tag{23}$$
$$for\ |v|\leq r_{\max}$$

Finally, the average beampattern can be written as

$$P_{av}\left(\phi\right) = \frac{1}{K}+\left(1-\frac{1}{K}\right)\left|A_{\psi}\left(\phi\right)\right|^2\left|A_r\right|^2 \tag{24}$$

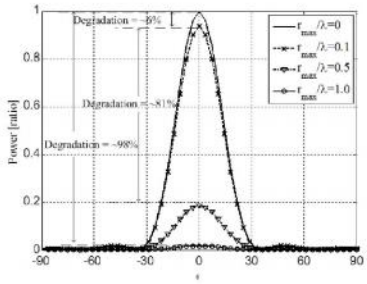

Fig.13: *Average beampattern with imperfection in network radius estimation, r_k.*

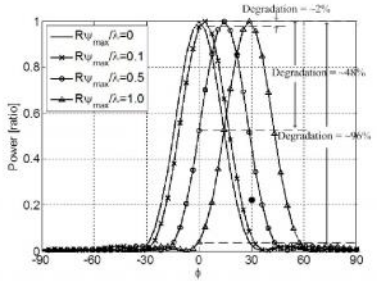

Fig.14: *Average beampattern with imperfection in phase estimation, ψ_k .*

where

$$A_r = E_{v_k}\left\{e^{j\frac{2\pi}{\lambda}v_k}\right\} = \frac{2}{\pi}\int_0^1 \cos\left(\frac{2\pi}{\lambda}r_{\max}t\right)\ln\frac{1+\sqrt{1-t^2}}{t}dt = {}_1F_2\left(\frac{1}{2};1,\frac{3}{2};-\left(\pi\frac{r_{\max}}{\lambda}\right)^2\right) \quad (25)$$

$$A_\psi(\phi) = \mathrm{E}_{z_k,\delta\psi_k}\left\{e^{j4\pi\tilde{R}z_k\sin\left(\frac{\phi_0+\delta\psi_k-\phi}{2}\right)}\right\} = \mathrm{E}_{\delta\psi_k}\left\{\frac{J_1\left(4\pi\tilde{R}\sin\frac{\phi-\delta\psi_k}{2}\right)}{2\pi\tilde{R}\sin\frac{\phi-\delta\psi_k}{2}}\right\} \quad (26)$$

According to this, estimated phase error $\delta\psi_k$ is uniform and distributed over range of $[-\psi_{max}, \psi_{max}]$ and $\sin\left((\phi+\delta\psi_k)/2\right) \approx (\phi+\delta\psi_k)/2$. Then, we obtain

$$A_\psi(\phi) \approx \frac{1}{2}\left(1-\frac{\phi}{\psi_{\max}}\right){}_1F_2\left(\frac{1}{2};\frac{3}{2},2;-\left(\pi\tilde{R}\left(\phi-\psi_{\max}\right)\right)^2\right) + \frac{1}{2}\left(1+\frac{\phi}{\psi_{\max}}\right){}_1F_2\left(\frac{1}{2};\frac{3}{2},2;-\left(\pi\tilde{R}\left(\phi+\psi_{\max}\right)\right)^2\right) \quad (27)$$

where ${}_mF_n(x)$ is hypergeometric function. Since the ${}_1F_2\left(\frac{1}{2};\frac{3}{2};-(x)^2\right)=1$ when x=0 and as the function has its symmetrical peak around phase error of $\phi = \pm\psi_{\max}$. Then, the function at main beam center can be defined by

$$A_\psi(\phi=0) = {}_1F_2\left(\frac{1}{2};\frac{3}{2},2;-\left(\pi\frac{R\psi_{\max}}{\lambda}\right)^2\right) \quad (28)$$

From our previous work, we has shown that the imperfection in network radius estimation degrades the gain of main beam while the imperfection in phase estimation deviates the main beam direction [9]. Some examples of imperfection in network radius estimation affecting the gain of main beam are shown in Fig. 13. For this case, the system is assumed to have an error free in phase estimation while estimation error in network radius r_k is assumed as $r_{max}/\lambda = 0.1$, $r_{max}/\lambda = 0.5$ and $r_{max}/\lambda = 1.0$. The obtained results show that the main beam's gain is extremely degraded when error in radius estimation is occurred. The main beam's gain is degraded by 6%, 81% and 98% when estimation error in network radius is $r_{max}/\lambda = 0.1$, $r_{max}/\lambda = 0.5$ and $r_{max}/\lambda = 1.0$, respectively. This is how to calculate the percentage degradation. For example in case of having $r_{max}/\lambda = 0.5$, the ratio of main beam is approximately 0.19 or 19%. Thus, the degradation of main beam's gain is 100-19 = 81% or 0.8.

Furthermore, some examples showing an effect of estimation error in phase are shown in Fig. 14. For this case, estimation of nodes location in terms of radius r_k is assumed to be perfect. Also, estimation error in phase ψ_k are assumed as $R\psi_{max}/\lambda = 0.1$, $R\psi_{max}/\lambda = 0.5$ and $R\psi_{max}/\lambda = 1.0$. The obtained results show that the directions of obtained main beam deviate from the direction of destination ($\phi_0 = 0°$). The deviated main beams are approximately at 3°, 15° and 30°. Thus, the main beam's gain is degraded by 2%, 48% and 96% respectively when comparing to the optimum beamforming. Maximum power ratio of main beam is denoted as 1.0 or 100%. For the case of $R\psi_{max}/\lambda = 0.5$, the ratio of main beam in direction of destination is approximately 0.52 or 52%. Thus, the degradation of main beam's gain is 100-52 = 48% or 0.48. Regarding this simulation results, we can conclude that the imperfection in network radius estimation degrades main beam's gain while the imperfection of phase estimation deviates the direction of main beam.

From running a number of simulations, we have

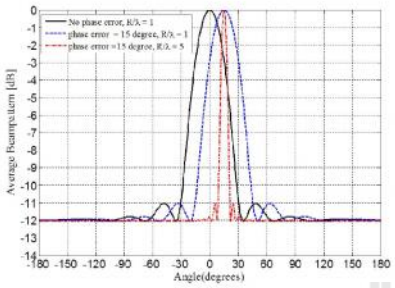

Fig.15: *Average beam pattern with various network radiuses and imperfection of estimated phase, ψ_k.*

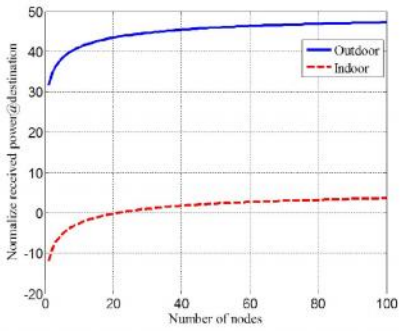

Fig.16: *Normalized received signal strength at destination with various N when $\tilde{R} = 5$.*

found that network radius $\tilde{R}$ is significant parameter for the systems. If utilizing a large network radius is allowed, a small amount of phase error can really affect the system performance as the main beam cannot be pointed to the destination. Some examples are shown in Fig. 15, the number of nodes is set as 16 and direction of destination is given at 0°. Note that in this figure we set an error free to the network radius. The figure shows that, when $\tilde{R} = 1$ and $\psi_{max} = 0.26$, gain at desired direction (0°) drops to -2 dB. In addition, this error is even more pronounced at -12 dB when network radius is wider.

According to simulation results shown in Section 3, path loss and node location estimation error tremendously degrade the beamforming gain of distributed beamforming networks. However, some simulations have revealed that increasing the number of nodes helps improving the beamforming gain. Nevertheless, this is hardly practical because increasing the number of nodes has impact to the system budget. Moreover, utilizing more number of nodes is limited according to available communication channels of the systems. Also an increase in network radius for improving the beamforming gain may be limited by the size of implemented area or environment. The simulation results in Section 4 show that the imperfection in network radius estimation degrades the gain of main beam while the imperfection in phase estimation deviates the direction of main beam. According to those degradation and limitation, we propose an idea to choose the optimum number of collaborative nodes and network radius for distributed beamforming networks in next section.

5. OPTIMUM NUMBER OF NODES AND NETWORK RADIUS

As the limitation of the number of node and accuracy of node location estimation discussed above, we propose the solution to select the optimum number of nodes N and network radius R for the distributed beamforming. In this section, we separate the proposed concept into two cases: Perfect Phase Synchronization and Imperfect Phase Synchronization as follows.

5.1 Perfect Phase Synchronization

For this case, synchronization between collaborate nodes and destination is assumed to be perfect. However, beamforming calibration has to be taken place before destination moves out from the main beam for the case of having mobility at destination. When synchronization between nodes and destination is perfect, only path loss between them as mentioned in Section 3 affects beamforming performance. From the (12), (13) and (16), the proposed algorithm for calculating the optimum number of nodes and network radius in case of perfect synchronization is as follow:

$$10\log\left(\frac{N}{1+0.09332}\right) + G_t + G_r + P_t - PL - S \geq 0 \quad (29)$$

when

N = Number of collaborative nodes.
$\tilde{R} = R/\lambda$
G_t = Transmitted gain (dBm)
G_r = Received gain (dBm)
P_t = Sensitivity of destination (dBm)
S = Sensitivity of destination (dBm)
PL = Path loss
f = Operation frequency (MHz)

The objective of proposed formula shown in (29) is to make the received-signal at destination higher than receiver sensitivity at destination. The first term shown in (29) is a distributed beamforming gain or directivity. We herein define the left-side term of (29) as "*normalized received signal*". As a result, we

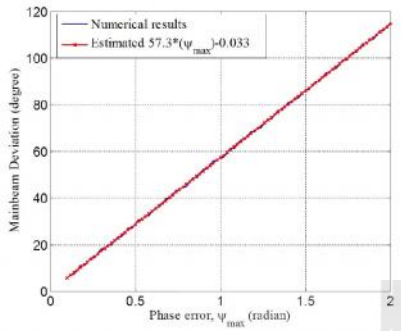

Fig.17: *Numerical and estimated results of main beam deviation vs. estimated phase error, ψ_{max}.*

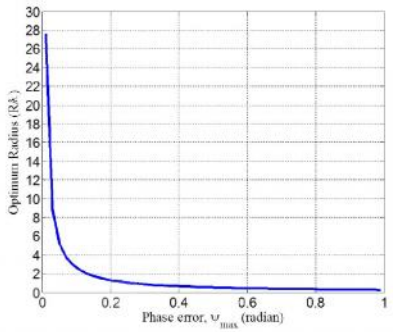

Fig.18: *optimum $\tilde{R}$ vs. estimated phase error, ψ_{max}.*

can select the number of collaborative nods N and network radius $\tilde{R}$ which corresponds to having normalized received signal higher than zero.

Fig. 16 shows some examples to select the proper number of N when $\tilde{R} = 5$. For this case, distance between collaborative networks and destination is assumed as 500 m, path loss in case of outdoor and indoor are -86 dB and -127 dB respectively. The path loss exponent, n is 3.3 and floor penetration factors, $L_f(n_f)$ is 9. Also f is assumed at 916 MHz, P_t is 10 dBm, G_r is 2.5 dBm, G_r is 5 dBm and sensitivity of base station S is -100 dBm. As we can see in this figure, in case of indoor, we should select a number of collaborative nodes N higher than 10 nodes so that destination can receive the transmitted signal having its signal strength higher than receiver sensitivity.

5.2 Imperfect Phase Synchronization

An existent synchronization in distributed beamforming system is often imperfect due to hardware error such as an estimation error in node location employing GPS or phase adjustment error. In this case calculation of the optimum number of N and $\tilde{R}$ is more critical than having perfect phase synchronization as discussed in Section 5.1. Because imperfect estimation in network radius degrades pattern gain while the imperfection in phase estimation deviates main beam direction. Therefore, we separate the proposed algorithm into two steps as follows. For the first step, we carefully select the optimum $\tilde{R}$ in order to maintain its main beam gain not lower than HPBW or -3 dB. Some examples for this case are shown in Fig. 15, when estimated phase error is 0.26 and $\tilde{R}$ is 5, the main beam gain is approximately -12 dB.

Step 1: from (10) and the numerical information shown in Fig. 17, we can find the deviation of main beam comparing to the phase error, ψ_{max}. The numerical results can be obtained from (24) and (28) while the estimated formula of main beam deviation can be taken from this figure as $57.3\psi_{max} - 0.033$. Therefore, the optimum solution is as follows.

$$\begin{aligned} &Main\ \ beam\ \ deviation < Half\ \ Power\ \ Beamwidth \\ &57.3\psi_{\max} - 0.033 < \left(\frac{0.26}{\tilde{R}}\right) \\ &\tilde{R} < \frac{0.26}{57.3\psi_{\max} - 0.033} \end{aligned} \tag{30}$$

The optimum $\tilde{R}$ is selected according to (30) and also Fig.18 informs the optimum value of $\tilde{R}$ when estimated phase error is occurred. For example, if the network has phase error, ψ_{max} of 0.1, then the network radius $\tilde{R}$ must be not higher than 2.5. Note that ψ_{max} is united in radian therefore we multiply (30) with $180/\pi$ for having its unit in degree.

Step 2: Since we get the optimum $\tilde{R}$ from the previous step. Then we consider an imperfect estimation in network radius which degrades the gain of main beam. Therefore we select the optimum N in order to allow the received signal at destination higher than receiver's sensitivity at destination when $\tilde{R}$ is given from Step 1. Finally, the proposed algorithm is as follows.

$$10\log\left(\frac{N}{1+0.09332}\right) L_r + G_t + G_r + P_t - PL - S \geq 0 \tag{31}$$

when L_r is loss factor of main beam degradation by imperfect estimation in radius (ratio) that we describe in Fig. 13. The L_r can be obtained by the information shown in Fig. 13 which shows the main beam degradation caused by imperfect estimation in network radius when r_{max}/λ is given in (25). For example, in case of having $r_{max}/\lambda = 0.5$, the ratio of main beam gain is approximately 0.19 or 19% compared to optimum normalized power of 1 or 100%.

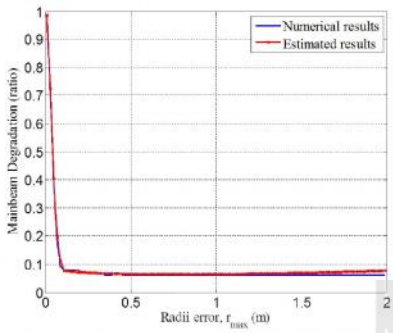

Fig.19: *Relationship between radius error, r_{max} (m) and main beam degradation.*

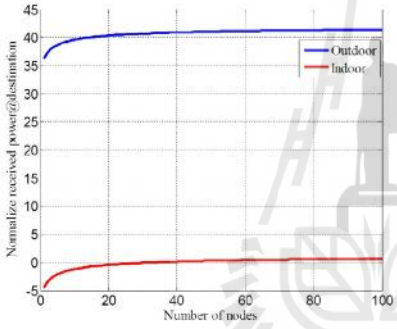

Fig.20: *Normalized received signal strength at destination when $\psi_{max} = 0.1$ and $r_{max} = 0.05$.*

Thus, main beam degradation is 100-19 = 81% or loss factor in main beam degradation caused by imperfect estimation in network radius. Therefore, we obtain L_r is 0.81.

Fig. 19 shows the numerical and estimated results of main beam degradation L_r vs. estimated radius error r_{max}. According to this figure, the estimated values of main beam degradation, L_r is defined as

$$L_r = -39063\,(r_{\max})^4 + 9792\,(r_{\max})^3 - 730\,(r_{\max})^2 + 5(r_{max}) + 1 \tag{32}$$

when $r_{max} \leq 0.1$

$$L_r = 0.084\,(r_{\max})^{-0.09} - 0.025 \tag{33}$$

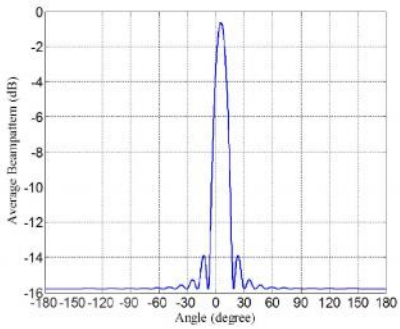

Fig.21: *Average beampattern utilized optimum $N = 38$ and $\tilde{R} = 2.6$ for $\psi_{max} = 0.1$ and $r_{max} = 0.05$.*

when $0.1 > r_{max} \leq 0.45$

$$L_r = 0.00091\,(r_{\max})^3 + 0.004262\,(r_{\max})^2 - 0.00671\,(r_{\max}) + 0.066227 \tag{34}$$

when $r_{max} > 0.45$

Finally we obtain the optimum N and $\tilde{R}$ utilizing (30), (31) and (32) to (34) in **Steps 1** and **Steps 2**. For example, we assume the distance between network and destination of 500 m. In addition, f is 916 MHz, P_t is 10 dBm, G_t is 2.5 dBm, G_r is 5 dBm, sensitivity is -100 dBm, path loss exponent, n is 3.3 and floor penetration factors, $L_f(n_f)$ is 9. Moreover phase and radius error are assumed as $\psi_{max} = 0.1$ and $r_{max} = 0.02$ respectively. Firstly, according to (30) or Fig. 18 utilized in **Steps 1**, the optimum $\tilde{R}$ for $\psi_{max} = 0.1$ is not larger than 2.6. Secondly, as the radius error, r_{max} is 0.02, then (32) in **Steps 2** is used to estimate the main beam degradation, thus we obtain $L_r = 0.85$. Finally we obtain the optimum number of nodes, N by using (31). Fig. 20 shows the normalized received signal calculated by (31) in **Steps 2**. As we can see in this figure, we should select N more than 38 nodes for indoor scenario. Therefore, we achieve the average beampattern employing optimum $N = 38$ and $\tilde{R} = 2.6$ as shown in Fig. 21. As we can see in this figure, we obtain the optimum average beam pattern that maintains its main beam gain not lower than HPBW or -3 dB. Moreover, the received signal at destination is also higher than sensitivity of receiver.

6. CONCLUSION

In the existent circumstances, the distributed beamforming performance is degraded by the phase synchronization error and path loss. However, increasing the number of nodes and network radius

in order to obtain higher beamforming gain is constrained. Therefore, this work has proposed the selection for an optimum number of nodes and network radius in order to receive higher signal over receiver's sensitivity at destination. The proposed idea provides ready-made formulas that are helpful for the distributed beamforming designers.

7. ACKNOWLEDGEMENT

The authors acknowledge the financial support from The Royal Golden Jubilee Ph.d Program (RGJ-Ph.D) 1.Q.TS/52/B.1.B.XX and Suranaree University of Technology, Thailand.

References

[1] Y. T. Lo, "A mathematical theory of antenna arrays with randomly spaced elements," *IEEE Trans. Antenna Prog.*, vol. 12, pp. 257-268, May 1964.

[2] R. Mudumbai, D.R. Brown, U. Madhow, and H.V. Poor, "Distributed transmit beamforming: challenges and recent progress," *IEEE Commun. Mag.*, vol. 47, no. 2, pp. 102-110, Feb. 2009.

[3] Y.-S. Tu, and G. J. Pottie, "Coherent cooperative transmission from multiple adjacent antennas to a distant stationary antenna through AWGN channels,"*Proc. IEEE 55th Veh. Tech. Conf.*, vol.1, 2002, pp. 130-134.

[4] R. Mudumbai, "Distributed transmit beamforming using feedback control," *IEEE Trans. Inf. Theory*, vol. 56, no. 1, pp. 411-426, Jan. 2010.

[5] R. Mudumbai, G. Barriac, and U. Madhow, "On the fea-sibility of distributed beamforming in wireless networks," *IEEE Trans. Wireless Commun.*, vol. 6, pp. 1754-63, May 200.

[6] I. Ozil, and D.R. Brown III, "Time-slotted Round-trip carrier synchronization," *Proc. 41st Asilomar Conf. Signals, Syst., Comput.*, 2007, pp. 1781-1785.

[7] H. Ochiai,P. Mitran, H. V. Poor, and V. Tarokh, "Collaborative beamforming for distributed wireless ad hoc sensor networks," *IEEE Trans. Signal process.*, vol. 53, no. 11, pp. 4110-4124, Nov. 2005.

[8] Official U.S. Government information about the Global Positioning System.(2007 Feb, 23). *GPS Performance Standards & Specifications* 1st edition [Online]. Available: http://www.gps.gov/technical/ps/

[9] Ian Poole. *Sources of Errors in GPS* 1st [Online]. Available:http://www.kowoma.de/en/gps/errors.htm

[10] P. Sriploy, P. Uthansakul, and M. Uthansakul, "An effect of imperfection in node location estimation on distributed beamforming", *9th Int. Conf. Elect. Eng./Electron., Comput., Telecommun. Inform. Tech.*, 2012, pp. 1-4.

[11] S. Sfar, G. J. Foschini, R. A. Valenzuela, L. Mailaender, D. Chizhik, K. Karakayali, and R. S. Blum, "Is relayed collaborative communication worth it?," *IEEE Asilomar Conf. Signals, Syst. Comput.*, 2008, pp. 146-150.

[12] A. N. Bishop, and P. N. Pathirana, "On the effect of path loss rates on the optimal receiver position in sensor networks," *IEEE Int. Conf. Inform. Automation*, 2006, pp. 126-128.

[13] P. Sriploy, P. Uthansakul, and M. Uthansakul, "Effect of path loss on the distributed beamforming for wireless sensor networks," *IEEE Int. Conf. Elect. Eng./Electron., Comput., Telecommun. Inform. Tech.*, 2013, pp. 1-4.

[14] A. Kalis, A. G. Kanatas, and G.P. Efthymoglou, "A co-operative beamforming solution for eliminating multi-hop communications in wireless sensor networks," *IEEE J. Selected Areas Commun.*, vol. 28, no. 7, pp. 1055-1062, Sept. 2010.

[15] K. Zarifi, A. Ghrayeb, and S. Affes, "Distributed beamforming for wireless sensor networks with improved graph connectivity and energy efficiency," *IEEE Trans. Signal Process.*, vol. 58. no. 3, pp. 1904-1921, Mar. 2010.

[16] T. S. Rappaport, *Wireless communications: principles and practice*, 2nd ed., Prentice Hall PTR Upper Saddle River, N.J., 2002.

[17] S. Saunders, *Antennas and Propagation for Wireless Communication Systems*, Wiley, 2000.

[18] H. O. Marcy, J. R. Agre, C. Chien, L. P. Clare, N. Romanov, and A. Twarowski, "Wireless sensor networks for area monitoring and integrted vehicle health management applications," *Proc. AIAA Guidance, Navigation, and Control Conf. Exhibit*, 1999, pp. 1-10.

[19] H. Abrach, J. Carlson, H. Dai, J. Rose, A. Sheth, B. Shucker, and R. Han , "MANTIS: system support for MultimodAl NeTworks of In-situ Sensors," *Proc. 2nd ACM Int. Workshop Wireless Sensor Networks Applicat.*, 2000, pp. 50-59.

Pongnarin Sriploy received the B.S. and M.S.degree in telecommunication engineering from Suranaree Univaersity of Technology, Nakhon Ratchasima, Thailand, in 2007 and 2009, respectively. He is currently pursuing the Ph.D. degree in telecommunication engineering at Suranaree Univaersity of Technology. From 2009 to 2011, he was a product engineer at Seagate Technology (Thailand) Ltd. His research interest includes the smart antenna and distributed beamforming.

Peerapong Uthansakul received the B.Eng and M.Eng of Electrical Engineering from Chulalongkorn University, Thailand, in 1996 and 1998 respectively, and Ph.D. degree (2007) in Information Technology and Electrical Engineering from The University of Queensland, Australia. From 1998 to 2001, he was employed as a telecommunication engineer at the Telephone Organization of Thailand. At present, he is working as Associate Professor in School of Telecommunication Engineering, Suranaree University of Technology, Thailand. His research interests include wave propagation modelling, MIMO, OFDM and advance wireless communications.

Leonardo L. Bravo-Roger received the B.Eng degree (1997) in Telecommunication Engineering from Suranaree University of Technology, Thailand, M.Eng degree (1999) in Electrical Engineering from Chulalongkorn University, Thailand, and Ph.D. degree (2007) in Information Technology and Electrical Engineering from The University of Queensland, Australia. She received 2nd prize Young Scientist Award from 16th International Conference on Microwaves, Radar and Wireless Communications, Poland, in 2006. At present, she is lecturer in School of Telecommunication Engineering, Suranaree University of Technology, Thailand. Her research interests include wideband/narrowband smart antennas, automatic switch beam antenna, DOA finder, microwave components, application of smart antenna on WLANs.

Hindawi Publishing Corporation
International Journal of Antennas and Propagation
Volume 2016, Article ID 7086234, 16 pages
http://dx.doi.org/10.1155/2016/7086234

Research Article

Nonfeedback Distributed Beamforming Using Spatial-Temporal Extraction

Pongnarin Sriploy and Monthippa Uthansakul

School of Telecommunication Engineering, Suranaree University of Technology, Nakhon Ratchasima 30000, Thailand

Correspondence should be addressed to Monthippa Uthansakul; mtp@sut.ac.th

Received 29 October 2015; Revised 20 January 2016; Accepted 26 January 2016

Academic Editor: Lei Yu

So far, major phase synchronization techniques for distributed beamforming suffer from the problem related to the feedback procedure as a base station has to send the feedback reference signal back to the transmitting nodes. This requires stability of communication channel or a number of retransmissions, introducing a complicated system to both transmitter and receiver. Therefore, this paper proposes an alternative technique, so-called nonfeedback beamforming, employing an operation in both space and time domains. The proposed technique is to extract a combined signal at the base station. The concept of extraction is based on solving a simultaneous linear equation without the requirement of feedback or reference signals from base station. Also, the number of retransmissions is less compared with the ones available in literatures. As a result, the transmitting nodes are of low complexity and also low power consumption. The simulation and experimental results reveal that the proposed technique provides the optimum beamforming gain. Furthermore, it can reduce Bit Error Rate to the systems.

1. Introduction

Nowadays, wireless communication networks provide a variety of applications such as wireless local area networks, cellular networks, or wireless sensor networks. These wireless networks have lots of advantages in flexibility and mobility for users compared with a wired communication. However, the transmission range of wireless communication systems is limited due to signal attenuation [1]. Therefore, nodes or sensors in the systems require a higher transmitted power to compensate the mentioned attenuation. This requirement is not practical due to the limited battery lifetime of nodes. To tackle the problem, array antennas may be employed at individual devices in order to enhance beamforming gain [2–7]. Unfortunately, the installation of multiple antennas on a mobile terminal is difficult due to its size and the limitation of power consumption [8–10]. Recently, a distributed beamforming has been proposed to handle the mentioned problem [11, 12], which has lots of advantages such as a significant increase in transmission range and an enhancement of both energy efficiency and Signal-to-Noise Ratio (SNR) [13–16].

The distributed beamforming concept is similar to smart antennas but the position of antennas (or nodes) is not fixed. Also, it could be said that the distributed beamforming is similar to virtual array antennas in which each node sends the same data at the same time to base station [17]. In the distributed beamforming networks, the transmitting nodes have to perform the synchronization in order to achieve phase alignment. Otherwise, the phase offsets or phase errors among all transmitted signals may degrade the combined signal at base station causing intersymbol distortion. Recently, lots of phase synchronization techniques have been proposed. These techniques can be classified into two types: closed-loop and open-loop synchronization techniques [18].

The closed-loop technique needs some feedback from base station to adjust the phase offsets among transmitting nodes. A one-bit feedback is one of the best techniques for closed-loop synchronization [19, 20]. In the mentioned work, every transmitting node in the networks has to randomly adjust its carrier signal phases. Then, all nodes transmit the same data to base station. After performing an estimation of received SNR at base station, one bit (0 or 1) is transmitted back to all nodes. The bit "0" means that SNR is worse than before so that each node has to randomly adjust its phases again. On the other hand, bit "1" means that SNR is better

than before so that all nodes have to update their latest phase adjustment. As we can see, this technique requires a large number of retransmissions from nodes to base station. For example, it requires at least $5N$ iterations in order to achieve 75% guarantee of perfect or maximum beamforming gain, where N stands for the number of transmitting nodes [21]. This may be considerably impractical as the battery life of nodes or mobile terminals is very limited. Moreover, a closed-loop feedback from base station to transmitting nodes may be unreliable when the communication channel is weak.

In order to overcome the mentioned problems, two open-loop phase synchronization techniques, master-slave and time-slot round-trip techniques, have been proposed to reduce the interaction between base station and nodes. For master-slave technique, one node in the networks is selected as a master node while all remaining nodes are assigned to be slave nodes. The phase synchronization in this technique is achieved by sending the reference signals between master and slave nodes [21]. Alternatively, for time-slot round-trip technique, the phase synchronization among transmitting nodes can be obtained by sending a reference data among themselves [22, 23]. The idea is based on the equivalence of round-trip transmission delays through a multihop chain between transmitting nodes and base station. According to these procedures, the open-loop techniques reduce the interaction among nodes and base station. However, both master-slave and round-trip techniques still require some feedback from base station. Also, this interaction increases a complexity to all transmitting nodes. In addition, nodes require a special hardware such as phase-locked loops to obtain a precise reference signal when performing phase synchronization.

Alternatively, a zero-feedback distributed beamforming technique has been lately proposed. This technique does not require any feedback signal from the base station and the unsynchronized carriers do not matter [24, 25]. However, this technique requires a large number of packet retransmissions. For example, in case of having 3 transmitting nodes, this technique requires at least 50 retransmissions (iterations) to obtain the beamforming gain at 9.1 dB [24]. Note that the maximum gain for this case is 9.5 dB. In addition, the number of required retransmissions exponentially increases when the number of nodes increases.

From above literatures, the major disadvantage of existing phase synchronization techniques can be concluded as follows: the one-bit feedback and zero-feedback require a large number of retransmissions, which extremely reduces the battery life of transmitting nodes. Also, the master-slave and round-trip techniques require the reference signal among transmitting nodes which increases a complexity to transmitting nodes.

To overcome those disadvantages, a nonfeedback distributed beamforming technique is proposed in this paper. Note that the authors use "nonfeedback" term to avoid any confusion with the conceptual term defined for "zero-feedback" that appeared in [24, 25]. In this paper, the proposed technique does not require any feedback signal from base station or interaction between transmitting nodes. Instead, the proposed technique requires a few number of retransmissions from nodes, which is only the same as the number of transmitting nodes, N. This is relatively small compared with the number of retransmissions for one-bit feedback and zero-feedback techniques. The proposed non-feedback beamforming performs an extraction of combined signal at base station which means that the transmitting nodes do not need to deal with phase synchronization anymore; hence they can save energy and also battery life. The concept of extraction is based on a classical equation solving using inverse matrix. This procedure requires a few retransmissions from nodes. After performing a signal extraction, each extracted signal is properly weighted to obtain an appropriate phase alignment at base station. Finally, the base station obtains a combined signal with maximum beamforming gain. However, the retransmitted signals may be distorted when travelling through the communication channel.

This paper is organized as follows. Following an introduction including motivation and contribution of the proposed idea, the basic concept and definition of distributed beamforming techniques are presented in Section 2. Then, the proposed nonfeedback technique and its performance are discussed in Section 3. Afterwards, experimental studies are performed in Section 4 in order to validate the proposed concept. Finally, Section 5 concludes the paper.

2. Distributed Beamforming: Concept and Definition

The basic concept behind a distributed beamforming is similar to a traditional beamforming technique such as smart antennas in which the data is transmitted by array antennas located at one place. The phases of antennas are aligned so that the transmitted signals are gainfully combined at destination. For distributed beamforming networks, the transmitting nodes representing a group of single antenna elements are randomly distributed over the networks. As the nodes' locations are unknown the phase synchronization between nodes is the key challenge over a traditional beamforming. Figure 1 shows a configuration of distributed beamforming networks in which each transmitting node and base station are equipped with a single antenna element. All nodes and base station are stationary. It is assumed that N distributed nodes transmit a shared message $x(t)$ to base station over the Rayleigh flat fading channel. The mathematical model of distributed beamforming networks is shown in Figure 2 which is detailed as follows. The received pass-band complex signal, $Y_R(t)$, can be written as

$$Y_R(t) = \Re\left\{x(t)\sum_{n=1}^{N} h_n e^{j(\omega_n t+\phi_n)} + W(t)\right\}, \quad (1)$$

where $x(t)$ is a transmitted message, h_n is a fading coefficient, and A_n is a carrier signal amplitude at nth node. Also, $\omega_n = \omega_c + \Delta\omega_n$, where ω_c is a carrier signal frequency and $\Delta\omega_n$ is a frequency offset. In addition, $\phi_n = \phi_0 + \Delta\phi_n$, where ϕ_0 is a nominal phase and $\Delta\phi_n$ is a phase offset of the signal coming from nth node which depends on the relative mobility or node location between nth node and base station.

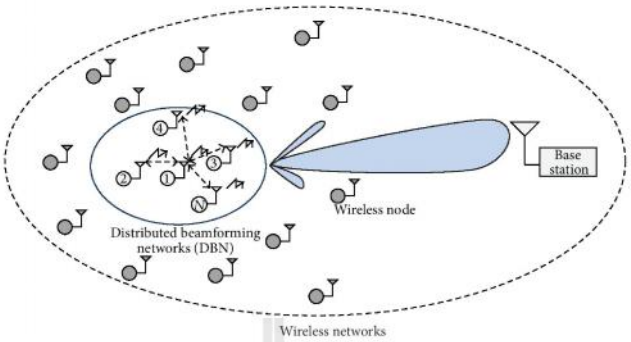

FIGURE 1: Configuration of wireless networks employing a distributed beamforming.

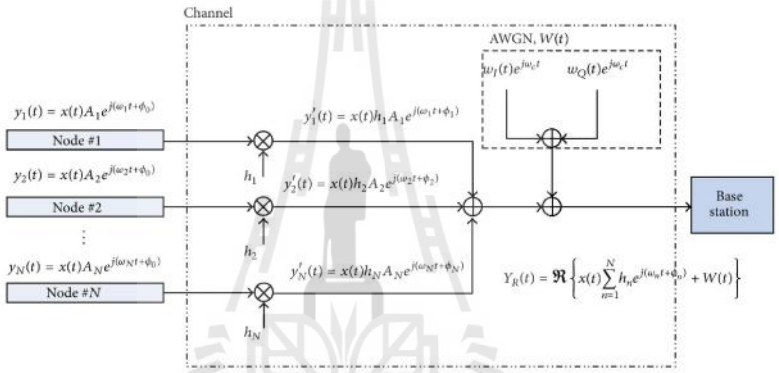

FIGURE 2: Mathematical model of wireless networks employing a distributed beamforming.

Furthermore, $W(t)$ is the Additive White Gaussian Noise (AWGN) which consists of in-phase, $w_I(t)$, and quadrature, $w_Q(t)$, components; that is, $W(t) = [w_I(t) + jw_Q(t)]e^{j\omega t}$. Therefore, the received signal power at base station can be expressed as follows [24]:

$$\begin{aligned}|Y_R(t)|^2 &= x(t)^2\left\{\sum_{n=1}^{N}h_n^2A_n^2\right.\\&\left.+2\sum_{n\neq m}[h_nh_m][A_nA_m]\cos(\omega_c t-\omega_c t+\phi_n-\phi_m)\right\}\\&+|W_{PB}(t)|^2 = x(t)^2\left\{\sum_{n=1}^{N}h_n^2A_n^2\right.\\&\left.+2\sum_{n\neq m}[h_nh_m][A_nA_m]\cos(\phi_n-\phi_m)\right\}+|W_{PB}(t)|^2.\end{aligned}\quad(2)$$

The phase offset between each node $(\phi_n - \phi_m)$ shown in (2) is relatively significant to the beamforming gain. Note that n and m are the index of transmitting node in the networks in which $n \neq m$. In the case of having a finite number of nodes N, the distributed beamforming gain can be defined as a normalized received power at base station, P_R, as

$$P_R = N\left\|\frac{x(t)}{N}\sum_{n=1}^{N}|h_n|^2|A_n|^2e^{j(\omega_c t+\phi_n)}\right\|^2+\|W(t)\|^2.\quad(3)$$

As the phases of transmitting nodes are random, thus we consider the normalized received power in form of an expected value. If we assume that the received signal amplitude from all nodes is $A_n = 1$, the average power of the transmitted signal is $P_T = 1$, and h_n are *i.i.d.* random variables then $E[h_n] = E[h]$

and $E|h_n^2| = 1$. Therefore, the average power of the received signal is adopted from [21] as follows:

$$
\begin{aligned}
E[P_R] &= \frac{x(t)^2}{N} \\
&\cdot E\left[\sum_{n=1}^{N} |h_n|^2 |A_n|^2 e^{j(\omega_c t+\phi_n)} \sum_{m=1}^{N} |A_m|^2 e^{j(\omega_c t+\phi_m)}\right] \\
&+ E\left[|W_{PB}(t)|^2\right] = \frac{x(t)^2}{N}\left(N + \frac{N(N-1)}{2}\right. \\
&\cdot \left. E\left[|h_n|^2 |A_1|^2 |A_2|^2 2\Re\left(e^{j(\omega_c t-\omega_c t+\phi_1-\phi_2)}\right)\right]\right) \\
&+ E\left[|W_{PB}(t)|^2\right] = \frac{x(t)^2}{N}\left(N + \frac{N(N-1)}{2}\right. \\
&\cdot \left. 2E\left[\cos(\phi_1-\phi_2)\right]\right) + E\left[|W_{PB}(t)|^2\right] = x(t)^2\{1 \\
&+ (N-1)E\left[\cos(\phi_1-\phi_2)\right]\} + E\left[|W_{PB}(t)|^2\right] \\
&= x(t)^2\{1 + (N-1) \\
&\cdot E\left[\cos(\phi_1)\cos(\phi_2) - \sin(\phi_1)\sin(\phi_2)\right]\} \\
&+ E\left[|W_{PB}(t)|^2\right] = x(t)^2\left\{1 + (N-1)E\left[\cos(\phi_i)\right]^2\right\} \\
&+ E\left[|W_{PB}(t)|^2\right],
\end{aligned}
\tag{4}
$$

where ϕ_i is a phase offset among nodes which is uniformly distributed around 0° between $[-\pi, \pi]$ interval. Figure 3 shows a normalized beamforming gain, $E[P_R]$, which is obtained using (4) upon varying the numbers of nodes in the networks. The "perfect distributed beamforming" term means that every received signal at base station is perfectly aligned. Note that the maximum beamforming gain is 1 as the signal normalization is performed at base station. For the case of having no phase offset (or $\phi_i = 0°$ here defined as a perfect distributed beamforming), the resulting beamforming gain is of maximum value. Otherwise, the systems experience an unstable low beamforming gain. According to these results, phase synchronization is a key success for distributed beamforming which is the focus of this paper. As mentioned in the Introduction, various phase synchronization techniques have been proposed with a common drawback of sending a large number of feedback signals and the requirement of additional hardware. Alternatively, this paper proposes a phase synchronization technique avoiding any feedback signal from base station and any interaction between transmitting nodes. The proposed nonfeedback phase synchronization is described in the next section.

3. Proposed Phase Synchronization

In this section, we propose a nonfeedback distributed beamforming which does not require any interaction between nodes and feedback signals. The phase synchronization is performed at base station. At base station, there are two major parts: (1) *RF front end operation* which converts the RF signals to the baseband signals and (2) *proposed nonfeedback technique* procedure which performs signal extraction and phase synchronization. Moreover, the performance comparison between the proposed technique and some existing techniques is presented afterwards.

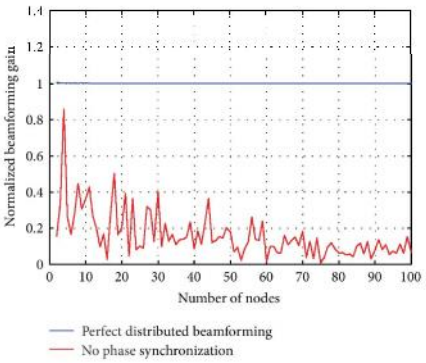

FIGURE 3: Beamforming gain in case of perfect beamforming and no phase synchronization.

When base station receives signals from N transmitting nodes, the composite received signal, $Y_R(t)$, is processed in the RF front end receiver in order to convert a pass-band received signal to digital baseband signal. The RF front end receiver consists of RF demodulator, band-pass filter, Analog-to-Digital Converter (ADC), and Digital Downconverter (DDC). Then, the proposed nonfeedback technique is applied to the output baseband signal, $Y''(k)$, which includes a signal extraction and a weighting process. The mentioned procedures are detailed as follows.

3.1. RF Front End Operation. In RF front end, we assume that the received signal amplitude, A_n, is equal to 1. The combined received signals at base station when they are coming from all transmitting nodes can be written as

$$
\begin{aligned}
Y_R(t) &= \Re\left\{\sum_{n=1}^{N} y_n'(t) + W(t)\right\} \\
&= \Re\left\{x(t)\sum_{n=1}^{N} h_n e^{j(\omega_n t+\phi_n)} + W(t)\right\} \\
&= x(t)\sum_{n=1}^{N}\left[h_n\cos(\omega_n t + \phi_n)\right] \\
&\quad + \underbrace{w_I(t)\cos(\omega_c t) - w_Q(t)\sin(\omega_c t)}_{\Re\{W_{PB}(t)\}},
\end{aligned}
\tag{5}
$$

when $y_n'(t)$ is a signal from the nth node, $\omega_n = \omega_c + \Delta\omega_n$ in which ω_c is a carrier signal frequency and $\Delta\omega_n$ is a frequency offset, $\phi_n = \phi_0 + \Delta\phi_n$, where ϕ_0 is a nominal phase, $\Delta\phi_n$ is a

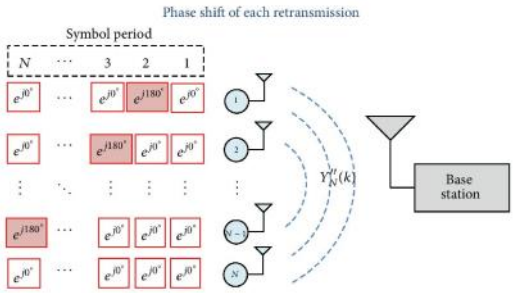

FIGURE 4: Proposed phase shifting pattern.

phase offset, and $W(t)$ is AWGN which consists of in-phase $w_I(t)$ and quadrature $w_Q(t)$ components. Then, the received signal that appeared in (5) is modulated and downconverted using RF modulator and DDC in order to obtain the digital baseband signal as follows:

$$Y''(k) = x(k)\sum_{n=1}^{N} h_n e^{-j(\Delta\Omega_n k+\Phi_n)} + W_{BB}(k), \quad (6)$$

where k is a sampling time variable, $\Delta\Omega_n$ is a frequency offset, and Φ_n is a phase offset at kth sampling time. In addition, $W_{BB}(k)$ is a baseband AWGN and $W_{BB}(k) = w_I(k) + jw_Q(k)$.

Equation (6) presents the baseband signal which can be degraded by the phase offset, Φ_n. Thus, the baseband signal of each transmitting node requires a phase synchronization in order to obtain the maximum beamforming gain. Therefore, $Y''(k)$ is passed to the procedure of proposed nonfeedback technique which is presented in the following section.

3.2. Proposed Nonfeedback Technique. In this paper, a nonfeedback technique is proposed employing a signal extraction at base station to achieve a phase synchronization for distributed beamforming networks. The received signal, $Y''(k)$, mentioned earlier is processed in two steps: *Spatial-Temporal Extraction* and *Optimum Weighting*.

Step 1 (Spatial-Temporal Extraction). The combined signal that appeared in (6) needs to be extracted before performing a phase synchronization. The steps of signal extraction are as follows.

All transmitting nodes in the networks transmit the similar message to the base station at the same time. This transmission repeats only N times where N stands for the number of transmitting nodes in the networks. For each retransmission, the transmitting nodes adjust their phases according to a fixed phase adjustment pattern matrix, $\mathbf{A}_{NN}$, which can be obtained by the following algorithm. Note that this retransmission does not require any interaction among transmitting nodes:

(1) At 1st symbol period, all transmitting nodes send the signal without any phase adjustment.

(2) At the nth symbol period, where $n = [2, 3, \ldots, N]$, only $(n-1)$th transmitting node shifts its phase by 180°. For example, at the 2nd symbol period, the 1st node shifts its phase by 180° and, at the 3rd symbol period, the 2nd node shifts its phase by 180° as seen in Figure 4 which shows the summary of proposed phase adjustment pattern.

(3) Repeat phase shifting pattern until N symbol period.

According to the proposed phase adjustment pattern as presented above, we obtain the fixed coefficient matrix $\mathbf{A}_{NN}$ by retransmitting signal for N times as shown in the following equations:

$$\mathbf{A}_{NN} = \begin{bmatrix} 1 & 1 & \cdots & 1 & 1 \\ e^{j180^\circ} & 1 & \cdots & 1 & 1 \\ 1 & e^{j180^\circ} & \cdots & 1 & 1 \\ \vdots & \vdots & \ddots & \vdots & \vdots \\ 1 & 1 & \cdots & e^{j180^\circ} & 1 \end{bmatrix}. \quad (7)$$

After having completed N retransmissions, all received signals are simultaneously arranged to form vector $\mathbf{Y}''_N$ as follows:

$$\mathbf{Y}''_N(k) = \mathbf{A}_{NN}\mathbf{y}_N(k) + \mathbf{W}_{BB,N}(k) \quad (8)$$

or

$$\begin{bmatrix} Y''_1(k) \\ Y''_2(k) \\ Y''_3(k) \\ \vdots \\ Y''_N(k) \end{bmatrix} = \underbrace{\begin{bmatrix} 1 & 1 & \cdots & 1 & 1 \\ e^{j180^\circ} & 1 & \cdots & 1 & 1 \\ 1 & e^{j180^\circ} & \cdots & 1 & 1 \\ \vdots & \vdots & \ddots & \vdots & \vdots \\ 1 & 1 & \cdots & e^{j180^\circ} & 1 \end{bmatrix}}_{\mathbf{A}_{NN}} \begin{bmatrix} y_1(k) \\ y_2(k) \\ y_3(k) \\ \vdots \\ y_N(k) \end{bmatrix}$$

$$+\begin{bmatrix} W_{BB,1}(k) \\ W_{BB,2}(k) \\ W_{BB,3}(k) \\ \vdots \\ W_{BB,N}(k) \end{bmatrix}, \tag{9}$$

where $\mathbf{Y}''_N(k)$ is the vector of combined received signal obtained by retransmitting signal for N times. $\mathbf{y}_N(k)$ is the vector of transmitted message from nth node, $n = [1, 2, \ldots, N]$, and $\mathbf{W}_{BB,N}(k)$ is the vector of baseband AWGN. Equation (9) confirms that the retransmitting signal of $\mathbf{Y}''_N(k)$ provides the coefficient matrix $\mathbf{A}_{NN}$.

From the combined signal vector that appeared in (8), $\mathbf{Y}''_N(k)$ can be extracted by applying an inverse matrix $\mathbf{A}^{-1}_{NN}$ as seen in (10). Thus, we can extract the combined signal by utilizing the inverse matrix as follows:

$$\mathbf{A}^{-1}_{NN}\mathbf{Y}''_N(k) = \mathbf{A}^{-1}_{NN}\mathbf{A}_{NN}\mathbf{y}_N(k) + \mathbf{A}^{-1}_{NN}\mathbf{W}_{BB,N}(k). \tag{10}$$

Then, the expression of $\mathbf{y}_N(k)$ that appeared in (8) becomes

$$\mathbf{y}_N(k) + \mathbf{A}^{-1}_{NN}\mathbf{W}_{BB,N}(k) = \mathbf{A}^{-1}_{NN}\mathbf{Y}''_N(k). \tag{11}$$

Equation (11) represents the extracted signals from each node, $\mathbf{y}_N(k) + \mathbf{A}^{-1}_{NN}\mathbf{W}_{BB,N}(k)$ which can be extracted by applying the proposed $\mathbf{A}^{-1}_{NN}$. Equation (11) also reveals that the extracted signals are affected by baseband AWGN, $\mathbf{A}^{-1}_{NN}\mathbf{W}_{BB,N}(k)$.

This proposed technique will be demonstrated through an example of a beamforming network that is composed of four transmitting nodes, $N = 4$. Note that each transmitting node and base station are equipped with a single antenna element. Also, all nodes are stationary and the operating frequency is 2.45 GHz. The received signals at base station are assumed to be equal to 1 having SNR of 20 dB, referring to the minimum SNR of commercial Wi-Fi networks [26]. This confirms the feasibility of proposed concept when operated in real circumstances having rich noise signal. The phase offset is distributed over $-\pi$ to π. The utilized frequency offset is referred to as a typical frequency offset of clock crystals which is 1–20 parts per million (ppm) [24]. As the operating frequency is 2.45 GHz, the maximum frequency offset is $2.45\,\text{GHz} \times 20 \times 10^{-6} = 49\,\text{kHz}$ and the minimum frequency offset is $2.45\,\text{GHz} \times 1 \times 10^{-6} = 2.45\,\text{kHz}$. Thus, the frequency offset is distributed over −49 kHz to 49 kHz. As the systems are stationary, the effect of fading channel is now neglected. Thus, the received signal amplitude from all nodes is assumed to be 1. As the focus of this paper is only phase synchronization, the perfect timing synchronization across all nodes is assumed in this system.

In case of $N = 4$, expressions (8) can be rewritten as follows:

$$\mathbf{Y}''_4(k) = \mathbf{A}_{44}\mathbf{y}_4(k) + \mathbf{W}_{BB,4}(k) \tag{12}$$

or

$$\begin{bmatrix} Y''_1(k) \\ Y''_2(k) \\ Y''_3(k) \\ Y''_4(k) \end{bmatrix} = \underbrace{\begin{bmatrix} 1 & 1 & 1 & 1 \\ e^{j180^\circ} & 1 & 1 & 1 \\ 1 & e^{j180^\circ} & 1 & 1 \\ 1 & 1 & e^{j180^\circ} & 1 \end{bmatrix}}_{\mathbf{A}_{44}} \begin{bmatrix} y_1(k) \\ y_2(k) \\ y_3(k) \\ y_4(k) \end{bmatrix} + \begin{bmatrix} W_{BB,1}(k) \\ W_{BB,2}(k) \\ W_{BB,3}(k) \\ W_{BB,4}(k) \end{bmatrix}, \tag{13}$$

where $Y''_1(k)$, $Y''_2(k)$, $Y''_3(k)$, and $Y''_4(k)$ are the received signal from retransmissions for the first, second, third, and fourth time, respectively. Also $y_1(k)$, $y_2(k)$, $y_3(k)$, and $y_4(k)$ are the transmitting signal, where $W_{BB,1}(k)$, $W_{BB,2}(k)$, $W_{BB,3}(k)$, and $W_{BB,4}(k)$ are baseband AWGN. Then, we can extract the original signal by utilizing the inverse matrix $\mathbf{A}^{-1}_{44}$ as follows:

$$\mathbf{y}_4(k) + \mathbf{A}^{-1}_{44}\mathbf{W}_{BB,4}(k) = \mathbf{A}^{-1}_{44}\mathbf{Y}''_4(k) \tag{14}$$

or

$$\begin{bmatrix} y_1(k) \\ y_2(k) \\ y_3(k) \\ y_4(k) \end{bmatrix} + \underbrace{\begin{bmatrix} 0.5 & -0.5 & 0 & 0 \\ 0.5 & 0 & -0.5 & 0 \\ 0.5 & 0 & 0 & -0.5 \\ -0.5 & 0.5 & 0.5 & 0 \end{bmatrix}}_{\mathbf{A}^{-1}_{44}} \begin{bmatrix} W_{BB,1}(k) \\ W_{BB,2}(k) \\ W_{BB,3}(k) \\ W_{BB,4}(k) \end{bmatrix} = \underbrace{\begin{bmatrix} 0.5 & -0.5 & 0 & 0 \\ 0.5 & 0 & -0.5 & 0 \\ 0.5 & 0 & 0 & -0.5 \\ -0.5 & 0.5 & 0.5 & 0 \end{bmatrix}}_{\mathbf{A}^{-1}_{44}} \begin{bmatrix} Y''_1(k) \\ Y''_2(k) \\ Y''_3(k) \\ Y''_4(k) \end{bmatrix}. \tag{15}$$

Figure 5(a) shows the original signals of 4 transmitting nodes which are separately sent to base station, $y_1(k)$, $y_2(k)$, $y_3(k)$, and $y_4(k)$. As we can see in the figure, the initial phase of each signal is 4.5°, 108.1°, −105.9°, and −25.5°. Note that the phase of transmitting signals is random using uniform distribution. After all original signals are transmitted, they are destructively combined at base station. Figure 5(b) shows the 4 retransmissions of combined signals, $Y''_1(k)$, $Y''_2(k)$, $Y''_3(k)$, and $Y''_4(k)$, for the first, second, third, and fourth time, respectively. As we can see, the maximum combination of received signal cannot be achieved as their phases are not suitably aligned. Thus, we propose an extraction of received signal at base station by applying the inverse matrix as shown in (14). After having done the proposed extraction, Figure 5(c) shows the 4 extracted signals $\mathbf{y}_4(k) + \mathbf{A}^{-1}_{44}\mathbf{W}_{BB,4}(k)$ obtained from (14) or (15). As we can see in the comparison between Figures 5(a) and 5(c), phases of extracted signals are similar to original signals at 4.8°, 110.7°, −104.3°, and

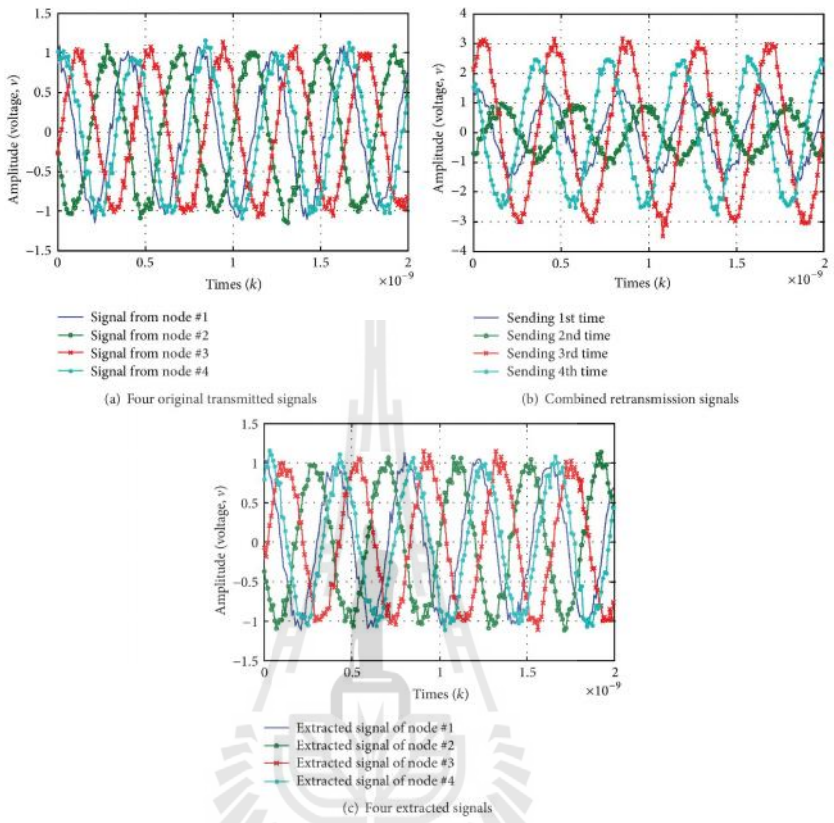

(a) Four original transmitted signals

(b) Combined retransmission signals

(c) Four extracted signals

FIGURE 5: Simulation results from Spatial-Temporal Extraction.

−26.3°. At this point, phase offsets among those 4 signals still remain in which a suitable phase synchronization technique is required next.

Step 2 (Optimum Weighting). After we obtain the correct extracted signals as pointed out in previous step, the signals are sent to the weighting procedure. In this process, the phases of extracted signals will be synchronized by the following simple algorithm. The transmitted signal from the 1st node is given to be a reference signal. Then, signals from remaining nodes $y_n(k)$ will be weighted by shifting their phases from 0° to 360° in order to find the best weighting coefficients which provide the maximum combined signal strength between the reference node $y_1(k)$ and the remaining nodes $y_n(k)$, where $n = [2, 3, \ldots, N]$. As a result, the synchronized signals have equal phases referring to the chosen reference signal. Figure 6 presents the flow chart of the proposed phase synchronization concept. In the process of finding the best weighting coefficients, we can choose a weighting step size larger than 1° in order to reduce the processing time. Figure 7 shows a normalized beamforming gain upon employing several weight steps varied from 1° to 100°. In this simulation, we assume that the received signal amplitude from all nodes is equal to 1 having SNR = 20 dB, the number of nodes is 20, and the phase offset is uniformly distributed over 0° to 360°. As we can see in this figure, a large weighting step provides the lower beamforming gain. This is because a large weighting step may skip the Optimum Weighting value. However, the weighting step of ~10° provides a similar beamforming gain as employing a

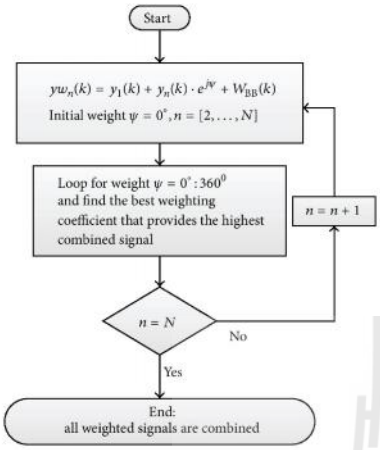

FIGURE 6: Summary flow chart of proposed phase synchronization.

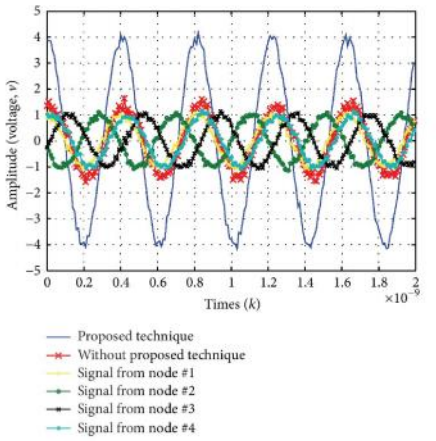

FIGURE 8: Received signal at base station from 4 transmitting nodes.

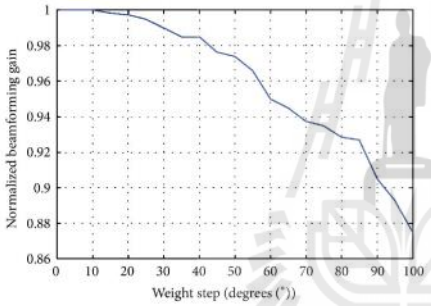

FIGURE 7: Normalized beamforming gain versus weighting step.

smaller weighting from 1° to 10°. Thus, we can utilize the weighting step of 10° to reduce the processing time.

After having done signal extraction and phase synchronization, we obtain the gainfully combined signal in a continuous time domain, $Y_{opt}(t)$, as shown in Figure 8. We finally obtain the maximum 4 times of transmitted signal amplitudes using the proposed techniques. The phase of combined signal equals the phase of the reference node $y_1(k)$. Without a phase synchronization, a lower beamforming gain is achieved due to the phase offset.

The simulation results in this section also reveal that the proposed nonfeedback technique has an efficiency over the one-bit feedback and zero-feedback techniques as the proposed technique requires a lower number of retransmissions comparing to the one-bit feedback and zero-feedback techniques. The proposed nonfeedback technique provides $N^2/N = N$ beamforming gain per transmission while the work presented in [18] has stated that the one-bit feedback offers $N^2/5N = N/5$ beamforming gain per transmission with the requirement of at least $5N$ retransmissions in order to achieve 75% guarantee of maximum beamforming gain. For example, considering employing 3 nodes in the networks, the proposed one and one-bit feedback offer gain per transmission of $3^2/3 = 3$ and $3/5 = 0.6$, respectively. In addition, from [24], in case of having 3 transmitting nodes, the zero-feedback technique provides $3^2/50 = 0.18$ beamforming gain per transmission as it requires at least 50 retransmissions in order to achieve ≈95% guarantee of maximum beamforming gain. As we can see, the proposed concept offers higher beamforming gain per one transmission comparing to other techniques.

The next section presents the beamforming gain comparison between the proposed technique and some existing phase synchronization techniques.

3.3. *Performance Comparison.* In this section, the average beamforming gains of some existing techniques and the proposed one are compared where the number of transmitting nodes is varied from 2 to 10 nodes. Note that the number of iterations for an average value is 100. In the simulation, we assume that the received signals at base station have unit amplitudes, $A_n = 1$, and SNR of 20 dB. The random initial phase of each node is uniformly distributed over $-\pi$ to π. The effects of fading channel and Doppler are neglected. The number of retransmitting signals (retransmissions) is limited to 50. Also, this paper focuses on only phase synchronization and the perfect timing and frequency synchronization across all transmitting nodes are assumed in this system. For the

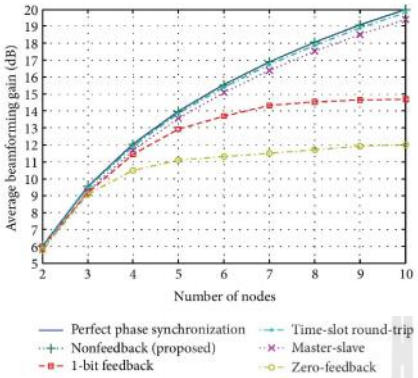

FIGURE 9: Beamforming gain of proposed nonfeedback technique versus other techniques.

proposed nonfeedback beamforming, we utilize the weighting step of 10°. Note that the reason of choosing the step size has been mentioned in the previous section.

As seen in Figure 9, the obtained results show that the average beamforming gains for the cases of proposed nonfeedback and time-slot round-trip are equal to the case of perfect phase synchronization. Although nonfeedback and time-slot round-trip techniques are comparable in terms of beamforming gain, the proposed nonfeedback technique is preferable as it does not require any feedback from base station while the time-slot round-trip technique requires a reference signal transmitted back from base station. Moreover, the proposed nonfeedback technique does not require any interaction between nodes while time-slot round-trip technique does. Although the master-slave technique also does not require any feedback from the base station it requires an interaction between transmitting nodes. This introduces a complexity to the systems. Moreover, the beamforming gain of the master-slave technique may be distorted by an uncompensated VCO phase drift. This phase drift occurred by the internal oscillator noise and over time of phase compensation in the open-loop mode, while the slave nodes are transmitting. Thus, the slave's carrier signals can be drifted out of phase [21].

According to the number of retransmissions which is limited to 50, the one-bit feedback and zero-feedback techniques provide lower beamforming gain compared with the proposed one. This is because the one-bit feedback and zero-feedback technique require a large number of retransmissions to achieve the maximum beamforming gain. The one-bit feedback technique requires the number of retransmissions to be at least $5N$ retransmissions to achieve 75% guarantee of maximum beamforming gain [18]. Thus, the one-bit feedback requires the number of retransmissions to be larger than 50 to achieve the maximum beamforming gain upon having 10 transmitting nodes, $N = 10$. Figure 9 shows that the 10 transmitting nodes for one-bit feedback technique provide (14.7 dB/20 dB) × 100 = 73.5% of the maximum beamforming gain which is close to the numerical results of [18]. Figure 9 also presents that the one-bit feedback technique cannot provide the maximum beamforming gain when $N > 3$. The reason is that only 50 retransmissions may be not enough to achieve the maximum beamforming gain while the zero-feedback requires at least 50 and 250 retransmissions to achieve ≈95% of the maximum beamforming gain upon having 3 and 4 transmitting nodes, respectively [24]. That means only 50 retransmissions are not enough to achieve the maximum beamforming gain when $N \geq 3$.

In summary, the proposed nonfeedback technique has the following advantages over other phase synchronization techniques: It offers higher effective gain with lower number of retransmissions. Also, it avoids interactions between transmitting nodes and also does not require any feedback signal from the base station.

4. An Experimental Study of the Proposed Nonfeedback Distributed Beamforming Technique

In a real circumstance, the proposed nonfeedback distributed beamforming can be affected by characteristic of communication channel such as phase variation or fading. Therefore, the experimental study of proposed techniques is considered in order to validate the proposed technique. A testbed consisting of two transmitting nodes and one base station was developed under SDR technology. We utilize a Universal Software Radio Peripheral (USRP) as it provides high speed ADCs, DACs, FPGA, and USB interface support [27, 28]. The experiments are separated into two parts: (A) *an experiment for received signal power* and (B) *an experiment for BER*. The first one is to prove if the proposed concept provides a gainfully combined signal at base station while the latter is to confirm the enhancement of system performance in terms of BER.

4.1. An Experiment on Received Signal Power. Figure 10 shows the configuration of experiment setup to measure the received signal power. A cosine wave is transmitted using USRP1 which includes two transmitting nodes, nodes #A and #B. Note that XCVR2450 is employed as a daughter board for both cases. Then, base station receives the transmitted signal and conveys it to laptop for data recording. We use a single laptop in order to avoid the problem of timing synchronization among transmitting nodes. As the transmitted cosine wave is very sensitive to frequency offset, two daughter boards (or RF boards) on a single USPR1 are chosen. The USRP1 is connected to a laptop which is operated by Ubuntu 10.04. Figure 11(a) presents the configuration of transmitting nodes (#A and #B) which are placed at the sidewall. Figure 11(b) presents the placement of base station which is situated 7 meters away from the two transmitting nodes. According to a distance between the base station and laptop which is limited to about 2 meters (a maximum range of USB cable), we utilize a transmission line to extend a

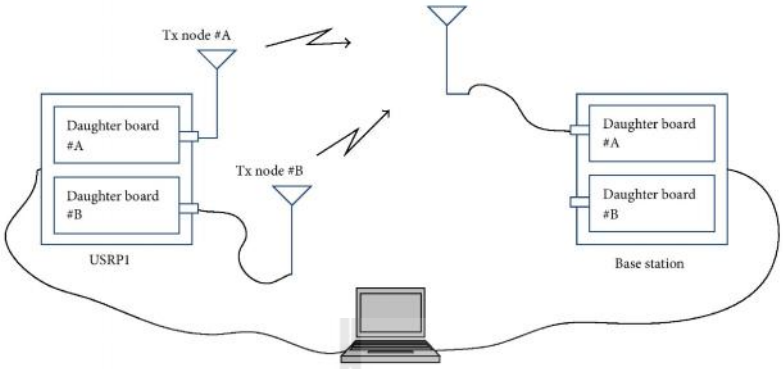

FIGURE 10: Configuration of measurement for received signal power.

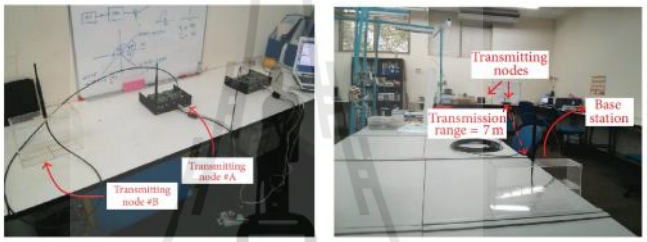

(a) Two transmitting nodes (b) Base station

FIGURE 11: The configuration of the experiment on received signal power.

communication range; the transmission lines are connected between USRP1 and antenna as shown in Figure 10. A loss of used transmission line is −16.2 dB. Therefore, the 7 meters is the longest distance to ensure that the received signal is not too weak. We cannot use a farther distance as the USRP is very sensitive for the signal strength. The antennas having gain of 3 dBi are employed at both transmitting nodes and base station.

For the programming, we utilize GNU Radio Companion (GRC) version 3.7.4 which can build GNU Radio flow graphs using a graphical user interface. Figure 12(a) presents a block diagram of the transmitting nodes. Note that the phase differences between the two transmitting nodes are random by the node locations as shown in Figure 11(a). The "Signal Source" generates a cosine wave which has the setup parameters as follows: signal amplitude is 1 volt, signal frequency is 1 kHz, carrier frequency is 2.45 GHz, and sampling rate is 250 kHz. Then, the signal is weighted by a "Phase Shifter" considered as a weighting coefficient. This weighting coefficient depends on the proposed phase adjustment patterns shown in Figure 4. Finally, the signals are transmitted by "UHD USRP Sink" where UHD is the USRP Hardware Driver compatible for all USRPs. Note that the transmitting gain of USRP parameter in GRC is 29 dB. Note that the testbed has two transmitting nodes ($N = 2$). Thus, the required number of transmission is 2 times as the proposed nonfeedback beamforming technique requires only N transmissions to perform beamforming when N is the number of transmitting nodes. Figure 12(b) presents a block diagram of base station. The received signal is obtained by "UHD USRP Source." Then, the received signal is locked to the center frequency and downconverted to baseband signal by a "Costas Loop." The loop bandwidth of Costas Loop is 0.0065 radians per sample. Finally, the signal is saved at "File Sink." The saved files are used for an offline processing to be performed for the proposed technique as shown in Figure 12(c). The saved files are loaded by "File Source." The "File Source #1" and "File Source #2" are obtained at the 1st- and 2nd-time transmission, respectively. Then, the "Extraction" proposed in Section 3.2 provides the two extracted signals which related to the signal transmitted

Table 1: Mean and standard deviation of measured average magnitude.

	1 × 1 A	1 × 1 B	2 × 1 1st	2 × 1 2nd	2 × 1 on	2 × 1 off
Mean (v)	0.012	0.026	0.030	0.030	0.038	0.026
Standard deviation (v)	0.0022	0.0037	0.0042	0.0046	0.0051	0.0078

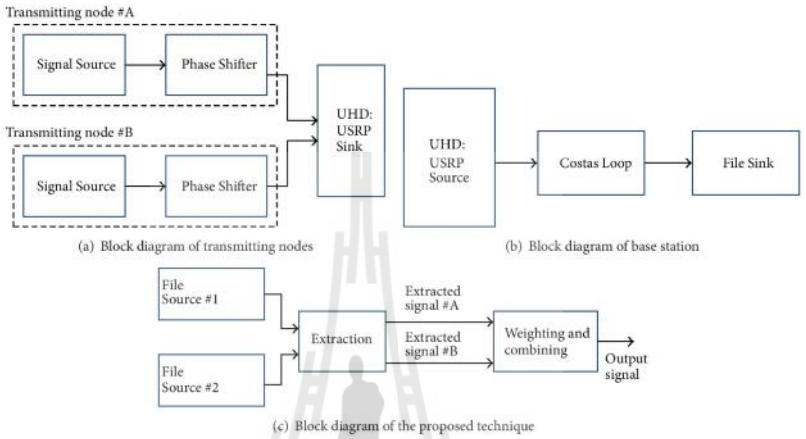

(a) Block diagram of transmitting nodes

(b) Block diagram of base station

(c) Block diagram of the proposed technique

Figure 12: The programming block diagram for experiment on received signal power.

from nodes #A and #B. Finally, the extracted signals are weighted and combined according to proposed weighting algorithm discussed in Section 3.2.

The measured results are presented in a histogram of average combined magnitude at base station. Note that this magnitude is average from 100-time data recording. Figure 13(a) shows the results in the case of only a single node (node #A) that transmits a cosine wave to base station while Figure 13(b) is for the case when only node #B transmits a cosine wave to base station. Figures 13(c) and 13(d) show the average of combined magnitude when both nodes #A and #B transmit a signal for the 1st time and 2nd time, respectively. Then, Figure 13(e) shows the output of combined signal when the proposed beamforming scheme has been performed. But when the proposed scheme is off (without phase synchronization), the combined signal turns to be lower as shown in Figure 13(f). As 100-time data of experiments is recorded, Table 1 shows a mean value and standard deviation of all cases. The results present that the proposed technique provides an optimum gain as 0.038 volts with respect to the optimum beamforming gain. Note that the optimum gain can be calculated by summation of the received signal power from nodes #A and #B (0.012 + 0.026 = 0.038). Thus, the gain of proposed technique is significantly better than that without phase synchronization which provides a signal gain as only 0.026 volts. Moreover, a standard deviation in case of proposed technique ($\sigma = 0.0051$) is lower than that in the case when the proposed scheme is off ($\sigma = 0.0078$). This implies that the proposed technique provides higher stability in terms of received signal power.

The experimental results in this section validate that the proposed technique provides a gainfully combined signal at base station. However, the power of received signal cannot totally guarantee the quality of the received data. This is because the received signal can be affected by transmission channel such as fading, noise, interference, and bit synchronization between the two transmitting nodes. Therefore, we further investigate the BER in the next section.

4.2. An Experiment on Bit Error Rate. A testbed for BER measurement is shown in Figure 14. In this experiment, we transmit the random binary bits to a base station. The number of transmitting bits is 1 million which has a carrier frequency at 2.45 GHz. The USRP is employed at base station and two USRPB100s are employed as the transmitting nodes, nodes #A and #B. SBX-120 is used as the daughter boards for USRPB100. All USRPs are connected to a laptop for data recording. The two transmitting nodes are placed at the sidewall as shown in Figure 15. The configuration of the base station is the same as the one for previous experiment shown in Figure 11(b). Also, all losses in transmission line have been calibrated before performing the measurement.

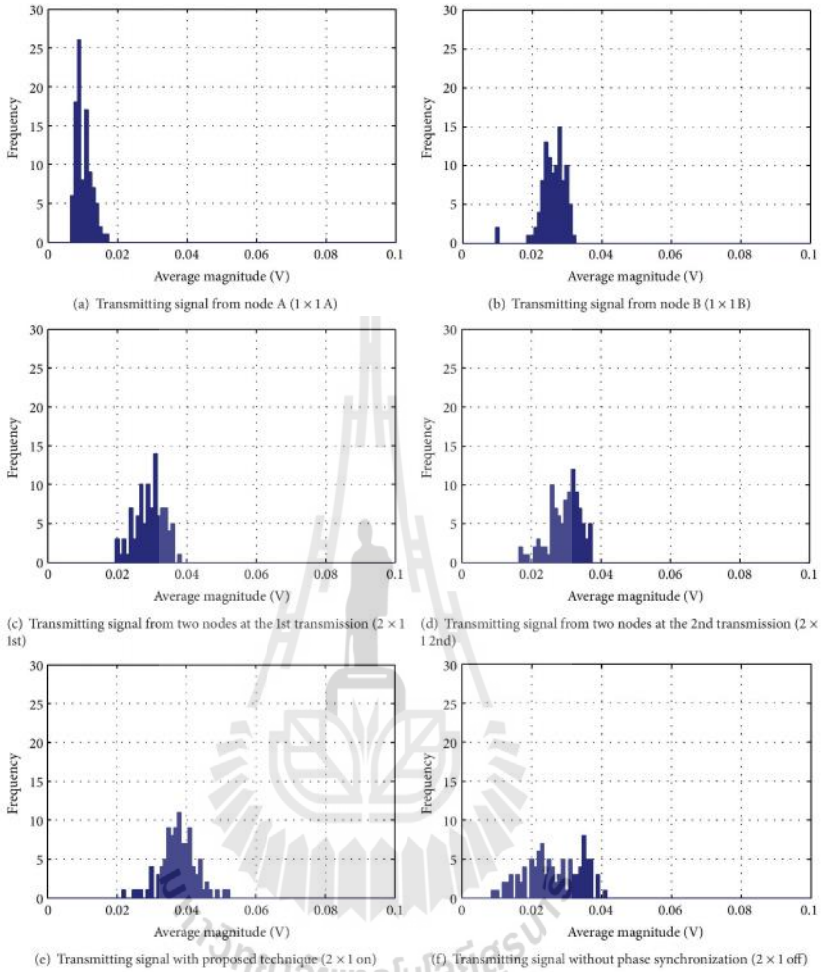

FIGURE 13: A histogram of average magnitude.

Figure 16(a) shows a block diagram of the transmitting nodes. The "Signal Source" generates the random binary bits which has sample rate of 250 kHz. Then, the signal is encoded by "Packet Encoder." In this block, the signal is wrapped into a packet which provides a payload length with a header, access code, and preamble. The setup parameters of this block are samples/symbol of 2 and bits/symbol of 1. Afterwards, the encoded signals are demodulated by the "Differential Binary Phase Shift Keying (DBPSK)" modulation. The setup parameter of this block is that an excess bandwidth (or roll-off factor) is 0.35 and Gray code is enabled. Then, the modulated signal is weighted by a "Phase Shifter" considered as weighting coefficient. Note that the mentioned weighting scheme has been proposed in Figure 4. Finally, the signals are transmitted at "UHD USRP Sink." The transmitted gain in GRC is 31 dB which related to the optimum transmitting gain.

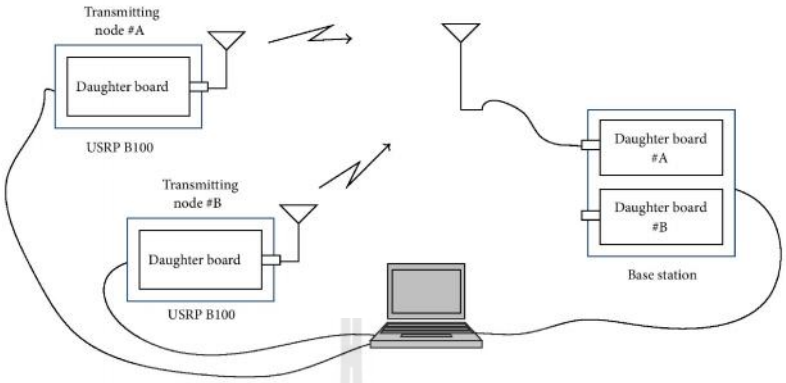

FIGURE 14: Configuration of measurement for BER.

FIGURE 15: Two transmitting nodes employing USRP B100.

Figure 16(b) shows a block diagram of base station including "UHD USRP Sink" and "File Sink." In the offline processing, the saved files are extracted, weighted, and combined as shown in Figure 16(c). After that, the combined signals are demodulated using "DBPSK Demodulation." The setup parameters of this block are as follows: an excess bandwidth (or roll-off factor) is 0.35, frequency lock loop bandwidth is 0.0628 radians per sample, phase recovery loop bandwidth is 0.0628, timing recovery loop bandwidth is 0.0628 radians per sample, and Gray code is enabled. Finally, a demodulated signal is decoded by "Packet Decoder."

The measurement results are presented in a histogram of BER where 100-time recorded data has been averaged. Note that the measured BER employing USRP is relatively sensitive with noise. Thus, the major portion of measured BER is the optimum case as 0.0 or the worst case as 0.5. Note that BER = 0.0 means that there is no bit error at all, while BER = 0.5 means that bit error turns out to be a half of transmitted bits; for example, bit error is 500,000 upon transmitting 1 million bits. Figure 17(a) presents the BER in the case of transmitting data from only node #A while Figure 17(b) presents the case when only node #B transmits the data. The results show that transmitting data from only a single node provides a low performance in terms of BER: the portion of BER = 0.0 which is only 11/100 in the case of only node #A and the portion of BER = 0.0 which is only 22/100 in the case of only node #B. Then, the proposed technique is applied in order to enhance the BER. Figures 17(c) and 17(d) show the BER value at the base station when the two nodes transmit data at the 1st and 2nd time, respectively. Figure 17(e) shows the BER of combined signal at base station when the proposed technique has been applied. Figure 17(f) shows the BER for the case without the proposed technique. The results present that the proposed technique provides a lower BER than the case of transmitting signal from a single node and when the proposed technique is not applied. The portion of BER = 0.0 in case of using the proposed technique is 45/100. The portion of BER = 0.0 is only 25/100, 17/100, and 14/100 when the two nodes transmit data at the 1st and 2nd time and without phase synchronization, respectively. Table 2 shows a mean and standard deviation BER of all cases as the experiments have been recorded for 100 times. The results in this table confirm that the proposed technique makes the system BER lower comparing to other cases. The mean BER of the proposed technique is only 0.27 while the mean BER values in case of transmitting signal from a single node #A and a single node #B are 0.43 and 0.39, respectively. The mean BER is 0.35, 0.39, and 0.40 when the two nodes transmit data at the 1st and 2nd times and without phase synchronization, respectively. The BER performance obtained in the experiment is considered high as the received signals are too weak as shown in Table 1. However, the BER performance of proposed technique is significantly lower than the BER performance of using a single node (1×1 A and 1×1 B) and without phase synchronization (2×1 off). Therefore, the experimental results in this section validate

Table 2: Mean and standard deviation of measured BER.

	1 × 1 A	1 × 1 B	2 × 1 1st	2 × 1 2nd	2 × 1 on	2 × 1 off
Mean (v)	0.43	0.39	0.35	0.39	0.27	0.40
Standard deviation (v)	0.16	0.21	0.22	0.20	0.25	0.19

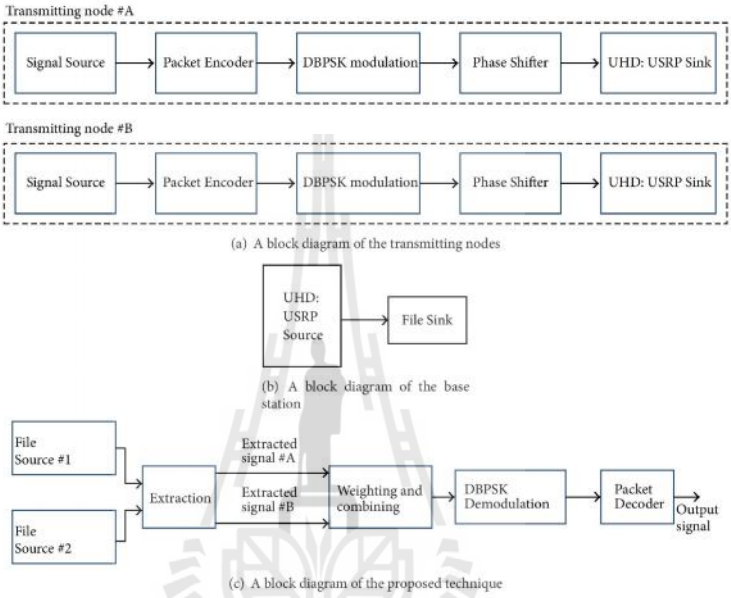

Figure 16: The programming block diagram experimental BER.

the proposed technique that it can be utilized to realize a distributed beamforming network with an optimum gain and lower BER.

5. Conclusion

This paper has proposed an alternative phase synchronization technique, so-called nonfeedback distributed beamforming technique. The proposed nonfeedback requires a lower number of retransmissions comparing to the one-bit feedback and zero-feedback techniques. Also, the proposed nonfeedback does not require any feedback signal or interaction between transmitting nodes. Using this technique, phase synchronization can be accomplished at base station instead of mobile terminals. From simulation results, the proposed nonfeedback technique provides a high beamforming gain compared with some existing phase synchronization techniques. Also, the proposed nonfeedback technique has been analyzed under real indoor environment. The measured results have revealed that the proposed technique provides the optimum beamforming gain. Also, it can enhance the system performance by lowering a Bit Error Rate (BER) comparing to the case when the phase synchronization is not applied.

Conflict of Interests

The authors declare that there is no conflict of interests regarding the publication of this paper.

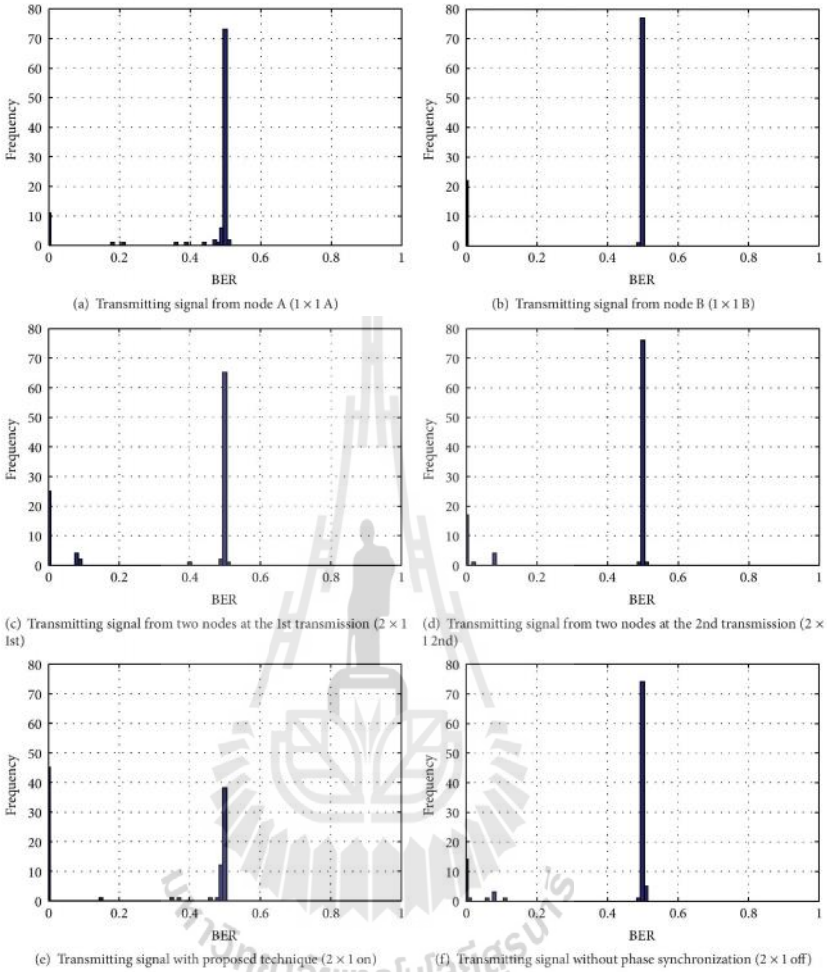

(a) Transmitting signal from node A (1 × 1 A)

(b) Transmitting signal from node B (1 × 1 B)

(c) Transmitting signal from two nodes at the 1st transmission (2 × 1 1st)

(d) Transmitting signal from two nodes at the 2nd transmission (2 × 1 2nd)

(e) Transmitting signal with proposed technique (2 × 1 on)

(f) Transmitting signal without phase synchronization (2 × 1 off)

Figure 17: A histogram of Bit Error Rate.

Acknowledgments

This work was supported in part by The Royal Golden Jubilee Ph.D. (RGJ-Ph.D.) Program no. 1.Q.TS/52/B.1.B.XX and Suranaree University of Technology, Thailand.

References

[1] P. Sriploy, P. Uthansakul, and M. Uthansakul, "Effect of path loss on the distributed beamforming for Wireless Sensor Networks," in *Proceedings of the 10th International Conference on Electrical Engineering/Electronics, Computer, Telecommunications and Information Technology (ECTI-CON '13)*, pp. 1–4, Krabi, Thailand, May 2013.

[2] C. A. Balanis, *Antenna Theory: Analysis and Design*, John Wiley & Sons, New York, NY, USA, 2nd edition, 1997.

[3] P. Meerasri, P. Uthansakul, and M. Uthansakul, "Self-interference cancellation-based mutual-coupling model for full-duplex single-channel MIMO systems," *International*

Journal of Antennas and Propagation, vol. 2014, Article ID 405487, 10 pages, 2014.

[4] A. Innok, P. Uthansakul, and M. Uthansakul, "Angular beamforming technique for MIMO beamforming system," *International Journal of Antennas and Propagation*, vol. 2012, Article ID 638150, 10 pages, 2012.

[5] M. Uthansakul and M. E. Bialkowski, "Investigations into a wideband spatial beamformer employing a rectangular array of planar monopoles," *IEEE Antennas and Propagation Magazine*, vol. 47, no. 5, pp. 91–99, 2005.

[6] C. Bunsanit, P. Uthansakul, and M. Uthansakul, "Refinement method for weighting scheme of fully spatial beamformer," *International Journal of Antennas and Propagation*, vol. 2012, Article ID 359847, 13 pages, 2012.

[7] P. Uthansakul, A. Innok, and M. Uthansakul, "Open-loop beamforming technique for MIMO system and its practical realization," *International Journal of Antennas and Propagation*, vol. 2011, Article ID 723719, 13 pages, 2011.

[8] F. Rayal, "Why have smart antennas not yet gained traction with wireless network operators?" *IEEE Antennas and Propagation Magazine*, vol. 47, no. 6, pp. 124–126, 2005.

[9] T. Kaiser, "When will smart antennas be ready for the market? Part I," *IEEE Signal Processing Magazine*, vol. 22, no. 2, pp. 87–92, 2005.

[10] M. Kosanovic and M. Stojcev, "Sensor node lifetime prolonging," in *Proceedings of the 20th Telecommunications Forum (TELFOR '12)*, pp. 178–181, Belgrade, Serbia, November 2012.

[11] Y. T. Lo, "A mathematical theory of antenna arrays with randomly spaced elements," *IEEE Transactions on Antennas and Propagation*, vol. 12, no. 3, pp. 257–268, 1964.

[12] H. Ochiai, P. Mitran, H. V. Poor, and V. Tarokh, "Collaborative beamforming for distributed wireless ad hoc sensor networks," *IEEE Transactions on Signal Processing*, vol. 53, no. 11, pp. 4110–4124, 2005.

[13] P. Sriploy, P. Uthansakul, and M. Uthansakul, "The optimum number of nodes and radius for distributed beamforming networks," *ECTI Transactions on Electrical Engineering, Electronics, and Communications (EEC)*, vol. 13, no. 2, pp. 35–47, 2014.

[14] S. Amini, D.-J. Na, and K. Choi, "Performance comparison between distributed beamforming and clustered beamforming," in *Proceedings of the 11th International Conference on Information Technology: New Generations (ITNG '14)*, pp. 174–179, IEEE, Las Vegas, Nev, USA, April 2014.

[15] L. Yang, K. A. Qaraqe, E. Serpedin, and M.-S. Alouini, "Performance analysis of distributed beamforming in a spectrum sharing system," *IEEE Transactions on Vehicular Technology*, vol. 62, no. 4, pp. 1655–1666, 2013.

[16] M. Dohler and Y. Li, *Cooperative Communications: Hardware, Channel and PHY*, John Wiley & Sons, Hoboken, NJ, USA, 2010.

[17] K. Yao, R. E. Hudson, C. W. Reed, D. Chen, and F. Lorenzelli, "Blind beamforming on a randomly distributed sensor array system," *IEEE Journal on Selected Areas in Communications*, vol. 16, no. 8, pp. 1555–1567, 1998.

[18] R. Mudumbai, D. R. Brown III, U. Madhow, and H. V. Poor, "Distributed transmit beamforming: challenges and recent progress," *IEEE Communications Magazine*, vol. 47, no. 2, pp. 102–110, 2009.

[19] R. Mudumbai, J. Hespanha, U. Madhow, and G. Barriac, "Scalable feedback control for distributed beamforming in sensor networks," in *Proceedings of the IEEE International Symposium on Information Theory (ISIT '05)*, pp. 137–141, Adelaide, Australia, September 2005.

[20] R. Mudumbai, J. Hespanha, U. Madhow, and G. Barriac, "Distributed transmit beamforming using feedback control," *IEEE Transactions on Information Theory*, vol. 56, no. 1, pp. 411–426, 2010.

[21] R. Mudumbai, G. Barriac, and U. Madhow, "On the feasibility of distributed beamforming in wireless networks," *IEEE Transactions on Wireless Communications*, vol. 6, no. 5, pp. 1754–1763, 2007.

[22] D. R. Brown and H. V. Poor, "Time-slotted round-trip carrier synchronization for distributed beamforming," *IEEE Transactions on Signal Processing*, vol. 56, no. 11, pp. 5630–5643, 2008.

[23] D. R. Brown III, B. Zhang, B. Svirchuk, and M. Ni, "An experimental study of acoustic distributed beamforming using round-trip carrier synchronization," in *Proceedings of the 4th IEEE International Symposium on Phased Array Systems and Technology (Array '10)*, pp. 316–323, Waltham, Mass, USA, October 2010.

[24] A. Bletsas, A. Lippman, and J. N. Sahalos, "Simple zero-feedback distributed beamforming with unsynchronized carriers," *IEEE Journal on Selected Areas in Communications*, vol. 28, no. 7, pp. 1046–1054, 2010.

[25] G. Sklivanitis and A. Bletsas, "Testing zero-feedback distributed beamforming with a low-cost SDR testbed," in *Proceedings of the 45th Asilomar Conference on Signals, Systems and Computers (ASILOMAR '11)*, pp. 104–108, Pacific Grove, Calif, USA, November 2011.

[26] Wi-Fi: Define Minimum SNR Values for Signal Coverage, May 2015, http://www.enterprisenetworkingplanet.com/netsp/article.php/3747656/.

[27] C. Clark, *Software Defined Radio: With GNU Radio and USRP*, McGraw-Hill, New York, NY, USA, 2008.

[28] Ettus Research Company, April 2015, http://www.ettus.com/.